Mathematical Problems in Engineering

Mathematical Models for Dealing with Risk in Engineering

Guest Editors: Jurgita Antucheviciene, Gang Kou, Vida Maliene, and Egidijus Rytas Vaidogas

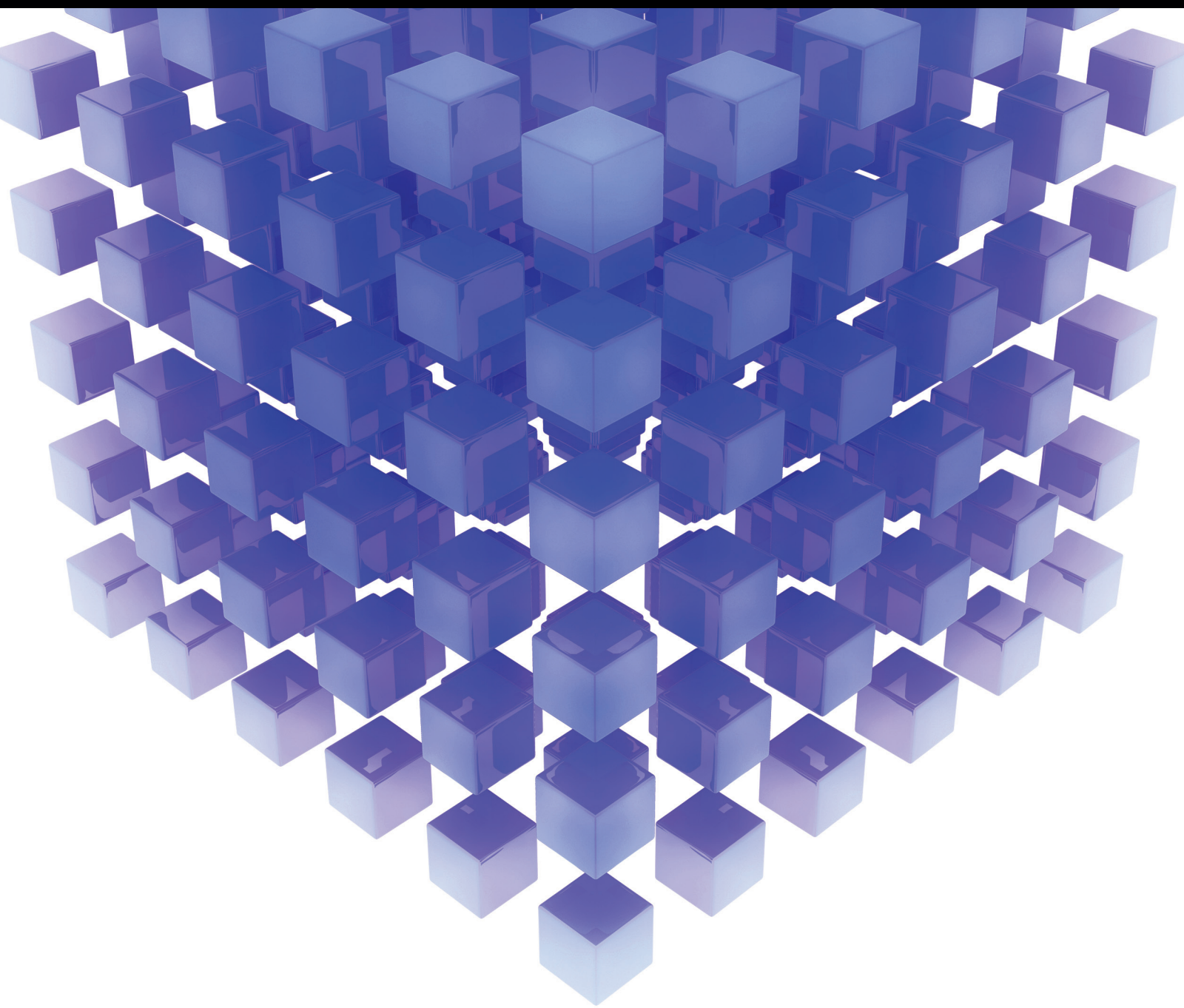

Mathematical Models for Dealing with Risk in Engineering

Mathematical Problems in Engineering

Mathematical Models for Dealing with Risk in Engineering

Guest Editors: Jurgita Antucheviciene, Gang Kou, Vida Maliene, and Egidijus Rytas Vaidogas

Editorial Board

Contents

Hindawi Publishing Corporation
Mathematical Problems in Engineering
Volume 2016, Article ID 2832185, 3 pages
http://dx.doi.org/10.1155/2016/2832185

Editorial

Mathematical Models for Dealing with Risk in Engineering

Jurgita Antucheviciene,[1] Gang Kou,[2] Vida Maliene,[3] and Egidijus Rytas Vaidogas[4]

[1]*Department of Construction Technology and Management, Faculty of Civil Engineering, Vilnius Gediminas Technical University, Saulėtekio Alėja 11, LT-10223 Vilnius, Lithuania*
[2]*School of Business Administration, Southwestern University of Finance and Economics, Chengdu 610072, China*
[3]*Department of the Built Environment, Faculty of Engineering and Technology, Liverpool John Moores University, Byrom Street, Liverpool L3 3AF, UK*
[4]*Department of Labour Safety and Fire Protection, Faculty of Civil Engineering, Vilnius Gediminas Technical University, Saulėtekio Alėja 11, LT-10223 Vilnius, Lithuania*

Correspondence should be addressed to Jurgita Antucheviciene; jurgita.antucheviciene@vgtu.lt

Received 15 August 2016; Accepted 15 August 2016

This special issue aims to provide recent developments in dealing with risk in various fields of engineering. Risk is a ubiquitous phenomenon of modern society. The concept of risk is variously understood and used in engineering, economics, and earth and social sciences [1–3]. An existence of risk arises from a possibility of adverse physical and economic phenomena that can cause damage to business, property, communication networks, and natural environment. In engineering, risk is commonly divided into speculative risk of potential economic losses or gains and nonspeculative or pure risk related to damaging phenomena, such as failures and accidents of physical objects as well as disturbances in computer networks and damage to information systems [4]. Currently, the assessment and management of pure risk are a well-established area with prospects of development and a number of unresolved problems [5–7].

Articles published in this special issue prove that risk assessment and management have many facets. Dealing with risk in engineering will require the application of a variety of approaches, ranging from sophisticated probabilistic and statistical models to straightforward engineering judgement and common sense decisions [8]. The management of risk calls for its assessment, and this in turn requires the quantification of the uncertainty of adverse events and consequences posed by each event. This is a standard, general scheme of risk assessment [9]. However, an application of this scheme will often require the solving of "local" problems, say, prediction of wind speeds, estimation of individual failure probabilities, or analysis of failure propagation in safety-critical systems. Articles included in this special issue are devoted to a solution of such "local" problems. Most of them are from various fields of engineering and informatics; some are devoted to solving risk-related problems in management. A part of articles is devoted to problems of safety and security, whereas another part deals with the problem of reliability. Risk analysis and reliability assessment are closely related areas sharing many aims, principles, and methodological tools [10–12]. In that sense, articles of the present special issue dealing with reliability can be seen as a contribution to risk assessment and management.

In the article "A Novel Approach to Evaluate the Time-Variant System Reliability of Deteriorating Concrete Bridges" by H. Tian et al., the authors propose a computational methodology developed for an assessment of time-variant reliability of concrete bridges. This methodology is based on the Monte Carlo simulation. It is used for evaluating system reliability of bridges subjected to environmental impacts. The lifetime structural performance of bridges is evaluated as well.

W. Liu et al. consider the problem of real-time railway traffic control when tracks break down at large railway stations. In the article "Real-Time Track Reallocation for Emergency Incidents at Large Railway Stations," the authors

propose a mathematical programming model aimed at minimizing the total occupational time of station bottleneck sections to avoid train delays. Additionally, an algorithm based on simulated annealing and genetic algorithm is proposed to solve the optimization problem.

In the article "Reliability of Foundation Pile Based on Settlement and a Parameter Sensitivity Analysis," S. Zhang et al. propose a formula of foundation pile reliability index. This index is related to the probability of excessive pile settlement through the distribution function of the standard normal probability distribution. Based on the formula of reliability index, authors analyze the sensitivity of this index to various statistical parameters of the pile: coefficients of variation of calculated settlement, permissible limit of the settlement, measured settlement, safety coefficient, and the mean value of calculation model coefficient.

The article "Risk Analysis Based on AHP and Fuzzy Comprehensive Evaluation for Maglev Train Bogie" by C. Fan et al. considers the safety of a maglev train bogie system. A new method combining analytic hierarchy process and fuzzy evaluation is proposed to assess hazards inherent in the bogie system and posed by potential multiple failures of bogie subsystems. This combination is seen as an alternative to standard methods of risk assessment, namely, fault tree analysis and event tree analysis.

In the article "Time-Independent Reliability Analysis of Bridge System Based on Mixed Copula Models" Y. Liu and X. Fan consider an estimation of the time-independent probability of bridge system failure. They propose mixed copula models for calculating joint failure probabilities of bridge systems. The copula models are used to express the nonlinear correlation between system failure modes. These models were developed by applying optimal copula functions with Bayesian selection criteria and the Monte Carlo method. Two-component and multiple-component systems with different configurations are considered in the article.

C.-C. Shih et al. studied fire safety in various laboratories in the article entitled "Investigation of Lab Fire Prevention Management System of Combining Root Cause Analysis and Analytic Hierarchy Process with Event Tree Analysis." Data on laboratory fire accidents are analyzed to identify the root causes of fires and draw out fire prevention strategies. The methods of root cause analysis, analytical hierarchy process, and event tree analysis are applied in combination to assess various strategies of fire protection in laboratories. The combination of these three methods is used to prioritize fire prevention measures.

In "Application of Probabilistic Method to Stability Analysis of Gravity Dam Foundation over Multiple Sliding Planes" by G. Wang and Z. Ma, the authors propose an approach to estimating the probability of instability of a concrete gravity dam foundation. The instability over multiple gliding places is considered. The problem of the instability probability calculation is solved by combining design point method with the method of divided differences. A performance function with nonnormal and correlated input variables is used for the probability estimation.

In the article "Quantification of Margins and Uncertainties Approach for Structure Analysis Based on Evidence Theory" C. Xie and G. Li address the problem of structural reliability assessment carried out as uncertainty propagation. Aleatory and epistemic uncertainties related to a mechanical structure are modeled and propagated by a combined application of the methodology known as a quantification of margins and uncertainties (QMU) and the evidence theory. The authors propose a technique that allows the reduction of computational costs of the Monte Carlo simulation used for the uncertainty propagation.

L. Zhao et al. consider an assessment of safety-critical systems in the article entitled "Failure Propagation Modeling and Analysis via System Interfaces." A novel approach to safety analysis based on system interface models is proposed. These models consider interactions between system components and the environment. The approach proposed by the authors is aimed at improving modeling of propagation of failures in the systems by applying interface automata and restricted reliability analysis.

In the article "The Method of Oilfield Development Risk Forecasting and Early Warning Using Revised Bayesian Network" Y. Zhong et al. propose a novel method for forecasting and early warning of risk related to oilfield development. This method uses neural networks to predict warning situation indices of oilfield development risk and risk warning degree. Bayesian network is applied to diagnose the reasons causing the risk. The risk considered in the article is of managerial nature.

In "Geometric Process-Based Maintenance and Optimization Strategy for the Energy Storage Batteries" by Y. Li et al., the authors analyze different main states in the life circle of energy storage batteries. In addition, they propose an optimized management strategy aimed at a minimization of long-run average costs of batteries. The strategy is used to define the time interval of detective and preventive maintenance and determine optimal corrective maintenance times related to health and reliability conditions.

In the article "Short-Term Wind Speed Forecasting Using the Data Processing Approach and the Support Vector Machine Model Optimized by the Improved Cuckoo Search Parameter Estimation Algorithm" by C. Wang et al., the authors study the problem of wind speed forecasting by means of a novel combination of data processing models. The combination is called the forecasting portfolio. It consists of empirical mode decomposition model and support vector machine model improved by a cuckoo search parameter estimation algorithm. The original data used for this forecasting are wind speed series recorded by wind turbines. The proposed forecasting portfolio is compared to alternative forecasting models by means of a case study.

In the article "A Grey Theory Based Approach to Big Data Risk Management Using FMEA" M. M. Silva et al. propose an approach to big data risk management based on failure mode and effect analysis (FMEA) and grey theory. The security-related risk posed by potential hacker attacks is considered. FMEA is used to determine and evaluate potential failure modes associated with big data dimensions in terms of data vulnerability. The grey analysis is applied to FMEA with the aim of allocating the relative importance of risk factors.

The risk factors and their relative weights are expressed in linguistic terms that evaluate data failure modes.

In "Vehicle Coordinated Strategy for Vehicle Routing Problem with Fuzzy Demands" by C. Liu et al., the problem of routing of cargo vehicles is solved. The demands of individual nodes in routes are considered to be uncertain (fuzzy). A fuzzy reasoning constrained program model is formulated for the vehicle routing problem with fuzzy demands and a hybrid ant colony algorithm is proposed to minimize the total travel distance, unloading times, and amount of waste caused by a service failure due to fuzzy demands.

In summary, the present special issue does not seek to systematize the very diverse field of risk assessment and management in engineering. This special issue rather demonstrates how many-sided dealing with risk can be.

Despite the certain randomness inherent in the submission of manuscripts for publication, we believe that this special issue could be interesting to all those who have to deal with risk in the vast field of engineering.

Acknowledgments

We would like to thank the authors of articles published in the issue for their contribution. We are grateful to all anonymous reviewers for their valuable work.

Jurgita Antucheviciene
Gang Kou
Vida Maliene
Egidijus Rytas Vaidogas

References

[1] J.-M. Flaus, *Risk Analysis. Socio-Technical and Industrial Systems*, John Wiley & Sons, Hoboken, NJ, USA, 2013.

[2] J. Ofungwu, *Statistical Applications for Environmental Analysis and Risk Assessment*, John Wiley & Sons, Hoboken, NJ, USA, 2014.

[3] L. Theodore and R. R. Dupont, *Environmental Health and Hazard Risk Assessment: Principles and Calculations*, CRC Press, Boca Raton, Fla, USA, 2012.

[4] E. R. Vaidogas, *The Business of Safety: Managing Occupational and Industrial Risks*, Technika, Vilnius, Lithuania, 2010.

[5] T. Aven, "Risk assessment and risk management: review of recent advances on their foundation," *European Journal of Operational Research*, vol. 253, no. 1, pp. 1–13, 2016.

[6] C. K. Pease and R. P. Gentry, "Systematic review in chemical risk assessment—a chemical industry perspective," *Environment International*, vol. 92–93, pp. 574–577, 2016.

[7] T. Aven, "Implications of black swans to the foundations and practice of risk assessment and management," *Reliability Engineering & System Safety*, vol. 134, pp. 83–91, 2015.

[8] N. Singpurwalla, *Reliability and Risk: A Bayesian Perspective*, John Wiley & Sons, Chichester, UK, 2006.

[9] L. T. Ostrom and C. A. Wilhelmsen, *Risk Assessment: Tools, Techniques and Their Applications*, John Wiley & Sons, Hoboken, NJ, USA, 2012.

[10] M. Rausand, *Risk Assessment: Theory, Methods, and Applications*, John Wiley & Sons, Hoboken, NJ, USA, 2011.

[11] M. Rousand, *Reliability of Safety-Critical Systems: Theory and Applications*, John Wiley & Sons, Hoboken, NJ, USA, 2014.

[12] D. J. Smith and K. G. L. Simpson, *Safety-Critical Systems Handbook*, John Wiley & Sons, Hoboken, NJ, USA, 2011.

Hindawi Publishing Corporation
Mathematical Problems in Engineering
Volume 2016, Article ID 9071394, 10 pages
http://dx.doi.org/10.1155/2016/9071394

Research Article

Vehicle Coordinated Strategy for Vehicle Routing Problem with Fuzzy Demands

Chang-shi Liu,[1,2,3,4] Gang Kou,[5] and Fu-hua Huang[1]

[1]*School of Management, Hunan University of Commerce, Changsha 410205, China*
[2]*Mobile E-Business Collaborative Innovation Center of Hunan Province, Hunan University of Commerce, Changsha 410205, China*
[3]*Key Laboratory of Hunan Province for Mobile Business Intelligence, Hunan University of Commerce, Changsha 410205, China*
[4]*Institute of Big Data and Internet Innovation, Hunan University of Commerce, Changsha 410205, China*
[5]*School of Business Administration, Southwestern University of Finance and Economics, Chengdu 611130, China*

Correspondence should be addressed to Gang Kou; kougang@swufe.edu.cn

Received 24 December 2015; Accepted 8 August 2016

Academic Editor: Thomas Hanne

The vehicle routing problem with fuzzy demands (VRPFD) is considered. A fuzzy reasoning constrained program model is formulated for VRPFD, and a hybrid ant colony algorithm is proposed to minimize total travel distance. Specifically, the two-vehicle-paired loop coordinated strategy is presented to reduce the additional distance, unloading times, and waste capacity caused by the service failure due to the uncertain demands. Finally, numerical examples are presented to demonstrate the effectiveness of the proposed approaches.

1. Introduction

The vehicle routing problem (VRP) was first proposed by Dantzig and Ramser [1]. The VRP has since been the topic of many operational studies. VRP consists of designing efficient routes to serve a number of nodes with a fleet of vehicles. Each node is visited exactly once by one vehicle. The activity of the vehicle is bounded by certain constraints. Each vehicle starts at the depot and returns to the same depot after completing its task. Most VRP studies employ the vehicle uncoordinated strategy; that is, there is no coordination between the vehicles, and each vehicle completes only its own task. There are many significant VRP results based on this case, including those of Clarke and Wright [2], Solomon [3], Laporte [4], Figliozzi [5], Sprenger and Mönch [6], Pillac et al. [7], Kou et al. [8], and Kou et al. [9].

The vehicle routing problem with fuzzy demands (VRPFD) is an extension of the VRP; that is, the demand of each node is uncertain, subjective, ambiguous, and/or vague [10]. The VRPFD is widely employed for many real applications due to their numerous uncertainties, including garbage collection systems, product recall systems, and raw milk collection systems (collecting raw milk from dairy farmers for milk powder production enterprises). There are also several classical studies that refer to the VRPFD, such as Bertsimas [11], Cao and Lai [12], Kuo et al. [13], Kou and Lin [14], Kou et al. [15], Allahviranloo et al. [16], and Hu et al. [17]. The VRPFD typically assumes that the real value of a node's demand is known when the vehicle reaches the node, whereas the vehicle's route is planned in advance. After serving v nodes, the vehicle might not be able to service the $v + 1$ node once it arrives due to insufficient capacity. In such situations, if the vehicle uncoordinated strategy is employed, the vehicle must return to the depot and unload what it has picked up thus far and then return to the node where it had a "service failure" and continue to serve the remaining nodes. Thus, "additional distance" and "additional unloading times" are introduced due to the "service failure." However, there are also vehicles with surplus capacity after completing their own tasks, introducing "waste capacity." All of these cases result in increasing logistics cost. To the authors' knowledge, few researchers have addressed the problem of minimizing the "additional distance" and "waste capacity," let alone "additional unloading times," in the VRPFD.

In this paper, vehicle coordinated strategy (VCS) is defined such that each vehicle finishes its own assigned task first; then, if there is a vehicle with surplus capacity, the vehicle must help any vehicle that has not completed its own task according to the specified vehicle coordination rules [18, 19]. Only a few VRP studies have considered VCS. Shang and Cuff [20] considered a multiobjective vehicle routing heuristic for a pickup and delivery problem. They assumed that the fleet size is not predetermined and that customers are allowed to transfer between vehicles. These transfers can occur at any location and between any two vehicles. Yang et al. [21] proposed a mixed-integer programming formulation for the offline version of the real-time VRP and compared five rolling horizon strategies for the real-time version. To some extent their work is relevant to vehicle coordination. Liu et al. [18] proposed a simple general VCS for the VRP with deterministic demands. Lin [19] designed a VCS with single or multiple vehicle uses. The VCS is defined as allowing vehicles to travel to transfer items to another vehicle returning to the depot, provided that no time window constraints are violated. Sprenger and Mönch [6] studied a methodology to solve a cooperative transportation planning problem motivated by a real-world scenario found in the German food industry. Several manufacturers with the same customers but complementary food products share their vehicle fleets to deliver to their customers. They designed a heuristic to solve the problem. The results of extensive simulation experiments demonstrated that the cooperative setting outperforms the noncooperative one. Hu et al. [22] presented a feasible routing solution to accommodate the changes (such as customer's demand changes, delivery time window changes, disabled roads induced by traffic accidents or traffic jams, and vehicle breakdowns) and to minimize the negative impacts on the existing distribution process in real-time VRP. They handle these disruptions by readjusting vehicle routes in real time to improve vehicles' efficiency and enhance service quality. To a certain extent their work is relevant to vehicle coordination. However, all investigations assumed that the customers were uniformly distributed in certain regions and that the demands were deterministic. To the authors' knowledge, few studies have employed the VCS in the VRPFD.

Thus, in this paper, the fuzzy reasoning constrained program model for VRPFD is formulated, and the hybrid ant colony algorithm is designed to minimize total travel distance. In particular, the two-vehicle-paired loop coordinated strategy (TVPLCS) is presented to reduce the "additional distance," "additional unloading times," and "waste capacity" caused by the service failure due to the uncertain demands. Finally, numerical examples are presented to demonstrate the effectiveness of the proposed approaches.

The remainder of this paper is organized as follows. In Section 2, the fuzzy reasoning constrained program model for VRPFD is formulated. In Section 3, we design a hybrid ant colony algorithm for VRPFD. In Section 4, in particular, we present the TVPLCS to minimize the "additional distance," "additional unloading times," and "waste capacity". In Section 5, we give numerical examples to demonstrate the effectiveness of the proposed approaches. Finally, we summarize the contributions of this paper.

2. VRPFD Assumptions and Model

2.1. VRPFD Assumptions. In this paper, the VRPFD assumes that there is only one depot denoted by 0, and there are n nodes with fuzzy demands served by m vehicles. The locations of the depot and nodes are known. The fuzzy demand of each node i is uncertain and only characterized by a triangular fuzzy number D_i, $D_i = (d_{i1}, d_{i2}, d_{i3})$. d_{i1} is the minimum of the demand of node i, d_{i3} is the maximum of the demand of node i, and d_{i2} is the most likely value. The distance c_{ij} between nodes i and node j is known. Each node is served exactly once by one vehicle. For simplicity, the capacity Q of each vehicle is the same, and the activity of the vehicle is only bounded by capacity constraints. Each vehicle starts at the depot and returns to the same depot after completing its task. The objective is to design a set of vehicle routes that minimizes the total logistics costs.

2.2. Deciding whether the Vehicle Serves the Next Node or Returns to the Depot. When the demand of each node is deterministic, it is easy for us to decide whether the vehicle is able to serve the next node after serving v nodes. However, while the demand at each node is uncertain and only characterized by a triangular fuzzy number $D_i = (d_{i1}, d_{i2}, d_{i3})$, it is difficult for us to decide whether the vehicle should serve the next node $v+1$ or return to the depot. We only know that the greater the vehicle's remaining capacity and the lesser the demand at the next node, the greater the vehicle's "chances" of being able to serve the next node. In this paper, we solve this problem by triangular fuzzy number theory proposed by Liu [23], which described as follows.

The membership function of triangular fuzzy number $D = (d_1, d_2, d_3)$ is defined as

$$\mu_D(x) = \begin{cases} 0, & x \le d_1 \text{ or } x \ge d_3 \\ \dfrac{(x - d_1)}{(d_2 - d_1)}, & d_1 \le x < d_2 \\ \dfrac{(d_3 - x)}{(d_3 - d_2)}, & d_2 \le x < d_3. \end{cases} \tag{1}$$

Let $\text{pos}\{\varepsilon\}$ be the occurrence possibility of event ε. For triangular fuzzy number $A = (a_1, a_2, a_3)$ and $B = \{b_1, b_2, b_3\}$, $\text{pos}\{A \le B\}$ is defined as

$$\begin{aligned} \text{pos}\{A \le B\} &= \sup\{\min\{\mu_A(x), \mu_B(y)\} \mid x \le y\} \\ &= \begin{cases} 1, & a_2 \le b_2 \\ \dfrac{(b_3 - a_1)}{(b_3 - b_2) + (a_2 - a_1)}, & a_2 > b_2,\ a_1 < b_3 \\ 0, & a_1 \ge b_3. \end{cases} \end{aligned} \tag{2}$$

Now, we can deduce that the occupied capacity Q_{vo} of the vehicle which had served v nodes is

$$Q_{vo} = \sum_{i=1}^{v} D_i = \left(\sum_{i=1}^{v} d_{i1}, \sum_{i=1}^{v} d_{i2}, \sum_{i=1}^{v} d_{i3} \right). \tag{3}$$

Also, the capacity Q of each vehicle can be presented as a triangular fuzzy number $Q = (Q, Q, Q)$. So, the remaining capacity Q_{vr} of the vehicle is

$$Q_{vr} = Q - Q_{vo} = \left(Q - \sum_{i=1}^{v} d_{i3}, Q - \sum_{i=1}^{v} d_{i2}, Q - \sum_{i=1}^{v} d_{i1}\right) = \left(Q_{vr1}, Q_{vr2}, Q_{vr3}\right). \quad (4)$$

Thus, the possibility $\text{pos}(D_{v+1} \le Q_{vr})$, which means that the demand of node $v+1$ is less than the remaining capacity, is

$$\text{pos}\left(D_{v+1} \le Q_{vr}\right) = \begin{cases} 1, & d_{v+1,2} \le Q_{vr2} \\ \dfrac{\left(Q_{vr3} - d_{v+1,1}\right)}{\left(Q_{vr3} - Q_{vr2}\right) + \left(d_{v+1,2} - d_{v+1,1}\right)}, & d_{v+1,2} > Q_{vr2},\ d_{v+1,1} < Q_{vr3} \\ 0, & d_{v+1,1} \ge Q_{vr3}. \end{cases} \quad (5)$$

Let $P^* \in [0, 1]$ be the decision maker's preference. A large value of P^* indicates that the decision maker is risk averse, and the decision maker aims to ensure service. In this case, $P^* \ge 0.6$. The possibility of "service success" is relatively high. In contrast, a small value of P^* means that the decision maker has an insatiable appetite for risk and tries to serve more nodes with each vehicle. In that case, $P^* \le 0.5$. The possibility of "service success" is relatively low.

Now, after serving v nodes, we can make a decision whether the vehicle should serve the next node $v+1$ or return to the depot 0. The decision was made as follows.

If $\text{pos}(D_{v+1} \le Q_{vr}) \ge P^*$, the vehicle should serve the next node $v+1$; else, the vehicle should return to the depot 0.

2.3. VRPFD Model. The notations used in the formulation of the VRPFD are described as follows.

i: node index ($i = 0$ stands for the depot).

n: number of nodes.

N: set of nodes.

S: nonempty proper subset of the set N.

D_i: fuzzy demand of each node i, $D_i = (d_{i1}, d_{i2}, d_{i3})$.

c_{ij}: distance between node i and node j.

k: vehicle index.

m: number of vehicles.

K: set of vehicles.

Q: capacity of the vehicle.

P^*: decision maker's preference, $P^* \in [0, 1]$.

The decision variables used in the formulation of the VRPFD are described as follows:

y_{ik}: {if node i is served by vehicle k, $y_{ik} = 1$; otherwise, $y_{ik} = 0$}.

x_{ijk}: {if vehicle k moves from node i to node j, $x_{ijk} = 1$; otherwise, $x_{ijk} = 0$}.

Thus, the fuzzy reasoning constrained program model of the VRPFD is mathematically formulated as follows:

$$\min \quad \sum_{k=1}^{m} \sum_{i=0}^{n} \sum_{j=0}^{n} c_{ij} x_{ijk} \quad (6)$$

$$\text{Subject to} \quad \text{pos}\left(\sum_{i \in N} D_i y_{ik} \le Q\right) \ge P^*, \quad \forall k \in K \quad (7)$$

$$\sum_{k \in K} y_{ik} = 1, \quad \forall i \in N \quad (8)$$

$$\sum_{i \in N} x_{ijk} = y_{jk}, \quad \forall j \in N,\ k \in K \quad (9)$$

$$\sum_{j \in N} x_{ijk} = y_{ik}, \quad \forall i \in N,\ k \in K \quad (10)$$

$$\sum_{j \in N} x_{ijk} = \sum_{j \in N} x_{jik} = y_{ik}, \quad \forall i \in N,\ k \in K \quad (11)$$

$$\sum_{k \in K} y_{0k} = m \quad (12)$$

$$\sum_{j \in N} x_{0jk} = \sum_{i \in N} x_{i0k} = 1, \quad \forall k \in K \quad (13)$$

$$\sum_{k \in K} \sum_{i \in S} \sum_{j \in S, j \ne i} x_{ijk} \le |S| - 1, \quad \forall S \subset N. \quad (14)$$

The object of the proposed VRPFD is to minimize the total distance. Constraint (7) ensures that all nodes are served within the vehicle's capacity at the values of the decision maker's preference. Constraint (8) ensures that each node is visited by one vehicle. Constraints (9) and (10) define the relationships between x_{ijk} and y_{ik}, respectively. Constraint (11) guarantees that a vehicle must enter and leave each node exactly once. Constraint (12) ensures that at most m vehicles are used. Constraint (13) ensures that vehicle routes start from the depot 0 and terminate at the same depot. Constraint (14) represents the subtour elimination constraint where $|S|$ stands for the cardinality of set S.

3. Hybrid Ant Colony Algorithm for VRPFD

The ant colony algorithm (ACA) is one of the most popular swarm-inspired methods in the field of computational intelligence. The first ACA was developed by Clolrni et al. [24]. It was successfully applied to the traveling salesman problem. The first ant system for the VRP was proposed by Bulleneimer et al. [25]. Doerner et al. [26] further improved this ant colony system using a savings-based heuristic. Recently, ACA has been applied to the VRP with different constraints, for example, Ellabib et al. [27], Gajpal and Abad [28], Yu et al. [29], and Fleming et al. [30]. By looking at success of above hybridised ant colony algorithms on VRP, we decided to develop hybrid ant colony algorithm (HACA) for VRPFD too.

Let Ω be the set of all candidate nodes in the dataset, let $U(h)$ be the set of nodes yet to be served by ant h, and let $\mathfrak{F}(h)$ be the set of nodes already served by ant h.

3.1. Transfer Probabilities. The probability p_{ij}^h that ant h chooses to serve node j having served node i is given by

$$p_{ij}^h = \begin{cases} \dfrac{\left[\tau_{ij}\right]^\alpha \times \left[\eta_{ij}\right]^\beta}{\sum_{r\in U(h)} \left[\tau_{ir}\right]^\alpha \times \left[\eta_{ir}\right]^\beta}, & j \in U(h) \\ 0, & \text{otherwise,} \end{cases} \tag{15}$$

where τ_{ij} is the pheromone density of edge (i, j); η_{ij} is the visibility of edge (i, j); α is the relative influence of the pheromone trails; and β is the relative influence of the visibility.

3.2. Pheromone Updating

3.2.1. Local Pheromone Updating Rule

Definition 1 (ant attraction). The ant attraction ∂/χ of edge (i, j) is the ratio of number ∂ of ants that have travelled edge (i, j) to the number χ of ants that have visited node i.

Each ant leaves constant quantity θ of pheromone on the edge it travels, and larger ant attraction χ/θ of edge (i, j) results in greater amount of ant travel on edge (i, j). Thus, more frequent local pheromone updating will result in a larger pheromone quantity τ_{ij} between all edges. The global searching of the ACO algorithm represents a handicap. To address this problem a local pheromone updating rule has been designed.

Let χ_h be the number of ants that visited node i before arrival of ant h at node i, and let ∂_h be the number of ants that travelled edge (i, j) before ant h travelled edge (i, j). The local pheromone update quantity of edge (i, j) caused by ant h can be calculated as

$$\Delta\tau_{ij}^h(t) = \begin{cases} \theta \times \left(1 - \dfrac{\partial_h}{\chi_h}\right), & \text{if ant } h \text{ traveled from node } i \text{ to } j \\ 0, & \text{otherwise.} \end{cases} \tag{16}$$

Let $\tau_{ij}^h(t)$ be the local pheromone quantity of edge (i, j) before updating; let $\tau_{ij}^h(t+1)$ be the local pheromone quantity of edge (i, j) after updating; and let ρ be the pheromone volatilization coefficient. Then, the local pheromone updating rule can be defined as

$$\tau_{ij}^h(t+1) = \rho \times \tau_{ij}^h(t) + \Delta\tau_{ij}(t), \quad \forall i,\ \forall j, i \neq j, \tag{17}$$

$$\Delta\tau_{ij}(t) = \sum_{h=1}^{m} \Delta\tau_{ij}^h(t). \tag{18}$$

3.2.2. Global Pheromone Updating Rule. If ant h has already served all n nodes, the global pheromone updating rule is employed. It is defined as

$$\tau_{ij}(t+n) = (1-\rho) \cdot \tau_{ij}(t) + \Delta\tau_{ij}(t), \tag{19}$$

$$\Delta\tau_{ij}(t) = \sum_{k=1}^{m} \Delta\tau_{ij}^h(t). \tag{20}$$

3.3. The Steps of HACA. The steps of the proposed HACA are depicted below.

Step 1 (algorithm initialization). (1) Set the values of the current iteration number nc, the maximum iteration number $\max ir$, the capacity value Q, the ant number m, and the decision maker's preference P^*. (2) Set all ants at the central depot 0, and let each ant start from the depot. (3) Let $Q_{vo} = 0$ be the initial occupied load of ant h, and the remaining capacity $Q_{vr} = Q - Q_{vo}$.

Step 2 (route construction). (1) Calculate the transfer probability p_{ij}^h. (2) Select node j according to the sequence of p_{ij}^h arranged in decreasing order. (3) If $\text{pos}(D_j \leq Q_{vr}) \geq P^*$, $j \in U(h)$, ant h must move to node j from the current node i, and the current node of ant h is changed to be j, $j \notin U(h)$, $j \in \mathfrak{F}(h)$, and the occupied load $Q_{vo} = Q_{vo} + d_j$; otherwise, ant h should return to the depot, $Q_{vo} = 0$, and move to the next node j. (4) Repeat this selection until $U(h) = \phi$.

Step 3 (pheromone updating). If $U(h) = \phi$, that is, ant h has already served all n nodes, the global pheromone updating rule is employed; otherwise, the local pheromone updating rule is employed.

Step 4 (judgment). If the total number of searching ants is smaller than m, return to step 2; otherwise, find the best solution by the path set $L = \{L_1, L_2, \ldots, L_m\}$ obtained with $\mathfrak{F}(h)$.

Step 5 (the 2-opt local search). (1) The obtained route is broken at random into three segments. (2) The middle segment must not contain the depot. (3) The route is then reconstructed by reversing the middle segment. (4) The route is updated whenever there is an improvement. (5) The process is repeated until there is no further improvement in the solution [28]. (6) If the new solution is better than the current solution, the new solution will replace the current solution.

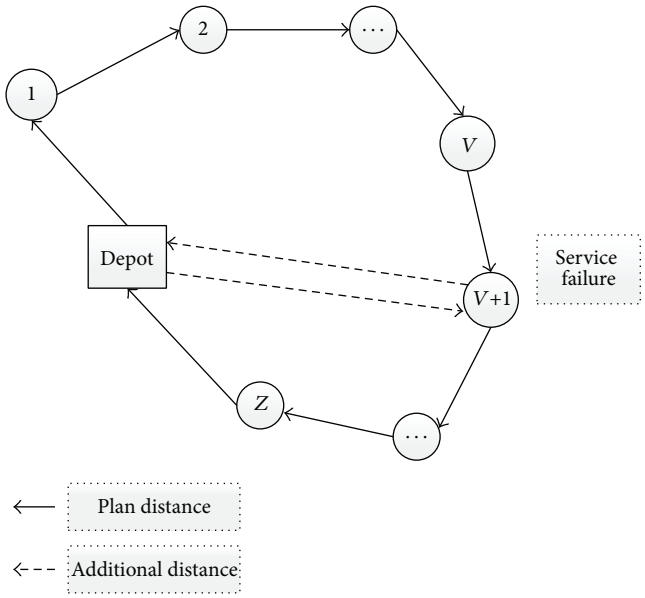

Figure 1: Service failure.

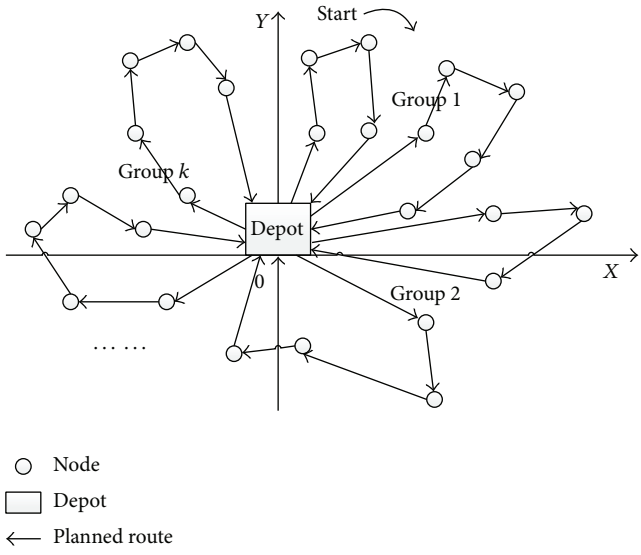

Figure 2: Vehicle grouping.

Step 6 (termination rule of the algorithm). If $nc < \max ir$, $nc = nc + 1$, return to step 2, and repeat the above steps; otherwise, terminate the HACA.

4. Two-Vehicle-Paired Loop Coordinated Strategy

As mentioned above, the VRPFD typically assumes that the "actual" value of a node's demand is known when the vehicle reaches the node, and the vehicle route is planned in advance. After serving v nodes, a vehicle might not be able to service the $v + 1$ node once it arrives due to its insufficient capacity. In such situations, if the vehicle uncoordinated strategy is employed, the vehicle must return to the depot, unload what it has picked up thus far, return to the node where it had a "service failure," and continue to service the remaining nodes (e.g., in raw milk collection systems). Thus, "additional distance" and "additional unloading times" are introduced due to the "service failure" (Figure 1). In contrast, there are also vehicles with surplus capacity after completing their own tasks; thus, "waste capacity" is created. All of these cases increase the logistics costs. To the authors' knowledge, few studies have considered the problem of how to effectively minimize the "additional distance" and "waste capacity," let alone reduce "additional unloading times," in the VRPFD.

After the optimal routes are obtained by the HACA (it is assumed that each route only served exactly by one vehicle), the two-vehicle-paired loop coordinated strategy (TVPLCS) is presented to minimize the "additional distance," "additional unloading times," and "waste capacity" in the VRPFD. The essence of the TVPLCS is that the vehicle with "surplus capacity" must help the vehicle with "insufficient capacity" according to the specified coordination rules after finish its own assigned task. The coordination rules of the TVPLCS are described as follows.

Coordination Rule 1. Assume that there are m planned vehicle routes and one depot 0 in two-dimensional coordinates. Put the depot on the origin of the two-dimensional coordinates. Starting from y-axis, divide the 2 adjacent routes into a coordinated group according to clockwise rotation (Figure 2). If the number of the routes is odd, there is one remaining route which is not assigned, and the vehicle will complete its own assigned task.

Coordination Rule 2. Each vehicle of the same coordinated group should finish its own assigned task first, and each vehicle first serves its "outer" nodes and then its "inner" nodes (Figure 3(a)). In this manner, if a vehicle has a "service failure," the "failure nodes" are near the other vehicle in the same coordinated group, thus promoting coordination between the two vehicles (Figure 3(b)).

Coordination Rule 2. If a vehicle completes its own task and has no surplus capacity, it should return to the depot and inform the other vehicle of its "task status."

Coordination Rule 4. If a vehicle completes its own task, has surplus capacity, and does not receive information from the other vehicle, the vehicle should wait and inform the other vehicle of its "task status" (Figure 4(a)). If the vehicle receives information from the other vehicle that the other vehicle is completing its own task, the first vehicle should return the depot (Figure 4(b)). If the vehicle receives information from the other vehicle that the other vehicle cannot complete its own task, the first vehicle should go to the node where the other vehicle had a "service failure" and continue to serve the remaining nodes. If the vehicle completes the remaining tasks, it should return the depot and inform the depot (Figure 4(c)); otherwise, the vehicle should return to the depot and inform the depot of its "remaining task status" (Figure 4(d)).

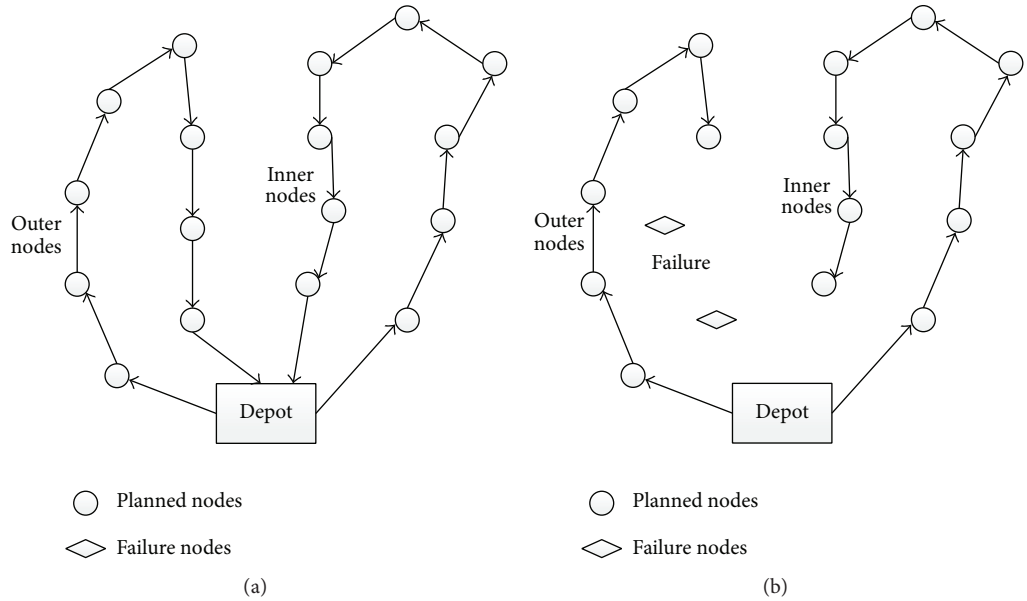

Figure 3: Coordination rule 2.

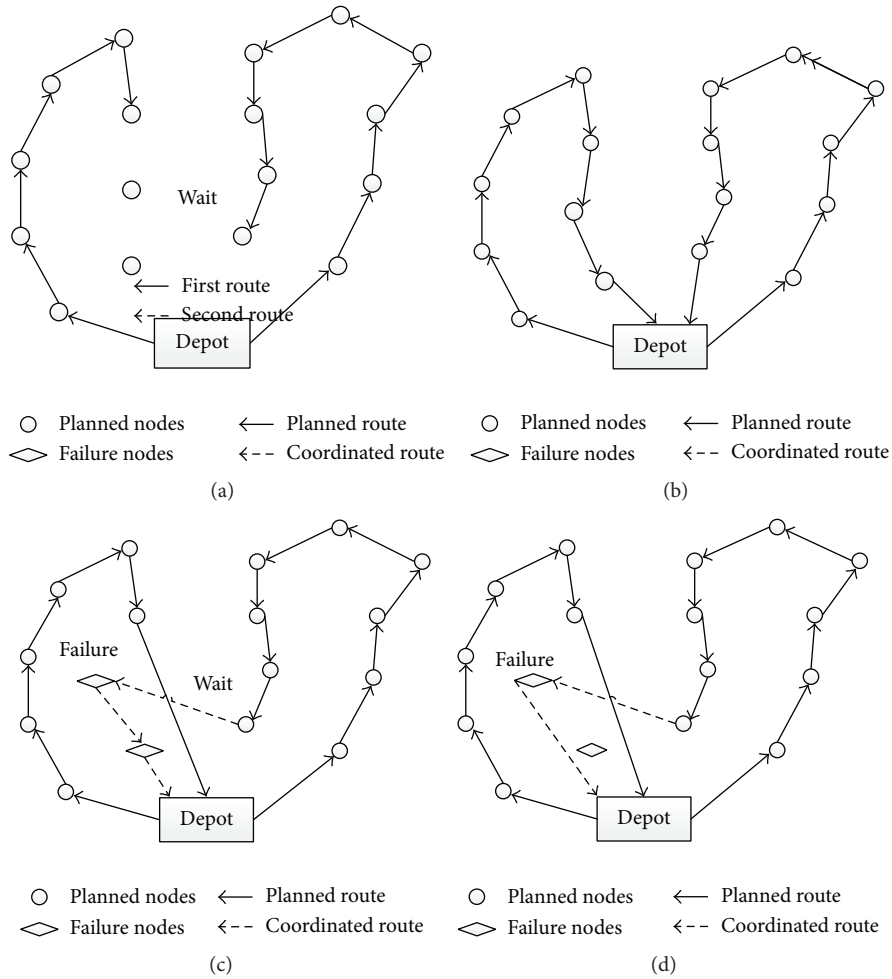

Figure 4: Coordination rule 4.

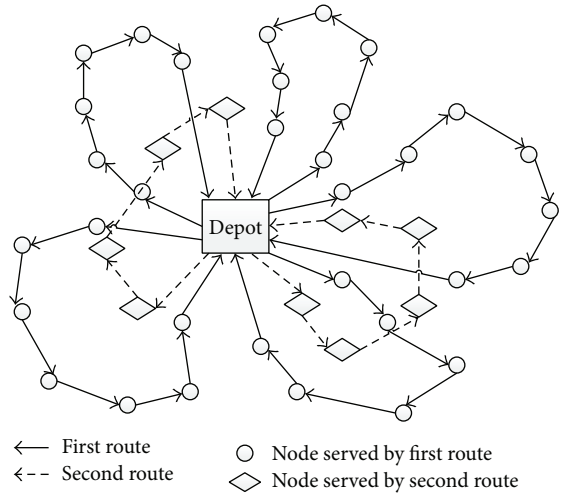

Figure 5: Coordination rule 5.

Coordination Rule 5. If all vehicles of all coordinated groups have returned to the depot and there are "remaining nodes" because of "service failure," the "remaining nodes" will be served by the vehicles of the second scheduling optimization, and the vehicle coordinated strategy will also be employed in the second service (Figure 5).

There are also some deficiencies in the TVPLCS, such as the "waiting" and "informing" between the two vehicles. "Waiting" means that if the vehicle completes its task and has surplus capacity, it must wait for the other vehicle's information. It may wait a long time due to different traffic circumstances, thus increasing the time cost. "Informing" means that when the vehicle completes its task, it must inform the other vehicle of its "task status." The "informing" problem can be easily solved using the advanced communication technology now available.

5. Experimental Results

The program for HACA was developed in Matlab 7.0. All computer experiments were performed on a PC (CPU 1.86 GHz, Memory 2 GB). The parameters for the HACA are set as follows: the ant number $m = 30$; the vehicle capacity value $Q = 150$ items; the maximum iteration number $\max ir = 200$; the pheromone volatilization coefficient $\rho = 0.9$; the relative influence of the pheromone trails $\alpha = 1$; the relative influence of the visibility $\beta = 2$; and the pheromone quantity $\theta = 15$.

Because the standard test instances for VRPFD are unavailable, the two-dimensional coordinates of the nodes and depot are generated randomly in $[100 \times 100]$ in this paper. The fuzzy demands of the nodes were also determined arbitrarily.

5.1. The Running Time of the HACA. In this experiment, the number of the test nodes is within the interval of 100–500 with a step of 100. Each instance runs 20 times. The average running time of each instance is used to be the solution. This is not real time problem and hence CPU times of HACA are acceptable. The results of running times are shown in Table 1.

Table 1: Running times of HACA.

Number of test nodes	100	200	300	400	500
Running time (seconds)	289.37	484.62	698.16	875.84	983.67

Table 2: Running times of HACA and HPSOGA.

Dataset	A-n33-k5	E-n51-k5	M-n101-k10	M-n151-k12
Running time of HACA (seconds)	20.16	81.24	296.71	437.62
Running time of HPSOGA (seconds)	20.64	88.09	388.32	635.59

To facilitate the comparison, HACA is also simulated in several benchmark datasets. The source of the datasets is http://www.coin-or.org/SYMPHONY/branchandcut/VRP/data/#V. These datasets are modified to the VRPFD datasets by generating fuzzy demand. The fuzzy demand $D_i = (d_{i1}, d_{i2}, d_{i3})$ is randomly generated for each dataset, where the original dataset is used as d_{i2} for each node. In this simulation, solution obtained by HACA is compared with HPSOGA designed by Kuo et al. [13]. Each instance runs 20 times. The average running time of each instance is shown in Table 2. The results in Table 2 prove that HACA has promising performance in solving VRPFD. HACA outperforms HPSOGA for all dataset.

5.2. The Efficiency of the TVPLCS. To determine efficiency of the TVPLCS we have developed an approach to estimate the "waste capacity," "additional distance," and "additional unloading times." The steps of the proposed calculation approach are described as follows.

Step 1. The method for processing fuzzy number into deterministic number proposed by the CA [31] is employed to estimate the "actual" demands d_i^a of each node.

Step 2. For each route planned by the HACA, the vehicle moves along the route, accumulating the sum Q^a of the "actual" demands of all nodes; that is, $Q^a = \sum_{i \in \text{route}} d_i^a$.

Step 3. If $Q^a \leq Q$, the vehicle can finish the task of this route, then the "waste capacity" is $Q - Q^a$; if $Q^a > Q$, the vehicle cannot finish the task of this route. The vehicle must return to the depot, unload what it has picked up thus far, return to the node where it had a "service failure," and continue to serve the remaining nodes. Now, we can calculate the "additional distance" and "additional unloading times" due to the "service failure." The "additional distance" is equal to length of second tour of the vehicle caused because of service failure in the first tour. The "additional unloading times" are the "service

Table 3: Travel distance results within 100 nodes.

P^*	TVPLCSHACA			HPSOGA		
	TPD	TAD	TD	TPD	TAD	TD
0.1	2,285.66	1,817.80	4,103.46	2,376.18	2,013.74	4,380.92
0.2	2,367.16	1,682.57	4,049.73	2,426.91	1,802.32	4,229.23
0.3	2,497.35	1,176.48	3,673.83	2,573.84	1,472.69	4,046.53
0.4	2,734.83	714.54	3,449.37	2,821.73	1058.36	3,880.09
0.5	2,610.92	673.27	3,284.19	2,783.41	952.71	3,736.12
0.6	3,016.73	283.24	3,298.97	3,133.28	509.16	3,642.44
0.7	3,236.51	0	3,236.51	3,292.41	407.65	3,700.06
0.8	3,347.26	0	3,347.26	3,384.74	368.52	3,753.26
0.9	3,469.80	0	3,449.80	3,794.37	0	3,794.37
1	3,577.56	0	3,577.56	3,836.91	0	3,836.91

failure" times. The "total distance" is the sum of the "total planned distance" and "total additional distance."

5.2.1. Test of the Travel Distance. For simplicity and perceptual intuition, we only test 100 nodes. To show the efficiency of the proposed approaches, we compare our TVPLCS based on the HACA (TVPLCSHACA) with the hybrid particle swarm optimization with genetic algorithm (HPSOGA) proposed by Kuo et al. [13]. HPSOGA employs vehicle uncoordinated strategy, and it is designed for VRPFD. This is to say, coordinating strategies/rules defined in Section 4 all were used in the experiment. At first, the coordination rule 1 is used. Then the coordination rule 2 is used. Also, the coordination rule 3 and coordination rule 4 are used; if the task is not finished, the coordination rule 5 must be used; else, the coordination rule 5 may not be used.

All test are calculated according to the decision maker's confidence P^*, where P^* varies within the interval of 0-1 with a step of 0.1. The average computational results of 10 times are calculated.

The "total planned distance" (TPD), "total additional distance" (TAD), and "total distance" (TD) are calculated. The results of TVPLCSHACA and HPSOGA are listed in Table 3.

From the results in Table 3, we can see the following: (1) with regard to TPD the result gained from the HACA is smaller than the result obtained by the HPSOGA. When $P^* = 0.9$, the former is 9.35% less than the latter. Even more, the former is 10.33% less than the latter while $P^* = 1$. (2) As mentioned above, TAD is due to the "service failures." The TAD result gained from the TVPLCSHACA is also smaller than the result obtained by the HPSOGA. Especially, when $0.4 \leq P^* \leq 0.6$, the former is close to almost half of the latter. This is to say, the TVPLCSHACA is useful for VRPFD, and TVPLCS can effectively reduce the TAD. When $P^* \geq 0.7$, TAD gained from the HACA is 0, which means that there is no "service failure" in each route. However, TAD gained from the HPSOGA is 0 while $P^* \geq 0.9$. That is, our approach is better than HPSOGA. (3) The TD of TVPLCSHACA is also smaller than the result obtained by the HPSOGA. The results can show the effectiveness of our proposed approaches.

Table 4: Results of the total vehicle number, waste capacity, and additional unloading times.

P^*	TVPLCSHACA				HDEA			
	PVN	TVN	TWC	TAUT	PVN	TVN	TWC	TAUT
0.1	13	22	0	9	13	26	166	13
0.2	13	21	0	8	14	25	182	12
0.3	14	21	0	7	14	25	186	11
0.4	15	21	0	6	15	25	198	9
0.5	16	20	51	4	16	25	223	8
0.6	17	20	87	3	17	24	257	7
0.7	18	18	125	0	18	23	261	5
0.8	18	18	114	0	19	23	273	4
0.9	19	19	89	0	20	20	127	0
1	19	19	81	0	20	20	118	0

5.2.2. Test of the Total Vehicle Number, Waste Capacity, and Additional Unloading Times. Also, we test the same 100 nodes which tested above. To show the efficiency of the proposed TVPLCS, we compare our TVPLCSHACA with the HDEA proposed by Erbao and Mingyong [12]. The algorithm employs vehicle uncoordinated strategy, and it is designed for VRPFD. All test are calculated according to the decision maker's confidence P^*, where P^* varies within the interval of 0-1 with a step of 0.1. The average computational results of 10 times are calculated. The "plan vehicle number" (PVN), "total vehicle number" (TVN), "total waste capacity" (TWC), and "total additional unloading times" (TAUT) are tested. The results of our TVPLCSHACA and the results of HDEA (HDEA employs vehicle uncoordinated strategy) are listed in Table 4. In Table 4, capacity unit is item.

The results in Table 4 indicate the following: (1) For PVN, the value gained by HACA is close to the result planed by HDEA, and the former is better than the latter. (2) With regard to TAUT, the value gained by TVPLCSHACA is much better than the result calculated by HDEA. When $P^* \leq 0.3$, the number of the former is 30% less than that of the latter. When $0.4 \leq P^* \leq 0.6$, the number of the former is 50% less than that of the latter. When $P^* \geq 0.7$, TAUT gained by TVPLCSHACA is 0. However, TAUT gained by HDEA is 0 till $P^* \geq 0.9$. So, TVPLCS can effectively cut down "additional unloading times" in VRPFD, especially when the value of decision maker's preference is relatively smaller. (3) About TWC, when $P^* \leq 0.4$, all numerical values gained by TVPLCSHACA are 0, but the results of HDEA are close to 200. In other words, when a vehicle has surplus capacity, the vehicle should serve the "failure nodes" of the other failure route according to the specified TVPLCS rules. TVPLCS could be usefully employed in reduction of the "waste capacity" in VRPFD, especially when the value of decision maker's preference is relatively smaller. (4) As for TVN, the value gained by TVPLCSHACA based on the HACA is less than the result planed by HDEA. When $P^* \leq 0.8$, the former is nearly 25% less than the latter. Thus, the TVPLCS is very useful for the VRPFD, especially when P^* is given a relatively smaller value. That is, the decision maker

Table 5: Results of total distance, vehicle number, and logistics cost.

P^*	TVPLCSHACA			HDEA		
	TD	TVN	TLC	TD	TVN	TLC
0.1	4,103.46	22	31,517.3	4,380.92	26	34,904.6
0.2	4,049.73	21	30,748.65	4,229.23	25	33,646.15
0.3	3,673.83	21	28,869.15	4,046.53	25	32,732.65
0.4	3,449.37	21	27,746.85	3,880.09	25	31,900.45
0.5	3,284.19	20	26,420.95	3,736.12	25	31,180.6
0.6	3,298.97	20	26,494.85	3,642.44	24	30,212.2
0.7	3,236.51	18	25,182.55	3,700.06	23	30,000.3
0.8	3,347.26	18	25,736.3	3,753.26	23	30,266.3
0.9	3,449.80	19	26,749	3,794.37	20	28,971.85
1	3,577.56	19	27,387.8	3,836.91	20	29,184.55

has an insatiable appetite for risk and wants to serve more nodes with each vehicle.

5.3. Determining the Reasonable Value of the Decision Maker's Preference. Now, we determine the reasonable value of the decision maker's preference based on the results listed in Tables 3 and 4. The TD in Table 3 and the TVN in Table 4 are selected to calculate the total logistics cost (TLC) for VRPFD. In this paper, it is assumed that the freight of TD is 5 yuan RMB per unit distance, and the fixed charge of TVN is 500 yuan RMB per vehicle. TLC is the sum of TD and TVN. The results of TLC are listed in Table 5.

From the results in Table 5 we can see the following: (1) When decision maker's preference $P^* \geq 0.6$, the decision maker is risk averse and aims to minimize service failures. The optimal value of P^* should be 0.6 or 0.7 according to TD. The best value of P^* should be 0.7 according to TLC and TVN. However, it is not easy for us to obtain a highly credible decision maker's preference due to the variability of customer demands in practice, especially when the operations of a distributing system are only starting up. (2) While $P^* \leq 0.5$, the decision maker is risk preference and wants to serve more nodes with each vehicle. All values of TD, TVN, and TLC tell us that the best value of P^* is 0.5. (3) The reasonable value of the decision maker's preference deduced from TVPLCSHACA is exactly the same as that inferred from HDEA.

6. Conclusions

This paper contributes to the research on the VRPFD in the following respects: (1) The fuzzy reasoning constrained program model and HACA are designed to optimize the vehicle routes, and the most appropriate values for the decision maker's confidence level P^* were obtained by simulation. That is, if decision maker is risk averse and aims to ensure service, the best value of P^* should be 0.7. If the decision maker has an insatiable appetite for risk and wants to serve more nodes with each vehicle, the best value of P^* should be 0.5. (2) In particular, the TVPLCS is presented to reduce the "additional distance," "unloading times," and the "waste capacity" caused by "service failure." Numerical examples are presented to demonstrate the effectiveness of our proposed approaches. Particularly, the TVPLCS is very useful for the VRPFD when the decision maker has an insatiable appetite for risk, especially when the operations of a distributing system are only starting up and the customers' demands are difficult to estimate.

For the future research, we may consider other nondeterministic side constraints in VRPFD, such as stochastic vehicle travel time, important customer with emergent service, and time window constraint that should be considered in order to fit the practical applications.

Competing Interests

The authors declare that they have no competing interests.

Acknowledgments

This research has been partially supported by grants from the National Natural Science Foundation of China (no. 71373216, no. 71471149 and no. 71222108), Major Project of the National Social Science Foundation of China (no. 15ZDB153), grants from the National Philosophy and Social Science Foundation of China (no. 15AJL006), Excellent Youth Project of Hunan Provincial Education Department of China (no. 15B131), and Key R & D program of Hunan Provincial Science and Technology Department of China (no. 2015ZK3049).

References

[1] G. B. Dantzig and J. H. Ramser, "The truck dispatching problem," *Management Science*, vol. 6, no. 1, pp. 80–91, 1959.

[2] G. Clarke and J. W. Wright, "Scheduling of vehicles from a central depot to a number of delivery points," *Operations Research*, vol. 12, no. 4, pp. 568–581, 1964.

[3] M. M. Solomon, "Algorithms for the vehicle routing and scheduling problems with time window constraints," *Operations Research*, vol. 35, no. 2, pp. 254–265, 1987.

[4] G. Laporte, "The vehicle routing problem: an overview of exact and approximate algorithms," *European Journal of Operational Research*, vol. 59, no. 3, pp. 345–358, 1992.

[5] M. A. Figliozzi, "Planning approximations to the average length of vehicle routing problems with time window constraints," *Transportation Research Part B: Methodological*, vol. 43, no. 4, pp. 438–447, 2009.

[6] R. Sprenger and L. Mönch, "A methodology to solve large-scale cooperative transportation planning problems," *European Journal of Operational Research*, vol. 223, no. 3, pp. 626–636, 2012.

[7] V. Pillac, M. Gendreau, C. Guéret, and A. L. Medaglia, "A review of dynamic vehicle routing problems," *European Journal of Operational Research*, vol. 225, no. 1, pp. 1–11, 2013.

[8] G. Kou, D. Ergu, and J. Shang, "Enhancing data consistency in decision matrix: adapting Hadamard model to mitigate judgment contradiction," *European Journal of Operational Research*, vol. 236, no. 1, pp. 261–271, 2014.

[9] G. Kou, Y. Lu, Y. Peng, and Y. Shi, "Evaluation of classification algorithms using MCDM and rank correlation," *International*

Journal of Information Technology & Decision Making, vol. 11, no. 1, pp. 197–225, 2012.

[10] E. Cao and M. Lai, "The open vehicle routing problem with fuzzy demands," *Expert Systems with Applications*, vol. 37, no. 3, pp. 2405–2411, 2010.

[11] D. J. Bertsimas, "A vehicle routing problem with stochastic demand," *Operations Research*, vol. 40, no. 3, pp. 574–585, 1992.

[12] C. Erbao and L. Mingyong, "A hybrid differential evolution algorithm to vehicle routing problem with fuzzy demands," *Journal of Computational and Applied Mathematics*, vol. 231, no. 1, pp. 302–310, 2009.

[13] R. J. Kuo, F. E. Zulvia, and K. Suryadi, "Hybrid particle swarm optimization with genetic algorithm for solving capacitated vehicle routing problem with fuzzy demand—a case study on garbage collection system," *Applied Mathematics and Computation*, vol. 219, no. 5, pp. 2574–2588, 2012.

[14] G. Kou and C. Lin, "A cosine maximization method for the priority vector derivation in AHP," *European Journal of Operational Research*, vol. 235, no. 1, pp. 225–232, 2014.

[15] G. Kou, Y. Peng, and G. Wang, "Evaluation of clustering algorithms for financial risk analysis using MCDM methods," *Information Sciences*, vol. 275, pp. 1–12, 2014.

[16] M. Allahviranloo, J. Y. J. Chow, and W. W. Recker, "Selective vehicle routing problems under uncertainty without recourse," *Transportation Research Part E: Logistics and Transportation Review*, vol. 62, pp. 68–88, 2014.

[17] Z.-H. Hu, J.-B. Sheu, L. Zhao, and C.-C. Lu, "A dynamic closed-loop vehicle routing problem with uncertainty and incompatible goods," *Transportation Research Part C: Emerging Technologies*, vol. 55, pp. 273–297, 2015.

[18] X. Liu, G. G. He, and W. W. Gao, "Modeling and algorithm for the multiple vehicles coordinated stochastic vehicle routing with time-constrain," *System Engineering*, vol. 23, pp. 105–109, 2005 (Chinese).

[19] C. K. Y. Lin, "A cooperative strategy for a vehicle routing problem with pickup and delivery time windows," *Computers and Industrial Engineering*, vol. 55, no. 4, pp. 766–782, 2008.

[20] J. S. Shang and C. K. Cuff, "Multicriteria pickup and delivery problem with transfer opportunity," *Computers & Industrial Engineering*, vol. 30, no. 4, pp. 631–645, 1996.

[21] J. Yang, P. Jaillet, and H. Mahmassani, "Real-time multivehicle truckload pickup and delivery problems," *Transportation Science*, vol. 38, no. 2, pp. 135–148, 2004.

[22] X. P. Hu, L. J. Sun, and L. L. Liu, "A PAM approach to handling disruptions in real-time vehicle routing problems," *Decision Support Systems*, vol. 54, no. 3, pp. 1380–1393, 2013.

[23] B. Liu, "Uncertain theory: an introduce to its axiomatic foundations," in *Fuzzy Variables, Fuzzy Sets and Systems*, S. Nahmias, Ed., vol. 1, pp. 97–110, Springer, Berlin, Germany, 2004.

[24] A. Clolrni, M. Dorigo, and V. Maniezzo, "Distributed optimization by ant colonies," in *Proceedings of the European Conference on Artificial Life (ECAL '91)*, pp. 134–142, Paris, France, 1991.

[25] B. Bulleneimer, R. F. Hartl, and C. Strauss, "Strauss, applying the ant system to the vehicle routing problem," in *Proceedings of the 2nd International Conference on Metaheuristics*, pp. 1–12, 1997.

[26] K. Doerner, M. Gronalt, R. F. Hartl, M. Reimann, C. Strauss, and M. Stummer, "Savings ants for the vehicle routing problem," in *Application of Evolutionary Computing*, pp. 11–20, Springer, Berlin, Germany, 2002.

[27] I. Ellabib, P. Calamai, and O. Basir, "Exchange strategies for multiple Ant Colony System," *Information Sciences*, vol. 177, no. 5, pp. 1248–1264, 2007.

[28] Y. Gajpal and P. L. Abad, "Multi-ant colony system (MACS) for a vehicle routing problem with backhauls," *European Journal of Operational Research*, vol. 196, no. 1, pp. 102–117, 2009.

[29] B. Yu, Z. Z. Yang, and B. Z. Yao, "A hybrid algorithm for vehicle routing problem with time windows," *Expert Systems with Applications*, vol. 38, no. 1, pp. 435–441, 2011.

[30] C. L. Fleming, S. E. Griffis, and J. E. Bell, "The effects of triangle inequality on the vehicle routing problem," *European Journal of Operational Research*, vol. 224, no. 1, pp. 1–7, 2013.

[31] C.-C. Chou, "The canonical representation of multiplication operation on triangular fuzzy numbers," *Computers & Mathematics with Applications*, vol. 45, no. 10-11, pp. 1601–1610, 2003.

Hindawi Publishing Corporation
Mathematical Problems in Engineering
Volume 2016, Article ID 9175418, 15 pages
http://dx.doi.org/10.1155/2016/9175418

Research Article

A Grey Theory Based Approach to Big Data Risk Management Using FMEA

Maisa Mendonça Silva,[1] Thiago Poleto,[2] Lúcio Camara e Silva,[1] Ana Paula Henriques de Gusmao,[2] and Ana Paula Cabral Seixas Costa[2]

[1] *Technology Centre, Department of Management Engineering, Universidade Federal de Pernambuco, Rodovia BR 104, Km 62, Nova Caruaru, 55002-960 Caruaru, PE, Brazil*
[2] *School of Engineering, Centre for Technology and Geosciences, Department of Management Engineering, Universidade Federal de Pernambuco, Caixa Postal 5125, 52.070-970 Recife, PE, Brazil*

Correspondence should be addressed to Maisa Mendonça Silva; maisa.ufpe@yahoo.com.br

Received 18 March 2016; Revised 3 July 2016; Accepted 26 July 2016

Academic Editor: Gang Kou

Big data is the term used to denote enormous sets of data that differ from other classic databases in four main ways: (huge) volume, (high) velocity, (much greater) variety, and (big) value. In general, data are stored in a distributed fashion and on computing nodes as a result of which big data may be more susceptible to attacks by hackers. This paper presents a risk model for big data, which comprises Failure Mode and Effects Analysis (FMEA) and Grey Theory, more precisely grey relational analysis. This approach has several advantages: it provides a structured approach in order to incorporate the impact of big data risk factors; it facilitates the assessment of risk by breaking down the overall risk to big data; and finally its efficient evaluation criteria can help enterprises reduce the risks associated with big data. In order to illustrate the applicability of our proposal in practice, a numerical example, with realistic data based on expert knowledge, was developed. The numerical example analyzes four dimensions, that is, managing identification and access, registering the device and application, managing the infrastructure, and data governance, and 20 failure modes concerning the vulnerabilities of big data. The results show that the most important aspect of risk to big data relates to data governance.

1. Introduction

In recent years, big data has rapidly developed into an important topic that has attracted great attention from industry and society in general [1]. The big data concept and its applications have emerged from the increasing volumes of external and internal data in organizations and it differs from other databases in four aspects: volume, velocity, variety, and value. Volume refers to the amount of data, velocity refers to the speed with which data can be analyzed and processed, variety describes the different kinds and sources of data that may be structured, and value refers to valuable discoveries hidden in large datasets [2]. The emphasis in big data analytics is on how data is stored in a distributed fashion that allows it to be processed in parallel on many computing nodes in distributed environments across clusters of machines [3].

Given the significance that big data has for business applications and the increasing interest in various fields, relevant works should be mentioned: [4] argued that consumer analytics lies at the junction of big data and consumer behavior and highlights the importance of the interpretation of the data generated from big data. Reference [5] examined the role of big data in facilitating access to financial products for economically active low-income families and microenterprises in China. Reference [6] investigated the roles of big data and business intelligence (BI) in the decision-making process. Reference [7] presented a novel active learning method based on extreme learning machines with inherent properties that make handling big data highly attractive. Reference [8] developed a selection algorithm based on evolutionary computation that uses the MapReduce paradigm to obtain subsets of features from big datasets. Reference [9] discussed the

advancement of big data technology, including the generation, management, and analysis of data. Finally, [10] described a brief overview of big data problems, including opportunities and challenges, current techniques, and technologies.

Big data processing begins with data being transmitted from different sources to storage devices and continues with the implementation of preprocessing, process mining and analysis, and decision-making [6]. Much of this processing takes place in parallel, which increases the risk of attack, and how best to guard against this is what big data management seeks to do [11].

Over the last few years, several researchers have proposed solutions for mitigating security threats. In [12], a taxonomy of events and scenarios was developed and the ranking of alternatives based on the criticality of the risk was provided by means of event tree analysis combined with fuzzy decision theory. Reference [13] developed a mathematical model to solve the problem according to the risk management paradigm and thereby provided managers with additional insights for making optimal decisions. There has also been research on the use of large network traces for mitigating security threats [14].

However, research analyzing the risks associated with big data is lacking. Moreover, from this perspective, information security measures are becoming more important due to the increasingly public nature of multiple sources. Hence, many issues related to big data applications can be addressed first by identifying the possible occurrences of failure and then by evaluating them. Consequently, this paper proposes the use of a specific Failure Mode and Effects Analysis (FMEA) method and Grey Theory, which allows for risk assessment at the crucial stages of the big data process. Both mathematical rigor, which is necessary to ensure the robustness of the model, and the judgments of those involved in the process, given the subjective characteristics of the types of assessments made, are considered in this model. This paper contributes to the literature in the following aspects. First, it offers new insights into how the different characteristics of big data are linked to risk in information security. Second, it provides a model risk analysis based on a multidimensional perspective of big data risk analysis.

The first section of the paper discusses big data and information security issues. Then, the discussion that follows relates to existing methodologies for information security and background information, which are necessary for developing the proposed approach. Next, we introduce the methodology and present a real case that illustrates how the methodology validates the proposed approach. Finally, the discussion presents the limitations of the research, suggested areas for further study, and concluding remarks.

2. Background

2.1. Big Data and Methodologies for Risk Management. As mentioned before, big data has different characteristics in terms of variety, velocity, value, and volume compared to classic databases. Consequently, big data risk management is more complex and is becoming one of the greatest concerns in the area of information security. Currently, another important point is that data availability and confidentiality are two top priorities regarding big data.

Recently, several works relating to big data and security have been published. Reference [15] proposed a new type of digital signature that is specifically designed for a graph-based big data system. To ensure the security of outsourced data, [16] developed an efficient ID-based auditing protocol for cloud data integrity using ID-based cryptography. In order to solve the problem of data integrity, [17] proposed a remote data-auditing technique based on algebraic signature properties for a cloud storage system that incurs minimal computational and communication costs. Reference [18] presented a risk assessment process that includes both risk arising from the interference of unauthorized information and issues related to failures in risk-aware access control systems.

There are many methods and techniques with respect to big data risk management. Table 1 lists and briefly describes qualitative methodologies for risk analysis.

Some approaches based on quantitative methods have also been proposed. Reference [19] presented an approach to the risk management of security information, encompassing FMEA and Fuzzy Theory. Reference [20] developed an analysis model to simultaneously define the risk factors and their causal relationships based on the knowledge from observed cases and domain experts. Reference [21] proposed a new method called the Information Security Risk Analysis Method (ISRAM) based on a quantitative approach.

As can be seen, the purpose of big data security mechanisms is to provide protection against malicious parties. Hence, researchers have also identified several forms of attacks and vulnerabilities regarding big data. Reference [22] investigated key threats that target VoIP hosts. Reference [23] analyzed the impact of malicious servers on different trust and reputation models in wireless sensor networks. Reference [24] examined a cloud architecture where different services are hosted on virtualized systems on the cloud by multiple cloud customers. Also, [25] outlined a discussion of the security and privacy challenges of cloud computing.

In this context, attacks themselves are becoming more and more sophisticated. Moreover, attackers also have easier access to ready-made tools that enable exploitation of platform vulnerabilities more effectively. For these reasons, the security risks of high volumes of data from multiple sources, complex data sharing, and accessibility-related issues arise in a big data environment. Therefore, there is an increasing need to develop and create new techniques for big data risk analysis.

2.2. Failure Mode and Effects Analysis (FMEA). FMEA was first proposed by NASA in 1963. The main objective of FMEA is to discover, prevent, and correct potential failure modes, failure causes, failure effects, and problem areas affecting a system [31]. According to FMEA, the risk priorities of failure modes are generally determined through the risk priority

Table 1: Qualitative methodologies for risk analysis.

Methods and techniques	Description and process	Author
CCTA risk analysis and management method (CRAMM)	Comprises three stages; the first two stages identify and analyze the risks to the system and the third stage recommends how these risks should be managed.	[26]
Expert system for security risk analysis and management (RAMeX)	Proposes examining the risk assessment portion of the risk management process in seven steps: define the problem, identify threats, determine the probability of occurrence, identify existing security, assess the business impact, assess security countermeasures, and generate report.	[27]
Facilitated risk analysis process (FRAP)	The process involves analyzing one system of the business operation at a time and convening a team of individuals who have business information needs and technical staff who have a detailed understanding of potential vulnerabilities of the system and related controls.	[28]
Information risk analysis methodologies (IRAM)	Provides three phases; first phase: conduct a comprehensive assessment of the business impact and determine the business security; second phase: assess threat and vulnerability of incidents occurring in a system; third phase: control selection.	[29]
Operationally critical threat, asset, and vulnerability evaluation (OCTAVE)	Organized into four phases: develop understanding of risk to the business, create a profile of each information asset that establishes clear boundaries and identify its security requirements, identify threats to each information asset, and mitigate this risk.	[30]

Table 2: Severity rating scale.

Rating	Effect	Severity of effect
10	Hazardous without warning	Failure is hazardous and occurs without warning; it suspends operation of the system and/or involves noncompliance with government regulations.
9	Serious	Failure involves hazardous outcomes and/or noncompliance with government regulations or standards.
8	Extreme	Big data is inoperable with loss of primary function; the system is inoperable.
7	High	The big data has severely affected performance but functions; the system may not operate.
6	Significant	The performance of big data is degraded; comfort or convenience functions may not operate.
5	Moderate	A moderate effect on the performance of big data; the product requires repair.
4	Very low	A small effect on the performance of big data; the product does not require repair.
3	Minor	A minor effect on the performance of the big data or system.
2	Very minor	A very minor effect on the performance of the big data or system.
1	None	No effect.

number (RPN), which assesses three factors of risk: occurrence (O), severity (S), and detection (D). Then, the RPN is defined by [32]

$$\text{RPN} = \text{O} \times \text{S} \times \text{D}. \quad (1)$$

Based on [33, 34], the classic proposal uses the 10-point linguistic scale for evaluating the O, S, and D factors. This scale is described in Tables 2, 3, and 4 for each risk factor. The failure modes with higher RPNs, which are viewed as more important, should be corrected with higher priorities than those with lower RPNs.

The FMEA method has been applied to many engineering areas. Reference [35] extended the application of FMEA to risk management in the construction industry using combined fuzzy FMEA and fuzzy Analytic Hierarchy Process (AHP). Reference [36] described failures of the fuel feeding system that frequently occur in the sugar and pharmaceutical industries [37]. Reference [38] proposed FMEA for electric power grids, such as solar photovoltaics. Reference [39] presented a basis for prioritizing health care problems.

According to [40], the traditional FMEA method cannot assign different weightings to the risk factors of O, S, and D and therefore may not be suitable for real-world situations. For these authors, introducing Grey Theory to the traditional FMEA enables engineers to allocate the relative importance of the risk factors O, S, and D based on the research and their

Table 3: Occurrence rating scale.

Rating	Description	Potential failure rate
10	Certain probability of occurrence	Failure occurs at least once a day or almost every time.
9	Failure is almost inevitable	Failure occurs predictably or every three or four days.
8 7	Very high probability of occurrence	Failure occurs frequently or about once per week.
6 5	Moderately high probability of occurrence	Failure occurs about once per month.
4 3	Moderate probability of occurrence	Failure occurs occasionally or once every three months.
2	Low probability of occurrence	Failure occurs rarely or about once per year.
1	Remote probability of occurrence	Failure almost never occurs; no one remembers the last failure.

Table 4: Detection rating scale.

Rating	Description	Definition
10	No chance of detection	There is no known mechanism for detecting the failure.
9 8	Very remote/unreliable	The failure can be detected only with thorough inspection and this is not feasible or cannot be readily done.
7 6	Remote	The error can be detected with manual inspection but no process is in place, so detection is left to chance.
5	Moderate chance of detection	There is a process for double checks or inspection but it is not automated and/or is applied only to a sample and/or relies on vigilance.
4 3	High	There is 100% inspection or review of the process but it is not automated.
2	Very high	There is 100% inspection of the process and it is automated.
1	Almost certain	There are automatic "shut-offs" or constraints that prevent failure.

experience. In general, the major advantages of applying the grey method to FMEA are the following capabilities: assigning different weightings to each factor and not requiring any type of utility function [41].

References [32, 33] pointed out that the use of Grey Theory within the FMEA framework is practicable and can be accomplished. Reference [42] examined the ability to predict tanker equipment failure. Reference [43] proposed an approach that is expected to help service managers manage service failures. Thus, Grey Theory is one approach employed to improve the evaluation of risk.

2.3. Grey Theory. Grey Theory, introduced by [44], is a methodology that is used to solve uncertainty problems; it allows one to deal with systems that have imperfect or incomplete information or that even lack information. Grey Theory comprises grey numbers, grey relations (which this paper uses in the form of Grey Relational Analysis, GRA), and grey elements. These three essential components are used to replace classical mathematics [45].

In grey system theory, a system with information that is certain is called a white system; a system with information that is totally unknown is called a black system; a system with partially known and partially unknown information is called a grey system [46]. Reference [47] argued that, in recent days, grey system theory is receiving increasing attention in the field of decision-making and has been successfully applied to many important problems featuring uncertainty such as supplier selection [48, 49], medical diagnosis [50], work safety [40], portfolio selection [51], and classification algorithms evaluation and selection [52].

According to [53], a grey system is defined as a system containing uncertain information presented by a grey number and grey variables. Another important definition is that of a grey set X (of a universal set U), which is defined by its two mappings $\underline{\mu_X}(x)$ and $\overline{\mu_X}(x)$ as follows:

$$\begin{aligned} \underline{\mu_X}(x) &: x \longrightarrow [0,1], \\ \overline{\mu_X}(x) &: x \longrightarrow [0,1], \end{aligned} \tag{2}$$

where $\overline{\mu_X}(x) \geq \underline{\mu_X}(x)$, $x \in X$, $X = R$, and $\overline{\mu_X}(x)$ and $\underline{\mu_X}(x)$ are the upper and lower membership functions in X, respectively.

A grey number is the most fundamental concept in grey system theory and can be defined as a number with uncertain information. Therefore, a white number is a real number $x \in \mathbb{R}$, and a grey number, written as $\otimes x$, refers to an indeterminate real number that takes its possible values from within an interval or a discrete set of numbers. In other words, a grey number, $\otimes x$, is then defined as an interval with a known lower limit and a known upper limit, that is, as $\otimes x\ [\underline{x}, \overline{x}]$. Supposing there are two different grey numbers

denoted by $\bigotimes x_1$ and $\bigotimes x_2$, the mathematical operation rules of general grey numbers are as follows:

$$\begin{aligned}
&\bigotimes x_1 + \bigotimes x_2 = \left[\underline{x_1} + \underline{x_2}, \overline{x_1} + \overline{x_2}\right],\\
&\bigotimes x_1 - \bigotimes x_2 = \left[\underline{x_1} - \overline{x_2}, \overline{x_1} + \underline{x_2}\right],\\
&\bigotimes x_1 \times \bigotimes x_2 = \left[\min\left(\underline{x_1}\,\underline{x_2}, \underline{x_1}\,\overline{x_2}, \overline{x_1}\,\underline{x_2}, \overline{x_1}\,\overline{x_2}\right),\right.\\
&\quad \left.\max\left(\underline{x_1}\,\underline{x_2}, \underline{x_1}\,\overline{x_2}, \overline{x_1}\,\underline{x_2}, \overline{x_1}\,\overline{x_2}\right)\right],\\
&\bigotimes x_1 \div \bigotimes x_2 = \left[\underline{x_1}, \overline{x_1}\right] \times \left[\frac{1}{\underline{x_2}}, \frac{1}{\overline{x_2}}\right],\\
&k \times \bigotimes x_1 = \left[k\underline{x}, k\overline{x}\right].
\end{aligned} \tag{3}$$

GRA is a part of Grey Theory and can be used together with various correlated indicators to evaluate and analyze the performance of complex systems [54, 55]. In fact, GRA has been successfully used in FMEA and its results have been proven to be satisfactory. Compared to other methods, GRA has competitive advantages in terms of having shown the ability to process uncertainty and to deal with multi-input systems, discrete data, and data incompleteness effectively [55]. In addition, [41] argues that results generated by the combination of Grey Theory and FMEA are more unbiased than those of traditional FMEA, and [42] claims that combining Fuzzy Theory and Grey Theory with FMEA leads to more useful and practical results.

GRA is an impact evaluation model that measures the degree of similarity or difference between two sequences based on the degree of their relationship. In GRA, a global comparison between two sets of data is undertaken instead of using a local comparison by measuring the distance between two points [56]. Its basic principle is that if a comparability sequence translated from an alternative has a higher grey relational degree between the reference sequence and itself, then the alternative will be the better choice. Therefore, the analytic procedure of GRA normally consists of four parts: generating the grey relational situation, defining the reference sequence, calculating the grey relational coefficient, and finally calculating the grey relational degree [55, 57]. The comparative sequence denotes the sequences that should be evaluated by GRA and the reference sequence is the original reference that is compared with the comparative sequence. Normally, the reference sequence is defined as a vector consisting of $(1, 1, \ldots, 1, \ldots, 1)$. GRA aims to find the alternative that has the comparability sequence that is the closest to the reference sequence [43].

2.4. Critical Analysis. Big data comprises complex data that is massively produced and managed in geographically dispersed repositories [63]. Such complexity motivates the development of advanced management techniques and technologies for dealing with the challenges of big data. Moreover, how best to assess the security of big data is an emerging research area that has attracted abundant attention in recent years. Existing security approaches carry out checking on data processing in diverse modes. The ultimate goal of these approaches is to preserve the integrity and privacy of data and to undertake computations in single and distributed storage environments irrespective of the underlying resource margins [11].

However, as discussed in [11], traditional data security technologies are no longer pertinent to solving big data security problems completely. These technologies are unable to provide dynamic monitoring of how data and security are protected. In fact, they were developed for static datasets, but data is now changing dynamically [64]. Thus, it has become hard to implement effective privacy and security protection mechanisms that can handle large amounts of data in complex circumstances.

In a general way, FMEA has been extensively used for examining potential failures in many industries. Moreover, FMEA together with Fuzzy Theory and/or Grey Theory has been widely and successfully used in the risk management of information systems [12], equipment failure [42], and failure in services [43].

Because the modeling of complex dynamic big data requires methods that combine human knowledge and experience as well as expert judgment, this paper uses GRA to evaluate the level of uncertainty associated with assessing big data in the presence or absence of threats. It also provides a structured approach in order to incorporate the impact of risk factors for big data into a more comprehensive definition of scenarios with negative outcomes and facilitates the assessment of risk by breaking down the overall risk to big data. Finally, its efficient evaluation criteria can help enterprises reduce the risks associated with big data.

Therefore, from a security and privacy perspective, big data is different from other traditional data and requires a different approach. Many of the existing methodologies and preferred practices cannot be extended to support the big data paradigm. Big data appears to have similar risks and exposures to traditional data. However, there are several key areas where they are dramatically different.

In this context, variety and volume translate into higher risks of exposure in the event of a breach due to variability in demand, which requires a versatile management platform for storing, processing, and managing complex data. In addition, the new paradigm for big data presents data characteristics at different levels of granularity and big data projects often encompass heterogeneous components. Another point of view states that new types of data are uncovering new privacy implications, with few privacy laws or guidelines to protect that information.

3. The Proposed Model

In this paper, an approach to big data risk management using GRA has been developed to analyze the dimensions that are critical to big data, as described by [65], based on FMEA and [31, 32]. The approach proposed is presented in Figure 1.

The new big data paradigm needs to work with far more than the traditional subsets of internal data. This paradigm incorporates a large volume of unstructured information, looks for nonobvious correlations that might drive new

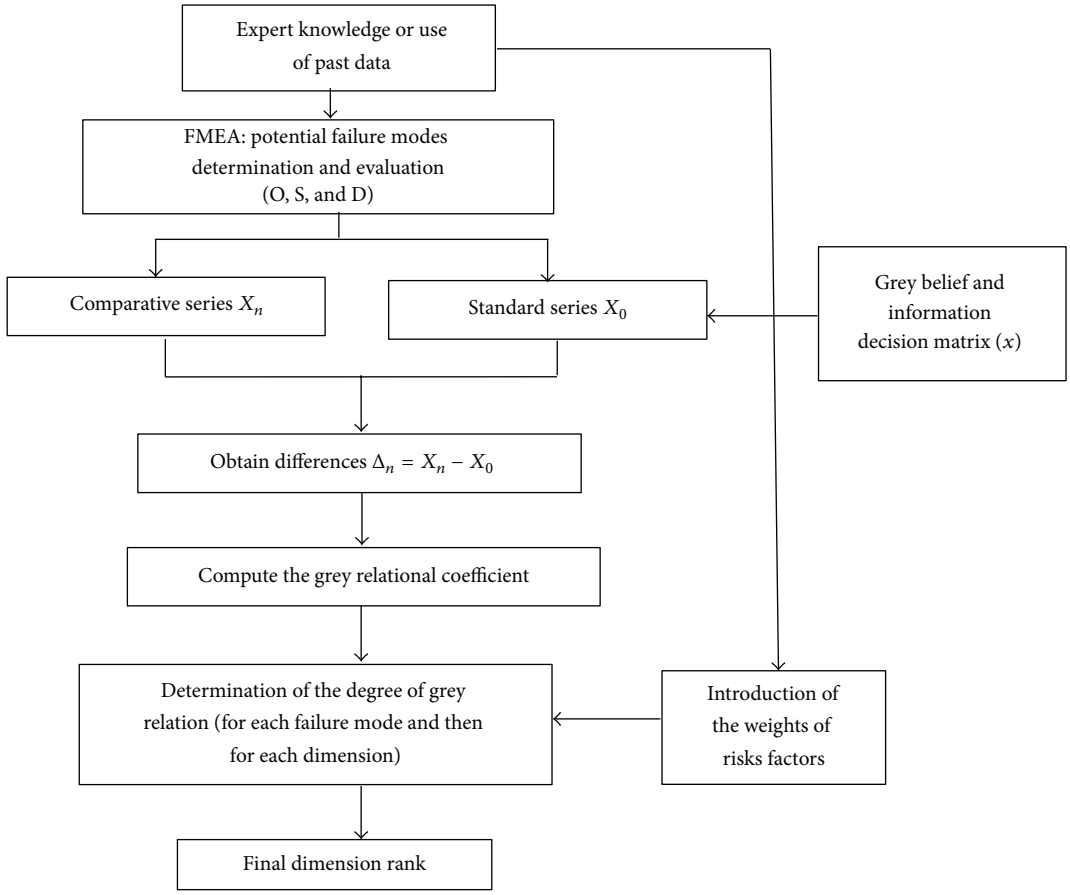

Figure 1: Flowchart of the proposed FMEA and Grey Theory based approach.

hypotheses, and must work with data that float into the organization in real time and that require real-time analysis and response. Therefore, in this paper, we analyzed the processing characteristics of the IBM Big Data Platform for illustrative purposes, but it is important to note that all big data platforms are vulnerable to both external and internal threats. Therefore, since our analysis model based on the probability of the occurrence of failure covers a wide view of the architecture of big data, it is eligible for analyzing other platforms, such as cloud computing infrastructures [66] and platforms from business scenarios [67]. Finally, our model considers the possible occurrence of failures in the distributed data and then we consider its implementation in a distributed way.

3.1. Expert Knowledge or Past Data regarding Previous Failures. The first step in the approach consists of expert identification or use of past data. The expert is the person who knows the enterprise systems and their vulnerability and is thus able to assess the information security risk of the organization in terms of the four dimensions [65]. One may also identify a group of experts in this step, and the analysis is accomplished by considering a composition of their judgments or the use of a dataset of past failures. The inclusion of an expert system in the model is also encouraged.

According to [68], an expert is someone with multiple skills who understands the working environment and has substantial training in and knowledge of the system being evaluated. Risk management models have widely used expert knowledge to provide value judgments that represent the expert's perceptions and/or preferences. For instance, [69] provides evidence obtained from two unbiased and independent experts regarding the risk of release of a highly flammable gas near a processing facility. References [70, 71] explore a risk measure of underground vaults that considers the consequences of arc faults using a single expert's a priori knowledge. Reference [19] proposes information security risk management using FMEA, Fuzzy Theory, and expert knowledge. Reference [72] analyzes the risk probability of an underwater tunnel excavation using the knowledge of four experts.

3.2. Determination and Evaluation of Potential Failure Modes (FMEA). In a general way, this step concerns the determination of the failure modes associated with the big data dimensions (Figure 2) in terms of their vulnerabilities. Each dimension is described in Table 5.

Furthermore, these dimensions can be damaged by various associated activities. Table 6 presents failure modes relating to the vulnerability of big data for each dimension.

Table 5: Description of dimensions.

Dimension	Description
Identification and access management	Given the opportunity to increase knowledge by accessing big data, it is necessary that only authorized persons can access it; thus, big data requires confidentiality and authenticity; to address this problem, [58] mentioned that sometimes both are needed simultaneously; this source recommended and proposed three different schemes: an encryption scheme, a signature scheme, and a sign-encryption scheme
Device and application registration	Data provenance refers to information about the history of a creation process; in other words, it refers to a mechanism that can be used to validate whether input data is coming from an authenticated source to guarantee a degree of information integrity [59]; then, provenance-related security and trustworthiness issues also arise in the system [60]; they include the registration of devices in machine-to-machine (M2M) and Internet-of-Things (IoT) networks, which can be considered one of the major issues in the area of security [61]
Infrastructure management	As big data physical infrastructures increase, difficulties associated with designing effective physical security also arise; thus, we use the term "system health" to describe the intersection of the information worker and the nominal conditions for infrastructure management monitoring of big data for security purposes, which include technical issues regarding the interoperability of services [62]
Data governance	Data governance can ensure appropriate controls without inhibiting the speed and flexibility of innovative big data approaches and technologies, which need to be established for different management levels with a clear security strategy

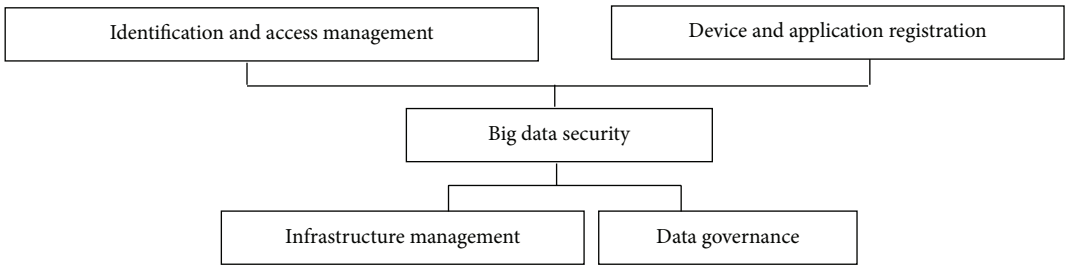

Figure 2: Big data dimensions.

In fact, the determination of the failure modes is achieved using the FMEA methodology and evaluated regarding its occurrence (O), severity (S), and detection (D).

3.3. Establish Comparative Series. An information series with n decision factors, such as chance of occurrence, severity of failure, or chance of lack of detection, can be expressed as follows:

$$X_i = \left(X_i(1), X_i(2), \ldots, X_i(k)\right). \tag{4}$$

These comparative series can be provided by an expert or any dataset of previous failures, based on the scales described in Tables 2–4.

3.4. Establish the Standard Series. According to [41], the degree of relation can describe the relationship of two series; thus, an objective series called the standard series is established and expressed as $X_0 = (X_0(1), X_0(2), \ldots, X_0(k))$, where k is the number of risk factors (for this work, $k = 3$, i.e., occurrence, severity, and detection). According to FMEA, as the score becomes smaller, the standard series can be denoted as $X_0 = (X_0(1), X_0(2), \ldots, X_0(k)) = (1, 1, \ldots, 1)$.

3.5. Obtain the Difference between the Comparative Series and the Standard Series. To discover the degree of the grey relationship, the difference between the score of the decision factors and the norm of the standard series must be determined and expressed by a matrix calculated by

$$\Delta_{0j}(k) = \left\| X_0(k) - X_j(k) \right\|, \tag{5}$$

where j is the number of failure modes in the analysis [31].

3.6. Compute the Grey Relational Coefficient. The grey relational coefficient is calculated by

$$\gamma\left(X_0(k), X_j(k)\right) = \frac{\Delta_{\min} - \zeta\Delta_{\max}}{\Delta_{0j}(k) - \zeta\Delta_{\max}}, \tag{6}$$

where ζ is an identifier, normally set to 0.5 [31]. It only affects the relative value of risk, not the priority.

Table 6: Failure modes associated with each dimension of big data.

Dimensions	Associated activities
A1: Identification and access management	A1.1: Loss of secret keys
	A1.2: Cryptanalysis of a ciphered signal
	A1.3: Secret password divulged to any other user
	A1.4: Intentional access to network services, for example, proxy servers
	A1.5: Spoofing: impersonation of a legitimate user
A2: Device and application registration	A2.1: Facility problems
	A2.2: Failure of encryption equipment
	A2.3: Unauthorized use of secure equipment
	A2.4: Ineffective infrastructure investment
	A2.5: Failure of application server
A3: Infrastructure management	A3.1: Cabling problems
	A3.2: Failure of radio platform transmission
	A3.3: Failure of cipher audio (telephone) and video
	A3.4: Failure of sensor networks
	A3.5: Failure of potential of energy
	A3.6: Unauthorized readout of data stored on a remote LAN
A4: Data governance	A4.1: Failure of interpretation and analysis of data
	A4.2: Failure of audit review of implemented policies and information security
	A4.3: Failure to maximize new business value
	A4.4: Failure of real-time demand forecasts

3.7. Determine the Degree of Relation. Before finding the degree of relation, the relative weight of the decision factors is first decided so that it can be used in the following formulation [31]. In a general way, it is calculated by

$$\Gamma\left(X_i, X_j\right) = \sum_{k=1}^{n} \beta_k \gamma\left(X_i(k), X_j(k)\right), \tag{7}$$

where β_k is the risk factors' weighting and, as a result, $\sum_{k=1}^{n} \beta_k = 1$.

3.8. Rank the Priority of Risk. This step consists of dimension ordering. Based on the degree of relation between the comparative series and the standard series, a relational series can be constructed. The greater the degree of relation, the smaller the effect of the cause [31].

4. An Illustrative Example

To demonstrate the applicability of our proposition based on FMEA and Grey Theory, an example based on a real context is presented in this section. The steps performed are the same as shown in Figure 1, explained in Section 3. Following these steps, the expert selected for this study is a senior academic with more than 20 years' experience. She holds a Ph.D. degree in information systems (IS), has published 12 papers in this field, and also has experience as a consultant in IS to companies in the private sector.

In the following step of the proposed model, the four dimensions associated with the potential failures of big data are represented according to Figure 2 and described in Table 5. Furthermore, Table 6 presents the failure modes relating to the vulnerability of big data for each dimension. Based on these potential failures, Tables 7 and 8 show the establishment of comparative and standard series for occurrence, severity, and detection, respectively.

To proceed to a grey relational analysis of potential accidents, it is necessary to obtain the difference between comparative series and standard series, according to (4). Table 9 shows the result of this difference.

In order to rank the priority of risk, it is necessary to compute both the grey relational coefficient (Table 10) and the degree of relation (Table 11) using (5), (6), and (7). Therefore, the greater the degree of relation, the smaller the effect of the cause. Assuming equal weights for risk factors, Table 11 also presents the degree of grey relation for each failure mode and dimension and final ranking.

From the analysis of failures using the proposed approach, we have shown that big data is mainly in need of structured policies for data governance. This result was expected because the veracity and provenance of data are fundamental to information security; otherwise, the vulnerabilities may be catastrophic or big data may have little value for the acquisition of knowledge. Data governance is also an aspect that requires more awareness because it deals with large amounts of data and directly influences operational costs.

Since the model works with a recommendation rather than a solution and compatible recommendations depend on expert knowledge, it is important to test the robustness of

Table 7: Comparative series.

Dimensions	Associated activities	O	S	D
A1: Identification and access management	A1.1: Loss of secret keys	5	7	4
	A1.2: Cryptanalysis of a ciphered signal	5	5	4
	A1.3: Secret password divulged to any other user	2	7	5
	A1.4: Intentional access to network services, for example, proxy servers	6	5	7
	A1.5: Spoofing: impersonation of a legitimate user	6	5	7
A2: Device and application registration	A2.1: Facility problems	8	7	5
	A2.2: Failure of encryption equipment	6	9	5
	A2.3: Unauthorized use of secure equipment	6	5	4
	A2.4: Ineffective infrastructure investment	8	5	4
	A2.5: Failure of application server	5	4	5
A3: Infrastructure management	A3.1: Cabling problems	6	5	4
	A3.2: Failure of radio platform transmission	2	9	4
	A3.3: Failure of cipher audio (telephone) and video	2	7	4
	A3.4: Failure of sensor networks	5	7	2
	A3.5: Failure of potential of energy	2	7	2
	A3.6: Unauthorized readout of data stored on a remote LAN	5	5	4
A4: Data governance	A4.1: Failure of interpretation and analysis of data	8	9	5
	A4.2: Failure of audit review of implemented policies and information security	8	9	4
	A4.3: Failure to maximize new business value	8	7	5
	A4.4: Failure of real-time demand forecasts	8	7	7

Table 8: Standard series.

Dimensions	Associated activities	O	S	D
A1: Identification and access management	A1.1: Loss of secret keys	1	1	1
	A1.2: Cryptanalysis of a ciphered signal	1	1	1
	A1.3: Secret password divulged to any other user	1	1	1
	A1.4: Intentional access to network services, for example, proxy servers	1	1	1
	A1.5: Spoofing: impersonation of a legitimate user	1	1	1
A2: Device and application registration	A2.1: Facility problems	1	1	1
	A2.2: Failure of encryption equipment	1	1	1
	A2.3: Unauthorized use of secure equipment	1	1	1
	A2.4: Ineffective infrastructure investment	1	1	1
	A2.5: Failure of application server	1	1	1
A3: Infrastructure management	A3.1: Cabling problems	1	1	1
	A3.2: Failure of radio platform transmission	1	1	1
	A3.3: Failure of cipher audio (telephone) and video	1	1	1
	A3.4: Failure of sensor networks	1	1	1
	A3.5: Failure of potential of energy	1	1	1
	A3.6: Unauthorized readout of data stored on a remote LAN	1	1	1
A4: Data governance	A4.1: Failure of interpretation and analysis of data	1	1	1
	A4.2: Failure of audit review of implemented policies and information security	1	1	1
	A4.3: Failure to maximize new business value	1	1	1
	A4.4: Failure of real-time demand forecasts	1	1	1

this information and therefore to conduct sensitivity analysis. Thus, different weightings, based on the context, may also be used for different risk factors, as suggested by [33]. Table 12 presents a sensitivity analysis conducted in order to evaluate the performance and validity of the results of the model. As can be seen, the final ranking of risk is the same for all the different weightings tested (±10%).

5. Discussion and Conclusions

The main difficulties in big data security risk analysis involve the volume of data and the variety of data connected to different databases. From the perspective of security and privacy, traditional databases have governance controls and a consolidated auditing process, while big data is at an early

Table 9: Difference between comparative series and standard series.

Dimensions	Associated activities	O	S	D
A1: Identification and access management	A1.1: Loss of secret keys	4	6	3
	A1.2: Cryptanalysis of a ciphered signal	4	4	3
	A1.3: Secret password divulged to any other user	1	6	4
	A1.4: Intentional access to network services, for example, proxy servers	5	4	6
	A1.5: Spoofing: impersonation of a legitimate user	5	4	6
A2: Device and application registration	A2.1: Facility problems	7	6	4
	A2.2: Failure of encryption equipment	5	3	4
	A2.3: Unauthorized use of secure equipment	5	4	3
	A2.4: Ineffective infrastructure investment	7	4	3
	A2.5: Failure of application server	4	3	4
A3: Infrastructure management	A3.1: Cabling problems	5	4	3
	A3.2: Failure of radio platform transmission	1	8	3
	A3.3: Failure of cipher audio (telephone) and video	1	6	3
	A3.4: Failure of sensor networks	4	6	1
	A3.5: Failure of potential of energy	1	6	1
	A3.6: Unauthorized readout of data stored on a remote LAN	4	4	3
A4: Data governance	A4.1: Failure of interpretation and analysis of data	7	8	4
	A4.2: Failure of audit review of implemented policies and information security	7	8	3
	A4.3: Failure to maximize new business value	7	6	4
	A4.4: Failure of real-time demand forecasts	7	6	6

stage of development and hence continues to require structured analysis to address threats and vulnerabilities. Moreover, there is not yet enough research into risk analysis in the context of big data.

Thus, security is one of the most important issues for the stability and development of big data. Aiming to identify the risk factors and the uncertainty associated with the propagation of vulnerabilities, this paper proposed a systematic framework based on FMEA and Grey Theory, more precisely GRA. This systematic framework allows for an evaluation of risk factors and their relative weightings in a linguistic, as opposed to a precise, manner for evaluation of big data failure modes. This is in line with the uncertain nature of the context. In fact, according to [40], the traditional FMEA method cannot assign different weightings to the risk factors of O, S, and D and therefore may not be suitable for real-world situations. These authors pointed out that introducing Grey Theory into the traditional FMEA method enables engineers to allocate relative importance to the O, S, and D risk factors based on research and their own experience. In a general way, another advantage of this proposal is that it requires less effort on the part of experts using linguistic terms. Consequently, these experts can make accurate judgments using linguistic terms based on their experience or on datasets relating to previous failures.

Based on the above information, the use of our proposal is justified to identify and assess big data risk in a quantitative manner. Moreover, this study comprises various security characteristics of big data using FMEA: it analyzes four dimensions, identification and access management, device and application registration, infrastructure management, and data governance, as well as 20 subdimensions that represent failure modes. Therefore, this work can be expected to serve as a guideline for managing big data failures in practice.

It is worth stating that the results presented greater awareness of data governance for ensuring appropriate controls. In this context, a challenge to the process of governing big data is to categorize, model, and map data as it is captured and stored, mainly because of the unstructured nature of the volume of information. Then, one role of data governance in the information security context is to allow for the information that contributes to reporting to be defined consistently across the organization in order to guide and structure the most important activities and to help clarify decisions. Briefly, analyzing data from the distant past to decide on a current situation does not mean that the data has higher value. From another perspective, increasing volume does not guarantee confidence in decisions, and one may use tools such as data mining and knowledge discovery, proposed in [73], to improve the decision process.

Indeed, the concept of storage management is a critical point, especially when volumes of data that exceed the storage capacity are considered [11]. In fact, the emphasis of big data analytics is on how data is stored in a distributed fashion, for example, in traditional databases or in a cloud [66]. When a cloud is used, data can be processed in parallel on many computing nodes, in distributed environments across clusters of machines [3]. In conclusion, big data security must be seen as an important and challenging feature, capable of generating significant limitations. For instance, several electronic devices that enable communication via networks, especially via the Internet, and which place great emphasis on mobile trends allow for an increase in volume, variety, and even speed of data, which can thereby be defined as big

Table 10: Grey relational coefficient.

Dimensions	Associated activities	O	S	D
A1: Identification and access management	A1.1: Loss of secret keys	0.625	0.5	0.714286
	A1.2: Cryptanalysis of a ciphered signal	0.625	0.625	0.714286
	A1.3: Secret password divulged to any other user	1	0.5	0.625
	A1.4: Intentional access to network services, for example, proxy servers	0.555556	0.625	0.5
	A1.5: Spoofing: impersonation of a legitimate user	0.555556	0.625	0.5
A2: Device and application registration	A2.1: Facility problems	0.454545	0.5	0.625
	A2.2: Failure of encryption equipment	0.555556	0.416667	0.625
	A2.3: Unauthorized use of secure equipment	0.555556	0.625	0.714286
	A2.4: Ineffective infrastructure investment	0.454545	0.625	0.714286
	A2.5: Failure of application server	0.625	0.714286	0.625
A3: Infrastructure management	A3.1: Cabling problems	0.555556	0.625	0.714286
	A3.2: Failure of radio platform transmission	1	0.416667	0.714286
	A3.3: Failure of cipher audio (telephone) and video	1	0.5	0.714286
	A3.4: Failure of sensor networks	0.625	0.5	1
	A3.5: Failure of potential of energy	1	0.5	1
	A3.6: Unauthorized readout of data stored on a remote LAN	0.625	0.625	0.714286
A4: Data governance	A4.1: Failure of interpretation and analysis of data	0.454545	0.416667	0.625
	A4.2: Failure of audit review of implemented policies and information security	0.454545	0.416667	0.714286
	A4.3: Failure to maximize new business value	0.454545	0.5	0.625
	A4.4: Failure of real-time demand forecasts	0.454545	0.5	0.5

Table 11: The degree of grey relation for each failure mode and each dimension and the final rank.

Dimensions	Associated activities	Degree of grey relation	Degree of grey relation (dimension)	Risk ranking
A1: Identification and access management	A1.1: Loss of secret keys	0.613095	0.619312	3
	A1.2: Cryptanalysis of a ciphered signal	0.654762		
	A1.3: Secret password divulged to any other user	0.708333		
	A1.4: Intentional access to network services, for example, proxy servers	0.560185		
	A1.5: Spoofing: impersonation of a legitimate user	0.560185		
A2: Device and application registration	A2.1: Facility problems	0.526515	0.588648	2
	A2.2: Failure of encryption equipment	0.532407		
	A2.3: Unauthorized use of secure equipment	0.631614		
	A2.4: Ineffective infrastructure investment	0.597944		
	A2.5: Failure of application server	0.654762		
A3: Infrastructure management	A3.1: Cabling problems	0.631614	0.712743	4
	A3.2: Failure of radio platform transmission	0.710317		
	A3.3: Failure of cipher audio (telephone) and video	0.738095		
	A3.4: Failure of sensor networks	0.708333		
	A3.5: Failure of potential of energy	0.833333		
	A3.6: Unauthorized readout of data stored on a remote LAN	0.654762		
A4: Data governance	A4.1: Failure of interpretation and analysis of data	0.498737	0.50965	1
	A4.2: Failure of audit review of implemented policies and information security	0.528499		
	A4.3: Failure to maximize new business value	0.526515		
	A4.4: Failure of real-time demand forecasts	0.484848		

Table 12: Sensitivity analysis.

Weights of risk factors	Degree of grey relation (dimension) and risk ranking
Occurrence: 0.30 Severity: 0.35 Detection: 0.35	D1: 0.616667 (3) D2: 0.591629 (2) D3: 0.645833 (4) D4: 0.512405 (1)
Occurrence: 0.36 Severity: 0.32 Detection: 0.32	D1: 0.621429 (3) D2: 0.586264 (2) D3: 0.641071 (4) D4: 0.507446 (1)
Occurrence: 0.35 Severity: 0.30 Detection: 0.35	D1: 0.621528 (3) D2: 0.589271 (2) D3: 0.644097 (4) D4: 0.512216 (1)
Occurrence: 0.32 Severity: 0.36 Detection: 0.32	D1: 0.61754 (3) D2: 0.58815 (2) D3: 0.64246 (4) D4: 0.507597 (1)
Occurrence: 0.35 Severity: 0.35 Detection: 0.30	D1: 0.619742 (3) D2: 0.585045 (2) D3: 0.639633 (4) D4: 0.504329 (1)
Occurrence: 0.35 Severity: 0.35 Detection: 0.30	D1: 0.618968 (3) D2: 0.591531 (2) D3: 0.646032 (4) D4: 0.513907 (1)

data content. This fact adds more value to large volumes of data and allows for the support of organizational activities, bequeathing even more importance to the area of data processing, which now tends to work in a connected way that goes beyond the boundaries of companies.

This research contributes as a guide for researchers in the analysis of suitable big data risk techniques and in the development of response to the insufficiency of existing solutions. This risk model can ensure the identification of failure and attacks and help the victim decide how to react when this type of attack occurs. However, this study has limitations. For instance, it does not measure the consequences of a disaster occurring in the field of big data. This measurement could be carried out based on [74]. Future work should focus on developing a model to ensure the working of data governance and should recommend specific actions to ensure the safety of big data and to help managers choose the best safeguards to reduce risks. Further studies may also consider security-related issues in the fields of enterprise architecture, information infrastructure, and cloud-based computing.

Competing Interests

The authors declare that they have no competing interests.

Acknowledgments

This research was partially supported by Universidade Federal de Pernambuco and GPSID, Decision and Information Systems Research Group.

References

[1] R. Tinati, S. Halford, L. Carr, and C. Pope, "Big data: methodological challenges and approaches for sociological analysis," *Sociology*, vol. 48, no. 4, pp. 663–681, 2014.

[2] M. Chen, S. Mao, and Y. Liu, "Big data: a survey," *Mobile Networks and Applications*, vol. 19, no. 2, pp. 171–209, 2014.

[3] H. Hu, Y. Wen, T.-S. Chua, and X. Li, "Toward scalable systems for big data analytics: a technology tutorial," *IEEE Access*, vol. 2, pp. 652–687, 2014.

[4] S. Erevelles, N. Fukawa, and L. Swayne, "Big Data consumer analytics and the transformation of marketing," *Journal of Business Research*, vol. 69, no. 2, pp. 897–904, 2016.

[5] N. Kshetri, "Big data's role in expanding access to financial services in China," *International Journal of Information Management*, vol. 36, no. 3, pp. 297–308, 2016.

[6] T. Poleto, V. D. H. de Carvalho, and A. P. C. S. Costa, "The roles of big data in the decision-support process: an empirical investigation," in *Decision Support Systems V—Big Data Analytics for Decision Making: First International Conference, ICDSST 2015, Belgrade, Serbia, May 27–29, 2015, Proceedings*, vol. 216 of *Lecture Notes in Business Information Processing*, pp. 10–21, Springer, Berlin, Germany, 2015.

[7] E. G. Horta, C. L. de Castro, and A. P. Braga, "Stream-based extreme learning machine approach for big data problems," *Mathematical Problems in Engineering*, vol. 2015, Article ID 126452, 17 pages, 2015.

[8] D. Peralta, S. del Río, S. Ramírez-Gallego, I. Triguero, J. M. Benitez, and F. Herrera, "Evolutionary feature selection for big data classification: a MapReduce approach," *Mathematical Problems in Engineering*, vol. 2015, Article ID 246139, 11 pages, 2015.

[9] X. Song, Y. Wu, Y. Ma, Y. Cui, and G. Gong, "Military simulation big data: background, state of the art, and challenges," *Mathematical Problems in Engineering*, vol. 2015, Article ID 298356, 20 pages, 2015.

[10] C. L. Philip Chen and C.-Y. Zhang, "Data-intensive applications, challenges, techniques and technologies: a survey on Big Data," *Information Sciences*, vol. 275, pp. 314–347, 2014.

[11] A. Siddiqa, I. A. T. Hashem, I. Yaqoob et al., "A survey of big data management: taxonomy and state-of-the-art," *Journal of Network and Computer Applications*, vol. 71, pp. 151–166, 2016.

[12] A. P. H. De Gusmão, L. C. E Silva, M. M. Silva, T. Poleto, and A. P. C. S. Costa, "Information security risk analysis model using fuzzy decision theory," *International Journal of Information Management*, vol. 36, no. 1, pp. 25–34, 2016.

[13] W. T. Yue, M. Çakanyildirim, Y. U. Ryu, and D. Liu, "Network externalities, layered protection and IT security risk management," *Decision Support Systems*, vol. 44, no. 1, pp. 1–16, 2007.

[14] K. Singh, S. C. Guntuku, A. Thakur, and C. Hota, "Big Data Analytics framework for Peer-to-Peer Botnet detection using Random Forests," *Information Sciences*, vol. 278, pp. 488–497, 2014.

[15] S. Hou, X. Huang, J. K. Liu, J. Li, and L. Xu, "Universal designated verifier transitive signatures for graph-based big data," *Information Sciences*, vol. 318, pp. 144–156, 2015.

[16] J. Zhang and Q. Dong, "Efficient ID-based public auditing for the outsourced data in cloud storage," *Information Sciences*, vol. 343-344, pp. 1–14, 2016.

[17] M. Sookhak, A. Gani, M. K. Khan, and R. Buyya, "Dynamic remote data auditing for securing big data storage in cloud computing," *Information Sciences*, 2015.

[18] N. Baracaldo and J. Joshi, "An adaptive risk management and access control framework to mitigate insider threats," *Computers and Security*, vol. 39, pp. 237–254, 2013.

[19] M. M. Silva, A. P. H. de Gusmão, T. Poleto, L. C. E. Silva, and A. P. C. S. Costa, "A multidimensional approach to information security risk management using FMEA and fuzzy theory," *International Journal of Information Management*, vol. 34, no. 6, pp. 733–740, 2014.

[20] N. Feng, H. J. Wang, and M. Li, "A security risk analysis model for information systems: causal relationships of risk factors and vulnerability propagation analysis," *Information Sciences*, vol. 256, no. 20, pp. 57–73, 2014.

[21] B. Karabacak and I. Sogukpinar, "ISRAM: information security risk analysis method," *Computers and Security*, vol. 24, no. 2, pp. 147–159, 2005.

[22] R. Farley and X. Wang, "Exploiting VoIP softphone vulnerabilities to disable host computers: attacks and mitigation," *International Journal of Critical Infrastructure Protection*, vol. 7, no. 3, pp. 141–154, 2014.

[23] V. K. Verma, S. Singh, and N. P. Pathak, "Impact of malicious servers over trust and reputation models in wireless sensor networks," *International Journal of Electronics*, vol. 103, no. 3, pp. 530–540, 2016.

[24] V. Varadharajan and U. Tupakula, "Counteracting security attacks in virtual machines in the cloud using property based attestation," *Journal of Network and Computer Applications*, vol. 40, no. 1, pp. 31–45, 2014.

[25] H. Takabi, J. B. D. Joshi, and G.-J. Ahn, "Security and privacy challenges in cloud computing environments," *IEEE Security and Privacy*, vol. 8, no. 6, pp. 24–31, 2010.

[26] SANS, "A Qualitative Risk Analysis and Management Tool-CRAMM," 2002.

[27] M. P. Kailay and P. Jarratt, "RAMeX: a prototype expert system for computer security risk analysis and management," *Computers & Security*, vol. 14, no. 5, pp. 449–463, 1995.

[28] T. R. Peltier, *Facilitated Risk Analysis Process (FRAP)*, Auerbach Publications, 2000.

[29] J. Creasey, "A complete information risk management solution For ISF members using IRAM and STREAM," in *Managing Information Risk*, pp. 1–7, 2013.

[30] C. Alberts and A. Dorofee, *Managing Information Security Risks: The OCTAVE Approach*, Addison-Wesley, 2002.

[31] R. J. Mikulak, R. McDermott, and M. Beauregard, *The Basics of FMEA*, vol. 2, CRC Press, Boca Raton, Fla, USA, 2009.

[32] A. Pillay and J. Wang, "Modified failure mode and effects analysis using approximate reasoning," *Reliability Engineering and System Safety*, vol. 79, no. 1, pp. 69–85, 2003.

[33] M. Ben Daya and Abdul Raouf, "A revised failure mode and effects analysis model," *International Journal of Quality & Reliability Management*, vol. 13, no. 1, pp. 43–47, 1996.

[34] J. B. Bowles and C. E. Peláez, "Fuzzy logic prioritization of failures in a system failure mode, effects and criticality analysis," *Reliability Engineering and System Safety*, vol. 50, no. 2, pp. 203–213, 1995.

[35] M. Abdelgawad and A. R. Fayek, "Risk management in the construction industry using combined fuzzy FMEA and fuzzy AHP," *Journal of Construction Engineering and Management*, vol. 136, no. 9, pp. 1028–1036, 2010.

[36] A. Mariajayaprakash and T. Senthilvelan, "Failure detection and optimization of sugar mill boiler using FMEA and Taguchi method," *Engineering Failure Analysis*, vol. 30, pp. 17–26, 2013.

[37] O. Kaljević, J. Djuriš, Z. Djurić, and S. Ibrić, "Application of failure mode and effects analysis in quality by design approach for formulation of carvedilol compression coated tablets," *Journal of Drug Delivery Science and Technology*, vol. 32, pp. 56–63, 2016.

[38] A. Colli, "Failure mode and effect analysis for photovoltaic systems," *Renewable and Sustainable Energy Reviews*, vol. 50, pp. 804–809, 2015.

[39] C. Kahraman, I. Kaya, and Ö. Şenvar, "Healthcare failure mode and effects analysis under fuzziness," *Human and Ecological Risk Assessment*, vol. 19, no. 2, pp. 538–552, 2013.

[40] J. Wei, L. Zhou, F. Wang, and D. Wu, "Work safety evaluation in Mainland China using grey theory," *Applied Mathematical Modelling*, vol. 39, no. 2, pp. 924–933, 2015.

[41] C.-L. Chang, P.-H. Liu, and C.-C. Wei, "Failure mode and effects analysis using grey theory," *Integrated Manufacturing Systems*, vol. 12, no. 3, pp. 211–216, 2001.

[42] Q. Zhou and V. V. Thai, "Fuzzy and grey theories in failure mode and effect analysis for tanker equipment failure prediction," *Safety Science*, vol. 83, pp. 74–79, 2016.

[43] Y. Geum, Y. Cho, and Y. Park, "A systematic approach for diagnosing service failure: service-specific FMEA and grey relational analysis approach," *Mathematical and Computer Modelling*, vol. 54, no. 11-12, pp. 3126–3142, 2011.

[44] J.-L. Deng, "Control problems of grey systems," *Systems & Control Letters*, vol. 1, no. 5, pp. 288–294, 1982.

[45] J. L. Deng, "Introduction to grey system theory," *The Journal of Grey System*, vol. 1, no. 1, pp. 1–24, 1989.

[46] H. Kuang, M. A. Bashar, K. W. Hipel, and D. M. Kilgour, "Grey-based preference in a graph model for conflict resolution with multiple decision makers," *IEEE Transactions on Systems, Man, and Cybernetics: Systems*, vol. 45, no. 9, pp. 1254–1267, 2015.

[47] H. Kuang, D. M. Kilgour, and K. W. Hipel, "Grey-based PROMETHEE II with application to evaluation of source water protection strategies," *Information Sciences*, vol. 294, pp. 376–389, 2015.

[48] M. S. Memon, Y. H. Lee, and S. I. Mari, "Group multi-criteria supplier selection using combined grey systems theory and uncertainty theory," *Expert Systems with Applications*, vol. 42, no. 21, pp. 7951–7959, 2015.

[49] D. Golmohammadi and M. Mellat-Parast, "Developing a grey-based decision-making model for supplier selection," *International Journal of Production Economics*, vol. 137, no. 2, pp. 191–200, 2012.

[50] Z. Li, G. Wen, and N. Xie, "An approach to fuzzy soft sets in decision making based on grey relational analysis and Dempster-Shafer theory of evidence: an application in medical diagnosis," *Artificial Intelligence in Medicine*, vol. 64, no. 3, pp. 161–171, 2015.

[51] R. Bhattacharyya, "A grey theory based multiple attribute approach for R&D project portfolio selection," *Fuzzy Information and Engineering*, vol. 7, no. 2, pp. 211–225, 2015.

[52] G. Kou, Y. Lu, Y. Peng, and Y. Shi, "Evaluation of classification algorithms using MCDM and rank correlation," *International Journal of Information Technology and Decision Making*, vol. 11, no. 1, pp. 197–225, 2012.

[53] G.-D. Li, D. Yamaguchi, and M. Nagai, "A grey-based decision-making approach to the supplier selection problem," *Mathematical and Computer Modelling*, vol. 46, no. 3-4, pp. 573–581, 2007.

[54] H.-H. Wu, "A comparative study of using grey relational analysis in multiple attribute decision making problems," *Quality Engineering*, vol. 15, no. 2, pp. 209–217, 2002.

[55] Y. Kuo, T. Yang, and G.-W. Huang, "The use of grey relational analysis in solving multiple attribute decision-making problems," *Computers and Industrial Engineering*, vol. 55, no. 1, pp. 80–93, 2008.

[56] W.-S. Lee and Y.-C. Lin, "Evaluating and ranking energy performance of office buildings using Grey relational analysis," *Energy*, vol. 36, no. 5, pp. 2551–2556, 2011.

[57] C.-L. Chang, C.-C. Wei, and Y.-H. Lee, "Failure mode and effects analysis using fuzzy method and grey theory," *Kybernetes*, vol. 28, no. 8-9, pp. 1072–1080, 1999.

[58] G. Wei, J. Shao, Y. Xiang, P. Zhu, and R. Lu, "Obtain confidentiality or/and authenticity in big data by ID-based generalized signcryption," *Information Sciences*, vol. 318, pp. 111–122, 2015.

[59] B. Glavic, "Big data provenance: challenges and implications for benchmarking," in *Specifying Big Data Benchmarks*, pp. 72–80, 2014.

[60] J. Park, D. Nguyen, and R. Sandhu, "A provenance-based access control model," in *Proceedings of the 10th Annual International Conference on Privacy, Security and Trust (PST '12)*, pp. 137–144, Paris, France, July 2012.

[61] H.-C. Chen, I. You, C.-E. Weng, C.-H. Cheng, and Y.-F. Huang, "A security gateway application for End-to-End M2M communications," *Computer Standards and Interfaces*, vol. 44, pp. 85–93, 2016.

[62] R. A. Oliveira, N. Laranjeiro, and M. Vieira, "Assessing the security of web service frameworks against Denial of Service attacks," *Journal of Systems and Software*, vol. 109, pp. 18–31, 2015.

[63] K. Kambatla, G. Kollias, V. Kumar, and A. Grama, "Trends in big data analytics," *Journal of Parallel and Distributed Computing*, vol. 74, no. 7, pp. 2561–2573, 2014.

[64] G. Lafuente, "The big data security challenge," *Network Security*, vol. 2015, no. 1, pp. 12–14, 2015.

[65] National Institute of Standards and Technology—NIST, *Big Data Interoperability Framework: Security and Privacy*, vol. 4, NIST, Gaithersburg, Md, USA, 2015.

[66] R. Iqbal, F. Doctor, B. More, S. Mahmud, and U. Yousuf, "Big data analytics: computational intelligence techniques and application areas," *International Journal of Information Management*, 2016.

[67] J. Chen, Y. Tao, H. Wang, and T. Chen, "Big data based fraud risk management at Alibaba," *The Journal of Finance and Data Science*, vol. 1, no. 1, pp. 1–10, 2015.

[68] J. H. Purba, "A fuzzy-based reliability approach to evaluate basic events of fault tree analysis for nuclear power plant probabilistic safety assessment," *Annals of Nuclear Energy*, vol. 70, pp. 21–29, 2014.

[69] R. Ferdous, F. Khan, R. Sadiq, P. Amyotte, and B. Veitch, "Handling data uncertainties in event tree analysis," *Process Safety and Environmental Protection*, vol. 87, no. 5, pp. 283–292, 2009.

[70] T. V. Garcez and A. T. De Almeida, "Multidimensional risk assessment of manhole events as a decision tool for ranking the vaults of an underground electricity distribution system," *IEEE Transactions on Power Delivery*, vol. 29, no. 2, pp. 624–632, 2014.

[71] T. V. Garcez and A. T. De Almeida, "A risk measurement tool for an underground electricity distribution system considering the consequences and uncertainties of manhole events," *Reliability Engineering and System Safety*, vol. 124, pp. 68–80, 2014.

[72] E.-S. Hong, I.-M. Lee, H.-S. Shin, S.-W. Nam, and J.-S. Kong, "Quantitative risk evaluation based on event tree analysis technique: application to the design of shield TBM," *Tunnelling and Underground Space Technology*, vol. 24, no. 3, pp. 269–277, 2009.

[73] Y. Peng, G. Kou, Y. Shi, and Z. Chen, "A descriptive framework for the field of data mining and knowledge discovery," *International Journal of Information Technology and Decision Making*, vol. 7, no. 4, pp. 639–682, 2008.

[74] D. Feledi and S. Fenz, "Challenges of web-based information security knowledge sharing," in *Proceedings of the 7th International Conference on Availability, Reliability and Security (ARES '12)*, pp. 514–521, Prague, Czech Republic, August 2012.

Hindawi Publishing Corporation
Mathematical Problems in Engineering
Volume 2016, Article ID 4896854, 17 pages
http://dx.doi.org/10.1155/2016/4896854

Research Article

Short-Term Wind Speed Forecasting Using the Data Processing Approach and the Support Vector Machine Model Optimized by the Improved Cuckoo Search Parameter Estimation Algorithm

Chen Wang,[1] Jie Wu,[2] Jianzhou Wang,[3] and Zhongjin Hu[1]

[1]*School of Mathematics & Statistics, Lanzhou University, Lanzhou 730000, China*
[2]*School of Mathematics and Computer Science, Northwest University for Nationalities, Lanzhou 730030, China*
[3]*School of Statistics, Dongbei University of Finance and Economics, Dalian 116025, China*

Correspondence should be addressed to Jie Wu; 13519619146@126.com

Received 28 October 2015; Revised 12 February 2016; Accepted 11 May 2016

Academic Editor: Vida Maliene

Power systems could be at risk when the power-grid collapse accident occurs. As a clean and renewable resource, wind energy plays an increasingly vital role in reducing air pollution and wind power generation becomes an important way to produce electrical power. Therefore, accurate wind power and wind speed forecasting are in need. In this research, a novel short-term wind speed forecasting portfolio has been proposed using the following three procedures: (I) data preprocessing: apart from the regular normalization preprocessing, the data are preprocessed through empirical model decomposition (EMD), which reduces the effect of noise on the wind speed data; (II) artificially intelligent parameter optimization introduction: the unknown parameters in the support vector machine (SVM) model are optimized by the cuckoo search (CS) algorithm; (III) parameter optimization approach modification: an improved parameter optimization approach, called the SDCS model, based on the CS algorithm and the steepest descent (SD) method is proposed. The comparison results show that the simple and effective portfolio EMD-SDCS-SVM produces promising predictions and has better performance than the individual forecasting components, with very small root mean squared errors and mean absolute percentage errors.

1. Introduction

The demand for clean and renewable energy resources has increased significantly since the acid emissions and air pollution caused by burning fossil fuels have heavily polluted the world environment. As a clean and renewable resource, wind energy plays an increasingly vital role in energy supply and wind power generation becomes an important way to generate electrical power. However, the stochastic fluctuation of wind makes it problematic to forecast [1–3]. Therefore, effort to improve the accuracy of wind speed forecasting continues so as to lower the possibility of the power-grid collapse accident occurrence.

Wind speed forecasting is an important foundation and prerequisite for the prediction of wind power generation. The more accurate wind speed forecasting result can reduce wind rotating equipment and operation cost and improve limitation of wind power penetration. At the same time the precise prediction of wind speed helps dispatching department timely adjustments to the program, so as to reduce the impact of wind power on the grid and effectively avoid the adverse effect of wind farm on the power system, enhancing the competitiveness of wind power in the electricity market.

In literature studies, statistically based and neural network-based methods are two models pervasively used to forecast the wind speed [4–7]. With the development of artificial intelligent techniques, some artificial intelligent methods have been presented, such as Artificial Neural Networks, fuzzy logic methods, and support vector machine. Guo et al. [8] presented a wind speed strategy based on the chaotic time series modeling technique and the Apriori algorithm. Barbounis et al. [9] employed three different types of neural network (NN) models to forecast the hourly wind speed (up to 3 days) in a wind park located on the Greek island of Crete. However, there are several unknown parameters in the NN model. Thus, many researchers have indicated the need to

optimize the parameters in the NN model to improve wind speed forecasting accuracy. Wang and Hu [10] improved the performance of the back propagation (BP) NN model in the wind speed forecasting field by optimizing the parameters in the BP model. Both models, that is, the statistical and the NN-based models, have been used by Azad et al. [11] to solve the long-term wind speed forecasting problem for two stations in Malaysia. However, wind speed forecasting results obtained by the neural network models are not always superior to those obtained by other models. Chen and Yu [12] developed a new model by integrating the unscented Kalman filter with the support vector regression-based state-space model. Comparison results indicated that the new proposed model outperforms the NN model. Apart from the NN models, the parameter optimization strategy has also been applied to other wind speed forecasting models. Gani et al. [13] proposed that firefly algorithm combines with SVM algorithm for a problem of short-term wind speed forecast, where firefly algorithm is used to optimize the parameters of SVMs and successfully obtain the accuracy forecasting result. Compared with artificial intelligent models, statistical approaches are less expensive and intrusive and, hence, more practical in forecasting wind power generation. Statistical models are widely used to forecast model for short-term wind forecasting, predicting wind conditions several hours in advance, which is particularly useful for wind power generation [14]. But for the nonlinear wind speed time series is often not satisfactory, especially in multistep prediction, and the error will be significantly increased with the extension of the prediction time. The new paradigm of big data stream mobile computing is quickly gaining momentum [15], while wind speed forecasting results have been applied to many different areas [16].

It is found that the existing wind speed forecasting models have the following disadvantages: (1) some of the existing models have taken no account of the randomness, instability, and the large fluctuation of the wind speed data, which may lead to a high forecasting error. Therefore, in this research, a model based on the ensemble empirical mode decomposition (EEMD) technique is utilized to adaptively decompose the original wind speed data into a finite number of intrinsic mode functions with a similarity property to modeling. (2) The existing traditional parameter estimation methods, such as the moment estimation or the likelihood estimation, are not dynamic and need to solve some equations with a great deal of calculations. Therefore, the artificial intelligent parameter estimation method named the cuckoo search (CS) algorithm is used in this paper to estimate the unknown parameters in the forecasting model. (3) Though some researchers applied the artificial intelligent parameter estimation approaches to the parameter estimation, they just adopted the original approach without considering the deficiency of the approach. Thus, in this paper, the steepest descent (SD) method is used to optimize the CS algorithm so as to enhance the convergence rate. Based on the above motivations, in this research, a new short-term wind speed forecasting portfolio which not only can maintain the characteristics of the wind speed data but can also automatically estimate the unknown parameters in the forecasting model with a considerable convergence rate has been proposed through the following three procedures: (I) data preprocessing: apart from regular normalization preprocessing, the data are preprocessed through the EMD model, which reduces the effect of the noise on the wind speed data; (II) artificially intelligent parameter optimization introduction: the unknown parameters in the support vector machine (SVM) model are optimized by the cuckoo search (CS) algorithm; (III) parameter optimization approach modification: although the original CS algorithm is simple and efficient, it has disadvantages such as insufficient search vigor and slow search speed during the latter part of the search. Therefore, this paper proposes an improved parameter optimization approach based on the CS algorithm and the steepest descent (SD) method, which is abbreviated as the SDCS model. The performance of the developed EMD-SDCS-SVM model has been compared with those obtained by the individual forecasting components using the following two error evaluation criteria: the root mean squared error and the mean absolute percentage error.

The paper is organized as follows: Section 2 introduces related methodologies, Section 3 presents the simulation examples and discussions, and the last section presents concluding remarks.

2. Related Methodologies

2.1. Data Preprocessing Approach. Data preprocessing is a common way to improve forecasting accuracy, especially for data with high noise and different scales. This paper focuses on handling these two problems by using the EMD model and the normalization preprocessing approach, respectively.

2.1.1. Empirical Mode Decomposition Model. The EMD model is an adaptive decomposition approach proposed by Baccarelli et al. [15]. It is used in a wide range of applications, especially in dealing with nonlinear time series. The EMD model decomposes the original time series into several different sequences with different scales (also called the intrinsic mode function (IMF)) as well as a residual sequence. All IMFs must satisfy two requirements:

(a) The number of extreme points (all maximum and minimum points are included) must be equal to the number of zero crossings or differ by no more than one.

(b) In all cases, the average of the envelopes defined by the local maxima and minima must be zero.

With the above two limitations, a signal sequence $x(t)$ can be decomposed with the assistance of the EMD method [16] through the following steps.

Step 1. Calculate all the local extrema (including all the minimum and maximum values).

Step 2. Connect the local maxima by a cubic spline line to generate the upper envelope and similarly produce the lower envelope by connecting all the local minima with a cubic spline interpolation, represented by e_{upper} and e_{lower}, respectively.

Step 3. Calculate the average value of the two envelopes m_1 by

$$m_1 = \frac{\left(e_{\text{upper}} + e_{\text{lower}}\right)}{2}. \tag{1}$$

Step 4. Calculate the difference (h_1) between the data and m_1 by

$$h_1 = x(t) - m_1. \tag{2}$$

Step 5. Judge whether h_1 satisfies the two requirements of the IMFs. If not, regard h_1 as the original signal sequence; then $h_{11} = h_1 - m_{11}$. Repeat this process k times until h_{1k} which is calculated by $h_{1k} = h_{1(k-1)} - m_{1k}$ is an IMF. The first IMF sequence is obtained by

$$\text{IMF}_1 = h_{1k}. \tag{3}$$

Step 6. Calculate the first residual sequence according to

$$r_1 = x(t) - \text{IMF}_1. \tag{4}$$

Step 7. Regard r_1 as the raw data and return to Step 1 to repeat this procedure unless the final residue r_n turns into either a monotonic function or a function from which no more IMF sequences can be extracted.

Finally, the original signal sequence is decomposed into

$$x(t) = \sum_{i=1}^{n} \text{IMF}_i + r_n. \tag{5}$$

2.1.2. Normalization Preprocessing. To improve the training efficiency and the generalization ability of the SVM model, normalization preprocessing is used to address the IMF sequences obtained by the SVM model. Normalization preprocessing is defined as follows:

$$x_{\text{processed}} = \frac{x - x_{\min}}{x_{\max} - x_{\min}}, \tag{6}$$

where x and $x_{\text{processed}}$ represent the original data sequence and the preprocessed data sequence, respectively, and $x_{\min}$ and $x_{\max}$ denote the minimum and the maximum data in the original data sequence, respectively.

2.2. Support Vector Machine Model. The SVM model is the core of statistical machine learning theories. It can surmount difficulties that appear in the traditional machine learning methods, such as the curse of dimensionality, easily falling into local optima and overlearning. In addition, it has great generalization ability [17]. Therefore, the SVM model has long been an attractive tool with powerful capabilities in solving classification and regression problems. In this paper, we mainly focus on the SVM model for regression.

Suppose that there are m in-sample data points (or training samples) $(x_1, y_1), (x_2, y_2), \ldots, (x_m, y_m)$ where $x_i \in R^n$ denotes the input vector and $y_i \in R$ is the targeted output corresponding to the input vector x_i. The main purpose of the SVM for regression is to find a function $f(x)$ which satisfies the following two requirements: (a) the deviation between $f(x_i)$ and y_i is no greater than a given positive real number ε, for all $i = 1, 2, \ldots, m$, and (b) $f(x)$ is as flat as possible. In the SVM algorithm, f is defined by the formula

$$f(x) = \omega^T \phi(x) + b, \tag{7}$$

where $\phi : R^n \to F$ is a nonlinear mapping, b is the threshold value, and the unknown coefficients ω and b can be estimated by solving the following optimization problem:

$$\min_{\omega,b,\xi,\xi^*} \quad \frac{1}{2}\|\omega\|^2 + C\sum_{i=1}^{m}\left(\xi_i + \xi_i^*\right) \tag{8}$$

$$\begin{aligned} \text{subject to:} \quad & \left[\omega^T \phi(x) + b\right] - y_i \le \varepsilon + \xi_i \\ & y_i - \left[\omega^T \phi(x) + b\right] \le \varepsilon + \xi_i^* \\ & \xi_i, \xi_i^* \ge 0, \ i = 1, 2, \ldots, m, \end{aligned} \tag{9}$$

where C denotes the penalty coefficient, ξ_i and ξ_i^* are two slack variables, and ε is the tube size. Problem (8) can be solved by introducing two Lagrange multipliers α_i and α_i^* and minimizing the following Lagrange function L [14]:

$$\begin{aligned} L &= -\frac{1}{2}\sum_{i,j=1}^{m}\left(\alpha_i - \alpha_i^*\right)\left(\alpha_j - \alpha_j^*\right)\kappa\left(x_i, x_j\right) \\ &\quad - \varepsilon\sum_{i=1}^{m}\left(\alpha_i + \alpha_i^*\right) + \sum_{i=1}^{m} y_i\left(\alpha_i - \alpha_i^*\right) \\ L &= -\frac{1}{2}\sum_{i,j=1}^{m}\left(\alpha_i - \alpha_i^*\right)\left(\alpha_j - \alpha_j^*\right)\kappa\left(x_i, x_j\right) \\ &\quad - \varepsilon\sum_{i=1}^{m}\left(\alpha_i + \alpha_i^*\right) + \sum_{i=1}^{m} y_i\left(\alpha_i - \alpha_i^*\right) \end{aligned} \tag{10}$$

subject to

$$\sum_{i=1}^{m}\left(\alpha_i - \alpha_i^*\right) = 0, \quad 0 \le \alpha_i, \alpha_i^* \le C. \tag{11}$$

This calculation results in

$$\begin{aligned} \omega &= \sum_{i=1}^{m}\left(\alpha_i - \alpha_i^*\right)\phi(x), \\ f(x) &= \sum_{i=1}^{m}\left(\alpha_i - \alpha_i^*\right)\kappa\left(x_i, x\right) + b, \end{aligned} \tag{12}$$

where $\kappa(\cdot,\cdot)$ is called the kernel function. The following four types of kernel functions are commonly used [18, 19]: (a) linear kernel function: $\kappa(x, y) = x^T y$, (b) polynomial kernel function: $\kappa(x, y) = (x^T y + 1)^d$, (c) sigmoid kernel function: $\kappa(x, y) = \tanh(ax^T y + c)$, and (d) Gaussian kernel function: $\kappa(x, y) = \exp(-\|x - y\|^2/2\sigma^2)$, where a, c, d, and σ are kernel parameters.

(1) Determine the objective function $g(x)$, $x = (x_1, x_2, \ldots, x_d)^T$;
(2) Initialize the population of N host nests x_i ($i = 1, 2, \ldots, N$);
(3) **WHILE** (*The stop criterion has not met*)
(4) *Choose a cuckoo randomly by Lévy flights and evaluate its goodness of fit or quality* G_i;
(5) *Choose a nest among* N (*say* j) *randomly*;
(6) **IF** ($G_i > G_j$)
(7) Replace j by the new solution;
(8) **END IF**
(9) *Abandon a fraction* (p_a) *of worse nests and build new ones*;
(10) *Keep the best solutions* (*or nests with quality solutions*);
(11) Rank the solutions and find the current best solution;
(12) **END WHILE**
(13) *Post-process results;*

Algorithm 1: CS algorithm.

2.3. Artificial Intelligent Parameter Optimization

2.3.1. Original Cuckoo Search Algorithm. The CS algorithm was first developed by Sun et al. [20] in 2007. It is derived from the action of cuckoos laying their eggs in the nests of other birds to let those birds hatch eggs for them. However, once the host birds discover the cuckoo eggs, these eggs will be thrown away or the host birds will abandon their nests and rebuild a new nest elsewhere. The CS algorithm is constructed based on three assumptions: (a) Only one egg is laid by each cuckoo in a randomly selected nest; (b) The best nests will be carried over to the following generations; and (c) The number of available host nests is a constant, and the probability value of an egg laid by a cuckoo being discovered by the host bird is p_a which has the range of 0 to 1.

In the CS algorithm, each nest represents a solution. The pseudo code of the CS technique [21] presented in Algorithm 1 can aid in understanding the CS process.

The Lévy flight mentioned in the pseudo code of Algorithm 1 is generated according to:

$$x_i^{t+1} = x_i^t + \alpha \oplus \text{Lévy}(\lambda), \tag{13}$$

where $\alpha > 0$ is the step size, which should be related to the scale of the problem of interest. The product $\oplus$ indicates entry-wise multiplication location. A Lévy flight is considered when the step-lengths are distributed according to the following probability distribution:

$$\text{Lévy} \sim u = t^{-\lambda}, \quad 1 < \lambda \leq 3 \tag{14}$$

which has an infinite variance. Here, the consecutive steps of a cuckoo search essentially form a random walk process that obeys a power-law step-length distribution with a heavy tail.

2.3.2. Modified Cuckoo Search Method. Similar to other metaheuristic algorithms, the original CS algorithm is simple and efficient; however, it has disadvantages such as insufficient search vigor and slow search speed during the latter part of the search. As one of the oldest optimization algorithms, the steepest descent (SD) method [22] is simple and intuitive. Currently, there are many effective optimization algorithms established on the basis of this algorithm. In order to overcome the CS's shortcoming of slow convergence rate, the SD method is used to modify the CS algorithm, and the modified model is abbreviated as the SDCS model. In the SDCS model, the following equation substitutes for (13):

$$x_i^{t+1} = x_i^t + d_i^t, \tag{15}$$

where d_i^t is defined by

$$d_i^t = -\nabla g\left(x_i^t\right). \tag{16}$$

The SDCS process can be expressed by the following procedures.

Step 1. Initialize the initial points x^0, the end error $\varepsilon > 0$, and set $k = 0$.

Step 2. Calculate $\nabla f(x^k)$. If $\|\nabla f(x^k)\| = \| - \nabla g(x_i^k)\| \leq \alpha \oplus \text{Lévy}(\lambda) \leq \varepsilon$, terminate the iteration and output the value of x^k. Otherwise, go to Step 3.

Step 3. Set $p^k = -\nabla f(x^k)$.

Step 4. Conduct one-dimensional search. Get the value of t_k which satisfied equation $f(x^k + t_k p^k) = \min_{t \geq 0} f(x^k + t p^k)$; then set $x^{k+1} = x^k + t_k p^k$, $k := k + 1$, and return to Step 2.

The step size and step-length distribution function of the CS algorithm can be improved by using steepest descent due to its simplicity and flexibility. The final optimal solution can be obtained by modifying the step size and step-length distribution function constantly.

2.4. Proposed Novel Model. Based on the above methodologies, we propose a novel short-term wind speed forecasting portfolio with three steps (Figure 1): (I) data preprocessing: both the regular normalization preprocessing model and the EMD approach are used for data preprocessing, which reduces the effect of noise and different scales on the wind speed data; (II) artificially intelligent parameter optimization

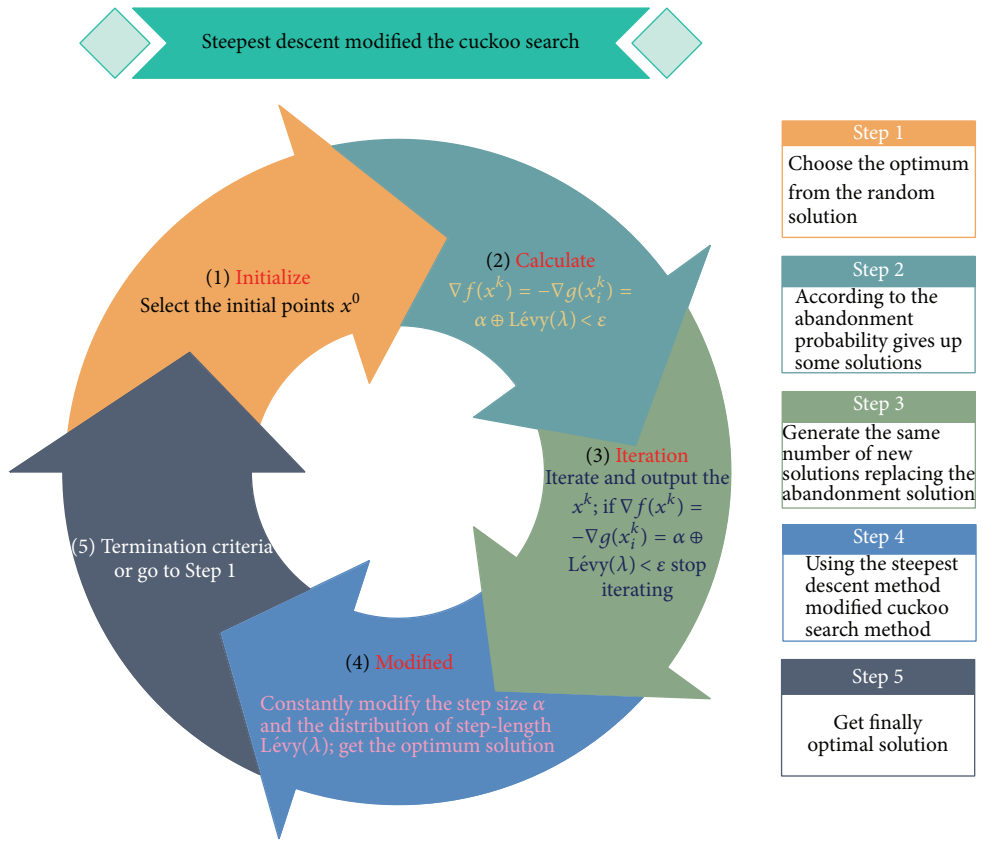

Figure 1: Flowchart of the SDCS algorithm.

introduction: the unknown parameters in the SVM model are optimized by the CS algorithm; (III) parameter optimization approach modification: although the original CS algorithm is simple and efficient, it has disadvantages such as insufficient search vigor and slow search speed during the latter part of the search. Therefore, this paper proposes an improved parameter optimization approach based on the CS algorithm and the steepest descent (SD) method, which we call the SDCS model. The final forecasting model is called the EMD-SDCS-SVM model.

The performance of SVM depends on a good set of parameters, including the penalty parameter and the parameter of the kernel function. The parameter adjustment and selection of support vector machine is still a difficult issue in the research field. The generalization performance of support vector machine is closely related to the selection of specific parameters in the model. The parameter of penalty coefficient C and kernel parameters σ must be selected by the users. However, in practical applications, the forecasting complexity control is more difficult, because the parameters of C and σ must be adjusted simultaneously.

(1) The Penalty Coefficient C. The penalty coefficient C is to balance the model between the complexity and the training error, so that the model has better extending ability. Furthermore, the parameter C can control the robustness of the forecasting model. The different training groups have different optimal values. For forecasting problems, if the parameter C is smaller, the punishment for miscalculation samples in the sample data is smaller. As a result, the training error becomes larger, and the system's generalization ability is poorer. When new data is forecasted by the model, the fitting error will be very high, and the phenomenon of "less learning" will appear. On the contrary, if the parameter C is too large, the weight of $(1/2)\|\omega\|^2$ will be smaller. Although the fitting error of the available data is very low, the fitting error of the new data is also very high. It is the so-called "overlearning" phenomenon. The generalization ability of the model is still very poor. Each sample data group has at least one suitable C, which makes the SVM generalization performance the best. Therefore, the correct choice of parameter C can improve the prediction accuracy of the model.

(2) The Kernel Function σ. For the kernel function of the SVM, the linear kernel function, polynomial kernel function, radial basis kernel function, and sigmoid function are usually the most used. The width σ of radial basis function is the same to all kernel functions, and σ can reflect corresponding width of inner product kernel for input. If σ is too small, it will lead to overfitting or memory of the training group. If σ is too large, it will make SVM discriminant function too gentle. Width of kernel function σ and the penalty coefficient C affect the shape of prediction curve of the support vector machine from different angles. In practical applications, too large or

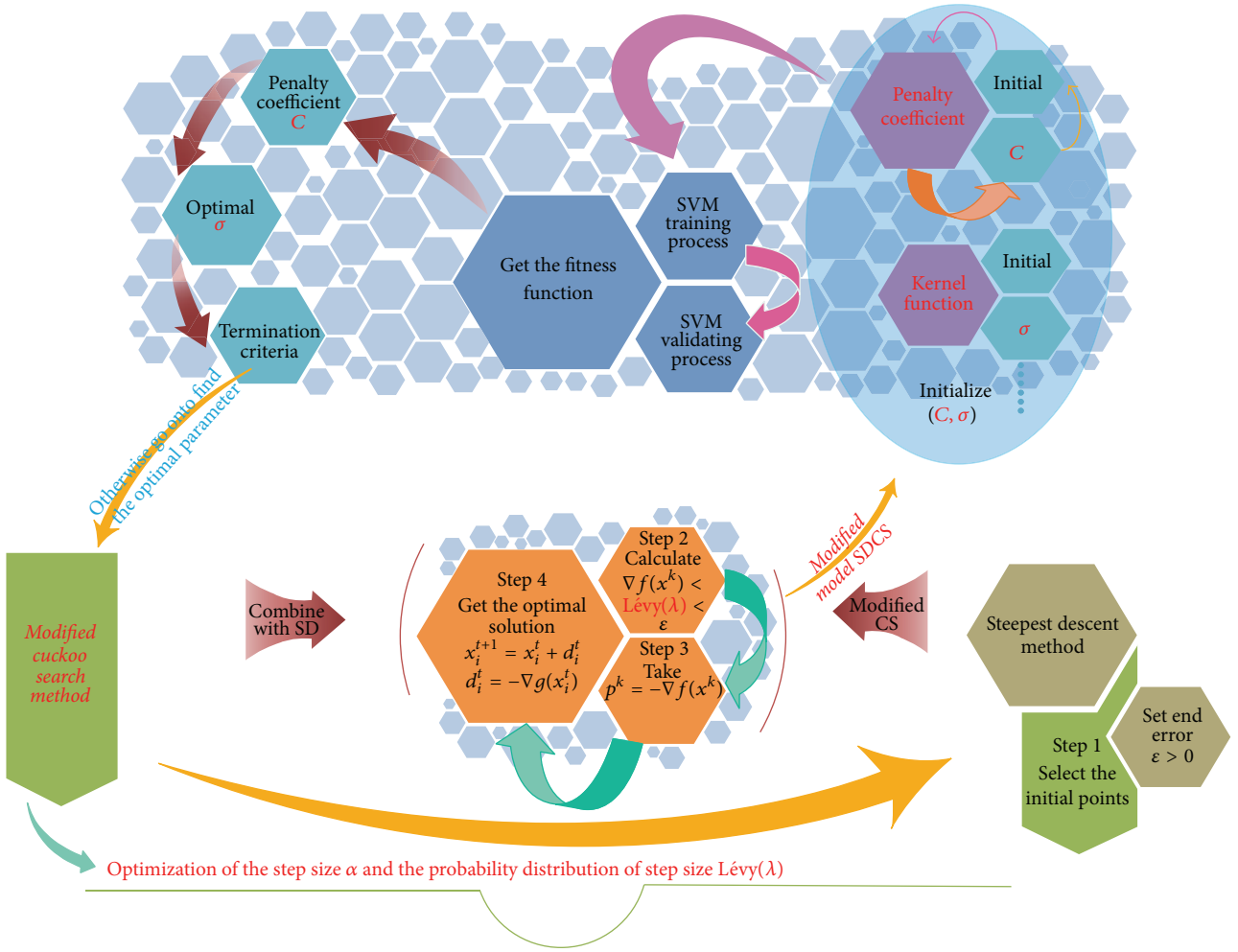

Figure 2: Process of objective model.

too small penalty coefficient C and kernel function σ will make the generalization performance of the support vector machine worse.

Based on the analysis of influences of each parameter on the performance of SVM, we put forward the time series forecasting model by using modified cuckoo search (SDCS) algorithm to optimize SVM parameters. It not only maintains the characteristics of time series, but also can select the parameters of SVM automatically, which eliminates the blindness and randomness caused by artificial selection. The main procedures of this EMD-SDCS-SVM are as follows.

Procedure 1. Collect wind speed time series data. Use the EMD to preprocess the wind speed data and reconstitute the new wind speed time series, which will be treated as the training sample of the SVM model.

Procedure 2. Determine the range of C and σ, the maximum step ($\text{step}_{\max}$), the minimum step ($\text{step}_{\min}$), and the maximum number of iterations $N_{\max}$. Set the probability of an egg laid by a cuckoo being discovered by the host bird as $p_a = 0.25$, and initialize the number of the host nests as $N = 25$. Each nest corresponds to a two-dimensional vector (C, σ).

Procedure 3. Search the optimum value of the two-dimensional vector (C, σ) according to the SDCS algorithm, and the detailed steps that need to be implemented in this procedure are shown in Figure 2.

Procedure 4. Use the optimum parameter values obtained in Procedure 3 and the processed data obtained in Procedure 1 to construct the forecasting model and obtain the forecasting results.

3. Simulation Examples and Discussions

3.1. Data Division and Parameter Initialization. Wind speed data recorded by four wind turbines (numbered #1, #2, #3, and #4) during the period from Jan 2, 2011, to Jan 6, 2011, with a time resolution of 10 minutes are used to verify the effectiveness of the new proposed hybrid model. The data from Jan 2 to Jan 5 are adopted as the in-sample data (i.e., training data), while those on Jan 6 are used as the out-of-sample data (i.e., testing data).

Step 1. The original wind speed series are decomposed into a high-frequency component and a low-frequency component,

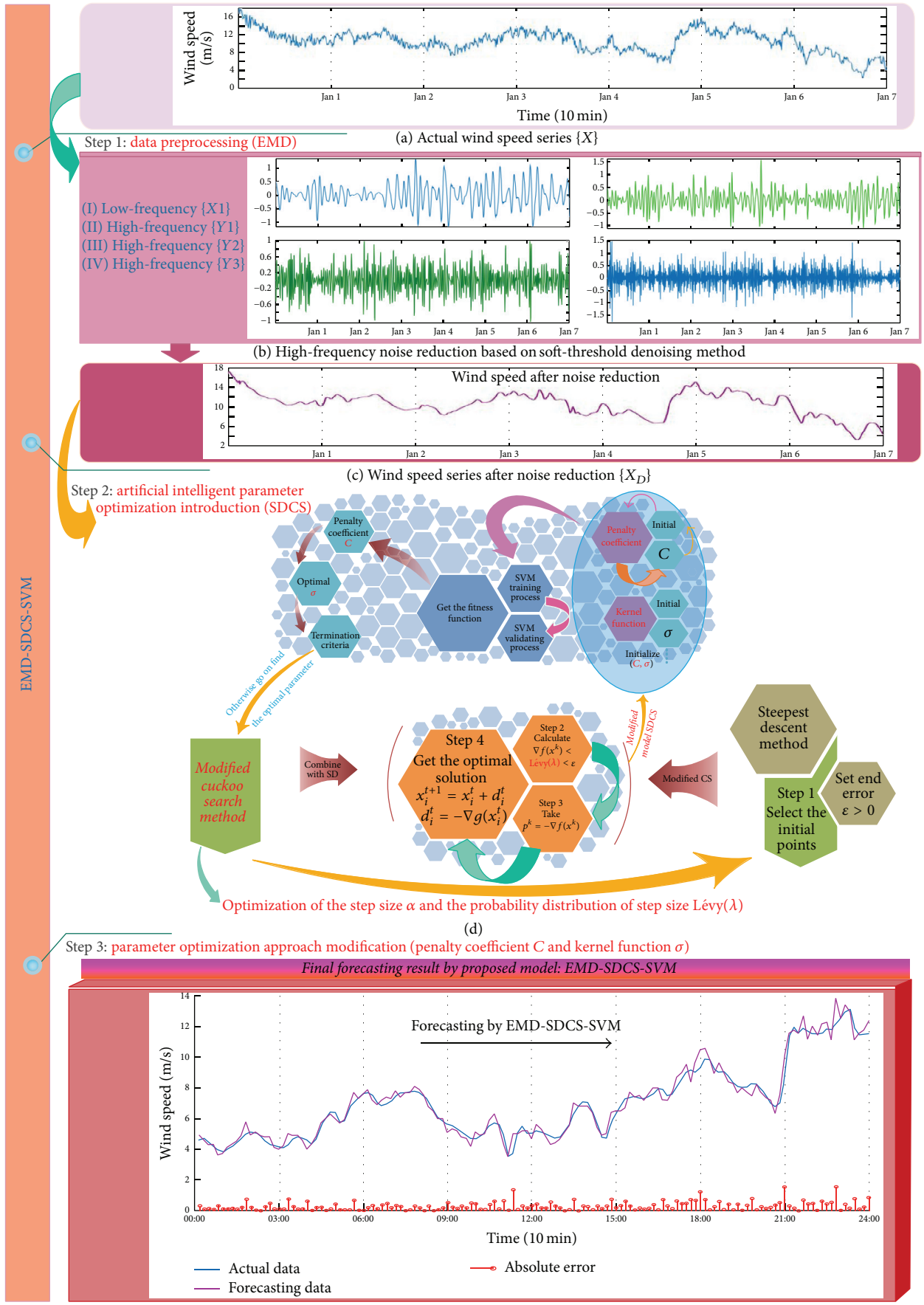

Figure 3: Procedures of the proposed forecasting portfolio.

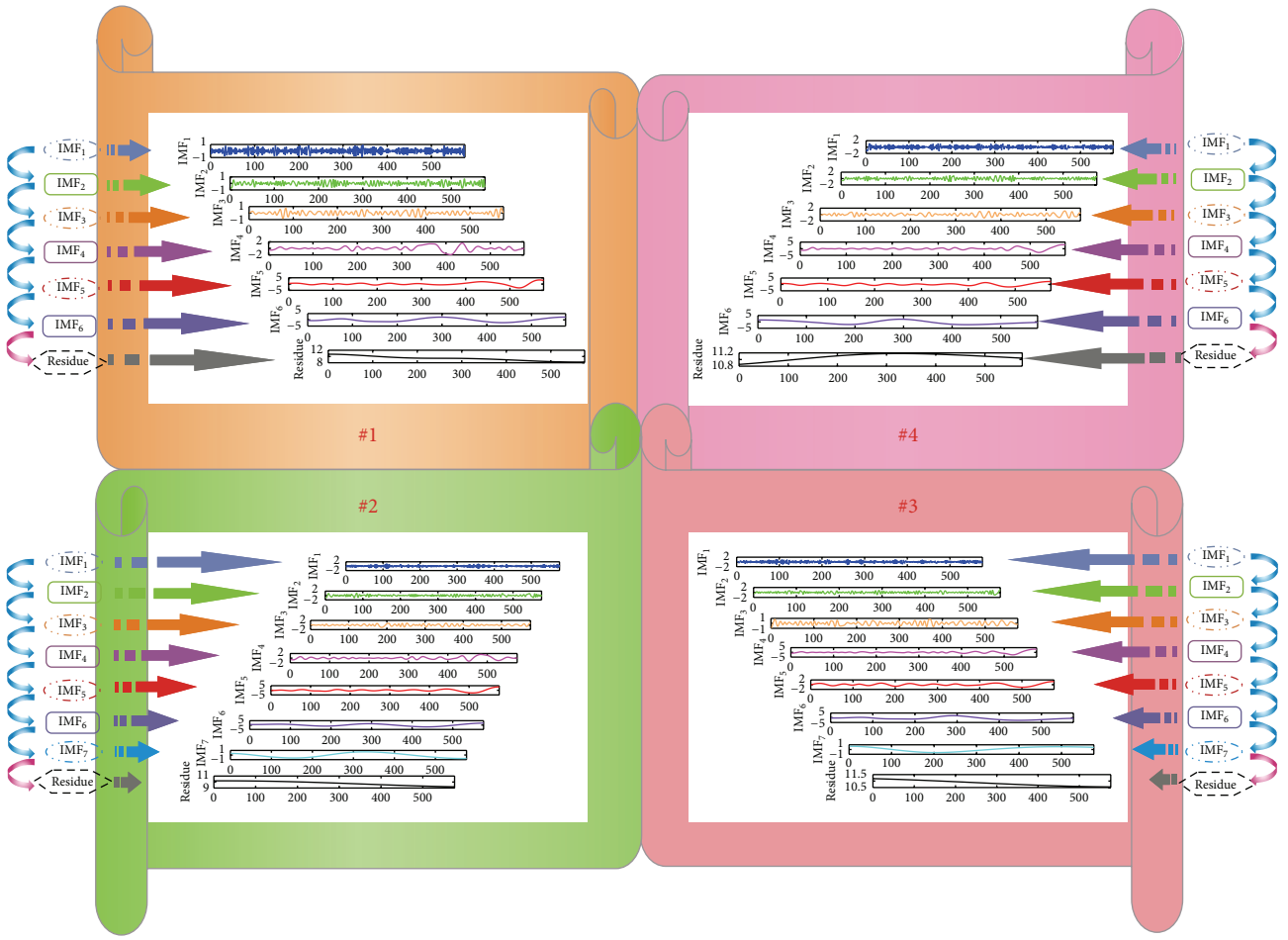

Figure 4: IMFs and residue results obtained by the EMD method.

which represents the noise signal and main features of the wind speed series (see Figures 3(a)–3(c)).

Step 2 (data splitting and normalization). The available wind speed series after noise reduction are split into the training set and the test set, which are denoted by including input sets and output sets for training parameters of SVM and consisting of inputs and outputs for the testing model's forecasting effectiveness, respectively. To establish the model, the training datasets and the input test sets are normalized with the same setting (see Figure 3(d)).

Step 3 (initialization: a SVM with two parameters). The penalty coefficient C and the kernel function σ are shown in Figure 3(e). The number of connection weights of the SVM is the size of the cities in the SDCS algorithm, namely, the dimension of the optimized parameters.

Step 4 (optimization). The objective function of the SDCS algorithm is given as follows:

$$x_i^{t+1} = x_i^t + \alpha \oplus \text{Lévy}(\lambda). \tag{17}$$

Step 5 (SVM construction). The best solution obtained by the SDCS algorithm is set to be the final connection weights of SVM training and construction. The terminal condition of network training is set to be the reach of maximum iterations or no further improvement (see Figures 3(d)–3(e)).

Step 6 (EMD-SDCS-SVM construction for the test dataset). The forecasting data of the output test sets are generated by importing the input test sets based on the established optimal SVM (see Figure 3(e)).

Step 7 (evaluation). The quality of the EMD-SDCS-SVM is assessed by the indices SDCS and SVM, which presents the validity and informativeness of EMD, respectively. With the aim of comprehensive evaluation, MAPE is calculated as well.

To employ the methodologies introduced in Section 2 of this paper, the parameters contained in the models are initialized as follows: in the CS algorithm, the number of the host nests is initialized as $N = 25$, and the probability of an egg laid by a cuckoo being discovered by the host bird is given as $p_a = 0.25$. The Gaussian kernel function is chosen for the SVM method. In the GA algorithm, the maximum number of iterations is initialized as 50, and the population size is 100. The probability of cross is 0.3 and the probability of mutation is 0.1. When the CS algorithm and GA are adapted for SVM

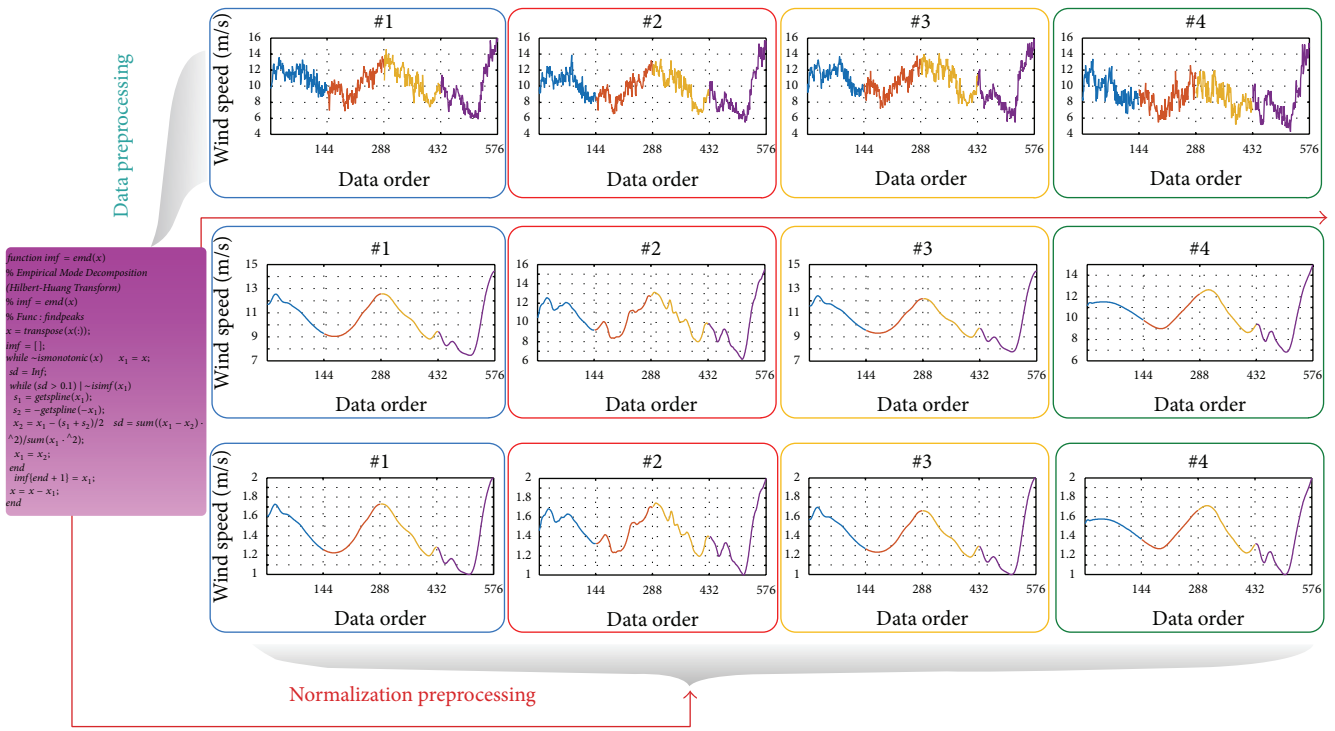

Figure 5: Denoised and normalized results of the original data.

optimization, the search interval of the penalty coefficient C is set to $[0.1, 100]$, while the search interval of the kernel function is set to $[0.01, 1000]$.

3.2. Data Preprocessing Results. Wind speed data are first preprocessed by the EMD method. Figure 4 shows the IMFs and residue results obtained by the EMD method for the four wind turbines. As indicated in Figure 4, for the #2 and #3 wind turbines, 7 IMF sequences are extracted from the original wind speed training dataset, while 6 IMF sequences are extracted for the other two wind turbines. According to the principle of denoising, eliminating the high-frequency sequence from the IMF sequences can assist in obtaining cleaner data sequence, that is, data sequence with lower noise. For this paper, the first IMF sequence obtained by the EMD method is eliminated from the original data sequence to improve the accuracy of wind speed forecasting. The visualization of the denoise preprocessing of the EMD method of the four wind turbines is shown in Figure 5. The final results after denoise processing with the EMD method and the normalization operation are also presented in Figure 5.

3.3. Forecasting Results. To validate the effectiveness of the EMD-SDCS-SVM model in wind speed forecasting, the model is used to forecast wind speed with four horizons: 1-step-ahead, 2-step-ahead, 4-step-ahead, and 6-step-ahead. The forecasting results obtained by this model are compared with those obtained by the nonparameterization method EMD-SVM, the unmodified parameterization method EMD-CS-SVM, and another parameterization method, EMD-GA-SVM, where GA is the abbreviation for the Genetic Algorithm [23].

Figure 6 presents the forecasting results of the four EMD-based models. In this figure, the wind speed data in the center of the circular rings with the value of 0 is the smallest, while the bigger the radius, the larger the wind speed value. The difference of the radius between each adjacent two circular rings is 5. As shown in Figure 6, the forecasting results obtained by these EMD-based models fit the actual wind speed data best when the forecasting horizon is 1-step-ahead, while the fit is the worst in the 6-step-ahead situation; that is, the deviation between the wind speed data forecast by the models and the actual wind speed data becomes larger as the forecasting horizon increases. In addition, the EMD-SVM and the EMD-GA-SVM methods deviate much more significantly from the actual data when compared to the other models.

In addition, the forecast results obtained by these models are analyzed according to the Quantile-Quantile (Q-Q) plot. The f quantile corresponding to a datum $q(f)$ means that approximately a decimal fraction f of the data can be found below the datum. The f quantile is calculated in the following manner: sort the data in a sequence $\{x_j\}_{j=1,2,\ldots,n}$ in an ascending order. The sorted data $\{x_{\langle i\rangle}\}_{i=1,2,\ldots,n}$ have rank $i = 1, 2, \ldots, n$. Then, the quantile value f_i for the datum $x_{\langle i\rangle}$ is computed by

$$f_i = \frac{i - 0.5}{n}. \tag{18}$$

Figure 6: Forecasting results comparisons among EMD-modified models.

The 0.25, 0.5, and 0.75 quantiles are called the lower quantile, the median, and the upper quantile, respectively. The Q-Q plot is used to compare the quantiles of two samples. If the two samples come from the same type of distribution, the plot will be a straight line. A straight reference line that passes through the lower quantile and the upper quantile is helpful for assessing the Q-Q plot. The greater the distance from this reference line, the more likely it is that the two samples come from populations with different distributions. The vertical and the horizontal axes of the Q-Q plot are the estimated quantiles from the two samples, respectively. If the sizes of these two samples are the same, the Q-Q plot is just a plot of the sorted data in the first sample against the sorted data in the second sample. As an example, Figure 7 provides an empirical Q-Q plot of the quantiles of the actual wind speed sequence versus the quantiles of the forecast data for the #4 wind turbine, where X represents the actual wind speed data sequence, and $Y1$, $Y2$, $Y3$, and $Y4$ denote the wind

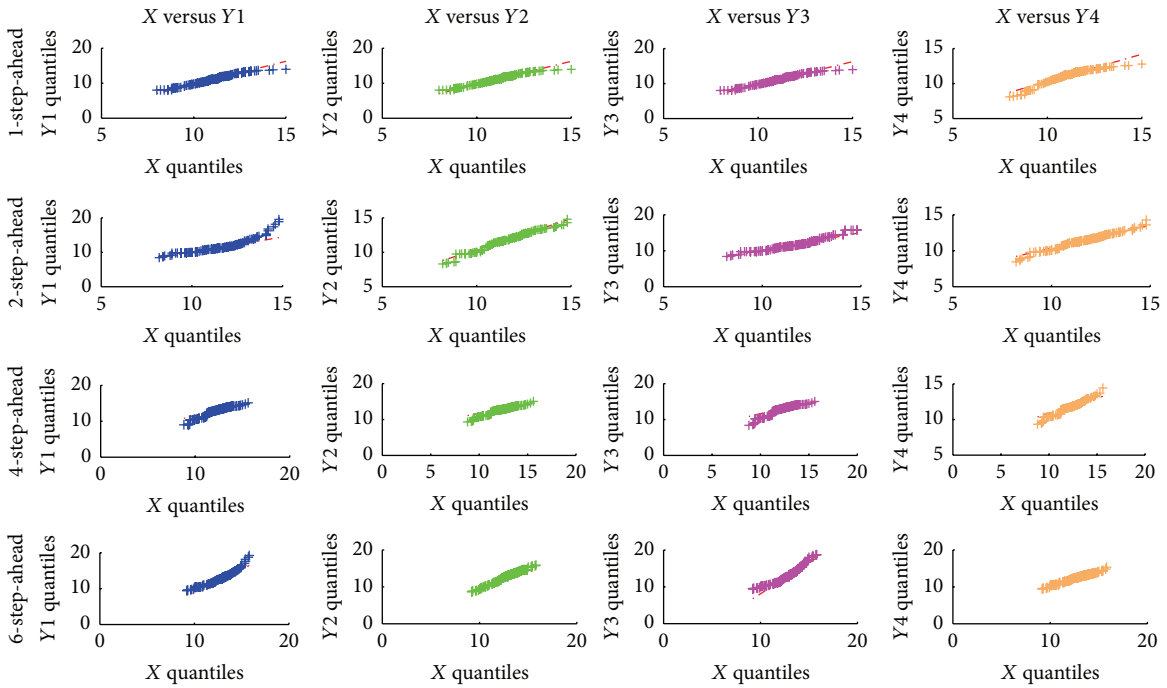

Figure 7: Empirical Q-Q plot of the quantiles of the actual wind speed sequence versus the quantiles of the forecasted data for the #4 wind turbine.

speed data sequences forecasted by the EMD-SVM model, the EMD-CS-SVM model, the EMD-GA-SVM model, and the EMD-SDCS-SVM model, respectively. The straight line shown in each subplot is just the extrapolated line which joins the lower and the upper quantiles, and the vertical axis and the horizontal axis in each subplot are the estimated quantiles from the corresponding forecast data sequence and the actual data sequence. As observed from Figure 7, the forecast values sometimes are larger than the actual values (corresponding to the plus symbol located above the straight line), while sometimes they are smaller than the actual values (corresponding to the plus symbol located below the straight line). Figure 7 also reveals that the EMD-SDCS-SVM model fits the actual wind speed data best when compared to the other three models.

3.4. Forecasting Error Comparison. Results presented in Section 3.2 provide graphical visualization of the performance of the different forecasting models. In this section, the superior performance of the EMD-SDCS-SVM model is shown quantitatively. To do this, two error evaluation criteria named the root mean squared error (RMSE) and the mean absolute percentage error (MAPE) are adopted and defined as follows:

$$\text{RMSE} = \sqrt{\frac{1}{n}\sum_{i=1}^{n}\left(x_i - \widehat{x}_i\right)^2},$$
$$\text{MAPE} = \frac{1}{n}\sum_{i=1}^{n}\left|\frac{x_i - \widehat{x}_i}{x_i}\right| \times 100\%, \tag{19}$$

where n is the number of data points in the out-of-sample data and x_i and $\widehat{x}_i$ are the actual value and the forecasted value, respectively.

From Table 1 and Figure 8, it can be seen that compared to the ANN forecasting models, the SVM models perform favorable forecasting accuracy; in particular in four- and six-step-ahead forecasting result, the SVM is superior to the ANN model of BPNN, Elman NN, and WNN.

The forecasting error results with different forecasting horizons of these 4 models are given in Table 2 and Figure 9. As observed from Table 2 and Figure 9, the forecasting error values become larger as the forecasting horizon increases. For the #1, #2, and #4 wind turbines, the EMD-SDCS-SVM model always obtains more accurate wind speed forecasting results than the other three models. In addition, for the #3 wind turbine, the EMD-SDCS-SVM model is superior to both the EMD-SVM and the EMD-CS-SVM models, which means that the proposed novel model EMD-SDCS-SVM has made promising predictions and has better performance than its individual forecasting components.

4. Conclusions

Wind speed forecasting plays a significant part in the economy and security of wind farm systems' operation. Accurate forecasting results have significant influence on the economy. Recently, academia and industry have paid more attention to wind speed forecasting. More accurate forecasting could reduce costs and risks, improve the security of power systems, and help administrators develop an optimal action program,

Table 1: Forecasting error results between SVM and ANN forecasting model.

Horizon	Wind turbine	Error type	SVM	BPNN	Elman NN	WNN	ARIMA	Horizon	Wind turbine	Error type	SVM	BPNN	Elman NN	WNN	ARIMA
1-step-ahead	1#	MSE	0.7306	1.9341	1.5646	2.3015	0.8544	4-step-ahead	1#	MSE	0.8133	2.1649	2.181	3.1542	1.2014
		MAPE	6.72	11.22	11.18	13.71	4.741			MAPE	7.01	12.25	14.03	17.81	6.882
	2#	MSE	0.4339	0.9645	1.1323	2.6048	0.9006		2#	MSE	0.8471	3.2995	2.1403	5.0735	1.5609
		MAPE	5.36	8.87	8.99	13.06	5.889			MAPE	7.58	14.08	12.99	20.23	7.373
	3#	MSE	0.4838	2.5618	1.4261	1.7689	0.9942		3#	MSE	0.8871	3.1718	2.7741	4.7698	1.8086
		MAPE	5.37	13.73	10.65	12.73	6.218			MAPE	7.19	14.28	15.76	19.77	7.280%
	4#	MSE	0.7954	1.8717	1.5713	3.2243	2.4862		4#	MSE	1.4467	3.6119	3.1221	6.4129	1.7779
		MAPE	8.19	12.73	12.11	14.13	7.283			MAPE	11.26	17.69	16.59	19.94	7.821
2-step-ahead	1#	MSE	0.639	1.2661	1.8282	3.6953	1.0663	6-step-ahead	1#	MSE	1.0364	2.708	2.6968	4.1962	1.3271
		MAPE	6.19	9.31	12.70	17.74	5.922			MAPE	8.03	13.56	16.90	18.40	6.709
	2#	MSE	0.5788	1.2924	1.6292	3.2163	1.0885		2#	MSE	1.0511	3.5101	2.5112	5.6064	2.0692
		MAPE	6.31	10.74	10.66	16.69	6.154			MAPE	8.44	14.90	14.27	22.60	7.954
	3#	MSE	0.6497	2.9984	1.8137	2.5426	1.5840		3#	MSE	1.0549	2.6744	2.9361	6.5295	1.3540
		MAPE	6.27	13.72	13.08	13.14	5.648			MAPE	7.84	12.49	16.29	20.57	7.380
	4#	MSE	1.0798	3.8907	1.8167	2.671	1.4168		4#	MSE	1.7788	4.7215	3.7118	4.8947	2.7558
		MAPE	9.58	18.82	13.46	15.94	6.955			MAPE	12.40	22.09	19.21	20.59	10.446

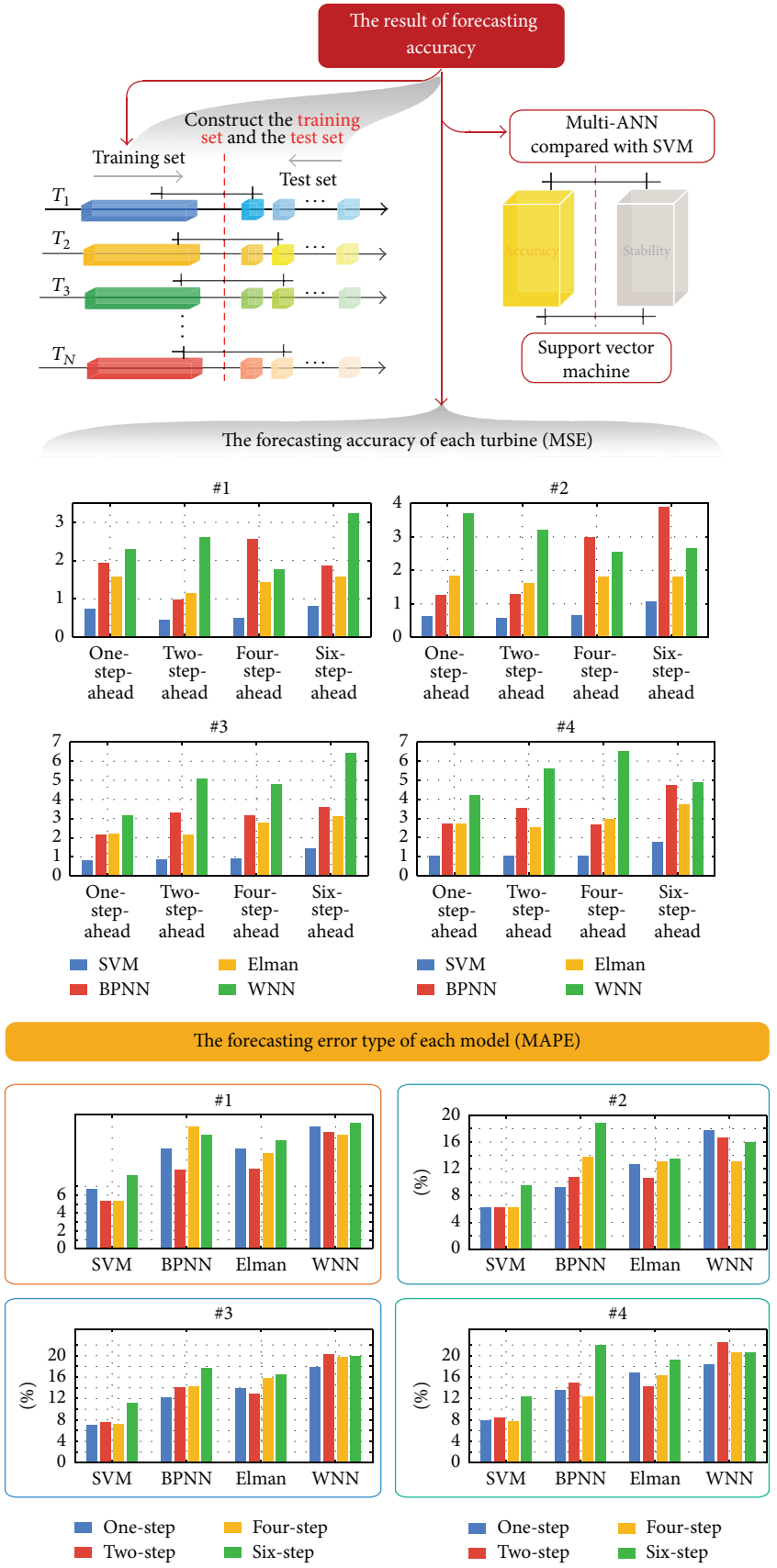

Figure 8: Forecasting results of SVM and others ANN.

Table 2: Forecasting error results with different forecasting horizons.

Horizon	Wind turbine	Error type	EMD-SVM	EMD-GA-SVM	EMD-CS-SVM	EMD-FA-SVM	EMD-SDCS-SVM	Horizon	Wind turbine	Error type	EMD-SVM	EMD-GA-SVM	EMD-CS-SVM	EMD-FA-SVM	EMD-SDCS-SVM
1-step-ahead	#1	MSE	0.6798	0.6798	0.6798	0.6460	0.6382	4-step-ahead	#1	MSE	0.9262	0.9262	0.9262	1.5420	0.7883
		MAPE	4.6937	4.6937	4.6937	4.924	4.4052			MAPE	6.3854	6.3854	6.3854	7.103%	5.5685
	#2	MSE	0.8628	0.8226	0.8534	0.9262	0.7959		#2	MSE	1.256	1.0524	1.1339	0.9147	1.011
		MAPE	6.0093	5.8184	5.9602	5.327	5.597			MAPE	8.2016	7.279	7.8073	6.197	6.8343
	#3	MSE	0.8256	0.7907	0.8304	0.9553	0.803		#3	MSE	1.0914	0.9676	1.1172	1.1185	1.0714
		MAPE	5.5431	5.2876	5.5765	6.234	5.2886			MAPE	7.2059	6.4716	7.3004	6.897	6.8158
	#4	MSE	0.8657	0.8514	0.9065	0.7401	0.8135		#4	MSE	1.1689	1.1094	1.3419	1.0754	1.0149
		MAPE	5.5708	5.5101	5.8196	5.493	5.1737			MAPE	6.8888	6.526	7.7831	6.548%	6.0562
2-step-ahead	#1	MSE	0.7707	0.7707	0.7707	0.9932	0.7184	6-step-ahead	#1	MSE	0.9982	0.9982	0.9982	1.8679	0.8342
		MAPE	5.3944	5.3944	5.3944	5.006	5.0049			MAPE	6.9568	6.9568	6.9568	9.435	5.898
	#2	MSE	1.0091	0.9242	0.9806	0.7437	0.8885		#2	MSE	1.4805	1.0856	1.2166	2.2042	1.0627
		MAPE	6.8987	6.4877	6.7938	5.892	6.0704			MAPE	8.9118	7.6722	8.3732	8.378%	7.0088
	#3	MSE	0.8876	0.8259	0.8963	1.2746	0.8674		#3	MSE	1.1505	0.9688	1.1615	1.7628	1.0857
		MAPE	5.9299	5.5404	5.9339	7.069	5.5753			MAPE	7.8968	6.643	7.9065	6.910	6.949
	#4	MSE	0.9916	0.9558	1.0946	1.0891	0.8804		#4	MSE	1.2147	1.0537	1.5362	2.8053	0.981
		MAPE	6.2854	5.8933	6.8798	6.587	5.4089			MAPE	7.3785	6.423	8.9868	8.532	6.1465

Figure 9: MSE and MAPE visualization of the four wind turbines.

thereby enhancing the economic social benefits of power-grid management. Therefore, it is highly desirable to develop techniques for wind speed forecasting to improve accuracy. However, individual models do not always achieve a desirable performance. The proper selection method of a hybrid model can reduce certain negative effects that are inherent to each of these individual models; moreover, the hybrid forecasting model can make full use of the advantages of each of the individual models and is less sensitive, in certain cases, to the factors that make the individual models perform in an undesirable manner.

In this paper, to enhance the forecasting capacity of the proposed combined model, consisting of three procedures, the data preprocessing procedure, the artificial intelligent parameter optimization introduction procedure, and the parameter optimization approach modification procedure were integrated. The SVM model used in this paper can handle data with nonlinear features, and the SD technique is adopted to enhance the convergence speed of the CS algorithm, which is utilized to optimize the parameters in the SVM model. The effectiveness and robustness of the proposed approach has been successfully tested by the real wind speed data sampled at four wind turbines. Based on the Q-Q plot and the error comparison, results show that the developed portfolio EMD-SDCS-SVM has made promising predictions and has better performance than its individual forecasting components despite very small MAPE and MSE values. For instance, the average MAPE values of the combined model were 0.7138%, 1.0281%, 4.8394%, 0.9239%, and 7.3367%, which are lower than those of BPNN, WNN, and Elman NN. By improving forecasting accuracy and stability, in the wind farm, a large amount of money and energy could be saved. The hybrid model can be applied to forecast the wind speed that can be used in wind power scheduling to produce various benefits, saving on economic dispatching, reducing production costs, and reducing the spinning reserve capacity of electrical power system. This model is also useful for supporting wind farm decision making in practice. The combined forecasting model, which has high precision, is a promising model for use in the future. In addition, this hybrid model can be utilized in other forecasting fields, such as product sales forecasting, tourism demand forecasting, early warning and flood forecasting, and traffic-flow forecasting.

Competing Interests

The authors declare that they have no competing interests.

References

[1] A. Tascikaraoglu, B. M. Sanandaji, K. Poolla, and P. Varaiya, "Exploiting sparsity of interconnections in spatio-temporal wind speed forecasting using Wavelet Transform," *Applied Energy*, vol. 165, pp. 735–747, 2016.

[2] M. Lydia, S. Suresh Kumar, A. I. Selvakumar, and G. E. P. Kumar, "Linear and non-linear autoregressive models for short-term wind speed forecasting," *Energy Conversion and Management*, vol. 112, pp. 115–124, 2016.

[3] Z. Men, E. Yee, F.-S. Lien, D. Wen, and Y. Chen, "Short-term wind speed and power forecasting using an ensemble of mixture density neural networks," *Renewable Energy*, vol. 87, pp. 203–211, 2016.

[4] H. Liu, H.-Q. Tian, Y.-F. Li, and L. Zhang, "Comparison of four Adaboost algorithm based artificial neural networks in wind speed predictions," *Energy Conversion and Management*, vol. 92, pp. 67–81, 2015.

[5] H. Liu, H. Q. Tian, X. F. Liang, and Y. F. Li, "New wind speed forecasting approaches using fast ensemble empirical model decomposition, genetic algorithm, Mind Evolutionary Algorithm and Artificial Neural Networks," *Renewable Energy*, vol. 83, pp. 1066–1075, 2015.

[6] Q. Hu, R. Zhang, and Y. Zhou, "Transfer learning for short-term wind speed prediction with deep neural networks," *Renewable Energy*, vol. 85, pp. 83–95, 2016.

[7] H. Liu, H.-Q. Tian, X.-F. Liang, and Y.-F. Li, "Wind speed forecasting approach using secondary decomposition algorithm and Elman neural networks," *Applied Energy*, vol. 157, pp. 183–194, 2015.

[8] Z. Guo, D. Chi, J. Wu, and W. Zhang, "A new wind speed forecasting strategy based on the chaotic time series modelling technique and the Apriori algorithm," *Energy Conversion and Management*, vol. 84, pp. 140–151, 2014.

[9] T. G. Barbounis, J. B. Theocharis, M. C. Alexiadis, and P. S. Dokopoulos, "Long-term wind speed and power forecasting using local recurrent neural network models," *IEEE Transactions on Energy Conversion*, vol. 21, no. 1, pp. 273–284, 2006.

[10] J. Wang and J. Hu, "A robust combination approach for short-term wind speed forecasting and analysis—combination of the ARIMA (Autoregressive Integrated Moving Average), ELM (Extreme Learning Machine), SVM (Support Vector Machine) and LSSVM (Least Square SVM) forecasts using a GPR (Gaussian Process Regression) model," *Energy*, vol. 93, pp. 41–56, 2015.

[11] H. B. Azad, S. Mekhilef, and V. G. Ganapathy, "Long-term wind speed forecasting and general pattern recognition using neural networks," *IEEE Transactions on Sustainable Energy*, vol. 5, no. 2, pp. 546–553, 2014.

[12] K. Chen and J. Yu, "Short-term wind speed prediction using an unscented Kalman filter based state-space support vector regression approach," *Applied Energy*, vol. 113, pp. 690–705, 2014.

[13] A. Gani, K. Mohammadi, S. Shamshirband, T. A. Altameem, D. Petković, and S. Ch, "A combined method to estimate wind speed distribution based on integrating the support vector machine with firefly algorithm," *Environmental Progress & Sustainable Energy*, vol. 35, no. 3, pp. 867–875, 2016.

[14] Y. J. Lin, U. Kruger, J. Zhang, Q. Wang, L. Lamont, and L. El Chaar, "Seasonal analysis and prediction of wind energy using random forests and ARX model structures," *IEEE Transactions on Control Systems Technology*, vol. 23, no. 5, pp. 1994–2002, 2015.

[15] E. Baccarelli, N. Cordeschi, A. Mei, M. Panella, M. Shojafar, and J. Stefa, "Energy-efficient dynamic traffic offloading and reconfiguration of networked data centers for big data stream mobile computing: review, challenges, and a case study," *IEEE Network*, vol. 30, no. 2, pp. 54–61, 2016.

[16] D. Liu, D. Niu, H. Wang, and L. Fan, "Short-term wind speed forecasting using wavelet transform and support vector machines optimized by genetic algorithm," *Renewable Energy*, vol. 62, pp. 592–597, 2014.

[17] S. J. Watson, L. Landberg, and J. A. Halliday, "Application of wind speed forecasting to the integration of wind energy into a large scale power system," *IEE Proceedings: Generation, Transmission and Distribution*, vol. 141, no. 4, pp. 357–362, 1994.

[18] N. E. Huang, Z. Shen, S. R. Long et al., "The empirical mode decomposition and the Hilbert spectrum for nonlinear and non-stationary time series analysis," *Proceedings of the Royal Society of London A*, vol. 454, no. 1971, pp. 903–995, 1998.

[19] Y. Gan, L. Sui, J. Wu, B. Wang, Q. Zhang, and G. Xiao, "An EMD threshold de-noising method for inertial sensors," *Measurement*, vol. 49, no. 1, pp. 34–41, 2014.

[20] H.-X. Sun, N.-N. Zhao, and X.-H. Xu, "Text region localization using wavelet transform in combination with support vector machine," *Journal of Northeastern University (Natural Science)*, vol. 28, no. 2, pp. 165–168, 2007.

[21] M. Bouzerdoum, A. Mellit, and A. M. Pavan, "A hybrid model (SARIMA-SVM) for short-term power forecasting of a small-scale grid-connected photovoltaic plant," *Solar Energy*, vol. 98, pp. 226–235, 2013.

[22] X. Wang, J. Wen, Y. Zhang, and Y. Wang, "Real estate price forecasting based on SVM optimized by PSO," *Optik*, vol. 125, no. 3, pp. 1439–1443, 2014.

[23] X.-S. Yang and S. Deb, "Cuckoo search via Lévy flights," in *Proceedings of the World Congress on Nature & Biologically Inspired Computing (NaBIC '09)*, pp. 210–214, Coimbatore, India, December 2009.

Hindawi Publishing Corporation
Mathematical Problems in Engineering
Volume 2016, Article ID 2720614, 13 pages
http://dx.doi.org/10.1155/2016/2720614

Research Article

Time-Independent Reliability Analysis of Bridge System Based on Mixed Copula Models

Yuefei Liu[1,2] and Xueping Fan[1,2]

[1] *Key Laboratory of Mechanics on Disaster and Environment in Western China, Lanzhou University, The Ministry of Education of China, Lanzhou, Gansu 730000, China*
[2] *School of Civil Engineering and Mechanics, Lanzhou University, Lanzhou 730000, China*

Correspondence should be addressed to Yuefei Liu; luiyuefei@126.com and Xueping Fan; fanxp@lzu.edu.cn

Received 25 December 2015; Accepted 19 May 2016

Academic Editor: Egidijus R. Vaidogas

The actual structural systems have many failure modes. Due to the same random sources owned by the performance functions of these failure modes, there usually exist some nonlinear correlations between the various failure modes. How to handle the nonlinear correlations is one of the main scientific problems in the field of structural system reliability. In this paper, for the two-component systems and multiple-component systems with multiple failure modes, the mixed copula models for time-independent reliability analysis of series systems, parallel systems, series-parallel systems, and parallel-series systems are presented. These obtained mixed copula models, considering the nonlinear correlation between failure modes, are obtained with the chosen optimal copula functions with the Bayesian selection criteria and Monte Carlo Sampling (MCS) method. And a numerical example is provided to illustrate the feasibility and application of the built mixed models for structural system reliability.

1. Introduction

Today's structural systems are becoming more complex and more sophisticated. Therefore, the evaluation of structural system reliability is becoming harder. This means that the derivations based on classical assumptions are no longer satisfactory for the analysis of systems in terms of reliability. The evaluation of today's real life systems needs more detailed and complicated statistical analysis. Dependence between the components is one of the intractable realistic assumptions that need to be carefully considered [1–4].

Especially for the actual bridge system, there exist many failure modes such as flexural failure and shearing failure. As the limit state functions (performance function) of these failure modes may have the same random sources, it is not mutually exclusive yet among failure modes [5–7]. Naturally, how to model the correlation among failure modes in aspect of the reliability analysis of structural systems is one of the most significant topics. The classic Pearson correlation coefficient is mainly used for characterizing the correlation among failure modes of structural system before; however, it has a few disadvantages. The copulas, unlike the Pearson correlation coefficient only applied for describing linear correlation, offer a flexible tool for deriving nonlinear dependence, especially tail dependence among failure modes. The aim of this study is to introduce the copula function as a useful tool for modeling the dependence among failure modes of bridge system. More recently, the copula theory has been primarily used in mechanical engineering [8] and hydraulic engineering [9] but little used in bridge engineering.

In this paper, firstly, several commonly used elliptical copulas and Archimedean copulas were introduced, and their application in the correlation analysis was also described in detail. And then based on the introduced copulas, with the aid of copula Bayesian selection criteria [7, 10, 11], a flexible mixed copula model is constructed, by means of linear weighted model, to model the nonlinear dependence among failure modes. For the two-component systems and multiple-component systems with multiple failure modes, the performance function value of failure modes is chosen as the copula functions' analytical variable to construct mixed copula model. With Monte Carlo Sampling method, the

unknown parameters of copula functions can be approximately determined; therefore, the mixed copula function, considering the correlation between failure modes, is built. And then use the built mixed copula model to solve the structural system's reliability. Finally, a numerical example is provided to illustrate the feasibility and application of the built mixed copula models.

2. Mixed Copula Models

The mixed copula models are commonly built through different combinations of several copula functions, which respectively possess various characteristics in aspect of the dependence modeling. For the complex and ever-changing correlations among random variables, they are not adequate for modeling the dependence by means of only a single copula function. Therefore, it is necessary to build a flexible mixed copula model to describe the complex dependence structures. Moreover, it is essential to select several appropriate copula functions from the existing copulas before building the mixed copula model. The Bayesian selection criteria are just chosen for constructing the mixed copula model, as this method is independent of the parameter estimation and may be applied to all known copula classes [7, 10].

2.1. Basic Theory about Copula Functions. Sklar's theory [12] clearly indicated that, given random variables $\mathbf{X} = (X_1, X_2, \ldots, X_n)$ with continuous marginal distribution functions $F_{X_1}, F_{X_2}, \ldots, F_{X_n}$ and n-dimensional joint distribution function F, there exists a unique copula function C such that, for all $\mathbf{x} = (x_1, x_2, \ldots, x_n) \in \mathbf{R}^n$,

$$\begin{aligned} &F(x_1, x_2, \ldots, x_n) \\ &\quad = C\left(F_{X_1}(x_1), F_{X_2}(x_2), \ldots, F_{X_n}(x_n)\right). \end{aligned} \tag{1}$$

According to (1), the joint probability density function of the random variable $\mathbf{X} = (X_1, X_2, \ldots, X_n)$ is given as follows:

$$\begin{aligned} &p(x_1, x_2, \ldots, x_n) \\ &\quad = c\left(F_{X_1}(x_1), F_{X_2}(x_2), \ldots, F_{X_n}(x_n)\right) \prod_{i=1}^{n} p_{X_i}(x_i), \end{aligned} \tag{2}$$

where $p_{X_i}(x_i)$ is the marginal probability density function (PDF) and $c(\mathbf{u})$ is the joint PDF of the copula function denoted as follows:

$$c(u_1, \ldots, u_n) = \frac{\partial^n C}{\partial u_1 \cdots \partial u_n}(u_1, \ldots, u_n). \tag{3}$$

If F_{X_i} for $i = 1, 2, \ldots, n$ have generalized inverse functions $F_{X_i}^{-1}$ for $i = 1, 2, \ldots, n$, then, (1) can be rewritten as follows:

$$\begin{aligned} &F\left(F_{X_1}^{-1}(u_1), F_{X_2}^{-1}(u_2), \ldots, F_{X_n}^{-1}(u_n)\right) \\ &\quad = C(u_1, u_2, \ldots, u_n), \end{aligned} \tag{4}$$

where $u_i = F_{X_i}$ $(i = 1, 2, \ldots, n)$, $(u_1, u_2, \ldots, u_n) = \mathbf{u}$.

Equation (4) reveals how to construct the copula function of a multivariate distribution with given marginal distributions. It follows from the probability integral transform that the random variables $U_i \equiv F_{X_i}(X_i)$, $i = 1, 2, \ldots, n$, are all uniformly distributed on $(0, 1)$. Conversely, $X_i = F_{X_i}^{-1}(U_i)$, $i = 1, 2, \ldots, n$, $\mathbf{U} = (U_1, U_2, \ldots, U_n)$; with this in mind, (4) is expressed as

$$\begin{aligned} &P(X_1 \le x_1, X_2 \le x_2, \ldots, X_n \le x_n) = P\left(X_1\right. \\ &\quad \left. \le F_{X_1}^{-1}(u_1), X_2 \le F_{X_2}^{-1}(u_2), \ldots, X_n \le F_{X_n}^{-1}(u_n)\right) \\ &\quad = P(U_1 \le u_1, U_2 \le u_2, \ldots, U_n \le u_n) \\ &\quad = C(u_1, u_2, \ldots, u_n). \end{aligned} \tag{5}$$

According to (1)–(5), the copula function organically combines each marginal distribution function with the multivariate joint distribution functions; therefore, it not only considers the dependence among random variables but also simplifies the probability modeling process for multivariate random variables.

2.2. Bayesian Selection Criteria of Copula Functions. Huard et al. [10] proposed the Bayesian copula selection method applied to the bivariate copula functions. Bayesian copula selection method was deduced by the Bayesian hypothesis testing to choose the best copula. However, we apply this method to choose not just the best one but also the better copulas as the candidate copulas for constructing the mixed copula model.

For the Bayesian copula selection criteria, it is essential to propose the optical copula function selection criteria described by

$$C_{\text{opt}} = \arg_{C_l} \max P(\mathrm{H}_t \mid D, I), \tag{6}$$

where C_{opt} is the optical copula function, H_t is denoted as the hypotheses that the right copula is copula C_l $(l = 1, 2, \ldots, L)$, as the candidate copulas, C_l is denoted by $C_l = C_l(u_i, v_i; \theta_i)$ $(i = 1, 2, \ldots, n)$, and n pair of quantiles (u_i, v_i) are supposed as n mutually independent pairs composing the data set D. Besides, I stands for some a priori information. According to Bayesian formula, it can be obtained that

$$P(\mathrm{H}_t \mid D, I) = \frac{P(D \mid \mathrm{H}_t, I) P(\mathrm{H}_t \mid I)}{P(D \mid I)}, \tag{7}$$

where $P(D \mid \mathrm{H}_t, I)$ is the likelihood, $P(\mathrm{H}_t \mid I)$ is the a priori copula family, and $P(D \mid I)$ is the normalization constant. The rank correlation coefficient Kendall's τ, denoted by $\tau = g_l(\theta)$ to be the correlation parameters for all the selected copulas, is introduced in order to give the formula for $P(\mathrm{H}_t \mid D, I)$:

$$\begin{aligned} &P(\mathrm{H}_t \mid D, I) \\ &\quad = \int_{\tau \in \Omega} \frac{P(D \mid \mathrm{H}_t, \tau, I) P(\mathrm{H}_t \mid \tau, I) P(\tau \mid I)}{P(D \mid I)} d\tau, \end{aligned} \tag{8}$$

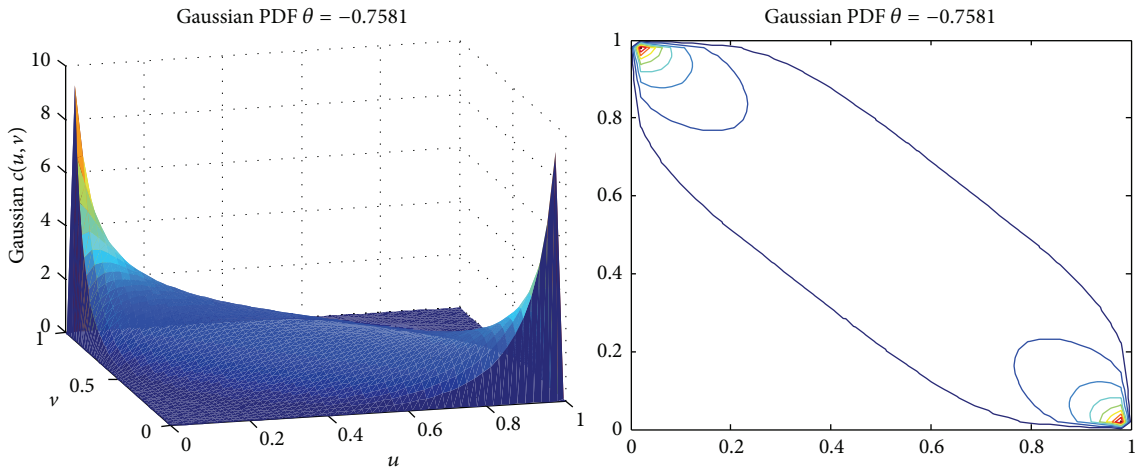

Figure 1: PDF and contour plots of Gaussian copula function.

where $P(D \mid \mathrm{H}_t, \tau, I)$ is the likelihood with respect to τ, because of the n mutually independent pairs, and is also described as the copula density:

$$P\left(D \mid \mathrm{H}_t, \tau, I\right) = \prod_{l=1}^{n} C_l\left(u_i, v_i; g_l^{-1}(\tau)\right). \tag{9}$$

Substituting (9) into (8), we obtain

$$P\left(\mathrm{H}_t \mid D, I\right) = \frac{1}{P\left(D \mid I\right)} \int_{\tau \in \Omega} \prod_{l=1}^{n} C_l\left(u_i, v_i; g_l^{-1}(\tau)\right) \cdot P\left(\mathrm{H}_t \mid \tau, I\right) P\left(\tau \mid I\right) d\tau, \tag{10}$$

where $P(D \mid I)$ is the normalization constant and $P(\mathrm{H}_t \mid \tau, I)P(\tau \mid I) = 1/\lambda(\Lambda)$, where $\lambda(\Lambda)$ is denoted as the Lebesgue measure of $\Lambda = [-1, 1]$ in this paper; therefore, (10) can be also expressed as follows:

$$P\left(\mathrm{H}_t \mid D, I\right) \propto \frac{1}{\lambda\left(\Lambda\right)} \int_{\Omega_l \cap \Lambda} \prod_{l=1}^{n} C_l\left(u_i, v_i; g_l^{-1}(\tau)\right) d\tau. \tag{11}$$

Obviously, the optimal copula function selection criteria can be described as the computation of the highest weight W_l:

$$W_l = \frac{1}{\lambda\left(\Lambda\right)} \int_{\Omega_l \cap \Lambda} \prod_{i=1}^{n} c_l\left(u_i, v_i; g_l^{-1}(\tau)\right) d\tau. \tag{12}$$

In especial, the "right" copulas include not just the best copula with the highest weight but also the better copula with higher weight for the mixed copula modeling in this paper.

Two particular classes of copulas that proved to be useful in dependence modeling are the elliptical and Archimedean classes [7, 13]. The four copulas (one of the elliptical copulas, Gaussian copula, and three of the Archimedean copulas, Gumbel copula, Clayton copula, and Frank copula) are employed as the candidates of the Bayesian copula selection criteria. Finally, the chosen ones are used for constructing the mixed copula model. Among the chosen copulas, Gaussian copulas and Frank copulas are able to capture symmetric dependence structures among random variables. Different from them, Gumbel copulas and Clayton copulas exhibit asymmetric dependence and Gumbel copulas are especially employed for describing upper tail dependence structures, while Clayton copulas are employed for that of the lower tail. And, then, the probability density function graphs and their contour plots are depicted as in Figures 1–4.

2.3. Modeling Method of Mixed Copula Models. There exist complex nonlinear correlations among failure modes; therefore, just one copula is not enough to characterize dependence structures among failure modes. With the aid of a weighted combination of the selected copula functions, a mixed copula is approximately constructed in order to describe the complex dependence structures among failure modes [7, 14]; namely,

$$C\left(\mathbf{u}, \mathbf{v}; \mathbf{a}, \boldsymbol{\theta}\right) = \sum_{i=1}^{N} a_i C_i\left(\mathbf{u}, \mathbf{v}; \theta_i\right) \quad (N \leq 4), \tag{13}$$

where C_i $(i = 1, 2, \ldots, N)$ are, respectively, denoted as one of the chosen copulas among the four copulas and $\mathbf{a} = (a_1, a_2, \ldots, a_N)$ is the weighting coefficient vector along with the inner parameter vector $\boldsymbol{\theta} = (\theta_1, \theta_2, \ldots, \theta_N)$ of the corresponding copulas, and $\mathbf{u}, \boldsymbol{\nu}$ are variables of the chosen copula functions, and what is more, $a_1 + a_2 + \cdots + a_N = 1$.

The copula function and Monte Carlo Simulation (MCS) method are contributed to the mixed copula model analysis. The specific steps can be stated as follows.

2.3.1. Monte Carlo Sampling (MCS). According to the distribution types of random variables for the performance functions of failure modes, the samples for the random variables can be obtained with MCS method. After substituting the samples into the corresponding performance functions, we can get the random sequence $\{g_j\}_i$, $i = 1, 2, \ldots, n$, $j = 1, 2, \ldots, N$, for each of the performance functions and obtain the sequences $\{F_j\}_i = F(\{g_j\}_i)$, $i = 1, 2, \ldots, n$, $j = 1, 2, \ldots, N$, of the corresponding empirical

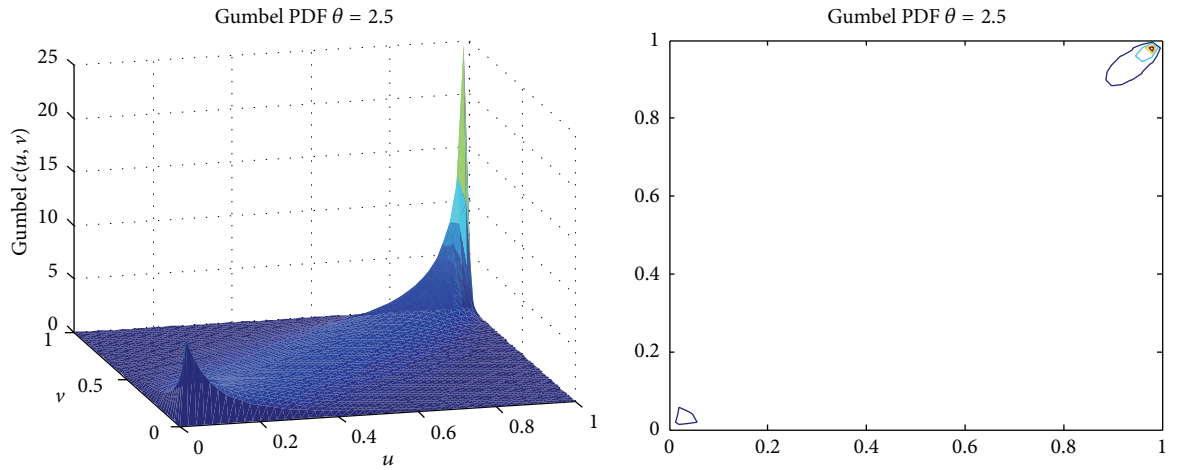

Figure 2: PDF and contour plots of Gumbel copula function.

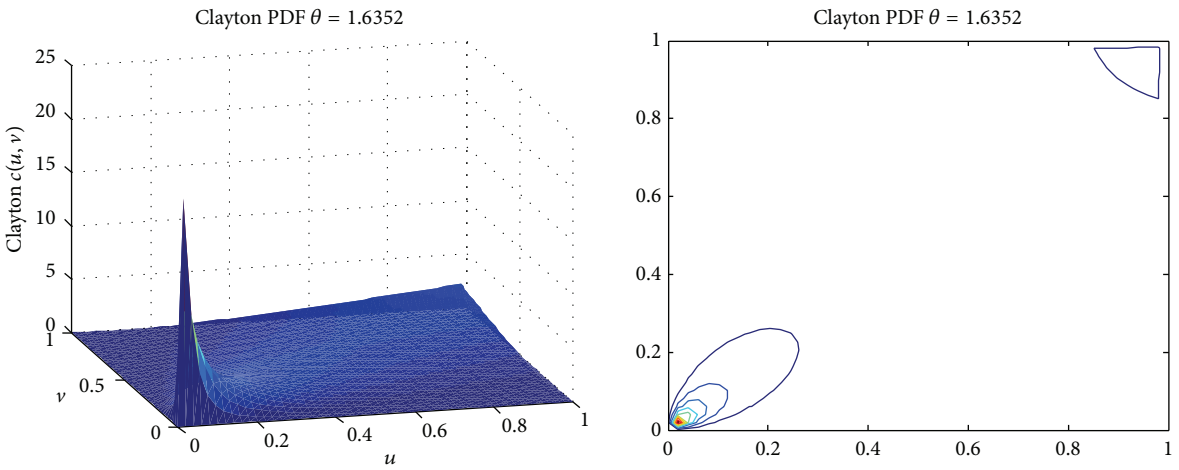

Figure 3: PDF and contour plots of Clayton copula function.

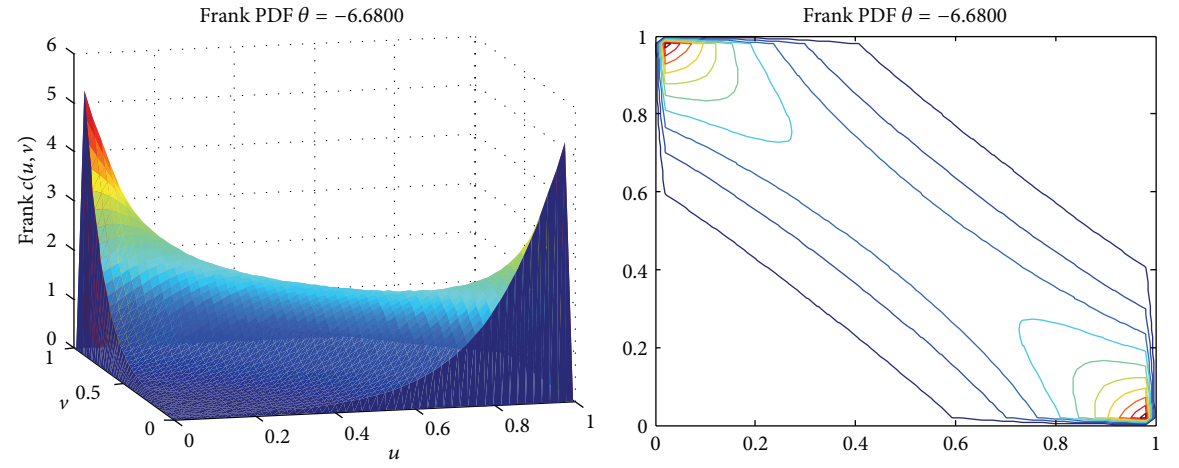

Figure 4: PDF and contour plots of Frank copula function.

Table 1: Basic cases of the parameters of copula functions.

Copula	$\tau = g(\theta)$	$\tau \in \Omega$	$\theta \in \Omega$
Gaussian	$\frac{2}{\pi}\arcsin\theta$	$[-1, 1]$	$[-1, 1]$
Gumbel	$1 - \theta^{-1}$	$[0, 1]$	$[1, +\infty)$
Clayton	$1 - \frac{2}{2+\theta}$	$(0, 1]$	$(0, +\infty)$
Frank	$1 - \frac{4}{\theta}\left(1 - \frac{1}{\theta}\int_0^\theta \frac{t}{e^t - 1}dt\right)$	$[-1, 0) \cup (0, 1]$	$(-\infty, 0) \cup (0, +\infty)$

distribution function by mean of Matlab software, where g is the performance function and F is the empirical distribution function.

2.3.2. Copula Function Selection. With the scatter plot of samples, we can judge approximate distribution features of the samples. Furthermore, it is extremely vital to determine which classes of copula functions to choose as the candidate copulas with Bayesian copula selection criteria. In this paper, the copula classes we chose are Gaussian copulas, Gumbel copulas, and Clayton copulas as well as Frank copulas, whose parameter domain along with the definition and the domain of Kendall's τ are listed in Table 1. The next is to build the mixed copula function through the selected copulas and (13).

2.3.3. Parameter Estimation for the Mixed Copula. Applying the least residual error quadratic sum method OLS, one of the curve fitting criteria, we can obtain parameters of the mixed copula function. And the formula of the OLS is represented as follows:

$$F_{\mathrm{OLS}} = \sqrt{\frac{1}{n}\sum_{i=1}^{n}\left(F\left(\left(F_1\right)_i, \left(F_2\right)_i, \ldots, \left(F_N\right)_i\right) - C\left(\left(F_1\right)_i, \left(F_2\right)_i, \ldots, \left(F_N\right)_i\right)\right)^2}, \tag{14}$$

where $F(\cdot)$ is the joint empirical distribution function of the empirical distribution function sequences for each performance function and $C((F_1)_i, (F_2)_i, \ldots, (F_N)_i)$ is the mixed copula function value. The unknown parameter value for the mixed copula function can be obtained by the optimization computation with the rule of OLS, while the optimized parameters must be determined to make sure that the value of F_{OLS} is the minimum.

2.3.4. Goodness-of-Fit Estimation for the Mixed Copula. Through MCS method, the values of joint empirical distribution functions and the corresponding mixed copula function are obtained, and, then, the scatter plot between them is drawn. Finally, the goodness of fit for the mixed copula can be determined through the scatter plot.

3. Mixed Copula Model Expressions about Joint Failure Probability of Structural System

3.1. Mixed Copula Model Expression about Joint Failure Probability of Two-Component Series System. For the two-component series system which is shown in Figure 5, suppose that the performance function of the component failure mode is

$$g_i(\mathbf{X}) = g_i\left(\mathrm{X}_1, X_2, \ldots, X_n\right), \quad i = 1, 2. \tag{15}$$

With (5), as a check, the probability that both failure modes occur is denoted as

$$\begin{aligned} &P\left(g_1(\mathbf{X}) \le 0, g_2(\mathbf{X}) \le 0\right) \\ &= P\left(F_{g_1}\left(g_1(\mathbf{X})\right) \le F_{g_1}(0), F_{g_2}\left(g_2(\mathbf{X})\right) \le F_{g_2}(0)\right) \\ &= P\left(U_1 \le F_{g_1}(0), U_2 \le F_{g_2}(0)\right) \\ &= C\left(F_{g_1}(0), F_{g_2}(0)\right) = C\left(p_{f_{g_1}}, p_{f_{g_2}}\right). \end{aligned} \tag{16}$$

$F_{\mathbf{g}}(0, 0) = C(F_{g_1}(0), F_{g_2}(0))$ is stated in the fundamental theorem of Sklar. Therefore, the failure probability of two-component series system (at least one failure mode of the two components occurred) can be solved as

$$\begin{aligned} p_f &= P\left(g_1(\mathbf{X}) \le 0 \cup g_2(\mathbf{X}) \le 0\right) \\ &= P\left(g_1(\mathbf{X}) \le 0\right) + P\left(g_2(\mathbf{X}) \le 0\right) \\ &\quad - P\left(g_1(\mathbf{X}) \le 0, g_2(\mathbf{X}) \le 0\right) \\ &= p_{f_{g_1}} + p_{f_{g_2}} - C\left(p_{f_{g_1}}, p_{f_{g_2}}\right), \end{aligned} \tag{17}$$

where $p_{f_{g_1}}, p_{f_{g_2}}$, respectively, denote the failure probability of the two failure modes and $C(\cdot)$ is two-component series system copula function.

3.2. Mixed Copula Model Expression about Joint Failure Probability of Two-Component Parallel System. For the two-component parallel system which is shown in Figure 6,

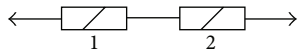

Figure 5: Two-component series system.

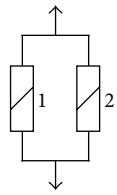

Figure 6: Two-component parallel system.

suppose that the performance function of the component failure mode is

$$g_i(\mathbf{X}) = g_i(X_1, X_2, \ldots, X_n), \quad i = 1, 2. \tag{18}$$

With (5) and (16), the failure probability of two-component parallel system (two failure modes of the two components meantime occurred) can be obtained:

$$p_f = P(g_1(\mathbf{X}) \le 0 \cap g_2(\mathbf{X}) \le 0) = C\left(p_{f_{g_1}}, p_{f_{g_2}}\right), \tag{19}$$

where $p_{f_{g_1}}, p_{f_{g_2}}$, respectively, denote the failure probability of the two failure modes and $C(\cdot)$ is two-component parallel system copula function.

3.3. Mixed Copula Model Expression about Joint Failure Probability of Multiple-Component Series System. For the multiple-component series system which is shown in Figure 7, suppose that the performance function of the component failure mode is

$$g_i(\mathbf{X}) = g_i(X_1, X_2, \ldots, X_n), \quad i = 1, 2, \ldots, N. \tag{20}$$

With (5), as a check, the probability that all the failure modes meantime occur is denoted as

$$\begin{aligned} &P(g_1(\mathbf{X}) \le 0, g_2(\mathbf{X}) \le 0, \ldots, g_N(\mathbf{X}) \le 0) \\ &\quad = P\left(F_{g_1}(g_1(\mathbf{X})) \le F_{g_1}(0), F_{g_2}(g_2(\mathbf{X}))\right. \\ &\quad \left. \le F_{g_2}(0), \ldots, F_{g_N}(g_N(\mathbf{X})) \le F_{g_N}(0)\right) = P\left(U_1\right. \\ &\quad \left. \le F_{g_1}(0), U_2 \le F_{g_2}(0), \ldots, U_N \le F_{g_N}(0)\right) \\ &\quad = C\left(F_{g_1}(0), F_{g_2}(0), \ldots, F_{g_N}(0)\right) \\ &\quad = C\left(p_{f_{g_1}}, p_{f_{g_2}}, \ldots, p_{f_{g_N}}\right). \end{aligned} \tag{21}$$

$F_{\mathbf{g}}(0, 0, \ldots, 0) = C(F_{g_1}(0), F_{g_2}(0), \ldots, F_{g_N}(0))$ is stated in the fundamental theorem of Sklar. Therefore, the failure probability of multiple-component series system (at least one failure mode of the multiple components occurred) can be solved as

$$\begin{aligned} p_f &= P(g_1(\mathbf{X}) \le 0 \cup g_2(\mathbf{X}) \le 0 \cup \cdots \cup g_N(\mathbf{X}) \le 0) \\ &= \sum_{i=1}^{N} P(g_i(\mathbf{X}) \le 0) - \sum_{i_1 < i_2} P\left(g_{i_1}(\mathbf{X}) \le 0, g_{i_2}(\mathbf{X})\right. \\ &\quad \left. \le 0\right) + \cdots + (-1)^{n+1} \sum_{i_1 < i_2 < \cdots < i_n} P\left(g_{i_1}(\mathbf{X}) \le 0, g_{i_2}(\mathbf{X})\right. \\ &\quad \left. \le 0, \ldots, g_{i_n}(\mathbf{X}) \le 0\right) + \cdots + (-1)^{N+1} P(g_1(\mathbf{X}) \le 0, \\ &\quad g_2(\mathbf{X}) \le 0, \ldots, g_N(\mathbf{X}) \le 0) = \sum_{i=1}^{n} p_{f_{g_i}} \\ &\quad - \sum_{i_1 < i_2} C\left(p_{f_{g_{i_1}}}, p_{f_{g_{i_2}}}\right) + \cdots + (-1)^{n+1} \\ &\quad \cdot \sum_{i_1 < i_2 < \cdots < i_n} C\left(p_{f_{g_{i_1}}}, p_{f_{g_{i_2}}}, \ldots, p_{f_{g_{i_n}}}\right) + \cdots \\ &\quad + (-1)^{N+1} C\left(p_{f_{g_1}}, p_{f_{g_2}}, \ldots, p_{f_{g_N}}\right), \end{aligned} \tag{22}$$

where $p_{f_{g_1}}, p_{f_{g_2}}, \ldots, p_{f_{g_N}}$, respectively, denote the failure probability of the multiple failure modes and $C(\cdot)$ is multiple-component series system copula function.

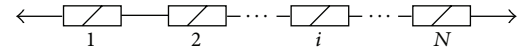

Figure 7: Multiple-component series system.

3.4. Mixed Copula Model Expression about Joint Failure Probability of Multiple-Component Parallel System. For the multiple-component parallel system which is shown in Figure 8, suppose that the performance function of the component failure mode is

$$g_i(\mathbf{X}) = g_i(X_1, X_2, \ldots, X_n), \quad i = 1, 2, \ldots, N. \tag{23}$$

With (5), the failure probability of two-component parallel system (all the failure modes of all the components meantime occurred) can be obtained:

$$\begin{aligned} p_f &= P(g_1(\mathbf{X}) \le 0, g_2(\mathbf{X}) \le 0, \ldots, g_N(\mathbf{X}) \le 0) \\ &\quad = P\left(F_{g_1}(g_1(\mathbf{X})) \le F_{g_1}(0), F_{g_2}(g_2(\mathbf{X}))\right. \\ &\quad \left. \le F_{g_2}(0), \ldots, F_{g_N}(g_N(\mathbf{X})) \le F_{g_N}(0)\right) = P\left(U_1\right. \\ &\quad \left. \le F_{g_1}(0), U_2 \le F_{g_2}(0), \ldots, U_N \le F_{g_N}(0)\right) \\ &\quad = C\left(F_{g_1}(0), F_{g_2}(0), \ldots, F_{g_N}(0)\right) \\ &\quad = C\left(p_{f_{g_1}}, p_{f_{g_2}}, \ldots, p_{f_{g_N}}\right), \end{aligned} \tag{24}$$

where $p_{f_{g_1}}, p_{f_{g_2}}, \ldots, p_{f_{g_N}}$, respectively, denote the failure probability of the N failure modes and $C(\cdot)$ is multiple-component parallel system copula function.

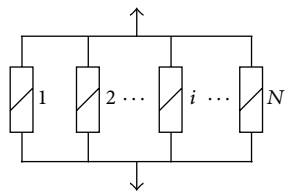

Figure 8: Multiple-component parallel system.

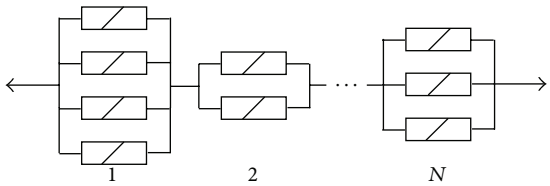

Figure 9: Series-parallel system.

3.5. Mixed Copula Model Expression about Joint Failure Probability of Series-Parallel System. For series-parallel system shown in Figure 9, in this paper, only the correlation between internal components of each subparallel system is considered, while the correlation between subparallel systems is not considered and considered to be mutually independent. Therefore, with (24), all the copula models of all the subparallel systems' failure probability can be obtained, and then, with (25), the failure probability of the series-parallel system can be solved:

$$\begin{aligned} p_{f_{\text{s-p}}} &= P\left(\bigcup_{i=1}^{N} F_i\right) = P\left(\bigcup_{i=1}^{N}\bigcap_{j}^{N_i} F_{ij}\right) \\ &= \sum_{i=1}^{N} P\left(F_i\right) - \sum_{i_1<i_2} \left\{P\left(F_{i_1}\right) P\left(F_{i_2}\right)\right\} + \cdots \\ &\quad + (-1)^{n+1} \sum_{i_1<i_2<\cdots<i_n} \left\{\prod_{k=i_1}^{i_n} P\left(F_k\right)\right\} + \cdots \\ &\quad + (-1)^{N+1} \prod_{i=1}^{N} P\left(F_i\right), \end{aligned} \tag{25}$$

where N is the total number of the subparallel systems; N_i is the total number of the components in the ith subparallel system; $F_i = \bigcap_{j=1}^{N_i} F_{ij}$ is the failure probability of the ith subparallel system; $F_{ij} = (g_{ij}(\mathbf{X}) \le 0)$ is the failure probability of the jth component in the ith subparallel system; $P(F_i)$, $i = 1, 2, \ldots, N$, can be solved with (24), which are the failure probability of the subparallel system considering correlation between internal components of each subparallel system.

3.6. Mixed Copula Model Expression about Joint Failure Probability of Parallel-Series System. For parallel-series system shown in Figure 10, in this paper, only the correlation between internal components of each subseries system is considered, while the correlation between subseries systems is not considered and considered to be mutually independent.

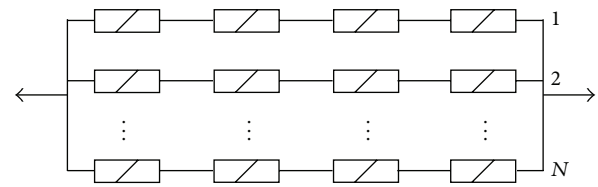

Figure 10: Parallel-series system.

Therefore, with (22), all the copula models of all the subseries systems' failure probability can be obtained, and then, with (26), the failure probability of the parallel-series system can be solved as

$$p_{f_{\text{p-s}}} = P\left(\bigcap_{i=1}^{N} F_i\right) = \prod_{i=1}^{N} P\left(F_i\right) = \prod_{i=1}^{N} P\left(\bigcup_{j=1}^{N_i} F_{ij}\right), \tag{26}$$

where N is the total number of the subseries systems; N_i is the total number of the components in the ith subseries system; $F_i = \bigcap_{j=1}^{N_i} F_{ij}$ is the failure probability of the ith subseries system; $F_{ij} = (g_{ij}(\mathbf{X}) \le 0)$ is the failure probability of the jth component in the ith subseries system; $P(F_i)$, $i = 1, 2, \ldots, N$, can be solved with (22), which are the failure probability of the subseries system considering correlation between internal components of each subseries system.

In this paper, firstly with First-Order Reliability Method (FORM), the structural reliability index and the corresponding failure probability of each failure mode can be solved, and then with the constructed mix copula functions, such as (17), (19), (22), (24), (25), and (26), the failure probability of structural system considering correlation between failure modes can be obtained.

4. Numerical Example: System Reliability Analysis of Simply Supported Cored Slab Bridge

For the simply supported cored slab bridge shown in Figure 11, the total span is 13 m, the computed span is 12.6 m, the clear width of bridge deck is 7 m, the width of footway on both sides of bridge deck is 1 m, and the whole bridge is composed of nine concrete cored slabs [15]. The design reference period of this bridge is 100 years. And this bridge has been served for 32 years. At the 32nd year, the resistance of each girder follows normal distribution; the distribution parameters are, respectively, 796.04 kN·m (mean value) and 91.783 kN·m (standard deviation).

Based on Figure 11 and reference [16], the failure criterion of bridge system is as follows: if any two adjacent girders both failed, then the whole bridge system failed. According to the failure criterion, the bridge system is a series-parallel system, which is shown in Figure 12.

The performance function of each girder's failure mode is

$$\begin{aligned} Z_i = g\left(X_{i1}, X_{i2}, X_{i3}\right) = g\left(R_i, G_i, Q_i\right) = R_i - G_i - Q_i, \\ i = 1, 2, \ldots, 9, \end{aligned} \tag{27}$$

Table 2: Distribution parameters of beams' dead load effects in 32nd year.

Girder number	1	2	3	4	5	6	7	8	9
Mean value/kN·m	212.86	221.79	223.91	230.74	260.69	230.74	223.91	221.79	212.86
Standard deviation/kN·m	9.68	9.68	9.68	9.68	9.68	9.68	9.68	9.68	9.68

Table 3: Distribution parameters of beams' maximum live load effects in 32nd year.

Girder number	1	2	3	4	5	6	7	8	9
Mean value/kN·m	85.42	96.42	116.8	144.4	180.9	144.4	116.8	96.42	85.42
Standard deviation/kN·m	12.71	14.35	17.38	21.49	26.92	21.49	17.38	14.35	12.71

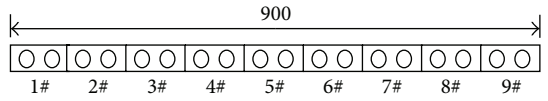

Figure 11: Cross section of bridge (unit: cm).

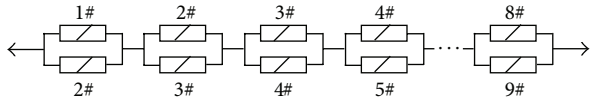

Figure 12: Series-parallel system.

where R_i is the resistance of the ith girder, G_i is the dead load effect of the ith girder, and Q_i is the live load effect of the ith girder. At the 32nd year, the distribution parameters about dead load effects are listed in Table 2, where the standard deviation is not changed, because, for load effect, the variation of variables is very small. And the distribution parameters about vehicle load effects are listed in Table 3, which occur due to symmetrical variable load and is not applicated to the unsymmetrical variable load.

Based on the reliability analysis method of two-component parallel system considering the correlation between failures modes described in Section 3.2, the reliability analysis processes of bridge system are as follows.

Because the bridge system is symmetrical, the subparallel systems (1#-2#, 2#-3#, 3#-4#, and 4#-5#) are used to analyze the reliability and failure probability of the bridge system.

Based on Tables 2 and 3 and (25), the scatter plot between two random sampling sequences of the corresponding limit state functions for the two failure modes of each subparallel system (1#-2#, 2#-3#, 3#-4#, and 4#-5#) can be obtained. Then, according to the characteristics of the obtained scatter plots, the candidate copula functions, which can approximately describe distribution features of the samples, can be selected, and then with Bayesian selection criteria described in Section 2.2, the suitable copula functions, from the selected candidate copula functions, can be obtained which can be used to build the mixed copula model. The parameters of the built mixed copula function for each subparallel system are listed in Table 4. Finally, the mixed copula modes, for each subparallel system, are built. Further, PDF plots and contour plots for the mixed copulas, the scatter plots between empirical distributions and mixed copula functions, and scatter plots for two limit state functions are presented, respectively, in Figures 13–16.

Table 4: Parameters of each of the mixed copulas for four subsystems.

	a	b	$1-a-b$	ρ	α	θ
1#-2#	0.7438	0.1958	0.0604	−0.1868	2.4872	4.4278
2#-3#	0.8521	0.1479	0	0.1014	2.4207	4.4078
3#-4#	0.9381	0.0619	0	0.1502	2.4611	4.3984
4#-5#	0.7690	0.2310	0	−0.3490	2.4814	4.4192

With FORM, the corresponding reliability indices to each girder's failure mode are, respectively,

$$\begin{aligned} \beta_1 &= 5.3429, \\ \beta_2 &= 5.1159, \\ \beta_3 &= 4.8484, \\ \beta_4 &= 4.4417, \\ \beta_5 &= 3.6869. \end{aligned} \tag{28}$$

Then, with the equation $p_f = \Phi(-\beta)$, the corresponding failure probability to each girder's failure mode is, respectively,

$$\begin{aligned} p_{f_{g_1}} &= 4.57 \times 10^{-8}, \\ p_{f_{g_2}} &= 1.56 \times 10^{-7}, \\ p_{f_{g_3}} &= 6.22 \times 10^{-7}, \\ p_{f_{g_4}} &= 4.46 \times 10^{-6}, \\ p_{f_{g_5}} &= 1.14 \times 10^{-4}. \end{aligned} \tag{29}$$

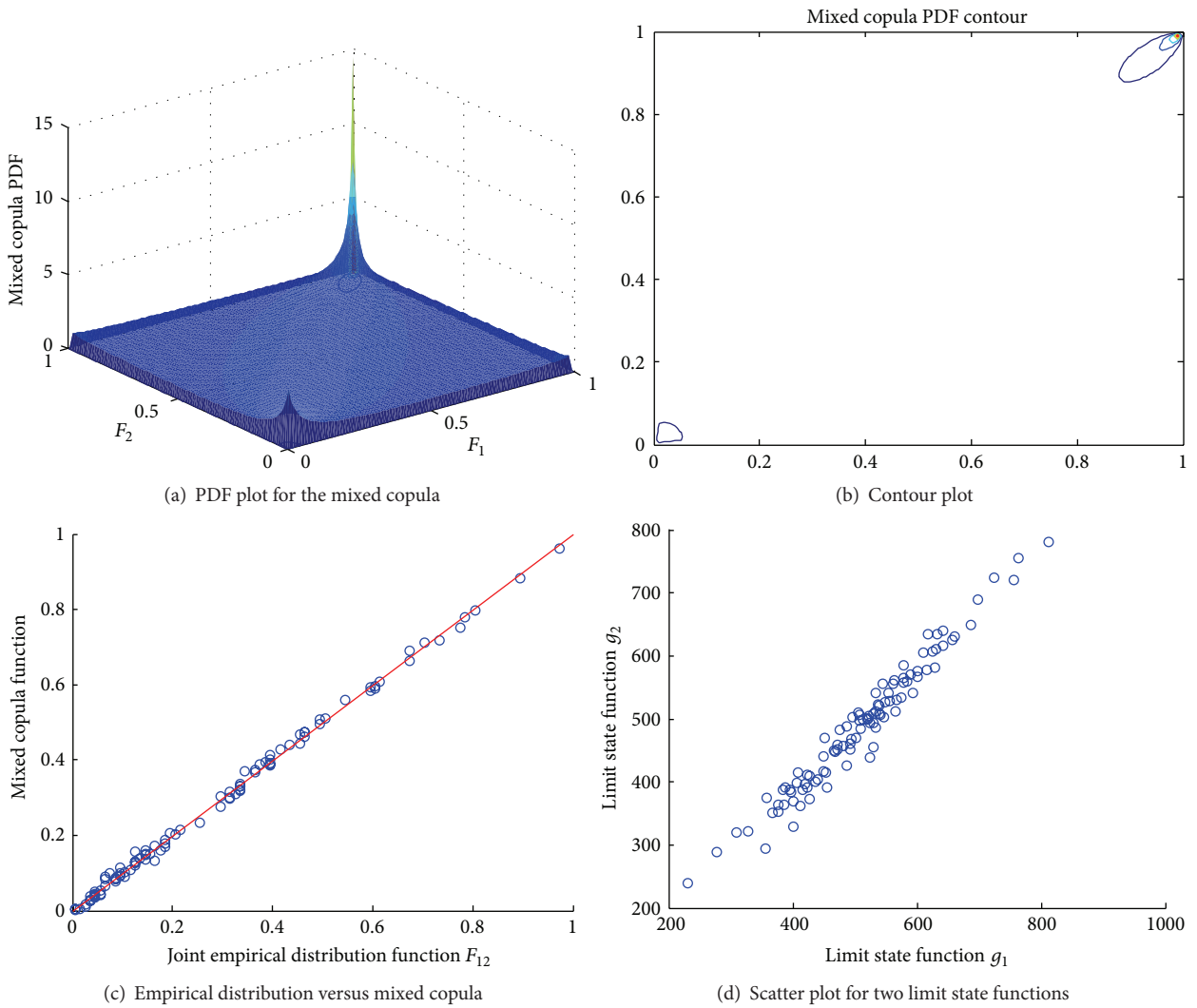

(a) PDF plot for the mixed copula

(b) Contour plot

(c) Empirical distribution versus mixed copula

(d) Scatter plot for two limit state functions

FIGURE 13: The subsystem 1#-2#.

With (19) and Table 4, the following can be obtained:

$$\begin{aligned} p_{f_{12}} &= C\left(p_{f_1}, p_{f_2}\right) = 8.61 \times 10^{-11}, \\ p_{f_{23}} &= C\left(p_{f_2}, p_{f_3}\right) = 3.12 \times 10^{-10}, \\ p_{f_{34}} &= C\left(p_{f_3}, p_{f_4}\right) = 1.32 \times 10^{-9}, \\ p_{f_{45}} &= C\left(p_{f_4}, p_{f_5}\right) = 1.31 \times 10^{-7}, \end{aligned} \tag{30}$$

where $p_{f_{12}}$ is the failure probability when girder 1# and girder 2# meantime failed, $p_{f_{23}}$ is the failure probability when girder 2# and girder 3# meantime failed, $p_{f_{34}}$ is the failure probability when girder 3# and girder 4# meantime failed, and $p_{f_{45}}$ is the failure probability when girder 4# and girder 5# meantime failed.

Suppose that failure modes between subsystems are mutually independent, and then the failure probability of structural system is approximately

$$\begin{aligned} p_f &= (-1)^2 \sum_{j=i+1,i=1}^{8} p_{f_{ij}} + (-1)^3 \sum_{t=k+1,j=i+1,k>i,i=1}^{7} p_{f_{ij}} p_{f_{kt}} \\ &+ \cdots + (-1)^9 \left(p_{f_{12}} p_{f_{23}} p_{f_{34}} p_{f_{45}} p_{f_{56}} p_{f_{67}} p_{f_{78}} p_{f_{89}}\right) \\ &\approx \sum_{j=i+1,i=1}^{8} p_{f_{ij}} - \sum_{t=k+1,j=i+1,k>i,i=1}^{7} p_{f_{ij}} p_{f_{kt}} = 2\left(p_{f_{12}}\right. \\ &+ \left. p_{f_{23}} + p_{f_{34}} + p_{f_{45}}\right) - 4\left(p_{f_{12}} p_{f_{23}} + p_{f_{12}} p_{f_{34}}\right. \\ &+ \left. p_{f_{12}} p_{f_{45}} + p_{f_{23}} p_{f_{34}} + p_{f_{23}} p_{f_{45}} + p_{f_{34}} p_{f_{45}}\right) - p_{f_{12}}^2 \\ &- p_{f_{23}}^2 - p_{f_{34}}^2 - p_{f_{45}}^2 = 2.65 \times 10^{-7}, \end{aligned} \tag{31}$$

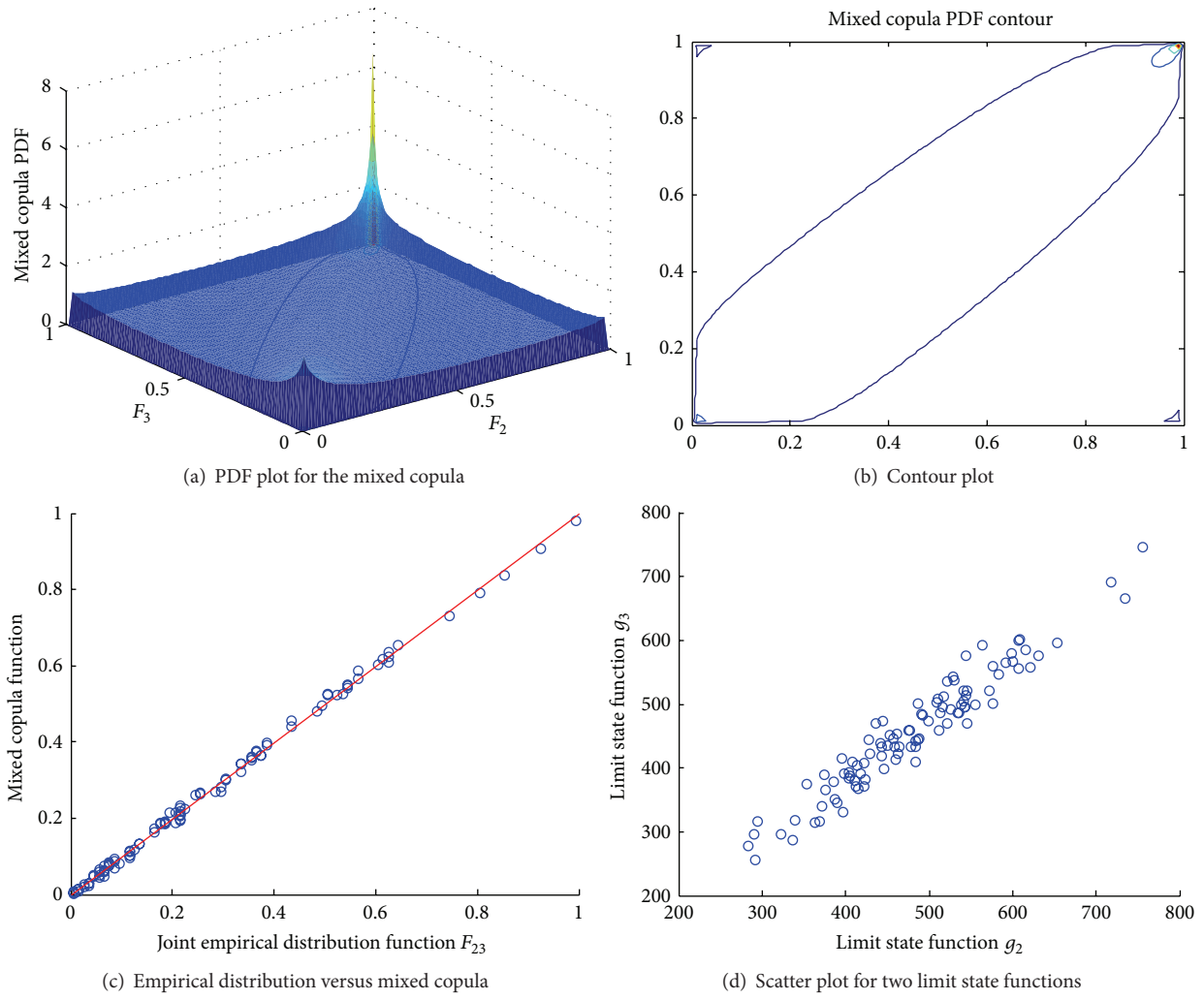

FIGURE 14: The subsystem 2#-3#.

where, because the structural system is symmetric, the failure probability of the subsystems at symmetric positions is the same. Namely, $p_{f_{12}} = p_{f_{89}}$, $p_{f_{23}} = p_{f_{78}}, \ldots, p_{f_{45}} = p_{f_{56}}$.

For each subparallel system, the failure probability without considering the correlation between the two components is

$$\begin{aligned} h_{f_{12}} &= p_{f_1} p_{f_2} = 7.13 \times 10^{-15}, \\ h_{f_{23}} &= p_{f_2} p_{f_3} = 9.70 \times 10^{-14}, \\ h_{f_{34}} &= p_{f_3} p_{f_4} = 2.77 \times 10^{-12}, \\ h_{f_{45}} &= p_{f_4} p_{f_5} = 5.08 \times 10^{-10}. \end{aligned} \tag{32}$$

Suppose that failure modes between subsystems are mutually independent, and the failure modes between the two components of each subsystem are also mutually independent; then, the failure probability of structural system [17] is approximately

$$\begin{aligned} p_f &= (-1)^2 \sum_{j=i+1,i=1}^{8} h_{f_{ij}} + (-1)^3 \sum_{t=k+1,j=i+1,k>i,i=1}^{7} h_{f_{ij}} h_{f_{kt}} \\ &\quad + \cdots + (-1)^9 \left(h_{f_{12}} h_{f_{23}} h_{f_{34}} h_{f_{45}} h_{f_{56}} h_{f_{67}} h_{f_{78}} h_{f_{89}} \right) \\ &\approx \sum_{j=i+1,i=1}^{8} h_{f_{ij}} - \sum_{t=k+1,j=i+1,k>i,i=1}^{7} h_{f_{ij}} h_{f_{kt}} = 2 \left(h_{f_{12}} \right. \\ &\quad \left. + h_{f_{23}} + h_{f_{34}} + h_{f_{45}} \right) - 4 \left(h_{f_{12}} h_{f_{23}} + h_{f_{12}} h_{f_{34}} \right. \\ &\quad \left. + h_{f_{12}} h_{f_{45}} + h_{f_{23}} h_{f_{34}} + h_{f_{23}} h_{f_{45}} + h_{f_{34}} h_{f_{45}} \right) - h_{f_{12}}^2 \\ &\quad - h_{f_{23}}^2 - h_{f_{34}}^2 - h_{f_{45}}^2 = 1.02 \times 10^{-9}. \end{aligned} \tag{33}$$

From the above solved system's failure probability shown in (31) and (33), it can be seen that the failure probability of the

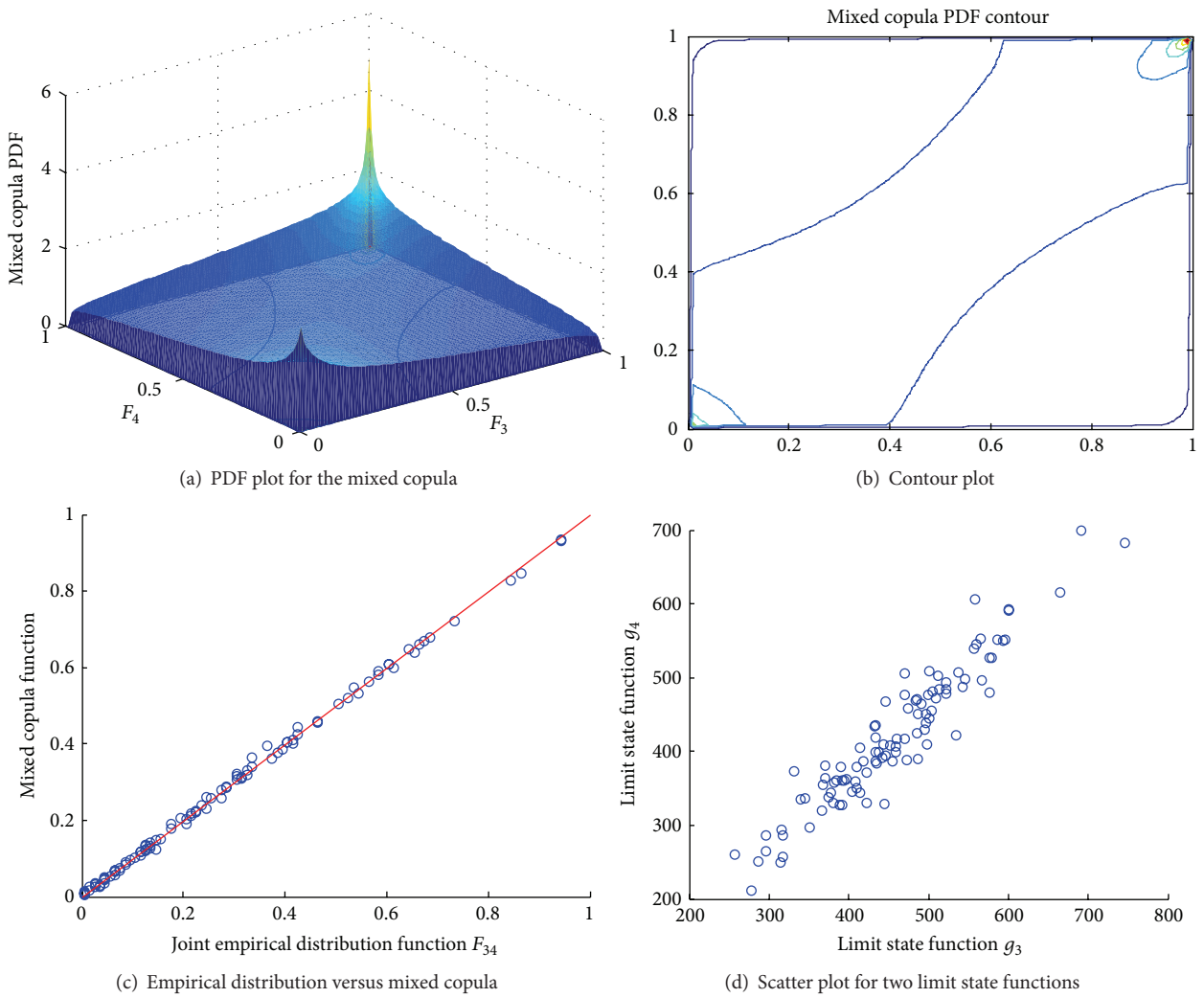

(a) PDF plot for the mixed copula

(b) Contour plot

(c) Empirical distribution versus mixed copula

(d) Scatter plot for two limit state functions

FIGURE 15: The subsystem 3#-4#.

series-parallel system considering the correlation between two adjacent girders is larger than the failure probability without considering the correlation between two adjacent girders, which showed that the series-parallel system considering the correlation between two adjacent girders more easily failed. Further, it is illustrated that considering the correlation between two adjacent girders of each subparallel system is essential and applicable for solving the reliability of the series-parallel system.

5. Conclusions

For the two-component systems and multiple-component systems with multiple failure modes, this paper presents the mixed copula models for reliability analysis of series systems, parallel systems, series-parallel systems, and parallel-series systems. The mixed copula model is obtained with the chosen optimal copula functions with the Bayesian method. Through a numerical example, it is illustrated that the calculated failure probability when considering the correlation between failure modes is larger than that without considering the correlation between failure modes. It is verified that the solved failure probability is conservative without considering the correlation between failure modes.

This paper provided a new method for characterizing the correlation between failure modes and solving the reliability of the system considering correlation between failure modes.

Competing Interests

The authors declare that they have no competing interests.

Acknowledgments

This work was supported by the Fundamental Research Funds for the Central Universities (lzujbky-2015-300, lzujbky-2015-301).

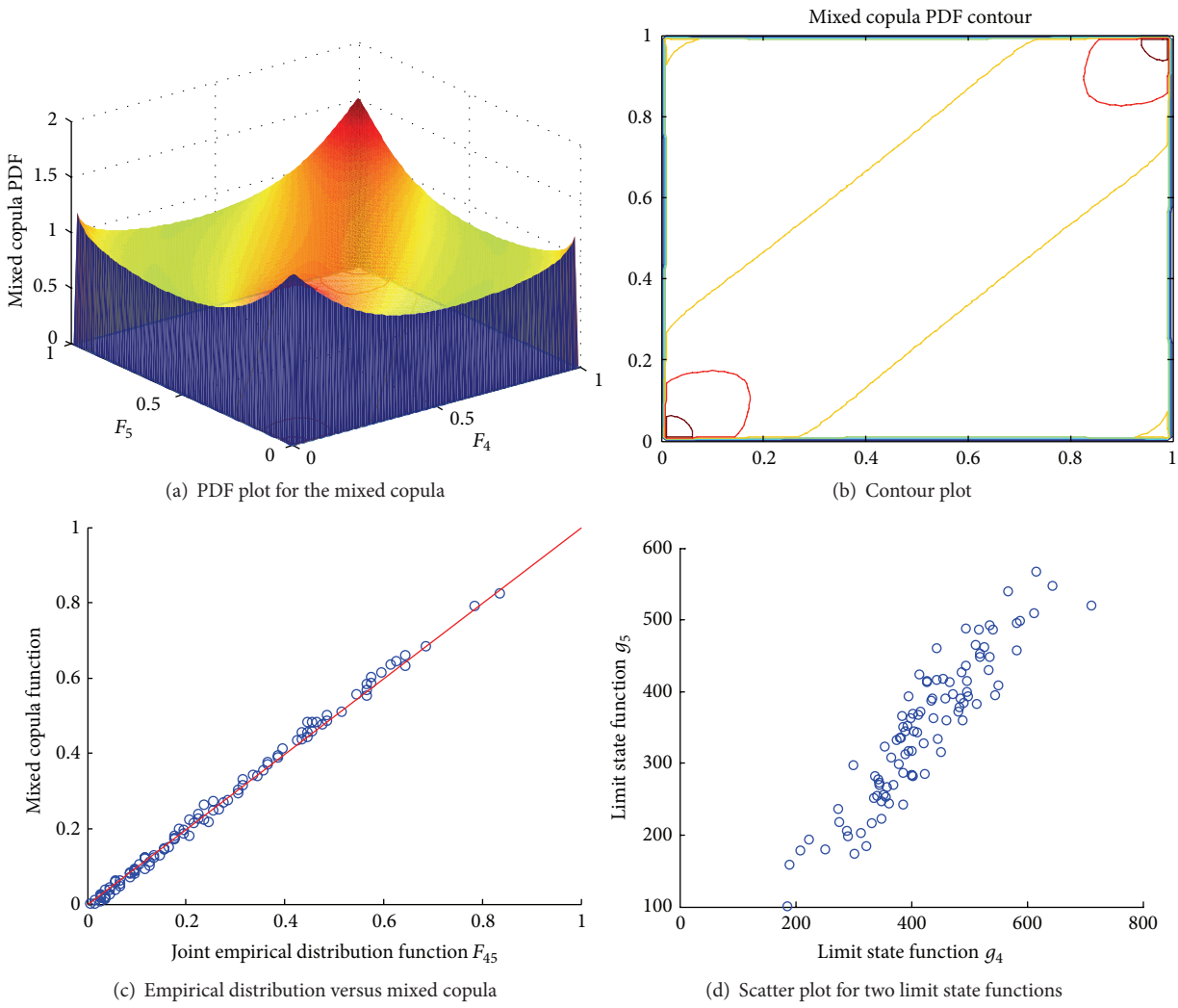

(a) PDF plot for the mixed copula

(b) Contour plot

(c) Empirical distribution versus mixed copula

(d) Scatter plot for two limit state functions

Figure 16: The subsystem 4#-5#.

References

[1] S. Eryilmaz, "Multivariate copula based dynamic reliability modeling with application to weighted-k-out-of-n systems of dependent components," *Structural Safety*, vol. 51, pp. 23–28, 2014.

[2] A. S. Balu and B. N. Rao, "Multicut-high dimensional model representation for structural reliability bounds estimation under mixed uncertainties," *Computer-Aided Civil and Infrastructure Engineering*, vol. 27, no. 6, pp. 419–438, 2012.

[3] L. Dueñas-Osorio and J. Rojo, "Reliability assessment of lifeline systems with radial topology," *Computer-Aided Civil and Infrastructure Engineering*, vol. 26, no. 2, pp. 111–128, 2011.

[4] D. V. Val, M. G. Stewart, and R. E. Melchers, "Life-cycle performance of RC bridges: probabilistic approach," *Computer-Aided Civil and Infrastructure Engineering*, vol. 15, no. 1, pp. 14–25, 2000.

[5] G. Li and G.-D. Cheng, "Correlation between structural failure modes and calculation of system reliability under hazard loads," *Engineering Mechanics*, vol. 18, no. 3, pp. 1–9, 2001.

[6] D.-Q. Li and S.-B. Wu, "System reliability analysis on main girder of plane gates considering multiple correlated failure modes," *Journal of Hydraulic Engineering*, vol. 40, no. 7, pp. 870–877, 2009 (Chinese).

[7] Y. Liu and D. Lu, "Reliability analysis of two-dimensional series portal-framed bridge system based on mixed copula functions," *Key Engineering Materials*, vol. 574, pp. 95–105, 2014.

[8] W. Q. Han, J. Y. Zhou, and K. Z. Sun, "Copulas in the mechanical components reliability analysis," in *Reliability Technology Academic Exchange Meeting and the 4th National Machinery Industry Reliability Engineering Branch of the Second Plebary Committee Conference Proceedings*, Xiangtan, China, 2010 (Chinese).

[9] Y. Y. Hou and S. B. Song, "Research of the joint distribution for flood peak and volume based on copula function," *Yellow River*, vol. 30, no. 11, pp. 39–44, 2010 (Chinese).

[10] D. Huard, G. Évin, and A.-C. Favre, "Bayesian copula selection," *Computational Statistics & Data Analysis*, vol. 51, no. 2, pp. 809–822, 2006.

[11] N. Fan, X. L. He, and Q. Zhao, "Optimal copula function selection based on Bayesian methodology," *Chinese Journal of Engineering Mathematics*, vol. 29, no. 4, pp. 516–522, 2012 (Chinese).

[12] A. Sklar, "Fonctions de répartition à n dimensions et leurs marges," *Publications de l'Institut de Statistique de l'Université de Paris*, vol. 8, pp. 229–231, 1959.

[13] R. B. Nelsen, *An Introduction to Copulas*, Springer, New York, NY, USA, 2006.

[14] L. Hu, *Essays in Econometrics with Applications in Macroeconomic and Financial Modelling*, Yale University, New Haven, Conn, USA, 2002.

[15] X. P. Fan, *Reliability Evaluation of Concrete Continuous Beam Bridge Based on Real-Time Monitoring Information*, School of Civil Engineering, Harbin Institute of Technology, Harbin, China, 2010.

[16] E. S. Gharaibeh, *Reliability and Redundancy of Structural Systems with Application to Highway Bridges*, University of Colorado, Denver, Colo, USA, 1999.

[17] R. E. Melchers, *Structural Reliability, Analysis and Prediction*, Ellis Horwood, Chichester, UK, 1987.

Hindawi Publishing Corporation
Mathematical Problems in Engineering
Volume 2016, Article ID 4264627, 12 pages
http://dx.doi.org/10.1155/2016/4264627

Research Article

Application of Probabilistic Method to Stability Analysis of Gravity Dam Foundation over Multiple Sliding Planes

Gang Wang and Zhenyue Ma

School of Hydraulic Engineering, Dalian University of Technology, No. 2 Linggong Road, Dalian 116024, China

Correspondence should be addressed to Gang Wang; ydwanggang@163.com

Received 9 March 2016; Accepted 5 June 2016

Academic Editor: Egidijus R. Vaidogas

The current challenge to the engineering profession is to carry out probabilistic methods in practice. The design point method in generalized random space (DPG method) associated with the method of divided difference can be utilized to deal with the complex problem of probability calculation of implicit performance function with nonnormal and correlated variables. For a practical concrete gravity dam, the suggested method is performed to calculate the instability probability of the dam foundation over multiple sliding places. The general conclusions drawn in the paper are identical to those in other research and the method is proved to be feasible, accurate, and efficient. As the same analysis principle, the method can also be used in other similar fields, such as in fields of slopes, earth-rock dams, levees, and embankments.

1. Introduction

It is a trend to use the probabilistic method for evaluation of the risk of failure in almost all engineering fields, including some in geotechnical or structural engineering [1–3]. The current challenge to the geotechnical and structural engineering profession is to carry out probabilistic methods in practice [4]. Many researchers have focused on the research topics of reliability-based design and risk analysis and made progress in resolving the problem about the instability failure of slopes, dams, levees, embankments, and other geotechnical or structural engineering fields in recent years [1, 4, 5].

The Monte Carlo method (MC) is usually used to estimate the reliability index, β. However this method is rarely adopted due to its huge calculation time [5, 6]. Besides MC, many other methods have been proposed for reliability analysis, such as the first-order reliability method (FORM) [1, 7], second-order reliability method (SORM) [8, 9], and some improved methods. In order to obtain β, the partial derivatives of performance function, $g(\mathbf{X})$, are needed in these methods. But, in geotechnical or structural engineering, $g(\mathbf{X})$ is usually implicit, and its partial derivatives are complex or difficult to be derived from implicit to explicit. Therefore, these conventional reliability methods only can be used to analyze small structures.

Always, the response surface methods (RSMs) are utilized to obtain the solution of β for reliability problem with implicit $g(\mathbf{X})$ for complex structures. Wong applied RSM to evaluate the reliability of a homogeneous slope [10]. Moore and Sa constructed confidence intervals about the difference in mean responses at the stationary point and alternate points based on the proposed delta method and F-projection method and compared coverage probabilities and interval widths [11]. Zheng and Das proposed an improved response surface method and applied that to the reliability analysis of a stiffened plate structure [12]. Guan and Melchers evaluated the effect of response surface parameter variation on structural reliability [13]. Gupta and Manohar used the response surface method to study the extremes of Von Mises stress in nonlinear structures under Gaussian excitations [14]. Wong et al. proposed an adaptive design approach to overcome the problem, which was that the solution of the reliability analysis initially diverged when the loading was applied in sequence in the nonlinear finite element (NLFE) analysis, and made several suggestions to improve the robustness of RSM [15]. Xu and Low used RSM to approximate the performance function of slope stability in slope reliability analysis, in which the response surface is taken as a bridge between standalone numerical packages and spreadsheet-based reliability analysis [16]. Cheng et al. presented a new

artificial neural network (ANN) based response surface method in conjunction with the uniform design method for predicting failure probability of structures [17]. Gavin and Yau described the use of higher order polynomials in order to approximate the true limit state more accurately in contrast to recently proposed algorithms which focused on the positions of sample points to improve the accuracy of the quadratic stochastic response surface method (SRSM) [18]. Zou et al. presented an accurate and efficient MC for limit state-based reliability analysis at both component and system levels, using a response surface approximation of the failure indicator function [19]. Nguyen et al. proposed an adaptive construction of the numerical design, in which the response surface was fitted by the weighted regression technique, which allowed the fitting points to be weighted according to their distance from the true failure surface and their distance from the estimated design point [20]. Similar to support vector machine- (SVM-) based RSM, Samui et al. adopted relevance vector machine- (RVM-) based first-order second-moment method (FOSM) to build a RVM model to predict the implicit performance function and evaluate the partial derivatives with sufficient accuracy [21]. Tan et al. discussed similarities and differences between radial basis function networks (RBFN) based RSMs and SVM-based RSMs, which indicated that there is no significant difference between them, and then proposed two new sampling methods and a hybrid RSM to reduce the number of evaluations of the actual performance function [22, 23].

However, RSM and its improved methods mentioned above are relatively complicated and need much more computing cost, since they have a lot of iterating calculations at different design points associated with numerical method (i.e., finite element method) to fit limit state curved surface, which is represented by $g(\mathbf{X}) = 0$. In this paper, a novel design point approach in generalized random space (DPG method) associated with the method of divided difference is proposed and applied to analyze the probability of gravity dam foundation instability over multiple sliding planes. In the method, implicit performance function with nonnormal and correlated variables is considered, and iterating calculation for β is performed in generalized random space directly. The whole procedure for reliability analysis does not need much preparation mathematically and is relatively simple for the complex engineering problems.

2. Basic Principle of Computing Instability Probability of Gravity Dam Foundation

Due to the complexity of foundation stability against sliding of gravity dam, for simplification, the instability probability is commonly evaluated using models of single or dual sliding plane(s) for the dam foundation [24]. However, instability of foundation over multiple sliding planes is a general case occurring in bedrock under most engineering geological conditions for a gravity dam. Therefore, it is necessary to apply a model of multiple sliding planes to analysis on instability probability of gravity dam foundation, but there is limited existing research regarding this case. In traditional deterministic analysis, equal safety coefficient method (namely, equal-K method) is used to analyze and assess the stability failure of dam foundation. In the method, factor of safety, K, is regarded as an unknown number in nonlinear equations and needs to be solved by iterative calculating numerically, similar to the application of the methods of Bishop, Spencer, and Janbu as well, which are widely used for stability analysis on slope. The reliability index β or failure probability p_f is calculated by implicit performance function, $g(\mathbf{X}) = K - 1$, associated with the factor of safety K. Accounting for this, the conventional FORM and its improved methods (such as JC method which combines the method of equivalent normalization transformation with FORM and is recommended by the Joint Committee of Structural Safety) cannot be directly applied since the partial derivatives of $g(\mathbf{X})$ with respect to the variable $\mathbf{X}$ cannot be evaluated directly [1, 25]. Hence, if a partial derivative of $g(\mathbf{X})$ is calculated by divided difference mathematically, the value of the derivative at any design point $\mathbf{x}^*$ will be worked out easily, and the limit state curved surface will not be fitted completely as RSM [1, 25]. Usually, the JC method associated with the method of divided difference could calculate design points by iteration on the actual limit state curved surface so that it could avoid fitting the overall curved surface. The method can provide sufficient accuracy and efficiency to calculate probability of failure as prone to dealing with complex problems for large projects, which has been verified by many examples in some literatures. So it is a good idea to use the similar method to calculate instability probability of gravity dam foundation over multiple sliding planes.

2.1. Uncertainty in the Analysis. Probabilistic methods can reveal the contributions of different components to the uncertainty in the analysis on the probability of failure of dam foundation for gravity dam. The uncertainty related to instability of dam foundation could be classified as follows: (1) the uncertainty of hydrographic and hydraulic parameters; (2) the uncertainty of mechanical parameters of rocks and soils; (3) the uncertainty of seismic excitation; (4) other uncertainty, underlying the process of dam design, construction, operation, management, and so on.

The second type of uncertainty above is studied mainly in the paper, and others are ignored by deterministic engineering applications just like in conventional analysis for dam stability against sliding. The uncertainty of mechanical parameters of rocks and soils might be enslaved to analysis methods, due to subjective or objective conditions, derived from the lack of knowledge, and so on. Always, the laboratory and *in situ* measured data of the properties of rocks or soils are inadequate. So there is demonstrable distinction between the measured values from the statistics of the small sampling and the true values of the actual physical and mechanical properties existing in real world.

Many of studies have shown that friction coefficient f' and cohesion force c' against shear fracture of rocks or discontinuities are two important uncertainty parameters

influencing the foundation stability of gravity dam. Firstly, by a great number of data of field measurements and their statistical back-analyses, there are obvious scatter in the spatial variation of the two shear strength parameters not only for rock mass and faults of different projects but also for different types of rock mass and faults at different locations in the same project. Chen et al. indicated that the variability of f' is nearly at the same level, but the variability of c' is not so by the study on the variability of the shear strength parameters of the foundation rock mass and faults at several dam sites in China [26, 27]. Secondly, the probability distributions and negative correlation of the two parameters cannot be ignored. The random parameters might be normally distributed or ln-normally distributed.

In our probabilistic analysis, the two parameters against shear fracture, f' and c', are to be regarded as random variables following some distributions, such as normal or ln-normal distribution, and considering their variability and correlation.

2.2. Performance Function for Computing Instability Probability

2.2.1. Equivalence Safety Factor Method for Foundation Instability over Multiple Sliding Planes. The sliding patterns of gravity dam foundation could be divided by slip paths over single, dual, and multiple plane(s). The last one is the general case for analysis of foundation instability of gravity dam by assuming the potential failure surface as shown in Figure 1. There are n slip planes of n sliding wedges from upstream to downstream in the foundation. The ith wedge is subjected to (a) the vertical normal stress σ and the horizontal shear stress τ induced by action of dam or other upside loads along the topside of the wedge, (b) dead load R_i, (c) force N_i and uplift U_i normal to the ith slip plane, (d) resistance Q_i provided by the $(i+1)$th wedge, (e) angle of inclination α_i of the interface between the ith and $(i+1)$th wedges, and (f) angle of inclination β_i, the length l_i, and the shear strength parameters f_i' and c_i' of the ith slip plane.

Based on the limit equilibrium method, the normal force N_i and applied shear T_i of the ith slip plane, respectively, are expressed as

$$N_i = \left(R_i + \int \sigma \mathrm{d}A_i\right)\cos\beta_i - \Big\lfloor Q_i \cos\left(\alpha_i + \beta_i\right) - Q_{i-1}\cos\left(\alpha_{i-1} + \beta_i\right) + \int \tau \mathrm{d}A_i \sin\beta_i \Big\rfloor - U_i \tag{1}$$

$$T_i = Q_{i-1}\sin\left(\alpha_{i-1} + \beta_i\right) - Q_i \sin\left(\alpha_i + \beta_i\right) + \left(R_i + \int \sigma \mathrm{d}A_i\right)\sin\beta_i + \int \tau \mathrm{d}A_i \cos\beta_i. \tag{2}$$

The stability factor of safety for the ith wedge is defined as

$$K_i = \frac{N_i f_i' + c_i' l_i}{T_i}. \tag{3}$$

So substituting the expressions for N_i and T_i into (3) for the typical wedge and according to the definition of equivalence safety factor method, $K_1 = K_2 = \cdots = K_n = K$, the general wedge and wedge interaction equation can be written as

$$K = \frac{Q_{i-1}\cos\left(\alpha_{i-1} + \beta_i\right) f_i' - Q_i \cos\left(\alpha_i + \beta_i\right) f_i' + p_i}{Q_{i-1}\sin\left(\alpha_{i-1} + \beta_i\right) - Q_i \sin\left(\alpha_i + \beta_i\right) + q_i}, \tag{4}$$

where $p_i = \lfloor (R_i + \int \sigma \mathrm{d}A_i)\cos\beta_i - \int \tau \mathrm{d}A_i \sin\beta_i - U_i \rfloor f_i' + c_i' l_i$, and $q_i = (R_i + \int \sigma \mathrm{d}A_i)\sin\beta_i + \int \tau \mathrm{d}A_i \cos\beta_i$.

The nonlinear equations (4) are in terms of K and Q_i $(i = 0, 1, \ldots, n)$, and $Q_0 = Q_n = 0$. So there are eventually n unknown numbers for n sliding wedges of dam foundation. Assuming $\alpha_i = 90^\circ$ according to conventional vertical slice method [26, 28–30], K and Q_i $(i = 1, \ldots, n-1)$ can be worked out by iterative calculation numerically.

2.2.2. Performance Function for Probability Calculation. The basic expression of the performance function for reliability analysis on dam foundation stability could be given as

$$Z = K - 1, \tag{5}$$

where K is the factor of safety mentioned in (4), which is the function in terms of variables $X_1, X_2, \ldots, X_l$. So (5) can be rewritten as

$$Z = K - 1 = g\left(X_1, X_2, \ldots, X_l\right), \tag{6}$$

where $g(X_1, X_2, \ldots, X_l)$ is the function associated with the random variables $X_1, X_2, \ldots, X_l$.

In the analysis of instability of foundation over multiple sliding planes, $Z = g(X_1, X_2, \ldots, X_l)$ is implicit function, and limit state equation, $Z = 0$, can be represented by nonlinear equation (4) above. Correspondingly, the random variables $X_1, X_2, \ldots, X_l$ $(l = 2n)$ are actually the strength parameters against shear fracture, f_i' and c_i', where $i = 1, 2, \ldots, n$.

2.3. Computing Method of Failure Probability with Nonnormal and Correlative Random Variables.

It is a problem to calculate instability probability with nonnormal and correlated random variables of dam rock base over multiple sliding planes. What is more, the random characteristics of the variables will influence the accuracy of the value of instability probability.

A well known method for calculating reliability index or probability of failure of a structure, MC simulation, is derived

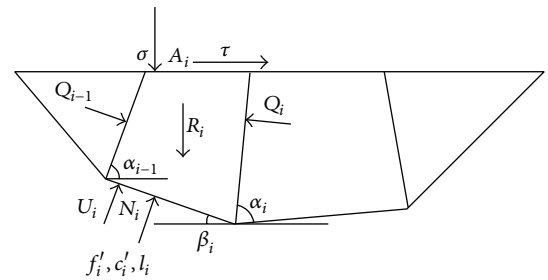

Figure 1: Illustration of multiple sliding planes for stability calculation of dam foundation.

from sampling principle. In the method, each continuous variable is replaced by a large number of discrete values generated from the underlying distribution. These values are used to compute a large number of values of function Z and its distribution. Finally, the probability of failure can be estimated to be equal to the number of failures which failed divided by the total number of calculations statistically. MC has been widely applied for reliability calculation due to its clear definition in spite of the low calculating efficiency, and under some circumstances it is always the unique method to verify the accuracy of any other probabilistic method.

Besides MC method, JC method is also a conventional method for calculating reliability index or probability of failure of a structure. When the random variables are nonnormally distributed, the treatment of equivalent normalization transformation [31] for the variables is performed rationally; however, when the random variables are correlative for each other, the problem becomes complicated because the calculation with nonnormal and correlative variables involves complex combining processes of equivalent normalization transformation and orthogonal transformation. Calculation of the eigenvalues of matrices must be conducted in the procedure in particular. Other approaches, such as the method of Rosenblatt or Nataf transformation, are also utilized to deal with the calculation with nonnormal and correlated variables [32, 33]. However, in the former method the joint cumulative distribution function of variables must be known and in the latter the ratio of coefficients of correlation between pre- and posttransformation of variables needs to be determined previously. The preconditions in the two methods are hardly ensured usually.

So a new reliability-based method, which is called design point method in generalized random space (DPG method), can be applied, since iterative calculation for β is performed in generalized random space directly by assuming that the value of coefficient of correlation of any two variables is not changed before and after variable transformation in generalized space based on the principle of isoprobabilistic transformation [34–37]. Obviously, the DPG method can be used in rather more general cases than JC method. When the variables are independent of each other, the former becomes the latter.

A set of random variables $X_1, X_2, \ldots, X_n$, describing the randomness in the geometry, material, loading, and so on, can form an n-dimensional generalized random space, in which there is a performance function $Z = g(X_1, X_2, \ldots, X_n)$ for the structure. Similar to the Euclidean random space in conventional reliability theory, the limit state of the structure is represented by $Z = 0$. $Z > 0$; then the structure is on the reliable state ("safe"). $Z < 0$; then the structure is on the failure state ("fail"). Figure 2 shows the principle of the DPG method.

To perform DPG method, firstly the angle of any two axes is defined as

$$\theta_{X_iX_j} = \pi - \arccos\left(\rho_{X_iX_j}\right), \tag{7}$$

where $\rho_{X_iX_j}$ is the coefficient of correlation for variables X_i and X_j. The coefficient of correlation for the two variables

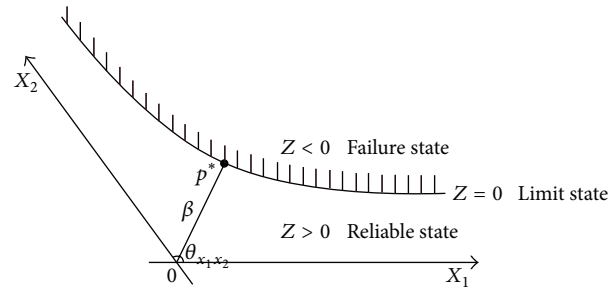

Figure 2: A conceptual illustration of the design point and reliability index in 2-dimensional generalized random space.

after transformation in generalized random space based on the principle of isoprobabilistic transformation is

$$\rho_{X_i'X_j'} \approx \rho_{X_iX_j}, \tag{8}$$

where X_i' and X_j' are arbitrary two variables by transformation in generalized space from X_i and X_j, respectively.

The mean and standard deviation of any variable X_i' are defined as

$$\begin{aligned} \mu_{X_i'} &= x_i^* - \sigma_{X_i'}\Phi^{-1}\left[F_i\left(x_i^*\right)\right], \\ \sigma_{X_i'} &= \frac{\varphi\left\{\Phi^{-1}\left[F_i\left(x_i^*\right)\right]\right\}}{f_i\left(x_i^*\right)}, \end{aligned} \tag{9}$$

where x_i^* is any component of the vector $\mathbf{x}^* = (x_1^*, x_2^*, \ldots, x_i^*, \ldots, x_n^*)$, which is the value of the vector $\mathbf{X} = (X_1, X_2, \ldots, X_n)$ at design point p^* shown in Figure 2; $f_i(\cdot)$ denotes the probability density function (PDF) of the random variables; and $F_i(\cdot)$ denotes the cumulative distribution function (CDF) of the random variables.

The reliability index at $\mathbf{x}^*$ is

$$\beta = \frac{\sum_{i=1}^{n}\left(\partial g/\partial X_i\right)\big|_{p^*}\left(\mu_{X_i'} - x_i^*\right)}{\left(\sum_{i=1}^{n}\sum_{j=1}^{n}\rho_{X_i'X_j'}\left(\left(\partial g/\partial X_i\right)\left(\partial g/\partial X_j\right)\right)\big|_{p^*}\sigma_{X_i'}\sigma_{X_j'}\right)^{1/2}} \tag{10}$$

and the sensitivity coefficient of any variable X_i is calculated as

$$\alpha_i' = \frac{\sum_{j=1}^{n}\rho_{X_i'X_j'}\left(\partial g/\partial X_j\right)\big|_{p*}\sigma_{X_j'}}{\sum_{j=1}^{n}\sum_{k=1}^{n}\rho_{X_j'X_k'}\left(\left(\partial g/\partial X_j\right)\left(\partial g/\partial X_k\right)\right)\big|_{p^*}\sigma_{X_j'}\sigma_{X_k'}}. \tag{11}$$

x_i^* for next iterative calculation is

$$x_i^* = \mu_{X_i'} + \beta\alpha_i'\sigma_{X_i'}. \tag{12}$$

The initial $\mathbf{x}^*$ are always the mean of random variable. When $\mathbf{x}^*$ converges by repeated calculation from (9) to (12), the resultant reliability index β and probability of failure $p_f = 1 - \Phi(\beta)$ are obtained finally.

2.4. Method of Divided Difference to Computing Partial Derivative of Implicit Performance Function. According to (10) and (11), the value of partial derivative of performance function at design point p^*, $(\partial g/\partial X_i)|_{p^*}$, needs to be calculated. When the performance function, $g(X_1, X_2, \ldots, X_n)$, is implicit, the method of one order divided difference can be utilized as

$$\begin{aligned}\left.\frac{\partial Z}{\partial X_i}\right|_{p^*} &= \left.\frac{\partial g}{\partial X_i}\right|_{p^*} \approx \frac{\Delta g}{\Delta x_i} \\ &= \frac{g\left(x_1, x_2, \ldots, x_i + \Delta x_i, \ldots, x_n\right)}{\Delta x_i} \\ &\quad - \frac{g\left(x_1, x_2, \ldots, x_i, \ldots, x_n\right)}{\Delta x_i}.\end{aligned} \tag{13}$$

From the practical experience of calculation, the computing efficiency and accuracy can be ensured while $\Delta x_i = (0.01 \sim 0.05)x_i$.

2.5. Computing Steps and Procedures. DPG method associated with method of divided difference to calculate the stability reliability index β or instability probability p_f of gravity dam foundation over multiple sliding planes has been proposed above and can be implemented easily within Matlab. There are six steps of the solution process:

(1) Regard all of the strength parameters against shear fracture, f_i' and c_i' $(i = 1, 2, \ldots, n)$, of the n slip planes under n sliding wedges as the random variables $\mathbf{X}$ that affect the foundation stability of gravity dam; generally assume the means of f_i' and c_i' as the initial value $\mathbf{x}^*$ at current design point p^*.

(2) Use the current $\mathbf{x}^*$ to calculate the means and standard deviations of the variables by (9).

(3) Calculate β at the current design point p^* by (10), and then perform sensitivity analyses according to (11). The critical calculation of partial derivative of performance function, $Z = g(\mathbf{X}) = K(\mathbf{X}) - 1$ (see (6)), is performed by divided difference calculation according to (13), in which the factor of safety K solved by nonlinear equations (4) at the limit state $(Z = 0)$ is considered.

(4) Use (12) to obtain the new $\mathbf{x}^*$ for next iterative calculation.

(5) Perform repeated calculation from Step (2) to Step (4) until the values of vector $\mathbf{x}^*$ are converged.

(6) Obtain the ultimate β and calculate the instability probability $p_f = 1 - \Phi(\beta)$ finally.

3. Assessment Standard

Dam failure is different from general safety accident. On the one hand, the consequence is very serious; sometimes it even causes destructive disasters; on the other hand, dam failure is affected by many natural factors and cannot be controlled by human. Therefore, risk standard of dam failure is a comprehensive index involving many factors, such as politics, economy, engineering technology, society, natural environment, and cultural background. If the risk standard is selected relatively low, the safety reliability resisting dam failure will be insufficient, and once failure takes place, the consequence will be serious; on the contrary, if the standard is relatively high, the project cannot bring anticipated economic benefit and may cause water waste and investment loss. From this point, many experts and researchers have studied the establishment of appropriate design standards. Based on the related data of different projects in the worldwide, the allowable probability of failure, P_y, is 1.1×10^{-4}/a for large and middle dams and the failure probability is unacceptable when it is larger than 1.0×10^{-3}/a. Among all the failure modes, stability failure accounts for about 10% of the total of dam failure according to ICOLD (the International Commission on Large Dams) Bulletin 99 (1995), "Dam FailuresStatistical Analysis," and Chinese "unified standard for reliability design of hydraulic engineering structures." Therefore, it is considered that the acceptable probability of stability failure is less than 1.1×10^{-5}/a, and the instability probability is unacceptable when it is larger than 1.0×10^{-4}/a.

In contrast, the allowable safety factor $[K]$ is 3.0 under normal loading condition according to deterministic limit equilibrium method in Chinese Design Specification of Concrete Gravity Dam (DL 5108-1999), and the target reliability index β_T is 4.2 for the hydraulic structures at Grade 1 and 3.7 for the hydraulic structures at Grade 2 in the relative reliability-based design codes.

4. Application

4.1. Basic Data. A hydropower station located in southeast China is for power generation singly without other comprehensive benefits. Its main body is roller compacted concrete gravity dam which has a maximum height of 119.0 m, the crest length of 284.0 m, and the elevation of 2564.00 m. This dam consists of 14 blocks and is numbered from number 1 to number 14 from left bank to right bank. Number 5 to number 8 are overflow structures; others are water retaining structures. The regulating storage of the reservoir is 0.254 billion m^3. The usual pool elevation under normal operation is 2560.0 m, and the corresponding tailwater elevation is 2471.61 m. The silt elevation is 2497.70 m. The uplift intensity factor is 0.25. The structure grade of the dam is Grade 2, so the design reference period N_d is 50 a according to the design specification. The allowable instability probability is $[P] = P_y \times N_d = 5.5\times10^{-4}$, and the probability is unacceptable when it is larger than 5×10^{-3}.

4.1.1. Engineering Geological Conditions. The geological exploration in the dam site has shown that there are a great number of lowly inclined weak structural planes and several fault-fractured zones within the foundation which are adverse to the dam stability. The geologic parameters of the bed base rock and the structural planes are listed in Tables 1 and 2, respectively.

Table 1: Geologic parameters of bed base rock in the dam site.

Class of rock mass	Dry density ρ/g/cm^3	Saturated compressive strength R_b/MPa	Bedrock/bedrock				Concrete/bedrock	
			Deformation module E_0/GPa	Poisson's ratio μ	Strength against shear fracture		Strength against shear fracture	
					f'	c'/MPa	f'	c'/MPa
II	2.65–2.70	80–100	15~21	0.20–0.25	1.20~1.35	1.50~1.60	1.10~1.20	1.10~1.15
III_1	2.60–2.65	60–80	8~12	0.25–0.30	1.10~1.20	1.00~1.30	1.00~1.07	0.90~1.00

Table 2: Geologic parameters of structural planes in the dam site.

Classification		Strength against shear fracture	
Category	Subcategory	f'	c'/MPa
Hard structural plane		0.60~0.70	0.10~0.15
Weak structural plane or fault-fractured zones	Clastic and fragment	0.45~0.50	0.10~0.15
	Clastic with mud	0.35~0.40	0.05~0.10
	Mud with silty grain clastic	0.25~0.30	0.01~0.05
	Clayey mud	0.18~0.25	0.002~0.010

Figure 3 shows the geologic section of typical sliding modes of number 6 overflow section. There are lowly inclined structural planes (mainly fh09, fh10, and fh11) and joints (fh152-2, etc.) below the dam base and steeply inclined faults (F16, F17, etc.) near to the dam heel. The geological characteristics of lowly inclined weak structural planes are listed in Table 3. Table 4 lists the slip paths and the values of the material properties of the sliding planes used for stability calculation.

4.1.2. Analyses of Slip Paths and Wedges. The slip paths of dam foundation are consisted of the faults, weak structural planes, joints, and rock bridges by their probable combinations (shown in Figure 3). For stability analysis of the dam foundation, the bed base rock will be divided in several wedges according to any different slip path. Figure 4 gives the divided wedges on Slip Path B, for example. There are one tensile fractured plane (B1-B2) below dam heal and three sliding planes (B2-B3, B3-B4, and B4-B5) at the bottom of the three wedges (Wedges I, II, and III).

4.1.3. Results from Deterministic Analyses. Under the normal loading condition, the safety factors are, respectively, 2.56, 2.45, and 10.71 for the three slip paths mentioned above by deterministic equivalence safety factor method without taking the variation of parameters into consideration. The first two factors of safety are less than the allowance safety factor, $[K] = 3.0$. So it is necessary to meet the stability of dam foundation against sliding by some effective engineering treatments.

In the next sections, the influence of randomness of strength parameters against shear fracture of sliding planes on foundation stability will be researched by DPG method associated with the method of divided difference proposed by the paper. That is, the foundation instability probability affected by the probability distribution, variability, and negative correlation of the two parameters, f' and c', is considered in detail.

4.2. Limit State Equations and Random Parameters. For the practical dam project, the limit state equations for the most adverse slip path, Slip Path B, of number 6 overflow section are expressed by (4) as follows:

$$\begin{aligned}
&KQ_0 \sin(\alpha_0 + \beta_1) - KQ_1 \sin(\alpha_1 + \beta_1) + Kq_1 \\
&\quad - Q_0 \cos(\alpha_0 + \beta_1) f_1' + Q_1 \cos(\alpha_1 + \beta_1) f_1' \\
&\quad - p_1 = 0, \\
&KQ_1 \sin(\alpha_1 + \beta_2) - KQ_2 \sin(\alpha_2 + \beta_2) + Kq_2 \\
&\quad - Q_1 \cos(\alpha_1 + \beta_2) f_2' + Q_2 \cos(\alpha_2 + \beta_2) f_2' \\
&\quad - p_2 = 0, \\
&KQ_2 \sin(\alpha_2 + \beta_3) - KQ_3 \sin(\alpha_3 + \beta_3) + Kq_3 \\
&\quad - Q_2 \cos(\alpha_2 + \beta_i) f_3' + Q_3 \cos(\alpha_3 + \beta_3) f_3' \\
&\quad - p_3 = 0,
\end{aligned} \tag{14}$$

where

$$\alpha_0 = \alpha_1 = \alpha_2 = 90^\circ,$$

$$\beta_1 = -14^\circ,$$

$$\beta_2 = -16^\circ,$$

$$\beta_3 = -14^\circ,$$

Table 3: Geologic characteristics of lowly inclined weak structural planes.

Name of structural planes	Occurrence	Width of fractured zone for weak structural planes/cm	Extension length/m	Type of structural planes
fh09	N40–60°W/NE ∠ 20–25°	2–30	210	Clastic with mud
fh10	N40–60°W/NE ∠ 20–25°	2–20	200	Clastic with mud
fh11	N40–60°W/NE ∠ 20–25°	2–8	125	Clastic and fragment
fh152-5	N80°E/NW ∠ 20°	2~5	/	Mud with silty grain clastic

Table 4: Description of the slip paths and the value of the material properties of the sliding planes.

Number of slip paths	Name of sliding planes comprising the paths	Angle of apparent dip/°	Characteristics	Strength against shear fracture	
				f'	c'/MPa
A	A1-A2	90	Tensile fractured plane at dam heal	0.000	0.000
	A2-A3	–16	Clastic with mud	0.375	0.075
	A3-A4	–16	Clastic and fragment	0.475	0.125
	A4-A5	–16	Clastic with mud	0.375	0.075
	A5-A6	0	Dam base	1.150	1.125
B	B1-B2	90	Tensile fractured plane at dam heal	0.000	0.000
	B2-B3	–14	Clastic with mud	0.375	0.075
	B3-B4	–16	Clastic and fragment	0.475	0.125
	B4-B5	–14	Clastic with mud	0.375	0.075
C	C1-C2	90	Tensile fractured plane at dam heal	0.000	0.000
	C2-C3	–15	Clastic and fragment	0.475	0.125
	C3-C4	–19	Rock bridge (II)	1.275	1.550
	C4-C5	–16	Mud with silty grain clastic	0.275	0.030
	C5-C6	–16	Rock bridge (III_1)	1.050	0.850

$$
\begin{aligned}
&p_i \\
&\quad = \left[\left(R_i + \int \sigma \mathrm{d}A_i\right)\cos\beta_i - \int \tau \mathrm{d}A_i \sin\beta_i - U_i\right] f_i' \\
&\qquad + c_i' l_i, \quad i = 1, 2, 3, \\
&q_i = \left(R_i + \int \sigma \mathrm{d}A_i\right)\sin\beta_i + \int \tau \mathrm{d}A_i \cos\beta_i, \\
&\qquad\qquad\qquad\qquad\qquad\qquad i = 1, 2, 3, \\
&\int \sigma \mathrm{d}A_i = V_i, \quad i = 1, 2, 3, \\
&\int \tau \mathrm{d}A_i = H_i, \quad i = 1, 2, 3, \\
&l_1 = 49.9\ \mathrm{m}, \\
&l_2 = 33.5\ \mathrm{m}, \\
&l_3 = 117.4\ \mathrm{m}, \\
&Q_0 = Q_3 = 0.
\end{aligned} \tag{15}
$$

According to the practical engineering experience and the special geological and mechanical parameters of the bed base rock of the example dam in the paper, the degree of scatter of the variation coefficients of the strength parameters against shear fracture is obvious, so the coefficients of variation of f' and c' are assumed to change in certain ranges. The statistical characteristics of f' and c' of Slip Path B used for calculation are listed in Table 5. According to Chinese "unified standard for reliability design of hydraulic engineering structures" (1994), the parameter distribution type of slip planes can be assumed in normal or ln-normal distributions for reliability analysis when the statistical data are not sufficient.

4.3. Resultant Analyses

4.3.1. Feasibility of DPG Method. Two methods, DPG and MC methods, are used to calculate the instability probabilities of Slip Path B during design reference period. Table 6 gives the calculated results obtained by the two methods; when f' and c' are both normally distributed, their variation coefficients, $\delta_{f'}$ and $\delta_{c'}$, are 0.2 and 0.3, respectively, and their coefficient of correlation, $\rho_{f'c'}$, is 0.

The instability probabilities of Slip Path B are, respectively, 1.310×10^{-4} and 1.244×10^{-4} calculated by MC and DPG methods, and the absolute and relative errors between the two methods are, respectively, 0.0007% and 5.3%. Thus, the two methods have nearly the same accuracy, but the latter requires less iterating calculation for convergence. Meanwhile, by

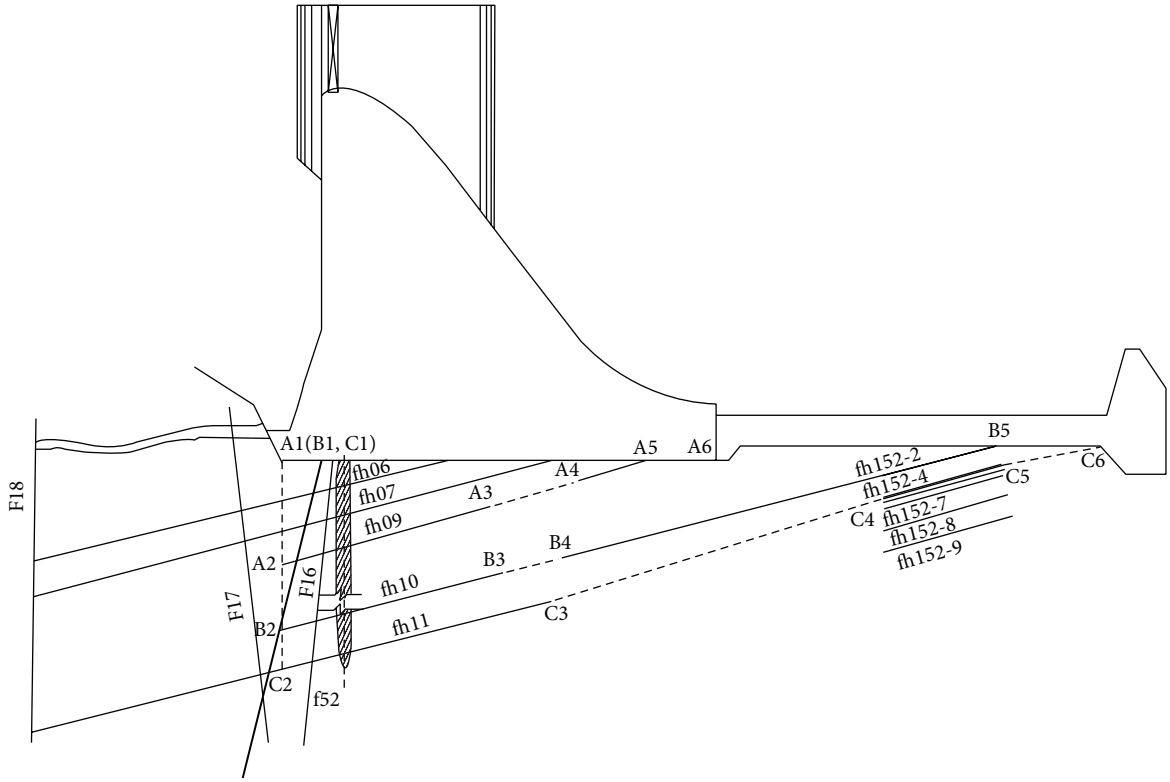

Figure 3: Geological profile and assuming slip paths of the dam foundation.

Table 5: Statistical characteristics of random variables of slip path B.

Slip plane	Random variable	Mean value	Variation coefficient	Probability distribution
B2-B3	f_1'	0.375	0.14~0.26	Normal/ln-normal distribution
	c_1'/MPa	0.075	0.15~0.45	Normal/ln-normal distribution
B3-B4	f_2'	0.475	0.18~0.33	Normal/ln-normal distribution
	c_2'/MPa	0.125	0.25~0.75	Normal/ln-normal distribution
B4-B5	f_3'	0.375	0.14~0.26	Normal/ln-normal distribution
	c_3'/MPa	0.075	0.15~0.45	Normal/ln-normal distribution

Table 6: Comparison of resultant instability probabilities calculated by MC and DPG method.

Method	Design points (sliding plane B2-B3)		β	p_f	Notes
	$f_1'^*$	$c_1'^*$/MPa			
MC	/	/	3.650	1.310×10^{-4}	The numbers of calculating performance function, $n = 1,000,000$, and the variation coefficient for p_f, $V_{p_f} = 0.0873$, when 95% confidence level is specified
DPG	0.107	0.039	3.664	1.244×10^{-4}	The numbers of calculating performance function, $n = 36$, with the step $\Delta x_i = 0.03x_i$, for divided difference calculation

DPG method the design points can be obtained easily, and the probability distributions, variability, and negative correlation of f' and c' can be taken into consideration for special research. So the DPG method suggested in the paper has much merit and is rational and feasible for the major research goal of the paper.

4.3.2. Analyses of the Effects of Correlation of f' and c' on Instability Probability. Table 7 lists the calculated results of the instability probabilities of Slip Path B by DPG method; when f' and c' are both normally distributed, $\delta_{f'}$ and $\delta_{c'}$ are 0.2 and 0.3, respectively, and the coefficient of correlation, $\rho_{f'c'}$, is within the range of −0.7~0.0. The negative value

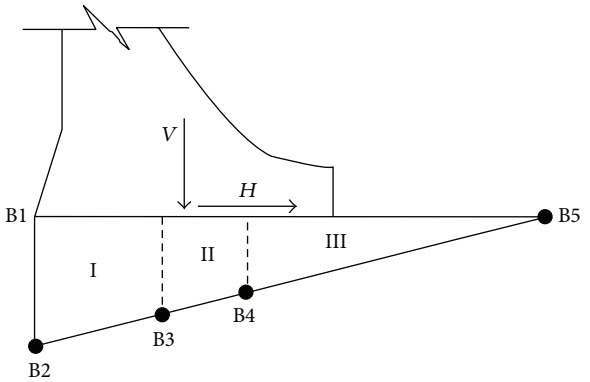

Figure 4: Wedges on Slip Path B. V: vertical load due to dam action. H: horizontal load due to dam action.

Table 7: Calculated results under the conditions of different $\rho_{f'c'}$ by DPG method.

Number	$\rho_{f'c'}$	Design points (sliding plane B2-B3)		β	p_f
		$f_1'^*$	$c_1'^*$/MPa		
1	0.0	0.107	0.039	3.664	1.244×10^{-4}
2	−0.1	0.100	0.044	3.789	7.554×10^{-5}
3	−0.2	0.092	0.050	3.929	4.262×10^{-5}
4	−0.3	0.082	0.057	4.086	2.194×10^{-5}
5	−0.4	0.071	0.065	4.264	1.005×10^{-5}
6	−0.5	0.058	0.075	4.467	3.961×10^{-6}
7	−0.6	0.042	0.087	4.704	1.275×10^{-6}
8	−0.7	0.022	0.102	4.984	3.106×10^{-7}

Note: if $\rho_{f'c'}$ is less than −0.8, $f_1'^*$ will be less than 0, and the simulation will be not converged at design points.

of $\rho_{f'c'}$ indicates the degree of negative correlation of f' and c'. It is clear from Table 7 that the resultant instability probability calculated decreases with the increasing of the absolute value of negatively correlated coefficient. $p_f = 1.244 \times 10^{-4}$ when $\rho_{f'c'} = 0.0$ (independent case), and $p_f = 3.106 \times 10^{-7}$ when $\rho_{f'c'} = -0.7$ (strongly negatively correlated case). By comparison, the values of the instability probability under the two cases are different in 3 orders of magnitude. Correspondingly, the values of the reliability index under the two cases are 3.664 and 4.984, respectively. Obviously the independent case is on the conservative side for simulation.

4.3.3. Analyses of the Effects in Different Distributions of f' and c' on Instability Probability. Figure 5 illustrates the resultant instability probability under four different cases of combinations of normal or ln-normal distributions of f' and c' for $\delta_{f'} = 0.2$ and $\delta_{c'} = 0.3$ by DPG method. In all cases, p_f tends to increase as $\rho_{f'c'}$ increases from −0.7 (negatively correlated) to 0 (independent). When f' is normally distributed, the instability probabilities are approximately identical whether c' is normally or ln-normally distributed. When f' is ln-normally distributed, the instability probabilities are smaller

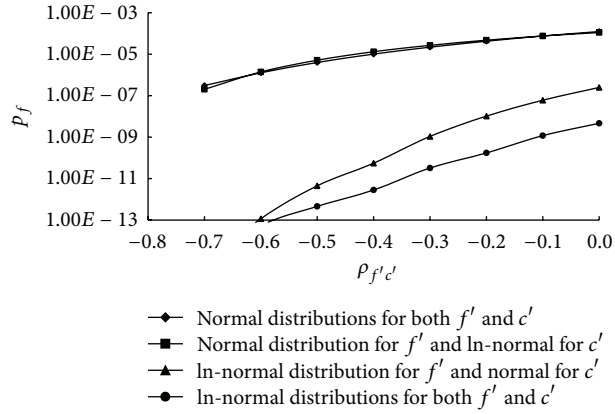

Figure 5: Relation of p_f and $\rho_{f'c'}$ assuming that f' and c' follow different distributions.

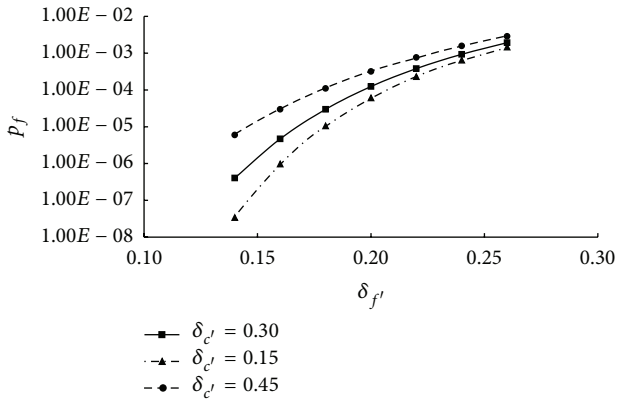

Figure 6: Relation of p_f and $\delta_{f'}$.

and the values calculated under the case that c' is in ln-normal distribution are less than in normal distribution at the same level of correlation of the two parameters. From the figure, $p_f = 1.24 \times 10^{-4}$ if f' and c' are both normally distributed, and $p_f = 4.64 \times 10^{-9}$ if the two parameters are both ln-normally distributed, for $\delta_{f'} = 0.2$, $\delta_{c'} = 0.3$, and $\rho_{f'c'} = 0.0$.

4.3.4. Analyses of the Effects of Variability of f' and c' on Instability Probability. On the basis of the above analyses, it is reasonable, simple, and conservative to assume that f' and c' are normally distributed and independent of each other unless otherwise demonstrated. Considering the range of the values of coefficients of variation, $\delta_{f'} = 0.14$~0.26, $\delta_{c'} = 0.15$~0.45, the calculations are made, and the curves about p_f varying with $\delta_{f'}$ and $\delta_{c'}$ are displayed in Figures 6 and 7. According to the resultant curves, p_f starts to apparently climb as $\delta_{f'}$ increases for different $\delta_{c'}$ (shown in Figure 6), and, in addition, p_f also tends to increase as $\delta_{c'}$ increases for different $\delta_{f'}$ (shown in Figure 7). However, $p_f = 1.92 \times 10^{-3}$ if $\delta_{f'} = 0.26$, and $p_f = 4.04 \times 10^{-7}$ if $\delta_{f'} = 0.14$ for $\delta_{c'} = 0.30$; meanwhile, $p_f = 3.18 \times 10^{-4}$ if $\delta_{c'} = 0.45$, and $p_f = 6.08 \times 10^{-5}$ if $\delta_{c'} = 0.15$ for $\delta_{f'} = 0.20$. There is the difference of p_f in 4 orders of magnitude between $\delta_{f'} = 0.14$ and 0.26 for

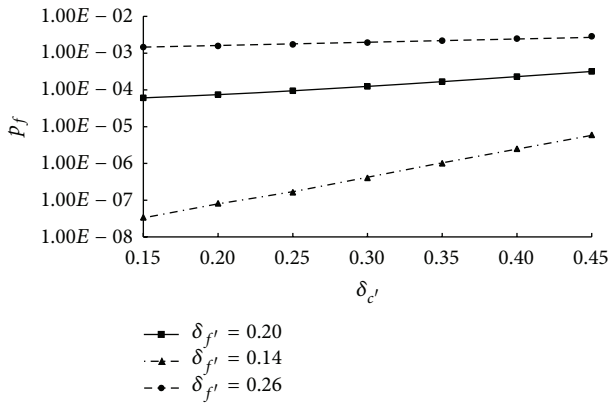

Figure 7: Relation of p_f and $\delta_{c'}$.

$\delta_{c'} = 0.30$; in contrast, under the latter case, there is the deference of p_f in one order of magnitude between $\delta_{c'} = 0.15$ and 0.45 for $\delta_{f'} = 0.20$. So the influence of the variability of f' is more apparent than that of c' on p_f despite the fact that the varying range of coefficients of variation of f' is less than that of c'.

4.3.5. Stability Safety Analyses and Assessments of the Practical Dam. The instability probability of the most adverse slip path of the example dam section (number 6 overflow section) mentioned above is 1.244×10^{-4} for $\delta_{f'} = 0.20$, $\delta_{c'} = 0.30$, and $\rho_{f'c'} = 0.0$. It is less than the allowable value of the instability probability, $[P] = 5.5 \times 10^{-4}$, but they are in the same order of magnitude. Meanwhile, it is 2.861×10^{-3} for $\delta_{f'} = 0.26$, $\delta_{c'} = 0.45$, and $\rho_{f'c'} = 0.0$. It is greater than $[P]$ but less than 5×10^{-3}, which is defined as unacceptable probability. In contrast, the factor of safety is 2.45 by deterministic method without taking the variation of parameters into consideration. The factor of safety is less than the allowable safety factor, $[K] = 3.0$; the reliability index is 3.66 for $\delta_{f'} = 0.20$, $\delta_{c'} = 0.30$, and $\rho_{f'c'} = 0.0$, which nearly equals the target reliability index, $\beta_T = 3.7$. Obviously, the conclusions are more or less different following three different safety standards. Generally, it has been verified that the deterministic method is most conservative in the three methods by the analyses of the practical dam in the paper and the conclusions from other literatures as well. From above analyses, the margins of safety of the foundation stability are not adequate for the example dam section and the enhancing treatments should be carried out especially for the fault-fractured zones and weak structural planes.

Similarly, the instability probabilities of the other two slip paths can be calculated by the DPG method. Assume that f' and c' of each sliding plane of each slip path are normally distributed and independent, and $\delta_{f'} = 0.20$, $\delta_{c'} = 0.30$, and $\rho_{f'c'} = 0.0$ for any slip plane. The resultant instability probabilities are listed in Table 8. The three slip paths can be seen as three main failure modes for the rock foundation of the example dam, and each failure mode is independent due to the independence of each shear strength parameter of any sliding plane. Three failure modes comprise a series failure system of dam foundation. So the overall probability of failure for the overall dam foundation system can be calculated by summing over the instability probabilities of the three slip paths. The final instability probability of the overall rock foundation is 2.053×10^{-4} for a conservative consideration.

Table 8: Resultant instability probabilities of three slip paths calculated by DPG method.

Slip paths	Reliability method (DPG)		Deterministic method
	β	p_f	K
A	3.772	8.094×10^{-5}	2.56
B	3.664	1.244×10^{-4}	2.45
C	5.612	9.993×10^{-9}	10.71

Note: the deterministic method is equivalence safety factor method without considering the variation of the parameters against shear fracture.

It should also be noted that for the example dam the coefficients of variation and negative correlation of the two key mechanical parameters of sliding planes were selected in the relatively wider ranges, which are summarized from the field and experimental data. In the calculation for Slip Path B, four combinations of distributions of the two parameters were detailedly taken into consideration. So the final results obtained for the example dam can reveal the performance about foundation stability of any similar gravity dam in general. We confirm that the randomness of f' is more significant than c', and, what is more, it is reasonable to assume a normal distribution and independence of each parameter in the absence of further information. The assumption will probably overestimate the probability of foundation instability of gravity dam in some degree.

5. Conclusions

In this paper the main goal has been to try applying probabilistic approach to calculate the instability probability of gravity dam foundation over multiple sliding planes rather than single or dual sliding plane(s) in traditional analysis. The simple and efficient probabilistic method, DPG method combined with a divided difference approximation to the partial derivatives, is proposed. The effects of randomness of the shear strength parameters of sliding planes for a practical typical gravity dam are analyzed in detail. The following conclusions can be obtained:

(1) By comparison between MC method and DPG method, the two methods have nearly the same accuracy, but the latter needs less cost for calculation. Meanwhile, the DPG method has much other merit. For example, the design points can be obtained easily during the calculating process, and probability distributions, variability, and correlation of variables can be taken into consideration rationally. Hence, the DPG method associated with the method of divided difference is feasible for the calculation of probability of failure with implicit performance function just like

the case of instability of dam foundation over multiple sliding planes.

(2) The randomness of material properties of sliding planes is a major contributor to the uncertainty of the foundation stability of a gravity dam. The randomness of the two parameters against shear fracture, f' and c', of the sliding planes may be described by assumption of their distributions, variability, and correlation. So the effects of the randomness of the parameters on resultant instability probability of gravity dam foundation can be analyzed based on these aspects. The study of the practical dam shows that (1) when both of the two parameters follow normal distribution, the resultant value of instability probability is greater than that which is calculated when one or both of the parameters do not follow normal distribution, and the distributed type of f' is dominant; (2) the stronger the negative correlation of the two parameters is, the smaller the instability probability calculated is; and (3) the instability probability tends to increase as the coefficients of variability of f' and c' increases, and the influence of the variability of f' is more apparent than that of c' on the instability probability. So it is reasonable to assume a normal distribution and independence of each parameter in the absence of further information. The assumption will probably overestimate the instability probability of gravity dam foundation. The spatial variation of f' is more significant than c' on the instability probability. All of the conclusions drawn in the paper are identical to those of other research.

(3) Currently, there are three kinds of safety indices—factor of safety, reliability index, and probability of failure—for engineering stability problem. The factor of safety is used in deterministic method. It is so convenient for engineers to utilize and have so much experience in designs of many existing gravity dam projects that has become a major index to assess foundation stability of gravity dam for a long time. However, the assessment method based on this index is relatively more conservative and should be improved upon undoubtedly. The trend is application of probabilistic approach, in which the reliability index or probability of failure will be utilized. Now, a fundamental problem is the lack of data. Field exploration is expensive and laboratory tests are always based on small numbers of samples, so there are seldom enough data to support meaningful statistical analyses and broad conclusions about the statistics of rock or soil properties. In a word, the current challenges to the profession are to make use of appropriate probabilistic methods in practice and to sharpen the investigations and analyses so that each additional data point provides maximal information.

(4) In the paper, we applied a simple, accurate, and efficient method to calculate the instability probability of concrete gravity dam foundation over multiple sliding places. It can also be utilized in other similar analyses of slopes, levees, embankments, earth-rock dams, and so on.

Competing Interests

The authors declare that they have no competing interests.

Acknowledgments

The research has been supported in part by National Natural Science Foundation of China under Grant no. 51309048.

References

[1] G. B. Baecher and J. T. Christian, *Reliability and Statistics in Geotechnical Engineering*, John Wiley & Sons, Chichester, UK, 2003.

[2] K. K. Phoon, *Reliability-Based Design in Geotechnical Engineering: Computations and Applications*, Taylor & Francis, New York, NY, USA, 2008.

[3] G. A. Fenton and D. V. Griffths, *Risk Assessment in Geotechnical Engineering*, John Wiley & Sons, New York, NY, USA, 2008.

[4] J. T. Christian and G. B. Baecher, "Unresolved problems in geotechnical risk and reliability," in *Proceedings of the GeoRisk 2011: Geotechnical Risk Assessment and Management (GSP 224), ASCE Specialty Conference*, pp. 50–63, Atlanta, Ga, USA, June 2011.

[5] J. T. Christian, C. C. Ladd, and G. B. Baecher, "Reliability applied to slope stability analysis," *Journal of Geotechnical Engineering*, vol. 120, no. 12, pp. 2180–2207, 1994.

[6] X.-S. Tang, D.-Q. Li, C.-B. Zhou, and K.-K. Phoon, "Copula-based approaches for evaluating slope reliability under incomplete probability information," *Structural Safety*, vol. 52, pp. 90–99, 2015.

[7] A. Der Kiureghian and T. Dakessian, "Multiple design points in first and second-order reliability," *Structural Safety*, vol. 20, no. 1, pp. 37–49, 1998.

[8] Y. J. Hong, J. Xing, and J. B. Wang, "A second-order third-moment method for calculating the reliability of fatigue," *International Journal of Pressure Vessels and Piping*, vol. 76, no. 8, pp. 567–570, 1999.

[9] H. U. Köylüoğlu and S. R. K. Nielsen, "New approximations for SORM integrals," *Structural Safety*, vol. 13, no. 4, pp. 235–246, 1994.

[10] F. S. Wong, "Slope reliability and response surface method," *Journal of Geotechnical Engineering*, vol. 111, no. 1, pp. 32–53, 1985.

[11] L. J. Moore and P. Sa, "Comparisons with the best in response surface methodology," *Statistics & Probability Letters*, vol. 44, no. 2, pp. 189–194, 1999.

[12] Y. Zheng and P. K. Das, "Improved response surface method and its application to stiffened plate reliability analysis," *Engineering Structures*, vol. 22, no. 5, pp. 544–551, 2000.

[13] X. L. Guan and R. E. Melchers, "Effect of response surface parameter variation on structural reliability estimates," *Structural Safety*, vol. 23, no. 4, pp. 429–444, 2001.

[14] S. Gupta and C. S. Manohar, "Improved response surface method for time-variant reliability analysis of nonlinear random structures under non-stationary excitations," *Nonlinear Dynamics*, vol. 36, no. 2–4, pp. 267–280, 2004.

[15] S. M. Wong, R. E. Hobbs, and C. Onof, "An adaptive response surface method for reliability analysis of structures with multiple loading sequences," *Structural Safety*, vol. 27, no. 4, pp. 287–308, 2005.

[16] B. Xu and B. K. Low, "Probabilistic stability analyses of embankments based on finite-element method," *Journal of Geotechnical and Geoenvironmental Engineering*, vol. 132, no. 11, pp. 1444–1454, 2006.

[17] J. Cheng, Q. S. Li, and R.-C. Xiao, "A new artificial neural network-based response surface method for structural reliability analysis," *Probabilistic Engineering Mechanics*, vol. 23, no. 1, pp. 51–63, 2008.

[18] H. P. Gavin and S. C. Yau, "High-order limit state functions in the response surface method for structural reliability analysis," *Structural Safety*, vol. 30, no. 2, pp. 162–179, 2008.

[19] T. Zou, Z. P. Mourelatos, S. Mahadevan, and J. Tu, "An indicator response surface method for simulation-based reliability analysis," *Journal of Mechanical Design, Transactions of the ASME*, vol. 130, no. 7, Article ID 071401, pp. 1–11, 2008.

[20] X. S. Nguyen, A. Sellier, F. Duprat, and G. Pons, "Adaptive response surface method based on a double weighted regression technique," *Probabilistic Engineering Mechanics*, vol. 24, no. 2, pp. 135–143, 2009.

[21] P. Samui, T. Lansivaara, and M. R. Bhatt, "Least square support vector machine applied to slope reliability analysis," *Geotechnical and Geological Engineering*, vol. 31, no. 4, pp. 1329–1334, 2013.

[22] X.-H. Tan, W.-H. Bi, X.-L. Hou, and W. Wang, "Reliability analysis using radial basis function networks and support vector machines," *Computers and Geotechnics*, vol. 38, no. 2, pp. 178–186, 2011.

[23] X.-H. Tan, M.-F. Shen, X.-L. Hou, D. Li, and N. Hu, "Response surface method of reliability analysis and its application in slope stability analysis," *Geotechnical and Geological Engineering*, vol. 31, no. 4, pp. 1011–1025, 2013.

[24] X. Chang, C. Jiang, W. Zhou, and D. Huang, "Equal safety factor method and its reliability analysis for rock foundation of dam," *Chinese Journal of Rock Mechanics and Engineering*, vol. 26, no. 8, pp. 1594–1602, 2007.

[25] J. T. Christian, "Geotechnical engineering reliability: how well do we know what we are doing?" *Journal of Geotechnical and Geoenvironmental Engineering*, vol. 130, no. 10, pp. 985–1003, 2004.

[26] Z. Chen, J. Xu, P. Sun, C. Wu, Y. Wang, and L. Chen, "Reliability analysis on sliding stability of gravity dams: part I: an approach using criterion of safety margin ratio," *Journal of Hydroelectric Engineering*, vol. 31, no. 3, pp. 148–159, 2012.

[27] Z. Chen, J. Xu, L. Chen, Y. Wang, P. Sun, and C. Wu, "Reliability analysis on sliding stability of gravity dams: Part II: determination of shear strength parameters and partial factors," *Journal of Hydroelectric Engineering*, vol. 31, no. 3, pp. 160–167, 2012 (Chinese).

[28] A. W. Bishop, "The use of the slip circle in the stability analysis of slopes," *Géotechnique*, vol. 5, no. 1, pp. 7–17, 1955.

[29] E. Spencer, "A method of analysis of the stability of embankments assuming parallel inter-slice forces," *Géotechnique*, vol. 17, no. 1, pp. 11–26, 1967.

[30] N. Janbu, *Slope Stability Computation in Embankment Dam Engineering*, John Wiley & Sons, New York, NY, USA, 1973.

[31] R. Rackwitz and B. Flessler, "Structural reliability under combined random load sequences," *Computers & Structures*, vol. 9, no. 5, pp. 489–494, 1978.

[32] M. Hohenbichler and R. Rackwitz, "Non-normal dependent vectors in structural safety," *ASCE Journal of Engineering Mechanics*, vol. 107, no. 6, pp. 1227–1238, 1981.

[33] P.-L. Liu and A. Der Kiureghian, "Multivariate distribution models with prescribed marginals and covariances," *Probabilistic Engineering Mechanics*, vol. 1, no. 2, pp. 105–112, 1986.

[34] O. Ditlevsen and H. O. Madsen, *Structural Reliability Methods*, John Wiley & Sons, New York, NY, USA, 1996.

[35] M. Lemaire, *Structural Reliability*, John Wiley & Sons, New York, NY, USA, 2009.

[36] G. F. Zhao, *Theory and Applications of Engineering Structural Reliability*, Dalian Institute of Technology Press, Dalian, China, 1996 (Chinese).

[37] Y. G. Li, G. F. Zhao, and B. H. Zhang, "Method for structural reliability analysis in generalized random space," *Journal of Dalian University of Technology*, vol. 33, supplement 1, pp. 1–5, 1993 (Chinese).

Hindawi Publishing Corporation
Mathematical Problems in Engineering
Volume 2016, Article ID 6419058, 5 pages
http://dx.doi.org/10.1155/2016/6419058

Research Article

Quantification of Margins and Uncertainties Approach for Structure Analysis Based on Evidence Theory

Chaoyang Xie[1,2] and Guijie Li[2]

[1]*School of Mechatronics Engineering, University of Electronic Science and Technology of China, Chengdu 611731, China*
[2]*Institute of Systems Engineering, China Academy of Engineering Physics, Mianyang 621900, China*

Correspondence should be addressed to Chaoyang Xie; xiezy@caep.cn

Received 14 February 2016; Revised 17 May 2016; Accepted 19 May 2016

Academic Editor: Egidijus R. Vaidogas

Quantification of Margins and Uncertainties (QMU) is a decision-support methodology for complex technical decisions centering on performance thresholds and associated margins for engineering systems. Uncertainty propagation is a key element in QMU process for structure reliability analysis at the presence of both aleatory uncertainty and epistemic uncertainty. In order to reduce the computational cost of Monte Carlo method, a mixed uncertainty propagation approach is proposed by integrated Kriging surrogate model under the framework of evidence theory for QMU analysis in this paper. The approach is demonstrated by a numerical example to show the effectiveness of the mixed uncertainty propagation method.

1. Introduction

The uncertainties of material properties, environment loads, and design models are inevitable in engineering. Uncertainty is usually classified into aleatory and epistemic types [1, 2], and the presence of uncertain factors introduces uncertainty in the reliability of the structure. Probabilistic approaches that deal with aleatory parameter uncertainty have been vastly investigated in typical structure reliability analysis. When sufficient data are not available or there is lack of information due to ignorance, the concept of subjective probability is well established for quantifying epistemic uncertainty. However, when the probabilities of rare events are very difficult to assess or events occur only once, the classical probability methodology may not be suitable because there is not enough statistic data [3, 4]. In order to overcome the lack of probabilistic method, the nonprobabilistic methods have been proposed and are more suitable to handle the epistemic uncertainty based on the Fuzzy theory, interval theory, evidence theory, and so forth. The theoretical concept and the application of the Quantification of Margins and Uncertainties (QMU) methodology were reported in the certification of reliability, safety of nuclear weapons stockpile, and risk-informed decision making process under restriction of test data in the last decade. Recently, the QMU methodology has been applied to more general complex systems, such as commercial nuclear power plants, reactor safety, and missile reliability [5, 6]. Eardley [7] described the main components (performance gates, margins, and uncertainties) of the QMU methodology. Under the key ideas and application procedures of QMU methodology, the uncertainty propagation that determines the output uncertainty from input uncertainty is a broad research area for QMU process. Reference [8] shows that evidence theory is a more general theory that can handle both types of uncertainty but it requires much more computational cost.

The objective of this paper is to propose an implementation framework of QMU under mixed uncertainty based on the evidence theory. To alleviate the computational costs, a stochastic surrogate model based on Kriging model and adaptive sampling method has been applied for uncertainty propagation for structure performance response. The rest of this paper is organized as follows. Section 2 briefly introduces the basic concept and metric of QMU. Section 3 details the mixed uncertainty propagation using evidence theory in QMU implementation. The new calculation scheme of mixed uncertainty analysis by integrating Kriging model and

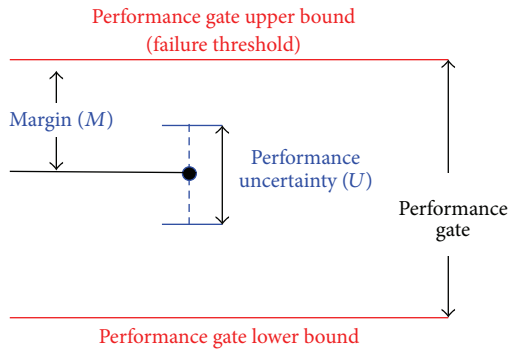

Figure 1: Notional illustration of the QMU.

adaptive sampling is presented. One case study is presented in Section 4 to demonstrate the new developed implementation.

2. The Concept and Metric of QMU

QMU is a decision-support methodology for complex technical decisions centering on performance thresholds and associated margins for engineering systems that are made under uncertainty [9]. The basic concept of the QMU is shown in Figure 1. The margin (M) is defined as the distance between the nominal response of the system and performance gate bound (e.g., a failure threshold not to be exceeded), whereas uncertainty (U) is described by the range of system responses caused by different sources of variability. A QMU metric, confidence factor (CF), has to be developed to quantify and certify the confidence of the system reliability, which can be defined as

$$\mathrm{CF} = \frac{M}{U}. \tag{1}$$

A CF sufficiently larger than one intuitively indicates safe conditions. In order to get the value of CF, three key elements should to be implemented as follows: (1) identification and specification of performance threshold(s); (2) identification and specification of associated performance margin(s), that is, measure(s) of exceeding performance thresholds; (3) quantified uncertainty in threshold and margin specifications.

3. The Mixed Uncertainty Propagation Based on Evidence Theory

3.1. Fundamentals of Evidence Theory. The measures of uncertainty provided by evidence theory [10] are known as belief (Bel) and plausibility (Pl), which lie in the interval $[0, 1]$. Evidence theory application involves the evidence specification of $(\mathscr{Y}, \mathbb{Y}, m)$, where $\mathscr{Y}$ denotes the universal set, $\mathbb{Y}$ denotes the collection of subsets $\mathscr{U}$ or set of focal elements of $\mathscr{Y}$, m is the basic probability assignment (BPA), and $m(\mathscr{U})$ should satisfy the following axioms of evidence theory: (1) $m(\mathscr{U}) \geq 0$ for any $\mathscr{U} \in \mathbb{Y}$; (2) $m(\mathscr{U}) = 0$ when $\mathscr{U} \notin \mathbb{Y}$; (3) $\sum m(\mathscr{U}) = 1$, for all $\mathscr{U} \in \mathbb{Y}$.

The Bel and Pl of a given event set A and B can be derived from the basic probability assignment by

$$\begin{aligned} \mathrm{Bel}(B) &= \sum_{A \subseteq B} m(A), \\ \mathrm{Pl}(B) &= \sum_{B \cap A \neq \phi} m(A). \end{aligned} \tag{2}$$

Resulting from (2), the belief function, Bel$(\cdot)$, is calculated by summing the BPAs that totally agree with event B, while the plausibility function, Pl$(\cdot)$, is calculated by summing BPAs that agree with event B totally and partially. Both Bel and Pl play roles similar to distribution functions in the standard probability and they give the lower and upper bounds of the event set.

3.2. Mixed Uncertainty Propagation Using Evidence Theory. The mixed uncertainty propagated from input parameters to systems output needs to be quantified for structure reliability analysis when aleatory and epistemic uncertainties exist. The performance function with aleatory and epistemic uncertainties can be given by

$$\begin{aligned} G(\mathbf{Z}) &= g(\mathbf{X}, \mathbf{Y}) \\ &= g(X_1, X_2, \ldots, X_{nX}, Y_1, Y_2, \ldots, Y_{nY}), \end{aligned} \tag{3}$$

where $\mathbf{X} = \{X_1, X_2, \ldots, X_{nX}\}$ represents the aleatory uncertainty variables described by probability distributions. For easy demonstration, we assume that the elements of $\mathbf{X}$ are independent. $\mathbf{Y} = \{Y_1, Y_2, \ldots, Y_{nY}\}$ is the vector of parameters with epistemic uncertainty described by evidence specification $(\mathscr{Y}_1, \mathbb{Y}_1, m_1), (\mathscr{Y}_2, \mathbb{Y}_2, m_2), \ldots, (\mathscr{Y}_n, \mathbb{Y}_n, m_n)$. The uncertainty associated with the model inputs $\mathbf{X}$ and $\mathbf{Y}$ are propagated through the model $g(\cdot)$ to the model output G. The joint evidence specification can be expressed by $(\mathscr{Y}, \mathbb{Y}, m_{\mathbf{Y}})$ and the joint BPA is defined by

$$m_{\mathbf{Y}}(\mathscr{U}) = \begin{cases} \prod_{k=1}^{nY} m_k(\mathscr{U}_k), & \mathscr{U} = \mathscr{U}_1 \times \mathscr{U}_2 \times \cdots \times \mathscr{U}_{nY} \\ 0, & \text{Otherwise.} \end{cases} \tag{4}$$

Let the number of the subsets of $\mathbf{Y}$ in the joint space be n. The probability of the system output value (G) is less than the threshold (c) which can be given by the following based on the total probability formula:

$$P = \sum_{i=1}^{n} \Pr\{G(\mathbf{X}, \mathbf{Y}) < c \mid \mathbf{Y}_i \in \mathscr{U}_i\} m_Y(\mathscr{U}_i), \tag{5}$$

where P is the probability of $G(\mathbf{Z}) < c$, which is denoted as event F. $\Pr\{\mathbf{Y}_i \in \mathscr{U}_i\} = m_{\mathbf{Y}}(\mathscr{U}_i)$ means the probability of the focal element $\mathscr{U}_i$ in joint space $\mathscr{Y}$ equals the joint BPA value. Because of the intervals in $\mathbf{Y}$, the minimum value (belief) and maximum value (plausibility) of P can be expressed by [11]

$$\begin{aligned} \mathrm{Bel}(F) &= P_{\min} \\ &= \sum_{i=1}^{n} m_{\mathbf{Y}}(\mathscr{U}_i) \Pr\{G_{\max}(\mathbf{X}, \mathbf{Y}) < c \mid \mathbf{Y}_i \in \mathscr{U}_i\}, \end{aligned} \tag{6}$$

$$\begin{aligned}\mathrm{Pl}(F) &= P_{\max} \\ &= \sum_{i=1}^{n} m_{\mathbf{Y}}(\mathcal{U}_i)\,\Pr\left\{G_{\min}(\mathbf{X},\mathbf{Y}) < c \mid \mathbf{Y}_i \in \mathcal{U}_i\right\}.\end{aligned} \tag{7}$$

3.3. The Solution Framework of Mixed Uncertainty Propagation. Equations (6)-(7) can be calculated using sampling methods such as MCS with large computational cost. The Kriging surrogate model [12, 13] can be employed to reduce the cost for uncertainty propagation. With training observations, the response and predicted mean square error for any given new point $\mathbf{x}'$ can be expressed as

$$\begin{aligned}\widehat{G}(\mathbf{x}') &= \mu + \mathbf{r}^T\mathbf{R}^{-1}(\mathbf{G} - \mathbf{A}\mu), \\ \widehat{e}(\mathbf{x}') &= \sigma^2\left[1 - \mathbf{r}^T\mathbf{R}^{-1}\mathbf{r} + \frac{\left(1 - \mathbf{A}^T\mathbf{R}^{-1}\mathbf{r}\right)^2}{\mathbf{A}^T\mathbf{R}^{-1}\mathbf{A}}\right],\end{aligned} \tag{8}$$

where $\mathbf{R}$ represents a correlation matrix, $\mathbf{r}$ is the correlation vector between $\mathbf{x}'$ and the observed samples, and $\mathbf{A}$ is an $n \times 1$ unit vector. This surrogate model is used to evaluate the uncertainty distribution of system output based on the traditional MCS method without calling the original performance function. The Maximum Confidence Enhancement adaptive sampling [13] is employed to ensure the surrogate model accuracy by adding new training sample.

The procedure of the kriging-based method for solving (7) is simply introduced as follows:

(1) Calculate the joint BPA of epistemic uncertainties variables $\mathbf{Y}$.

(2) Use the Latin hypercube sampling (LHS) to generate $N = (n+1)(n+2)/2$ sample points $\mathbf{x}_t = (x_{1,t}, \ldots, x_{n,t})$ $(t = 1, 2, \ldots, N)$ of the aleatory variables $\mathbf{X}$.

(3) For each $\mathbf{x}_t$, calculate the minimum output value of $G_{\min}(\mathbf{x}_t)$ in focal element $\mathcal{U}_i$ of joint space.

(4) Build Kriging model based on training data $\mathbf{x}_t$ and $G_{\min}(\mathbf{x}_t)$.

(5) Calculate the maximum Confidence point (x^*) from the MC sampling and update Kriging model by adding new training sample $(x^*, G_{\min}(x^*))$.

(6) Repeat steps (4)-(5) until the surrogate model approximate accuracy is satisfied.

(7) Calculate the probability boundary using the updated Kriging model and MC samples.

(8) Repeat steps (3)–(7) for each focal element of $\mathbf{Y}$.

(9) Compute the Pl(·) based on the joint BPA and probability of each focal element.

For the Bel(·) solution, the minimum output value $G_{\min}(\mathbf{x}_t)$ needs to change to the maximum output value $G_{\max}(\mathbf{x}_t)$.

3.4. Calculation of CF under the Evidence Theory Framework. As described in Section 2, the safety or reliability of a structural system will be measured by the Confidence Factor, CF.

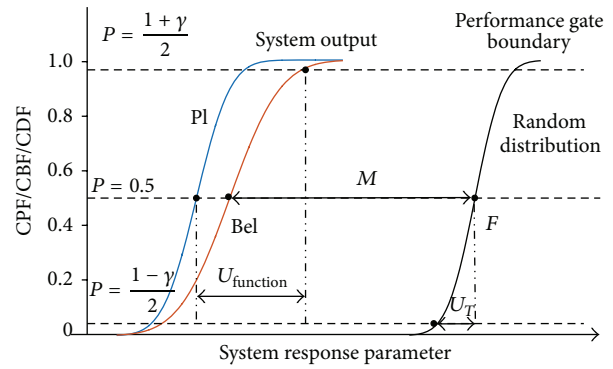

FIGURE 2: Demonstration of uncertainties and margins under belief and plausibility.

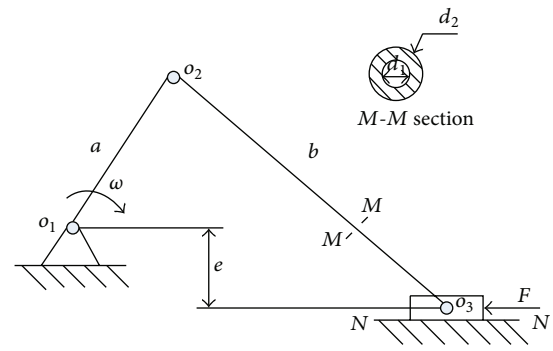

FIGURE 3: A crank-slider mechanism.

When the system output uncertainty is represented in terms of evidence theory measures with belief and plausibility, the demonstration of uncertainties and margins with distance between system output and performance gate boundary is shown in Figure 2. The performance gate boundary is a random variable.

The calculations of M and U to perform upper boundary are given by the following equations:

$$\begin{aligned}M &= \left|\mathrm{Bel}_{P=0.5} - F_{P=0.5}\right|, \\ U &= U_{\text{function}} + U_T \\ &= \left|\mathrm{Bel}_{P=(1+\gamma)/2} - \mathrm{Pl}_{P=0.5}\right| + \left|F_{P=0.5} - F_{P=(1-\gamma)/2}\right|,\end{aligned} \tag{9}$$

where the subscript P corresponds to the quantity of belief/plausibility/probability level and γ is the specified confidence level.

4. Application Example for Structure Analysis

Figure 3 shows a crank-slider mechanism [11]. The length of the crank a, the length of the coupler b, the external force P, Young's modulus of the material of the coupler E, and the yield strength of the coupler S are random variables. The coefficient of friction u between the ground and the slider and the offset e are epistemic variables. The random variables and epistemic variables with BPA are provided in Tables 1 and 2.

Table 1: Random variables.

Variable	Parameters symbol	Mean	Standard deviation	Distribution
X_1	a (mm)	100	0.01	Normal
X_2	b (mm)	400	0.01	Normal
X_3	P (KN)	280	28	Normal
X_4	E (GPa)	200	10	Normal
X_5	S (MPa)	290	29	Normal
X_6	d_1 (mm)	60	3	Normal
X_7	d_2 (mm)	25	2.5	Normal

Table 2: Uncertain variables with epistemic uncertainty.

Variable	Symbol	Intervals	BPA
Y_1	e	[100, 120]	0.2
		[120, 140]	0.4
		[140, 150]	0.4
Y_2	μ	[0.15, 0.18]	0.3
		[0.18, 0.23]	0.3
		[0.23, 0.25]	0.4

Table 3: Calculated CF vs different γ.

γ	M	U	CF
0.95	133.5	138	0.9674
0.9	133.5	117.5	1.136
0.8	133.5	93.5	1.428

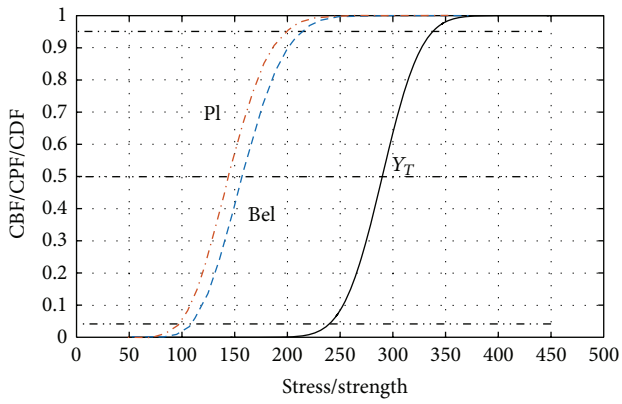

Figure 4: The uncertainty distribution of system performance and threshold.

The performance function is defined by the maximum stress as (10) and the boundary is the material strength:

$$Y = \frac{4P(b-a)}{\pi\left(\sqrt{(b-a)^2 - e^2} - \mu e\right)\left(d_2^2 - d_1^2\right)}. \quad (10)$$

The belief and plausibility measures of the maximum stress are calculated by the proposed adaptive sampling Kriging model approach, and these results are shown in Figure 4. The QMU analysis with different γ is summarized in Table 3. Results show that the confidence level is very sensitive for QMU analysis in risk-informed decision-making.

5. Conclusion

The mixed uncertainty propagation approach is proposed by integrated adaptive sampling method and Kriging model for QMU analysis in this paper. The technique is demonstrated by a numerical example to account for the QMU analysis process and the approach for mixed uncertainty propagation. The results indicate the potential effectiveness of the proposed QMU approach for the evaluation of structure reliability.

Competing Interests

The authors declare that there is no conflict of interests regarding the publication of this paper.

Acknowledgments

The authors acknowledge China Academy of Engineering Physics (CAEP) Foundation (2013ZK1.2) and Foundation of NSAF, Grant no. U1330130 (NSAF-U1330103).

References

[1] J. C. Helton, J. D. Johnson, W. L. Oberkampf, and C. J. Sallaberry, "Representation of analysis results involving aleatory and epistemic uncertainty," *International Journal of General Systems*, vol. 39, no. 6, pp. 605–646, 2010.

[2] J. C. Helton and W. L. Oberkampf, "Alternative representations of epistemic uncertainty," *Reliability Engineering & System Safety*, vol. 85, no. 1–3, pp. 1–10, 2004.

[3] R. Rackwitz, "Reliability analysis—a review and some perspectives," *Structural Safety*, vol. 23, no. 4, pp. 365–395, 2001.

[4] S.-K. Au and J. L. Beck, "Estimation of small failure probabilities in high dimensions by subset simulation," *Probabilistic Engineering Mechanics*, vol. 16, no. 4, pp. 263–277, 2001.

[5] X. Du, P. K. Venigella, and D. Liu, "Robust mechanism synthesis with random and interval variables," *Mechanism & Machine Theory*, vol. 44, no. 7, pp. 1321–1337, 2009.

[6] H.-Z. Huang, Z. L. Wang, Y. F. Li, B. Huang, N. C. Xiao, and L. P. He, "A nonprobabilistic set model of structural reliability based on satisfaction degree of interval," *Mechanika*, vol. 17, no. 1, pp. 85–92, 2011.

[7] D. Eardley, "Quantification of margins and uncertainties (QMU)," Tech. Rep. JSR-04-330, JASON, 2005.

[8] H. Shah, S. Hosder, and T. Winter, "Quantification of margins and mixed uncertainties using evidence theory and stochastic expansions," *Reliability Engineering & System Safety*, vol. 138, pp. 59–72, 2015.

[9] NAS/NRC (National Academy of Science/National Research Council), *Evaluation of Quantification of Margins and Uncertainties for Assessing and Certifying the Reliability of the Nuclear Stockpile*, National Academy Press, Washington, DC, USA, 2008.

[10] H.-R. Bae, R. V. Grandhi, and R. A. Canfield, "An approximation approach for uncertainty quantification using evidence theory," *Reliability Engineering & System Safety*, vol. 86, no. 3, pp. 215–225, 2004.

[11] X. P. Du, "Unified uncertainty analysis by the first order reliability method," *Journal of Mechanical Design*, vol. 130, no. 9, pp. 1–10, 2008.

[12] I.-K. Bang, D.-S. Han, G.-J. Han, and K.-H. Lee, "Structural optimization for a jaw using iterative Kriging metamodels," *Journal of Mechanical Science and Technology*, vol. 22, no. 9, pp. 1651–1659, 2008.

[13] Z. Wang and P. Wang, "A maximum confidence enhancement based sequential sampling scheme for simulation-based design," *Journal of Mechanical Design*, vol. 136, no. 2, Article ID 021006, 2014.

Hindawi Publishing Corporation
Mathematical Problems in Engineering
Volume 2016, Article ID 3161823, 12 pages
http://dx.doi.org/10.1155/2016/3161823

Research Article

Investigation of Lab Fire Prevention Management System of Combining Root Cause Analysis and Analytic Hierarchy Process with Event Tree Analysis

Cheng-Chan Shih,[1] Richard S. Horng,[2] and Shin-Ku Lee[3]

[1]*Department of Occupational Safety and Hygiene, Fooyin University, No. 151 Chin-Hsueh Road, Ta-Liao, Kaohsiung 831, Taiwan*
[2]*Department of Chemical Engineering, I-Shou University, No. 1, Sec. 1, Syuecheng Road, Dashu, Kaohsiung 840, Taiwan*
[3]*Research Center of Energy Technology and Strategy, National Cheng Kung University, No. 1, University Road, Tainan 701, Taiwan*

Correspondence should be addressed to Shin-Ku Lee; sklee1015@gmail.com

Received 17 February 2016; Accepted 22 May 2016

Academic Editor: Egidijus R. Vaidogas

This paper proposed a new approach, combining root cause analysis (RCA), analytic hierarchy process (AHP), and event tree analysis (ETA) in a loop to systematically evaluate various laboratory safety prevention strategies. First, 139 fire accidents were reviewed to identify the root causes and draw out prevention strategies. Most fires were caused due to runaway reactions, operation error and equipment failure, and flammable material release. These mostly occurred in working places of no prompt fire protection. We also used AHP to evaluate the priority of these strategies and found that chemical fire prevention strategy is the most important control element, and strengthening maintenance and safety inspection intensity is the most important action. Also together with our surveys results, we proposed that equipment design is also critical for fire prevention. Therefore a technical improvement was propounded: installing fire detector, automatic sprinkler, and manual extinguisher in the lab hood as proactive fire protections. ETA was then used as a tool to evaluate laboratory fire risks. The results indicated that the total risk of a fire occurring decreases from 0.0351 to 0.0042 without/with equipment taking actions. Establishing such system can make Environment, Health and Safety (EH&S) office not only analyze and prioritize fire prevention policies more practically, but also demonstrate how effective protective equipment improvement can achieve and the probabilities of the initiating event developing into a serious accident or controlled by the existing safety system.

1. Introduction

Laboratory operations are dangerous that require all workers to act properly at all times. Most organizations or universities have set up an Environment, Health and Safety (EH&S) office to protect people from accidents. They draw policies, develop programs, establish training and standard operating procedures (SOPs), and enforce their compliance to meet this goal [1, 2]. Despite this, laboratory accidents still continue to occur. The most common type of accidents that occur in laboratories is fires. There have been 25 serious fires in laboratories, each of which incurred losses in excess of 13 million GBP, since 1997 [3]. Sometimes, even if a laboratory accident does not cause any fatalities, or injuries, significant property damage [4, 5] could make such events devastating, if they result in research samples and experimental models being destroyed as well as the data loss from many years of hard work. For example, a laboratory fire occurred in National Taiwan Ocean University on July 23, 2004 [6]; while no one was injured, the loss of property was estimated to be 100,000 US dollars. But the valuable observation data obtained on the ecology of green turtles (*Chelonia mydas*) from 1994 to 2004 was totally destroyed. An approach based on merely established rules, regulations, and instructions

in safety manuals is unsatisfactory for valuable property protection. A proactive approach with control parameters to objectively measure its success is necessary.

The causes of laboratory accidents are usually very complex. Root cause analysis (RCA) provides a structural way, with regard to a particular event, to help investigators systematically identify root causes. Chang and Lin [7] reviewed 242 accidents of storage tanks that occurred over the last 40 years and found that fire and explosion accounted for 85% of the accidents. They used fishbone diagram to demonstrate the causes and effects; there are 8 primary causes and 52 secondary causes; six (6) major corrective actions and 40 secondary actions were also developed. Safety managers can establish protocols based on this complex information to help operating engineers handling similar situations in the future. However, they also need a way to estimate the impact of each cause and human corrective action for policy making. The analytic hierarchy process (AHP), proposed by Saaty [8], is a well-recognized multicriteria tool designed for dealing with complex decision-making problems. It models the problem into a hierarchical structure by incorporating levels: objectives (goals), criteria, subcriteria, and alternatives [9], and then, according to expert judgments, AHP estimates the impact of the elements at each level of the hierarchy [8–11]. This will help policy makers to make priority decisions. AHP has been widely applied to numerous fields for strategy planning, such as energy policy [12, 13], intelligent building systems [14], indicator modeling [15, 16], fire safety engineering [17], and evaluations of disaster carrying capacity [18]. However, the process is considered very subjective and needs a quantitative approach to objectively determine the probability of whether or not an initiating event still develops into a serious accident; most accidents are not due to a single event, but the results of many unnoticed events previously occurred. Event tree analysis (ETA) is an inductive technique intended to examine a sequence of events and their probability of occurrence. Several research works have been conducted using ETA for different applications. For instance, Novack et al. [19] used ETA to analyze accident scenarios attributed to oil spills. Abdelgawad and Fayek [20] proposed a hybrid framework based on combining failure mode and effect analysis (FMEA), fault trees, event trees, and fuzzy logic to calculate the expected monetary value of risk events in the construction industry. This method is useful as an objective decision making, where causes and effects are comprehensively taken into consideration when planning prevention actions. Many other risk management systems have also been proposed [21–26] elsewhere to carry out operating process risk assessments in laboratories, testing grounds, and practice factories.

Although many risk assessment methods have been proposed, few investigators have performed full risk or accident analyses and concept development, especially for college laboratory accidents. In this work, a management model combining RCA, AHP, and ETA is proposed. It contains risk concept development, decision-making process, and probability evaluation of various accident scenarios; fire accidents are chosen to demonstrate the feasibility of the proposed approach. We believe that it is a more effective system-based approach than the traditional one that is prescriptive based on safety manuals.

2. Methodology

Figure 1 illustrates this methodology, which is composed of five main steps. The first is to define the type of fire and fire source based on a general description of a large number of lab fire accidents in the literature. Then, in the second step, all this information is summarized using RCA to identify the root causes of the accident and to provide feasible accident prevention strategies. The third step is to analyze the priority of these strategies using AHP. Finally, ETA is used to complete the quantitative risk analysis and to assess each control measure recommended in this work. The research methods are described as follows.

2.1. Root Cause Analysis. In this study, an RCA task performance team was formed consisting of one EH&S officer, one expert from the Ministry of Education Environmental Protection Division, and three college professors. Information on 139 laboratory fire accidents that occurred in Taiwan was reviewed from published reports and incident news and books [4, 6, 23]. It is important to clearly define the source of risk (what started the fire), causes of the fires (established or assumed), and consequences. The data in the references were first collected and discussed and then analyzed to identify the root causes, construct the fishbone diagram, and propose prevention strategies.

2.2. The AHP Method. Two surveys were conducted in the second phase of AHP analysis: a general survey and an AHP survey. The general survey was to investigate the effects of current laboratory safety education/training and knowledge of the safety facility system. Two questions about laboratory safety education were used to assess the respondents' reactions to the laboratory safety education and three questions to assess their knowledge of the location, SOPs, and operating experience of the fire sprinkler system. The respondents were required to read the statements and indicate the extent of their agreement or disagreement using a five-point Likert-type, with 5 denoting "strongly agree." The questionnaires were given to the respondents via e-mail or personal visit. The AHP approach was used to assign weightings to the prevention strategies proposed in the first phase to improve laboratory fire safety and to prioritize them using a set of criteria. A decision hierarchy was first established before designing the paired comparison matrices. The AHP questionnaire was designed for data collection, and the format was developed with reference to the AHP matrix, as proposed by Saaty [8]. A total of 15 experienced respondents were selected to complete the AHP questionnaire. The demographic information revealed that all the respondents were highly experienced in different professional positions, with more than five years of work experience in laboratory safety management. When examining the consistency level of the collected questionnaires, only a consistency ratio (CR) less than 0.1 is considered acceptable. The relative importance

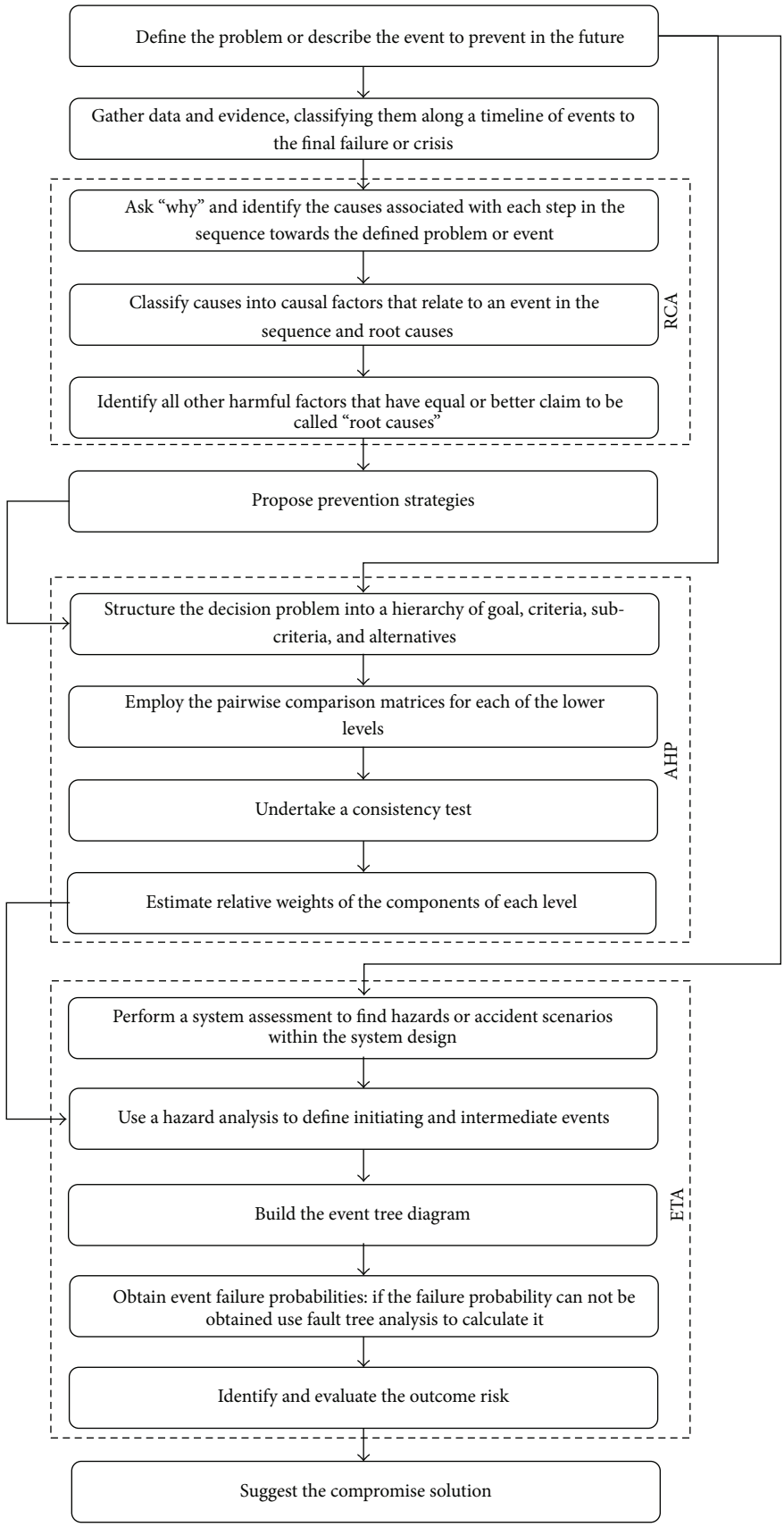

Figure 1: Methodology for laboratory fire safety strategies reducing the risk of fire accidents.

Table 1: Fundamental scale of the AHP [8].

Intensity of importance	Definition	Explanation
1	Equal importance	Two activities contribute equally to the objective
2	Weak	—
3	Moderate importance	Experience and judgment slightly favor one activity over another
4	Moderate plus	—
5	Strong importance	Experience and judgment strongly favor one activity over another
6	Strong plus	—
7	Very strong or demonstrated importance	An activity is favored very strongly over another; its dominance is demonstrated in practice
8	Very, very strong	—
9	Extreme importance	The evidence favoring one activity over another is of the highest possible order of affirmation
Reciprocals of above	If activity i has one of the above nonzero numbers assigned to it when compared with activity j, then j has the reciprocal value when compared with i	A reasonable assumption
Rationales	Ratios arising from the scale	If consistency were to be forced by obtaining numerical values to span the matrix

of the criteria and subcriteria was rated using the nine-point scale proposed by Saaty [8], as shown in Table 1, which shows the relative importance ranging from equal, moderate, strong, and very strong to extreme by 1, 3, 5, 7, and 9, respectively. The intermediate values between two adjacent levels are represented by 2, 4, 6, and 8.

2.3. Event Tree Analysis. Event tree analysis (ETA) is an inductive technique intended to examine a sequence of events and their probability of occurrence. In this work, an event tree starts with an initiating event, such as a component failure, and then the consequences of the event are followed through a series of possible paths. Each path is assigned a probability of occurrence, and the probabilities of the various outcomes are calculated.

3. Results and Discussion

3.1. Root Cause Analysis. The task performance team reviewed one hundred and thirty-nine (139) lab fire accidents from the literature and their root causes were collated involving fire origins, causes, and prevention strategies demonstrated in Tables 2–3 and Figures 2–7.

Table 2 shows the number of fire accidents and their origins; fire accidents occurred most frequently in chemistry laboratories, at a rate of about 68.3%, or 95 cases, much more than in physical (24 cases, 17.3%) and biological (20 cases, 14.4%) laboratories. Among the 95 cases, 23 (24.2%) were caused by electrical devices, and 44 (46.3%) were at the locations of the desk, hood, and storage places, due to inflammable materials used. Chemistry laboratories, by their nature, are of primary concern with regard to fire accidents; they may be highly destructive as leading to explosion and serious threat to human life, when they occurred. The causes

Table 2: Number of fire accidents by fire origin.

Location	Lab type		
	Chemical	Biological	Physical
Desk	16	1	1
Hood	13	1	0
Biosafety hood	0	5	0
Storage place	15	0	2
Electrical device	23	6	14
Equipment	12	1	1
Water tank	2	0	0
Exhaust duct	0	0	1
Trash can	1	1	0
Floor	6	0	2
Others	7	5	3
Total	95	20	24

of lab fire accidents can be classified into five categories, that is, chemical reaction fires, static electricity fires, equipment failure fires, fire due to operational errors (man-made fire), and fires caused by nature disaster. Chemical reaction fires are the most frequent type of fire, with 64 cases, and static electricity fires are the second, with 27 cases, as shown in Table 3. Chemical reaction and static electricity fires together account for 66% of the total cases, much more than those due to operational error (24 cases, 17%) and equipment failure (10 cases, 7%). Only one fire was caused by natural disaster the massive 921 earthquake which happened in Taiwan on September 21, 1999, with a magnitude of 7.6 on the Richter scale. Figure 2 shows details of the ignition factors causing chemical reaction fires, where runaway chemical reaction (29%) and the release of flammable materials (21%) are

Table 3: Cause of fire accidents in laboratory.

Laboratory	Cause						
	Chemical reaction	Static electricity	Equipment failure	Operational error	Nature disaster	Others	Total
Chemical	54	13	6	14	1	7	95
Physical	3	10	2	5	0	4	24
Biological	7	4	2	5	0	2	20

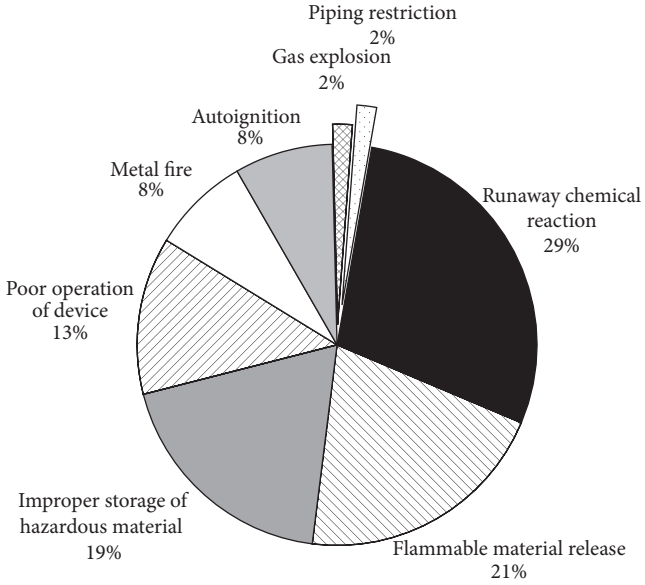

Figure 2: Percentage breakdown of root causes in chemical reaction fire casualties.

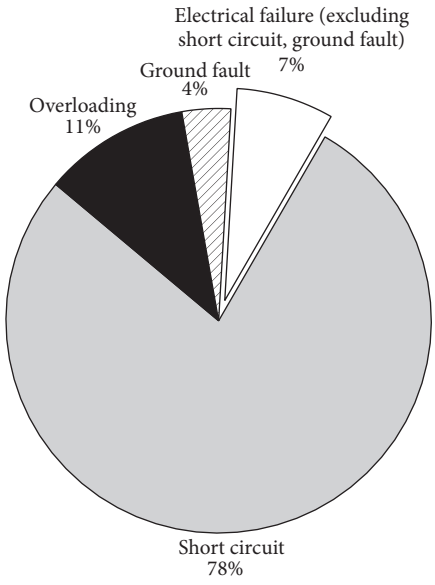

Figure 3: Percentage breakdown of root causes in static electricity fire casualties.

the most. The causes of static electricity fires, as shown in Figure 3, are mainly from short circuits (21 instances, 78%), electric wire overloading (three instances, 11%), and electrical failure (excluding short circuits and ground faults). Figure 4 indicates that the major causes of equipment failure fires were malfunctions (four instances) and overheating due to heater failure (three instances). The analysis of the 24 man-made fires shows that these accidents mainly resulted from human error rather than conscious risk taking; the main factors were negligence (14 instances), experimental mistakes, or misunderstanding the SOP (seven instances) and disobeying the safety rules. A fishbone diagram is thus developed, shown in Figure 5, to more clearly illustrate the relationship between an "effect" and all the possible "causes." And accordingly, the accident prevention strategies, in Figure 6, are also proposed. From above, it is clear that fire accidents have some form of human error involved, whether they are chemical experiment or electric fires. It is recommended that lab safety implementation plans must take human fallibility into consideration, including being overly optimistic about our ability to control our environments.

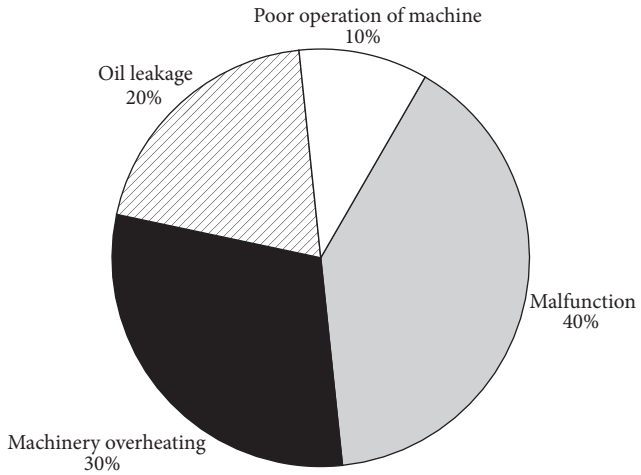

Figure 4: Percentage breakdown of root causes in equipment failure fire casualties.

3.2. AHP Analysis. AHP can model a complex problem in a simple hierarchy form for decision making. Our goal is shown at the top of Figure 9. When we consider the factors affecting fire prevention ability, five main criteria are found at level 1: man-made fire prevention (MMFP), mechanical and electrical fire prevention (MEFP), chemical fire prevention (CFP), personal protective equipment (PPE), and disaster experience learning (DEL). Each criterion is further divided into a number of subcriteria at level 2. The consistent data from 15 respondents are used to make pairwise comparisons between decision alternatives and criteria using a scaling ratio

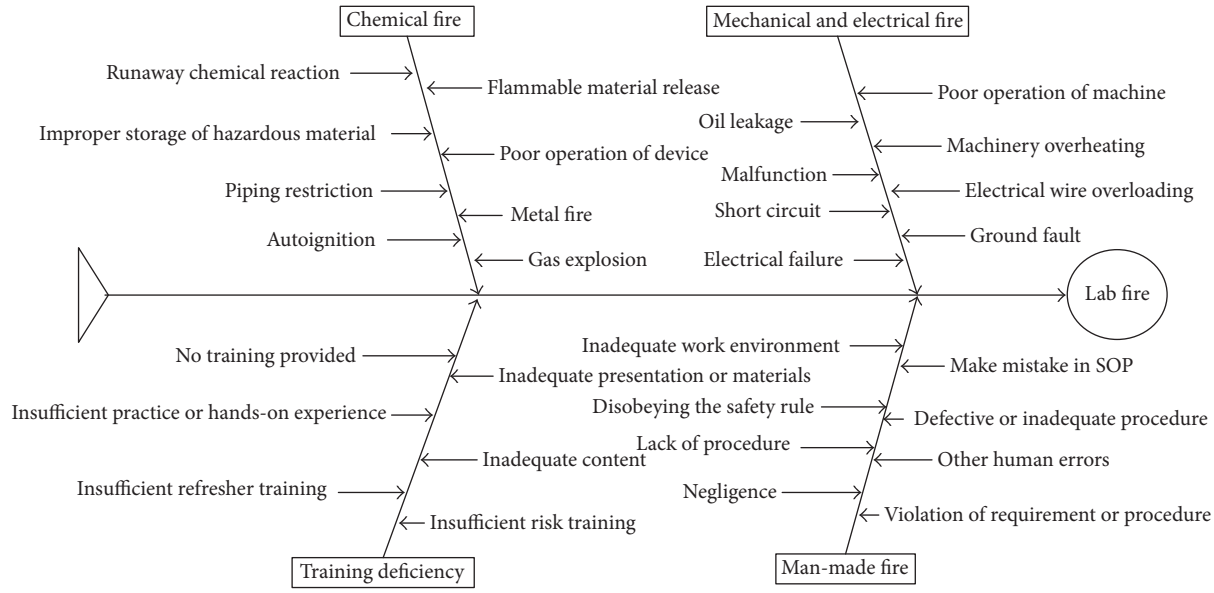

Figure 5: Lab fire cause and effect fishbone diagram.

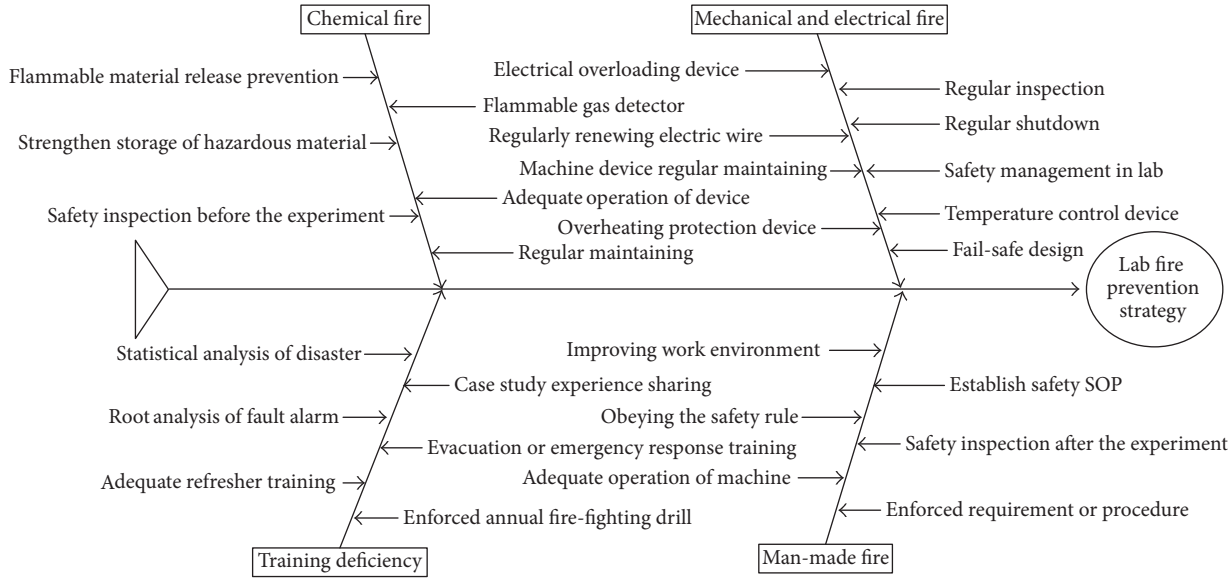

Figure 6: Lab fire prevention strategy fishbone diagram.

for the weighting of attributes. As discussed previously, we construct pairwise comparison matrices (main criteria and subcriteria) for each response. The judgment matrices are computed by using a commercial software package, Power Choice, to prioritize the criteria and alternatives. The local priority weights of all the main criteria and subcriteria are first calculated and then combined with all successive hierarchical levels in each matrix to obtain a global priority vector. The higher the mean weight of the global priority vector, the greater the relative importance. This will help lab safety decision makers find the most important control elements in their decision-making process. As shown in Table 6, the local priority of the main criteria weights from the lowest of 0.132 to the highest of 0.263, and the global priority weights from the lowest of 0.012 to the highest of 0.064. Chemical fire prevention (CFP) with local priority of 0.263 is evaluated as the main factor for respondents when selecting their fire prevention strategy, followed by MEFP (0.261) and PPE (0.202), and DEL (0.132); identifying risks in the working environment (0.062) is seen as the most effective way of the subcriteria items in CFP category, carrying out safety inspections after experiments (0.058) in MMFP category, strengthening maintenance and safety inspection intensity for electrical equipment (0.064) in MEFP category, developing a standard operating procedure for laboratory facilities (0.048) in PPE category, and evacuation

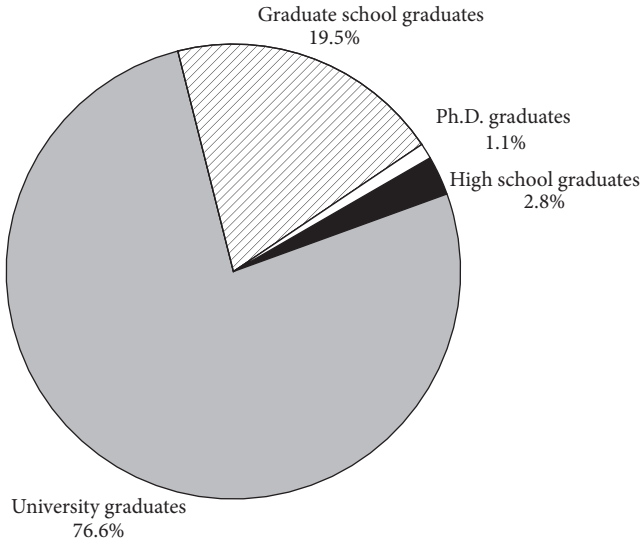

Figure 7: Percentage breakdown of respondents' education background.

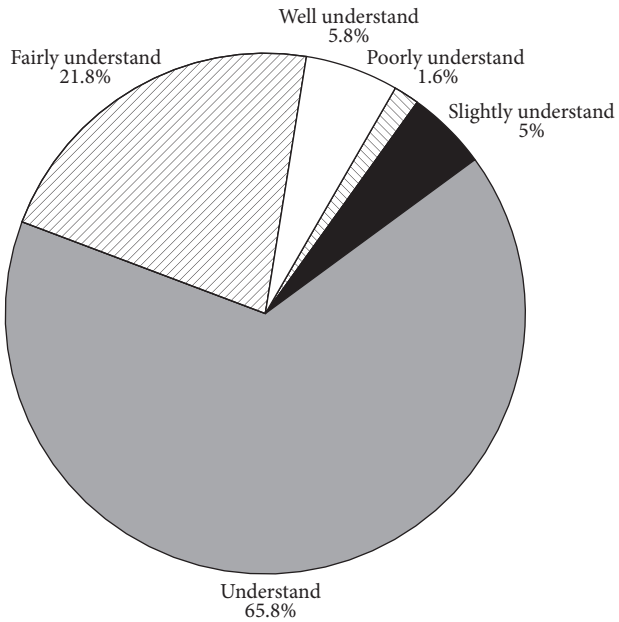

Figure 8: Percentage breakdown of the views of respondents on their understanding of risks.

and emergency response training (0.034) in DEL category. The weights of top 10 subcriteria are presented in Table 7 in descending order. The proposed priorities of these prevention strategies could assist EH&S officers and lab employees in selecting appropriate strategies for enhancing fire safety in laboratories. However, it is worth noting that eight of the top 10 subcriteria are either management or staff-education strategies, and only two are technology related.

A general questionnaire survey of 641 respondents (all with lab operating experience) about safety knowledge and training was conducted and 573 valid samples were collected. The results are shown in Figures 7 and 8 and Tables 4 and 5. Figure 7 presents that 76.6% of the respondents were university students, 19.5% graduate school students, 2.8% senior high school students, and 1% Ph.D. students. Table 4 indicates that 66.7% of the respondents received laboratory safety training, and more than 57.6% of them felt that it was important, although 6.8% said that they felt they did not benefit from it; research showed that, even under optimal training circumstances, individual differences related to a person's intention to learn play an important role in training effectiveness. On the other hand, nearly 33.3% of the respondents did not receive the laboratory safety training, but 60% of them agreed that it was important for improving laboratory safety. The Mann-Whitney U test for both types of respondents was conducted to quantify, subjectively and objectively, the effects of laboratory safety training. It revealed no significant differences ($p > 0.05$) in the satisfaction with the effect of safety education and perception of their safety behaviors. In terms of whether the respondents fully understood the fire dangers prevention and protection, before doing experiments, Figure 8 indicates that 27.6% of respondents thought so; most of laboratory staff replied that they realized the importance of accident prevention, but the results implied that 72.4% of the staff still perceive risks in the laboratory operations; Table 5 presents that most respondents (81.7%) knew the location of the safety protective equipment, and approximately 88.7% understood their standard operating procedures (SOPs), but only 42.2% had the experience of using the safety protective equipment. These results indicate that most training programs need improvement, especially for safety skills training curricula. Nearly 57.8% of respondents felt that there is room for improvement of their current lab safety training programs.

3.3. Event Tree Analysis. It is well known that hood is a critical part when conducting chemical experiments. Unfortunately, there is usually no fire protection within it. Previously we have found that fire accidents occurred frequently in chemistry laboratories. Therefore, we proposed hood safety improvement as a compensation for the insufficiency of management system to improve the fire safety level, namely, installing fire prevention equipment in the hood as proactive preventions from fire accidents: fire detector, automatic sprinkler, and manual extinguisher. ETA was used to explore the feasibility of reducing the risk of fire. The probability of extinguishing a fire due to fire detectors [27], automatic sprinklers [28], laboratory personnel, and fire brigades [29] was set as 0.94, 0.81, 0.51, and 0.97, respectively. The damage is divided into two in this work: research data loss and equipment property damage, with range from 1 to 5 being used for the degree damage, in order to quantitatively assess the consequences of a fire. Damage to research data is considered to be the most important event, since research data from years of work is difficult to recover if it is lost, while laboratory equipment is easier to replace. Degree of damage caused by fire in a laboratory is presented in Table 8.

Figure 10 shows the event tree analysis for a fire occurring in a hood without a fire system. The ETA results indicate that when there is no fire extinguisher system in the hood,

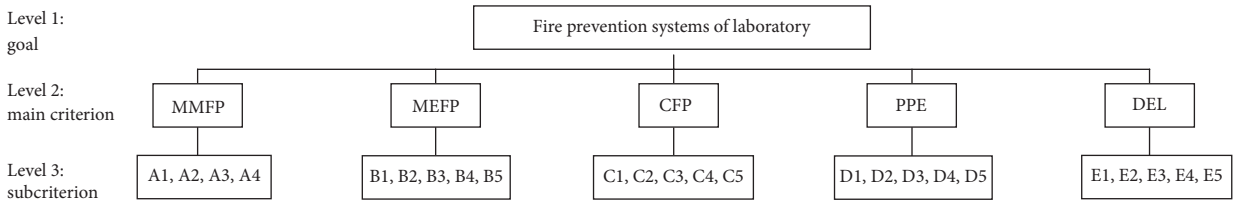

Legend for level 2, 3 attributes:

MMFP: man-made fire prevention

MEFP: mechanical and electrical fire prevention

CFP: chemical fire prevention

PPE: personal protective equipment

DEL: disaster experience learning

A1: practice safety inspections after experiments

A2: establish complete safety guide

A3: establish complete emergency response plan for disasters

A4: set up the disaster announcement procedures and emergency telephone number labels

B1: reinforce the protective devices for mechanical equipment

B2: strengthen maintenance and safety inspection intensity for electrical equipment

B3: fail-safe design

B4: strengthen the safety management of the laboratory

B5: increase the number of the fire detectors and fire extinguishers

C1: identify the risks in the working environment

C2: enhance the safety design of storage devices

C3: carry out safety inspections and labeling of storage devices

C4: strengthen the identification of hazard materials information using the Material Safety Data Sheets (MSDS) for chemicals

C5: enhance the detection technology in the working environment

D1: the personnel protective equipment regular maintenance

D2: develop the standard operation procedures for laboratory facilities

D3: strengthen the instrument operating education and training

D4: strengthen the health and safety education and training

D5: give safety lectures to new employees

E1: cause analysis of false alarm

E2: develop the accident investigation mechanism and database

E3: experience sharing

E4: evacuation and emergency response training

E5: carry out annual fire-fighting drill and check system

Figure 9: AHP model for the prioritization of the fire accident prevention strategies in lab.

Initiating event	Pivotal events				Probability		Consequence		Risk
	Fire detector works	Automatic sprinkler works	Manual extinguisher works	Fire brigade works	Outcomes	[F]	Equipment properties	Research data	
					1	0.7614	3	2	3.8070
					2	0.0911	3	3	0.5465
					3	0.0849	4	4	0.6791
					4	0.0026	5	5	0.0263
					5	0.0306	3	3	0.1836
					6	0.0285	4	4	0.2281
					7	0.0009	5	5	0.0088

Figure 10: Results of the ETA (for the hood without a fire system).

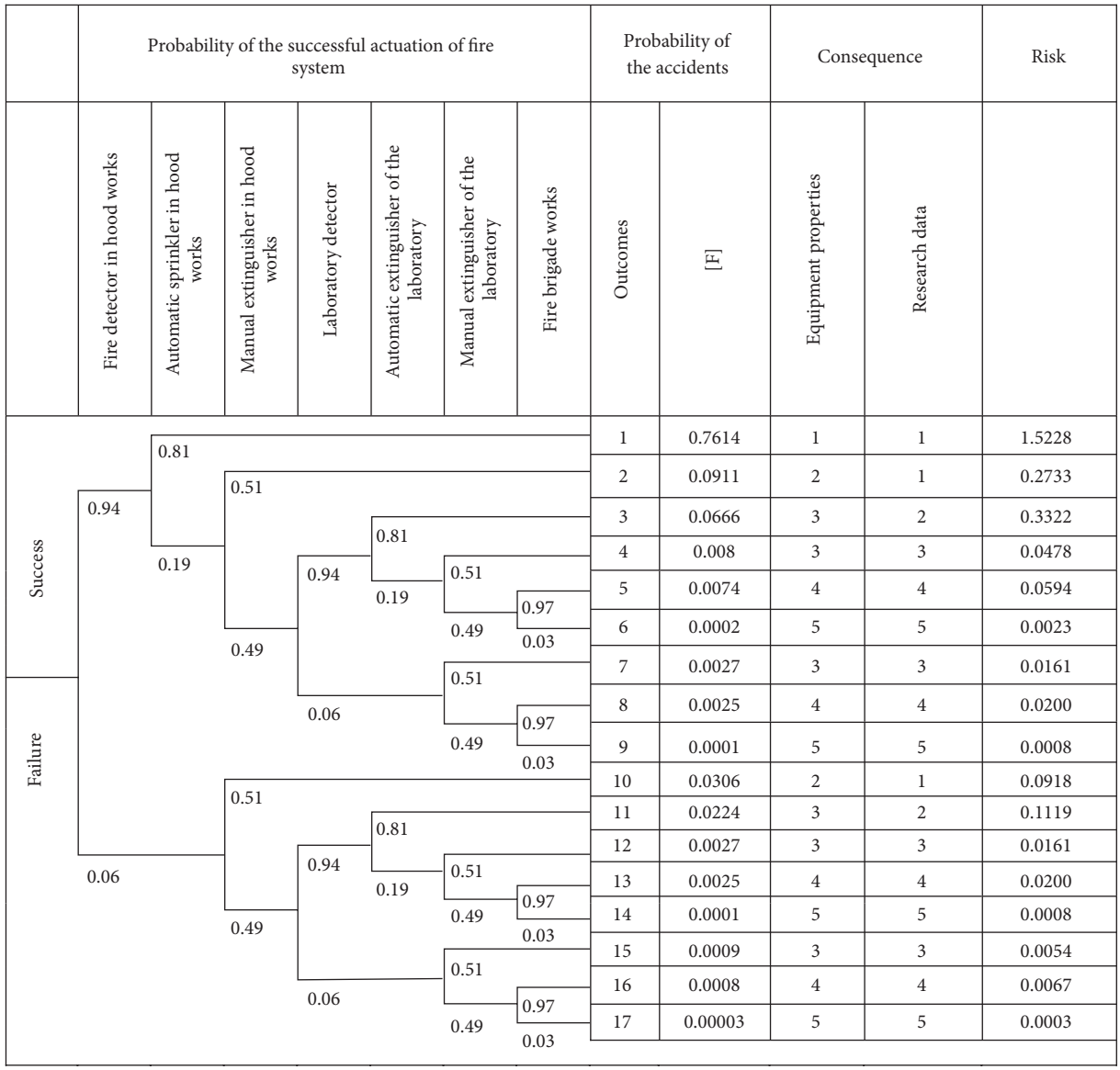

Figure 11: Results of the ETA (for the hood with a fire system).

Table 4: The effect of laboratory safety training.

		Do you benefit from laboratory safety training course?				
Received the training course		Strongly disagree	Disagree	Neither agree nor disagree	Agree	Strongly agree
Yes	Number (%)	5 (1.3%)	21 (5.5%)	136 (35.6%)	164 (42.9%)	56 (14.7%)
No	Number (%)	7 (3.7%)	4 (2.1%)	66 (34.6%)	72 (37.7%)	42 (22.0%)

Table 5: Survey on knowledge of the safety facility system.

Question	Yes	No
Do you know the location of the safety facility system (fire extinguisher, fire alarm button, emergency safety shower, personnel protective equipment, etc.)?	468 (81.7%)	105 (18.3%)
Do you understand the standard operating procedure (SOP) of the safety facility system?	508 (88.7%)	65 (11.3%)
Do you have experience with the safety facility system?	242 (42.2%)	331 (57.8%)

Table 6: Relative priorities of the selection criteria of the prevention strategies.

Main criterion	Local priority	Subcriterion	Local priority	Global priority	Rank
Man-made fire prevention	0.142	Practice safety inspection after the experiment	0.406	0.058	5
		Establish a complete safety guide	0.236	0.033	17
		Establish a complete emergency response plan for a disaster	0.169	0.024	22
		Set up disaster announcement procedures and emergency telephone number labels	0.189	0.027	20
Mechanical & electrical fire prevention	0.261	Reinforce the protective devices for mechanical equipment	0.195	0.051	6
		Strengthen maintenance and safety inspection intensity for electric equipment	0.246	0.064	1
		Fail-safe design	0.165	0.043	13
		Strengthen the safety management of the laboratory	0.232	0.061	3
		Increase the number of fire detectors and fire extinguishers	0.162	0.042	14
Chemical fire prevention	0.263	Identify the risks in the working environment	0.234	0.062	2
		Enhance the safety design of storage devices	0.227	0.060	4
		Carry out safety inspections and labeling of storage devices	0.186	0.049	8
		Strengthen the identification of the hazard materials information using Material Safety Data Sheets (MSDS) for chemicals	0.187	0.049	7
		Enhance detection technology in the working environment	0.166	0.044	12
Personnel safety protection	0.202	The personnel carry out regular maintenance	0.116	0.023	23
		Develop standard operation procedure for laboratory facilities	0.24	0.048	9
		Strengthen the instrument operating education and training	0.228	0.046	11
		Strengthen the health & safety education and training	0.178	0.036	15
		Give safety lectures to new employees	0.238	0.048	10
Disaster experience learning	0.132	Cause analysis of false alarms	0.093	0.012	24
		Develop an accident investigation mechanism and database	0.19	0.025	21
		Experience sharing	0.224	0.030	19
		Evacuation and emergency response training	0.26	0.034	16
		Annual fire-fighting drill and system checks	0.233	0.031	18

Table 7: Global percentage weights of the subcriteria of the hierarchy tree in descending order.

Rank	Subcriteria	Global percentage weight
1	Strengthen maintenance and safety inspection intensity for electrical equipment	6.4%
2	Identify the risks in the working environment	6.2%
3	Strengthen the safety management of the laboratory	6.1%
4	Enhance the safety design of storage devices	6.0%
5	Practice safety inspections after experiments	5.8%
6	Reinforce the protective devices for mechanical equipment	4.3%
7	Strengthen identification of the hazard materials information using the Material Safety Data Sheets (MSDS) for chemicals	4.9%
8	Carry out safety inspections and labeling of storage devices	4.9%
9	Develop standard operation procedures for laboratory facilities	4.8%
10	Give safety lectures to new employees	4.8%

Table 8: Degree of damage caused by fire in a laboratory.

Damage category	Degree of damage	Description of damage
Property	1	Less than 1,000 USD: nondamaged
	2	1,000~5,000 USD: slightly damaged
	3	5,000~50,000 USD: moderately damaged
	4	50,000~100,000 USD: heavily damaged
	5	More than 100,000 USD: severely damaged
Research data	1	100% restorable
	2	80% restorable
	3	50% restorable
	4	20% restorable
	5	0% restorable

and when the fire extinguisher system in laboratory fails, then outcomes 4 and 7 arise, and the total risk associated with a failed fire extinguisher system is 0.026 + 0.009 = 0.035. But when fire detectors and a fire extinguisher system are installed, three additional pivotal events are identified; namely, the fire detector works in the hood, the automatic sprinkler works, and the manual extinguisher works. The ETA for this case indicates that when the fire extinguisher system failure happens, as shown in Figure 11, the possible outcomes are 6, 9, 14, and 17. The total risk for the fire extinguisher failure is 0.0042. The results indicate that the total risk of a fire occurring in hood decreases from 0.0350 to 0.0042 when actions to improve hood safety are taken. According to these results, ETA, incorporated into the proposed management model, is very useful to evaluate the probability of whether safety strategies can successfully control the fire accidents or additional design is needed.

4. Conclusions

A system-based management model for lab fire prevention was investigated which combines RCA, AHP, and ETA with the information of questionnaire surveys in a loop. First, the information of 139 lab fire accidents was reviewed; a fishbone diagram was used to analyze the causes leading to accidents and prevention strategies were also developed; AHP with various levels of criteria was used to evaluate the priority of these strategies. We also found that, no matter what reasons, human error could be inevitable and it has to be considered seriously. Additional fire prevention equipment was thus proposed to be installed in the lab hood. ETA, an inductive management technique, was applied, to explore how effective these installations can achieve. The risks drop tremendously from 0.035 to 0.0042. Fire risks could largely be avoided if good engineering design is also involved in the safety management program. Combining root cause analysis (RCA), analytic hierarchy process (AHP), and event tree analysis (ETA) in a loop is able to develop and prioritize prevention strategies and more specifically evaluate whether these strategies can successfully control fire accidents or specific installation is needed.

Competing Interests

The authors declare that there is no conflict of interests regarding the publication of this paper.

Acknowledgments

This study was supported by the Ministry of Science and Technology of Taiwan under Projects MOST 103-2221-E-327-004 and MOST 104-3113-E-006-019-CC2.

References

[1] A. Keith Furr, *CRC Handbook of Laboratory Safety*, CRC Press, 5th edition, 2000.

[2] R. J. Alaimo, *Handbook of Chemical Health and Safety*, Oxford University Press, Oxford, UK, 2001.

[3] Environment, Health, and Safety Committee, *Fire Safety in Chemical Laboratories*, Royal Society of Chemistry, London, UK, 2007.

[4] Y. C. Chien, C. P. Chang, Y. C. Lin, H. S. Liu, and K. C. Lee, "The characteristics and potential causes of laboratory incident and injury in Taiwan," in *Proceedings of the the Occupational Safety & Hygiene International Symposium*, 2002.

[5] C. Shih, Y. C. Chien, T. P. Chia, and C. P. Chang, "Initial review of emergency response procedure for laboratories on campus," in *Proceedings of the Occupational Safety & Hygiene International Symposium*, 2002.

[6] S. Y. Lin, *Fire risk assessment of fume hood in laboratories [M.S. thesis]*, National Kaohsiung First University of Science and Technology, 2008.

[7] J. I. Chang and C.-C. Lin, "A study of storage tank accidents," *Journal of Loss Prevention in the Process Industries*, vol. 19, no. 1, pp. 51–59, 2006.

[8] T. L. Saaty, *The Analytic Hierarchy Process: Planning, Priority Setting, Resource Allocation*, McGraw-Hill, 1980.

[9] T. J. Crowe, J. S. Noble, and J. S. Machimada, "Multi-attribute analysis of ISO 9000 registration using AHP," *International Journal of Quality and Reliability Management*, vol. 15, no. 2, pp. 205–222, 1998.

[10] S.-O. Cheung, T.-I. Lam, M.-Y. Leung, and Y.-W. Wan, "An analytical hierarchy process based procurement selection method," *Construction Management and Economics*, vol. 19, no. 4, pp. 427–437, 2001.

[11] M. Hastak, "Advanced automation or conventional construction process?" *Automation in Construction*, vol. 7, no. 4, pp. 299–314, 1998.

[12] E. W. L. Cheng and H. Li, "Construction partnering process and associated critical success factors: quantitative investigation," *Journal of Management in Engineering*, vol. 18, no. 4, pp. 194–202, 2002.

[13] S. K. Lee, Y. J. Yoon, and J. W. Kim, "A study on making a long-term improvement in the national energy efficiency and GHG control plans by the AHP approach," *Energy Policy*, vol. 35, no. 5, pp. 2862–2868, 2007.

[14] J. K. W. Wong and H. Li, "Application of the analytic hierarchy process (AHP) in multi-criteria analysis of the selection of intelligent building systems," *Building and Environment*, vol. 43, no. 1, pp. 108–125, 2008.

[15] C.-M. Chiang and C.-M. Lai, "A study on the comprehensive indicator of indoor environment assessment for occupants' health in Taiwan," *Building and Environment*, vol. 37, no. 4, pp. 387–392, 2002.

[16] K.-F. Chang, C.-M. Chiang, and P.-C. Chou, "Adapting aspects of GBTool 2005—searching for suitability in Taiwan," *Building and Environment*, vol. 42, no. 1, pp. 310–316, 2007.

[17] R. M. Tavares, J. M. L. Tavares, and S. L. Parry-Jones, "The use of a mathematical multicriteria decision-making model for selecting the fire origin room," *Building and Environment*, vol. 43, no. 12, pp. 2090–2100, 2008.

[18] N. S. Arunraj and J. Maiti, "Risk-based maintenance policy selection using AHP and goal programming," *Safety Science*, vol. 48, no. 2, pp. 238–247, 2010.

[19] S. D. Novack, N. O. Siu, and S. G. Hill, "The use of event trees in oil spill prevention applications," *International Oil Spill Conference Proceedings*, vol. 1997, no. 1, pp. 527–534, 1997.

[20] M. Abdelgawad and A. R. Fayek, "Comprehensive hybrid framework for risk analysis in the construction industry using combined failure mode and effect analysis, fault trees, event trees, and fuzzy logic," *Journal of Construction Engineering and Management*, vol. 138, no. 5, pp. 642–651, 2012.

[21] C. Maio, M. C. Liu, and Y. C. Peng, "The practice on laboratory risk assessment," *Chemical Engineering*, vol. 49, no. 5, pp. 62–73, 2002.

[22] *AS/NZS 4360: 2004 Risk Management*, 2004: Standards Australia and Standards New Zealand.

[23] C. W. Lin, Y. C. Kuo, S. H. Kuo, and H. C. Wu, "Investigation on fires and explosions at university laboratories related to chemicals," in *Proceedings of the Annual Conference of the Chemical Engineering Safety*, 2003.

[24] J. Y. Peng and R. S. Sheu, "A study of risk management on the university campus safety," in *Proceedings of the International Seminar on Fundamental University Education*, 2006.

[25] J. Zakzeski, "Improving engineering research laboratory safety by addressing the human aspects of research management," *Journal of Chemical Health and Safety*, vol. 16, no. 3, pp. 5–20, 2009.

[26] T.-C. Wu, C.-W. Liu, and M.-C. Lu, "Safety climate in university and college laboratories: impact of organizational and individual factors," *Journal of Safety Research*, vol. 38, no. 1, pp. 91–102, 2007.

[27] R. W. Bukowski, E. K. Budnick, and C. F. Schemel, "Estimates of operation reliability of fire protection systems," in *Proceedings of the International Conference on Fire Research and Engineering*, 1999.

[28] W. E. Koffel, "Reliability of automatic sprinkler system," in *Proceedings of 2006 Fire Supersession and Detection Research Application Symposium*, 2006.

[29] Y. Yoshida, "Analysis of simulation evacuation World Trade Center," in *Proceedings of the CIB-CTBUH Conference on Tall Buildings: Strategies for Performance in the Aftermath of the World Trade Centre CIB*, Kuala Lumpur, Malaysia, October 2003.

Hindawi Publishing Corporation
Mathematical Problems in Engineering
Volume 2016, Article ID 8593612, 11 pages
http://dx.doi.org/10.1155/2016/8593612

Research Article

Failure Propagation Modeling and Analysis via System Interfaces

Lin Zhao,[1] Krishnaiyan Thulasiraman,[2] Xiaocheng Ge,[3] and Ru Niu[1]

[1]*State Key Laboratory of Rail Traffic Control and Safety, Beijing Jiaotong University, Beijing 100044, China*
[2]*School of Computer Science, University of Oklahoma, Norman, OK 73019, USA*
[3]*Institute of Railway Research, University of Huddersfield, Huddersfield HD1 3DH, UK*

Correspondence should be addressed to Lin Zhao; lzhao3@bjtu.edu.cn

Received 12 January 2016; Revised 30 March 2016; Accepted 5 April 2016

Academic Editor: Egidijus R. Vaidogas

Safety-critical systems must be shown to be acceptably safe to deploy and use in their operational environment. One of the key concerns of developing safety-critical systems is to understand how the system behaves in the presence of failures, regardless of whether that failure is triggered by the external environment or caused by internal errors. Safety assessment at the early stages of system development involves analysis of potential failures and their consequences. Increasingly, for complex systems, model-based safety assessment is becoming more widely used. In this paper we propose an approach for safety analysis based on system interface models. By extending interaction models on the system interface level with failure modes as well as relevant portions of the physical system to be controlled, automated support could be provided for much of the failure analysis. We focus on fault modeling and on how to compute minimal cut sets. Particularly, we explore state space reconstruction strategy and bounded searching technique to reduce the number of states that need to be analyzed, which remarkably improves the efficiency of cut sets searching algorithm.

1. Introduction

Our society is relying more and more on the safety of a number of computer-based systems, for example, the control system of managing air traffic or operating a nuclear power plant. These systems are usually called safety-critical systems, which are a class of engineered systems that may pose catastrophic risks to its operators, the public, and the environment. The development of these systems demands a rigorous process of system engineering to ensure that safety risks of the system, even if some of its components fail, are mitigated to an acceptable level. System safety analysis techniques are well established and are used extensively during the design of safety-critical systems.

The size, scale, heterogeneity, and distributed nature of current (and likely future) systems make them difficult to verify and to analyze, particularly for nonfunctional properties including availability, performance, and security, as well as safety. Due to the manual, informal, and error-prone nature of the traditional safety analysis process, the use of models and automatic analysis techniques as an aid to support safety-related activities in the development process has attracted increasing interest. Model-based safety analysis (MBSA), where the analysis is carried out on formal system models that take into account system behaviors in the presence of faults, has been proposed to address some of the issues specific to safety assessment. Recent work in this area has demonstrated some advantages of this methodology over traditional approaches, for example, the capability of automatic generation of safety artifacts, and shown that it is a promising way to reduce costs while further improving efficiency and quality of safety analysis process.

The existing approaches to MBSA, for example, ESACS/ISAAC [1, 2], AltaRica [3–5], Failure Propagation and Transformation Notation (FPTN) [6, 7], Hierarchically Performed Hazard Origin and Propagation Studies (HiP-HOPS) [8], and the AADL with its error annex [9], can be classified into two groups: (a) failure logic based or (b) system states based. Original MBSA techniques, such as FPTN and HiP-HOPS, have sought to unify classical safety analysis methods such

as Fault Tree Analysis (FTA) and Failure Modes and Effects Analysis (FMEA) and to provide a formalism for capturing a single authoritative safety model of the system. These approaches emphasized the model of failure propagation logic. The second group of MBSA approaches addresses the analysis of the transition of system states [10–12], in order to identify the routes that a system transits from a safe state to a hazardous state. Since these search-based techniques normally require exhaustive enumeration of all reachable states, they do not fully exploit the advantage of the internal structure of the state space and domain knowledge of safety analysis.

Safety is clearly an emergent property of a system that can only be determined in the context of the whole. As an emergent property, safety arises only when the system components interact with each other in an environment. Such property is controlled or enforced by a set of constraints related to behaviors of system components. Accidents often result from interactions among components that violate these constraints. In general, the term interaction is conceptually simple; it is a kind of action that occurs as two or more objects have an effect upon one another. In practice, interactions among the components dramatically increase the complexity of the overall system. It is intuitively obvious that growing interaction complexity poses a great challenge to engineer safety of the system. In some cases, although hazard identification and safety assessment had been undertaken for system components, the hazards could be missed apparently at least in part because they arise out of the complex and indirect interactions in a complex system, especially when the components of the system are independently developed or operated. The new challenge to MBSA due to the complexity of a system is that it is very hard to analyze all possible dysfunctional interactions in the system so that its hazardous states which reflect the effects of dysfunctional interactions and inadequate enforcement of safety constraints can be identified.

Using interface models to capture these interactions would offer twofold benefits. Interface information could be abstracted from the existing system design models conveniently. This is helpful to the tight integration of the systems and safety engineering processes. Furthermore, interface models are often more abstract and contain much less corresponding implementation details, which help to combat the state space explosion problem in the following automatic analysis.

In this paper, we propose an approach of model-based safety analysis which utilizes extended interface automata [13] to model the nominal behaviors as well as fault behaviors of the system. To avoid the exploration of the entire reachability set, we present a structural analysis strategy, which takes into account the inner structure of state space. This has made possible development of efficient algorithms for the purpose of safety analysis. By applying state space reduction and heuristic search, a much smaller reachable space needs to be explored and thus the efficiency of proposed minimal cut sets algorithm has been improved.

The rest of the paper is organized as follows. In Section 2, we introduce interface automaton as a formal model for safety analysis. In Section 3, we show how to use domain knowledge for efficient state space reduction and minimal cut sets generation. Section 4 mainly demonstrates our approach on a small yet realistic safety-related example where minimal cut sets are generated and analyzed. Conclusions and outlooks for future work are presented in Section 5.

2. Interfaces and Fault Modeling

2.1. Definitions and Notation. Interface automata give a formal and abstract description of the interactions between components and the environment. This formalism captures the temporal aspects of component interfaces, including input assumptions and output guarantees, in terms of I/O actions and the order in which they occur in automata. Input assumptions describe the possible behaviors of the component's external environment, while output guarantees describe the possible behaviors of the component itself.

Definition 1 (interface automata). An interface automaton is defined as a tuple $P = \langle \mathscr{V}_P, \mathscr{V}_P^{\text{Init}}, \mathscr{I}_P, \mathscr{O}_P, \mathscr{H}_P, \mathscr{T}_P \rangle$, where

(i) $\mathscr{V}_P$ is a finite set of states,

(ii) $\mathscr{V}_P^{\text{Init}} \subseteq \mathscr{V}_P$ is a set of initial states,

(iii) $\mathscr{I}_P$, $\mathscr{O}_P$, and $\mathscr{H}_P$ are mutually disjoint sets of input, output, and internal actions; one denotes by $\mathscr{A}_P = \mathscr{I}_P \cup \mathscr{O}_P \cup \mathscr{H}_P$ the set of all actions,

(iv) $\mathscr{T}_P \subseteq \mathscr{V}_P \times \mathscr{A}_P \times \mathscr{V}_P$ is a transition relation.

A trace on interface automaton is an alternating sequence consisting of states and actions, such as $p_0, a_0, p_1, a_1, \ldots, a_{k-1}, p_k$, where $p_i \in \mathscr{V}_P$ and $a_j \in \mathscr{A}_P$ ($i \in \{0, \ldots, k\}$ and $j \in \{0, \ldots, k-1\}$). If an action $a \in \mathscr{I}_P$ (resp., $a \in \mathscr{O}_P$, $a \in \mathscr{H}_P$), then $(v, a, v') \in \mathscr{T}_P$ is called an input (resp., output, internal) transition. We denote by $\mathscr{T}_P^{\mathscr{I}}$ (resp., $\mathscr{T}_P^{\mathscr{O}}$, $\mathscr{T}_P^{\mathscr{H}}$) the set of input (resp., output, internal) transitions. An action $a \in \mathscr{A}_P$ is enabled at a state $v \in \mathscr{V}_P$ if there is a transition $(v, a, v') \in \mathscr{T}_P$ for some $v' \in \mathscr{V}_P$. We denote by $\mathscr{I}_P(v)$, $\mathscr{O}_P(v)$, and $\mathscr{H}_P(v)$ the subsets of input, output, and internal actions that are enabled at the state v.

We illustrate the basic features of interface automata by applying them to the modeling of a railroad crossing control system. Figure 1 depicts the interfaces of three components modeling the train, controller, and gate, respectively. Two sensors are used to detect the approach and exit of the train. The state changes of the controller stand for handshaking with the train (via the actions *Approach* and *Exit*) and the gate (via the actions *Lower* and *Raise* by which the controller commands the gate to close or to open). When everything is ready, a signal *Enter* is sent to authorize the entrance of the train.

In the graphic representation, each automaton is enclosed in a box, whose ports correspond to the input and output actions. The symbols ? and ! are appended to the name of the action to denote that the action is an input and output action, respectively. An arrow without source denotes the initial state of the automaton.

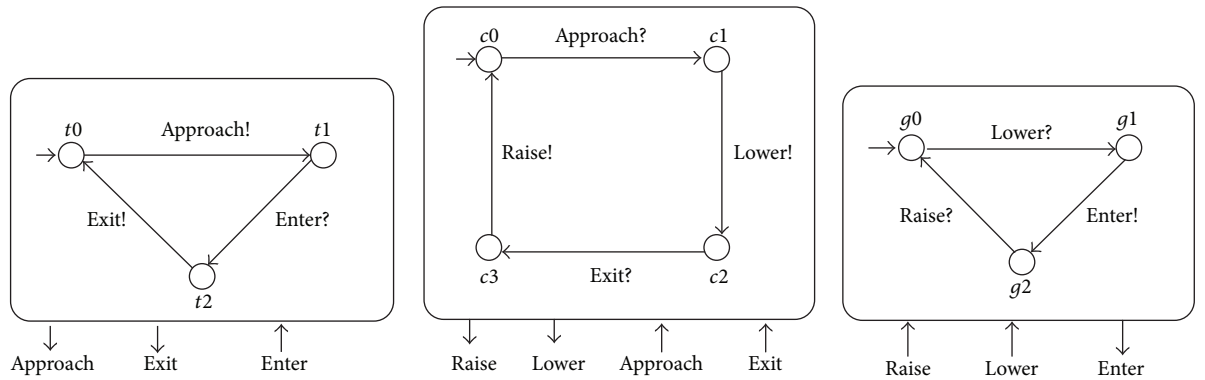

(a) Train (b) Controller (c) Gate

Figure 1: The interface models of railroad crossing control system.

The parallel composition of interface automata shows how they all relate and work together. In Alfaro and Henzinger's original paper of interface automata [13], providing a particular form of parallel composition mainly aimed to analyze the compatibility of components. In this paper, the compatibility is not our concern. Therefore, we abandon this kind of parallel composition, using a more traditional one which is common in automaton theory. Two interface automata P and Q are composable if $\mathcal{I}_P \cap \mathcal{I}_Q = \varnothing = \mathcal{O}_P \cap \mathcal{O}_Q$; that is, they have neither common inputs nor common outputs. We let $\text{shared}(P,Q) = \mathcal{A}_P \cap \mathcal{A}_Q$. In a composition, the two automata will synchronize on all common actions and asynchronously interleave all other actions.

Definition 2 (parallel composition). If P and Q are composable interface automata, the parallel composition $P \times Q$ is the interface automaton defined by

$$
\begin{aligned}
&\mathcal{V}_{P\times Q} = \mathcal{V}_P \times \mathcal{V}_Q,\\
&\mathcal{V}^{\text{Init}}_{P\times Q} = \mathcal{V}^{\text{Init}}_P \times \mathcal{V}^{\text{Init}}_Q,\\
&\mathcal{I}_{P\times Q} = \left(\mathcal{I}_P \cup \mathcal{I}_Q\right) \setminus \text{shared}\left(P,Q\right),\\
&\mathcal{O}_{P\times Q} = \left(\mathcal{O}_P \cup \mathcal{O}_Q\right) \setminus \text{shared}\left(P,Q\right),\\
&\mathcal{H}_{P\times Q} = \left(\mathcal{H}_P \cup \mathcal{H}_Q\right) \setminus \text{shared}\left(P,Q\right),\\
&\mathcal{T}_{P\times Q} = \left\{\left((v,u),a,\left(v',u\right)\right) \mid \left(v,a,v'\right) \in \mathcal{T}_P \wedge a\right.\\
&\quad \left.\notin \text{shared}\left(P,Q\right) \wedge u \in \mathcal{V}_Q\right\}\\
&\quad \cup \left\{\left((v,u),a,\left(v,u'\right)\right) \mid \left(u,a,u'\right) \in \mathcal{T}_Q \wedge a\right.\\
&\quad \left.\notin \text{shared}\left(P,Q\right) \wedge v \in \mathcal{V}_P\right\}\\
&\quad \cup \left\{\left((v,u),a,\left(v',u'\right)\right) \mid \left(v,a,v'\right) \in \mathcal{T}_P \wedge \left(u,a,u'\right)\right.\\
&\quad \left.\in \mathcal{T}_Q \wedge a \in \text{shared}\left(P,Q\right)\right\}.
\end{aligned}
\tag{1}
$$

The parallel composition of *train* and *controller* is shown in Figure 2(a). Here, we have only depicted the reachable states of the composition. The automaton $train \times controller \times gate$ in Figure 2(b), where all the actions have been hidden as internal ones after synchronization, describes the system function in an orderly and concise manner.

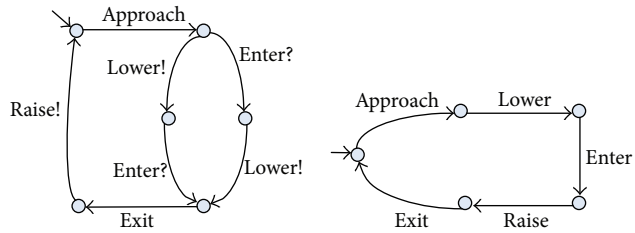

(a) Train × controller (b) Train × controller × gate

Figure 2: The parallel composition of interface models.

2.2. Fault Propagation Modeling on Interface Automata. For model-based safety analysis, failure modes must be explicitly modeled. Our approach to modeling fault behaviors is to specify them using the interface automata notation itself. The incorporation of the fault behaviors directly on the system interface models will promote ease of specification of complex fault behaviors for both the system design and safety engineers, allowing them to create simple but realistic models for precise safety analysis.

Fault modeling is aiming to specify the direct effects of failure modes. In our approach, this is done via importing new actions, states, and transitions to the existing models. There are two types of faults in interface automata: basic faults and propagating faults. Basic faults differ from propagating faults in their activation condition. Basic faults are intrinsic to a component and originate within the component boundary. Their activation occurs independently of other component failures and can be modeled using an independent input action.

The faults that get activated by interaction or interference due to error propagation are considered as propagating faults. In interface automata, propagating faults will be synchronized during the composition of two components and then

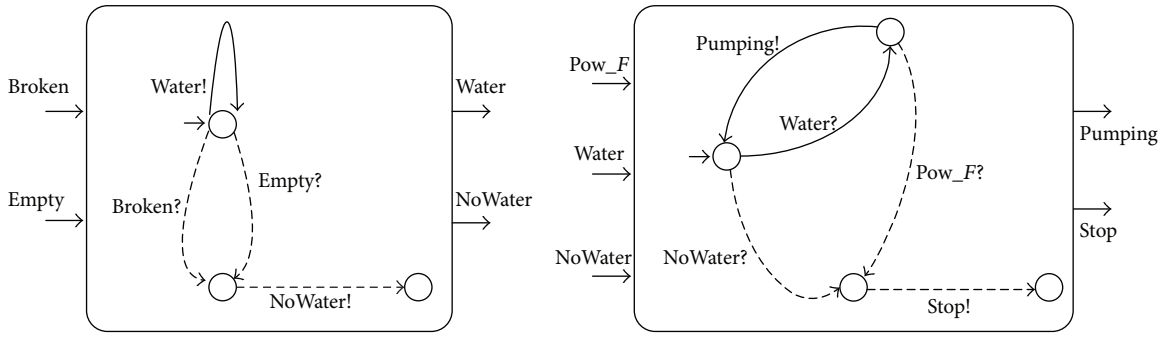

Figure 3: Basic faults and propagating faults in interface automata.

hidden as internal actions. We denote by $\mathscr{E}^{\mathrm{bf}}$ and $\mathscr{E}^{\mathrm{pf}}$, respectively, the mutually disjoint sets of basic faults and propagating faults.

Consider the cooling water supply system in Figure 3. This system consists of an electric pump and a water tank. Two components synchronize on action *Water*, which means there is water in the tank and the pump will start working (action *Pumping*). However, the tank may be broken or empty, denoted by input actions *Broken* and *Empty*. Here, *Broken* and *Empty* are basic faults since they originate within the tank component. *NoWater* is defined as a propagating fault to model the failure propagation from water tank to the pump. Also, there are other propagating faults, like power failure (action *Pow_F*) and the stop of pump (action *Stop*), between pump and other devices not listed in this example.

Our extension towards interface automata lies on two aspects. Firstly, as shown in Figure 3, the extended definition of interface automata could be regarded as a 7-tuple $P = \langle \mathscr{V}_P, \mathscr{V}_P^{\mathrm{Init}}, \mathscr{I}_P, \mathscr{O}_P, \mathscr{H}_P, \mathscr{T}_P, \mathscr{E}^{\mathrm{bf}}, \mathscr{E}^{\mathrm{pf}} \rangle$. Since $\mathscr{E}^{\mathrm{bf}}$ and $\mathscr{E}^{\mathrm{pf}}$ also have input or output attributes, they do not need special treatment during the composition. Besides, solid lines in the figure depict the nominal system interfaces, while the dash lines show the fault behaviors of each of the components. Based on the real system interfaces, this kind of extension is easy to perform and easy to understand and provides useful system insights and shared formal models between the design and safety analysis stages.

3. Algorithms Assist in Failure Analysis

Minimal cut set is the combination of basic faults which can guarantee occurrence of a top-level event (TLE), that is, a set of undesired states, but only has the minimum number of these faults. The key problem investigated in this paper is how to efficiently produce minimal cut sets through exhaustive state space exploration. We first give the following definitions of (minimal) cut sets.

Definition 3 (cut set). Let $P = \langle \mathscr{V}_P, \mathscr{V}_P^{\mathrm{Init}}, \mathscr{I}_P, \mathscr{O}_P, \mathscr{H}_P, \mathscr{T}_P \rangle$ be an interface automaton, $\mathscr{E}^{\mathrm{bf}}$ the set of basic faults, and top-level event TLE $\subseteq \mathscr{V}_P$. cs $\subseteq \mathscr{E}^{\mathrm{bf}}$ is a cut set of TLE if there exists a trace $t = p_0, a_0, p_1, a_1, \ldots, a_{k-1}, p_k$ on P satisfying the following:

(1) $p_0 \in \mathscr{V}_P^{\mathrm{Init}}$, $p_i \notin \mathscr{V}_P^{\mathrm{Init}}$ $(i \in \{1, \ldots, k\})$, and $p_k \in$ TLE;

(2) $\forall i \in \{0, \ldots, k-1\}$ $(a_i \in \mathscr{E}^{\mathrm{bf}} \rightarrow a_i \in \mathrm{cs})$;

(3) $\forall a \in \mathrm{cs} \rightarrow a \in t$.

Intuitively, a cut set is a combination of some basic faults which can lead to the occurrence of the given top-level event, that is, the set of all basic faults contained in a trace from initial states $\mathscr{V}_P^{\mathrm{Init}}$ to top-level event (TLE) is a cut set with respect to TLE. We use $\mathrm{CS}_{\mathrm{TLE}}^P$ to represent all cut sets on automaton P with respect to TLE. Minimal cut sets are formally defined as follows.

Definition 4 (minimal cut sets). Let $\mathrm{CS}_{\mathrm{TLE}}^P$ be the set of all cut sets on automaton P with respect to TLE. One has the set of all minimal cut sets of TLE on automaton P as follows:

$$\mathrm{MCS}_{\mathrm{TLE}}^P = \left\{ \mathrm{cs} \in \mathrm{CS}_{\mathrm{TLE}}^P \mid \forall \mathrm{cs}' \in \mathrm{CS}_{\mathrm{TLE}}^P \ \left(\mathrm{cs}' \subseteq \mathrm{cs} \longrightarrow \mathrm{cs}' = \mathrm{cs} \right) \right\}. \tag{2}$$

Based on the previous definitions, the computation of minimal cut sets is to find out all traces leading to the TLE, that is, all cut sets $\mathrm{CS}_{\mathrm{TLE}}^P$, and then minimize these sets.

3.1. State Space Reconstruction. Several automatic analysis techniques for minimal cut sets generation have been developed on a variety of models, for example, Petri net, finite state machine, NuSMV model, and AltaRica model. The main difficulty in this kind of search-based minimal cut sets generation is state space reduction, because in general the complexities of searching algorithms depend on the size of the state space.

We observed that, for safety analysis on interface models, only those actions that contribute to the occurrence of the predefined TLE need to be analyzed. During the state exploration, noncontributing actions could be ruled out as far as possible. This means that a majority of transitions relevant to internal and output actions could be peripheral to our core searching algorithm. Based on this observation, we develop a procedure of state space reduction.

To reconstruct the state space of the given interface models, our approach is to cluster states that are noncontributing to the occurrence of TLE into equivalent classes and eliminate

relevant transitions. The numbers of states and transitions are reduced using a restricted forward and backward reachability analysis from initial states and TLE, respectively. The result is a representation of the state space that is compact and minimal in some sense and keeps all necessary information about faults propagation.

Definition 5 (state space partition). Let P be an interface automaton, $\mathscr{E}^{\text{bf}}$ the set of basic faults, and top-level event TLE $\subseteq \mathscr{V}_P$. The set of states $\mathscr{V}_P$ consists of three disjoint parts, denoted by SafetyArea^P, TriggeringArea^P, and HazardCore^P, where

(i) SafetyArea^P is a forward closure $U \subseteq \mathscr{V}_P$ such that (1) $\mathscr{V}_P^{\text{Init}} \subseteq U$ and (2) if $u \in U$ and $(u, a, u') \in (\mathscr{T}_P^{\mathscr{O}} \cup \mathscr{T}_P^{\mathscr{H}})$, then $u' \in U$;

(ii) HazardCore^P is a backward closure $U \subseteq \mathscr{V}_P$ such that (1) TLE $\subseteq U$ and (2) if $u \in U$ and $(u', a, u) \in (\mathscr{T}_P^{\mathscr{O}} \cup \mathscr{T}_P^{\mathscr{H}})$, then $u' \in U$;

(iii) TriggeringArea^P $= \mathscr{V}_P \setminus$ (SafetyArea$^P \cup$ HazardCore^P).

Definition 5 divides the state space of an interface automaton into three separate areas based on top-level event (TLE). Intuitively, the set SafetyArea contains the reachable states of an automaton from the initial states by taking only internal or output transitions. In this area, the current running of the system is safe and there is no occurring of any basic faults. HazardCore consists of all states that can reach TLE through a series of continuous internal or output transitions. States within the scope of HazardCore could evolve into TLE without any external stimulation, that is, the occurrence of any basic fault. TriggeringArea is a complement set containing all states of $\mathscr{V}_P$ excepting those in SafetyArea $\cup$ HazardCore. According to this definition, all of the basic faults are contained in the TriggeringArea, which is the focus of our state exploration algorithm for minimal cut sets generation.

We use a directed graph DG_P, consisting of vertices and labeled edges, to denote the underlying transition diagram of an interface automaton P.

Definition 6 (state space reconstruction). Given an interface automaton P, *Reduced*(DG_P) is the reduced form of its original transition diagram by applying the following steps on DG_P:

(1) remove all transitions from TriggeringArea^P to SafetyArea^P;

(2) remove all transitions from HazardCore^P to SafetyArea^P or TriggeringArea^P;

(3) combine all states of SafetyArea^P into a new state Init;

(4) combine all states of HazardCore^P into a new state Top.

Definition 6 and Figure 4 show the process of our state space reduction strategy. All states in the set *SafetyArea* are merged into a new state *Init*. All states in the set *HazardCore* are combined into state *Top*. After removing all reverse transitions on the fault propagation path, we get a new state space for further analysis.

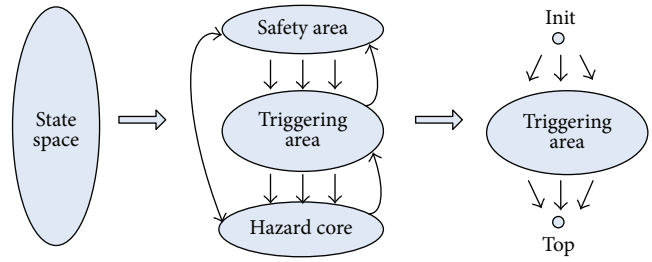

FIGURE 4: The reconstruction of system state space.

Theorem 7. *Let P be an interface automaton. If cs is a cut set with respect to top-level event (TLE), then there exists a trace t in Reduced(DG_P) from Init to Top, containing all elements of cs.*

Proof. Since the set of basic faults cs is a cut set of TLE, according to Definition 3, there is a trace $t' = p_0, a_0, p_1, a_1, \ldots, a_{k-1}, p_k$ in DG_P from $\mathscr{V}_P^{\text{Init}}$ to TLE satisfying $\forall a \in \text{cs} \rightarrow a \in t'$. By applying steps (3) and (4) of Definition 6 at both ends of this trace, respectively, we get a new path $t = \text{Init}, a_m, p_{m+1}, \ldots, p_n, a_n, \text{Top}$. Obviously, t is in *Reduced*(DG_P). During this process, only those internal and output transitions in SafetyArea^P and HazardCore^P are removed. Because all basic faults are defined as input actions, hence no basic fault is eliminated from t'; that is, trace t still contains all elements of cs. □

The essence of the search-based minimal cut sets generation is to find out all combinations of basic faults that contributed to the top-level event in DG_P. Theorem 7 shows that DG_P and *Reduced*(DG_P) are equivalent for this purpose, whereas the latter contains far fewer states and transitions. We use an example to illustrate the effectiveness of this approach. Reconsider the previous railroad crossing control system in Figure 1, which is in an ideal world where no errors occur. The next step is to extend these models such that failure modes are also correctly described. The following three failure modes are taken into account in this example:

(i) Failure of the sensors (actions *S1_F* and *S2_F*) which will prevent sending signals (actions *Approach* and *Exit*) when the train is approaching or exiting.

(ii) Failure of the brake (action *Bra_F*) which will lead to nonauthorized entering of the cross, that is, bypassing action *Enter*.

(iii) Failure of the barrier (action *Stuck*) which results in the barrier being stuck at any location; a new state g_3 is added to represent the stuck state of the barrier.

These failure modes are integrated into the formal interface models, as shown in Figure 5. This model extension provides us a failure propagation map on nominal system model,

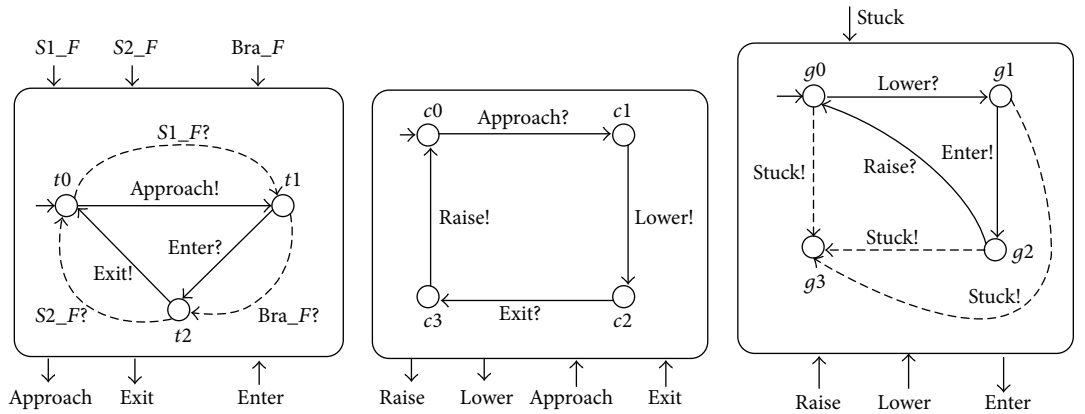

(a) Train (b) Controller (c) Gate

Figure 5: The extended interface models of railroad crossing control.

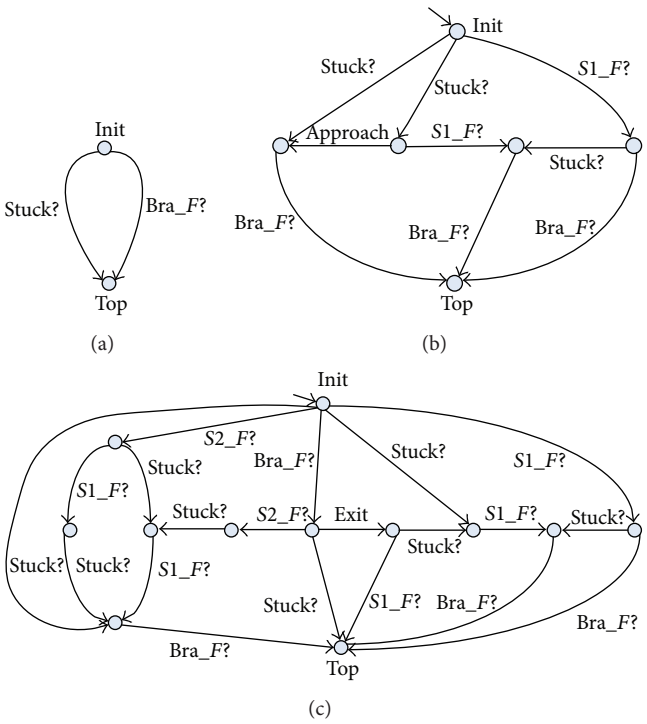

Figure 6: The reshaped state space *Reduced*(DG_{RC}).

reflecting both normal interactions and fault propagation. The safety goal of this system is clear:

SR 1: it must never happen that the train is on the crossing (at state t_2) and the crossing is not secured (at state g_0 or g_3).

RC = $train \times controller \times gate$ is the parallel composition of those extended interface models. There are 30 states and 63 transitions in the state space DG_{RC}. By using the state space reduction technique in Definition 6, we can obtain a reduced state space *Reduced*(DG_{RC}), as shown in Figure 6, which only contains 17 states and 31 transitions. For brevity, we use 3 separate subgraphs to represent the entire state space, while these subgraphs have the common endpoints *Init* and *Top*.

3.2. Minimal Cut Sets Generation. Here, we discuss the basic searching algorithm for cut sets generation using forward reachability analysis. The first step is to find all possible simple paths (paths without cycles) between two vertices, that is, *Init* and *Top*, in the graph *Reduced*(DG_P). To solve this problem, the traditional depth-first search algorithm could be adjusted in the following manner:

(1) Start at source vertex *Init* and perform a depth-first walk. All nodes on the path are pushed in a stack and set as *visited*.

(2) When the top element of the stack is target node *Top*, a path is successfully found. Record this path, pop out *Top*, and set it as *unvisited*.

(3) For the current top of the stack u, find its successor that is *unvisited* and push this node in the stack. If no such successor exists, pop out u and set u and its successors *unvisited*.

(4) Go back to step (2) until the stack is empty.

To better visualize this process, one can think of a search tree rooted at the vertex *Init*, and all simple paths leading to node *Top* constitute the body of this tree. As an illustration, consider the searching of Figure 6(b). The tree structure in Figure 7(a) depicts all simple paths between *Init* and *Top* generated by the above algorithm. Since a cut set only consists of basic faults, we get the following four cut sets from this tree by removing extra actions and duplicate paths:

$$\begin{gathered}\{\text{Stuck}, \text{Bra\_}F\},\\ \{\text{Stuck}, \text{S1\_}F, \text{Bra\_}F\},\\ \{\text{S1\_}F, \text{Bra\_}F\},\\ \{\text{S1\_}F, \text{Stuck}, \text{Bra\_}F\}.\end{gathered} \tag{3}$$

After finding all possible cut sets in *Reduced*(DG_P), it is easy to identify those minimal ones. According to

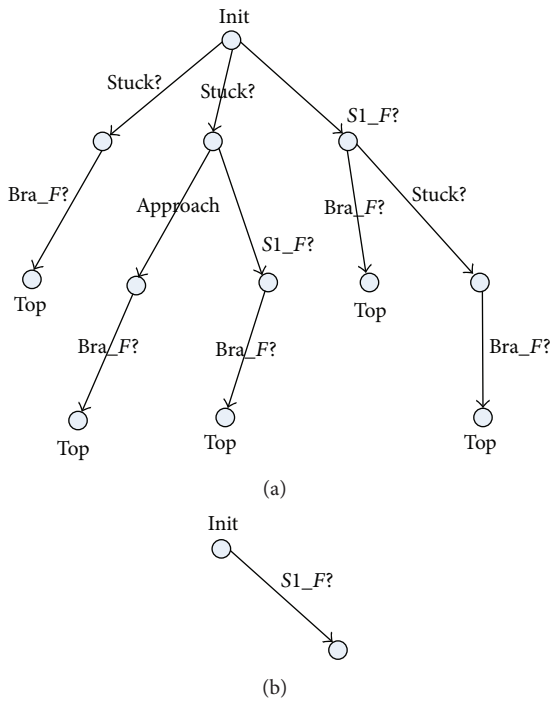

Figure 7: The comparison of different search strategies.

Definition 4, given two cut sets cs_1 and cs_2, if $cs_1 \subset cs_2$, cs_2 must not be a minimal cut set. This fact could be used to design a simple filter through pairwise comparison of these cut sets. It is worth noting that sorting this set of cut sets by size in advance will make the comparison more efficient. So far, we have presented a simple search-based algorithm for minimal cut sets generation.

Unfortunately, this naive algorithm has a major drawback: it needs to traverse all possible simple paths between *Init* and *Top* during the searching. However, from a practical perspective, some branches of the search tree could be pruned. Since the ultimate goal is to get minimal cut sets, according to Definition 4, no further extension of the current path is necessary if it contains a cut set which has been found in the previous exploration. Using this observation, we present a heuristic searching strategy based on a bounded breadth-first search to improve the performance of state space exploration.

The basic idea is to search for all simple paths between *Init* and *Top* whose lengths are bounded by some integer k. This problem can be efficiently solved in $Reduced(\mathrm{DG}_P)$ via a breadth-first search with bound k. The result is a set of cut sets whose lengths are no more than k, denoted by Ksets, and can therefore be used for guiding the branch pruning during the rest searching. Figure 7 shows a very distinct optimization effect on the graph $Reduced(\mathrm{DG}_{\mathrm{RC}})$. Firstly, we perform a bounded breadth-first search (let $k = 1$) on $Reduced(\mathrm{DG}_P)$. Via a breadth-first search with depth 1, the searching process will find two traces from *Init* to *Top*, which are exactly shown as Figure 6(a). Thus, we get

$$K\text{sets} = \{\{\text{Stuck}\}, \{\text{Bra\_}F\}\}. \quad (4)$$

We then use part of the state space (i.e., Figure 6(b)) to demonstrate the branches pruning effect of Ksets. Figure 7(a) shows the paths generated by the naive algorithm, while Figure 7(b) represents the results of the optimized algorithm which uses Ksets to prune superfluous paths. The comparison indicates that over half of the total vertices and edges are ruled out of the searching. In order to tail off the search space and boost converging rate of the algorithm, unnecessary branches are trimmed in terms of the results of the k bounded searching.

Algorithm 1 implements the above discussed techniques, which takes as input a directed graph $Reduced(\mathrm{DG}_P)$, a set of basic faults *BasicFaults*, and bounded searching result Ksets. The output *MCSList* returns all minimal cut sets as a list, which will be initialized with Ksets. The set cs is used to record all basic faults in the current path, and it will be added to the end of *MCSList* once the node *Top* in $Reduced(\mathrm{DG})$ is reached. All nodes on the current searching path are pushed into a stack S. If the top element of the stack is node *Top* or cs $\in$ *MCSList*, the algorithm will backtrack to continue the search for a new path by popping out the old stack top and trying out the unvisited neighbor of the new stack top. This procedure is repeated over and over until S gets empty. Procedure $Filter(MCSList)$ carries out the pairwise comparison of all elements in *MCSList* to get those minimal cut sets, as we mentioned before.

For $Reduced(\mathrm{DG}_{\mathrm{RC}})$ in Figure 6, computing $K\text{sets} = \{\{\text{Stuck}\}, \{\text{Bra\_}F\}\}$ with $k = 1$ firstly and then using Algorithm 1 to perform a full search in state space, we get all minimal cut sets $MCSList = \{\{\text{Stuck}\}, \{\text{Bra\_}F\}\}$. This result shows that the necessary and sufficient conditions for the occurrence of top-level event (i.e., a train is on the crossing, while the crossing is not secured) are as follows: the barrier is stuck or the brake fails, while sensors failure will not consequentially lead to a dangerous situation.

In this approach, the choosing of parameter k in the bounded searching is relatively flexible, depending on the size of $Reduced(\mathrm{DG})$. The role of Ksets will gradually change with the increasing of k. Obviously, if the value of k is big enough, all simple paths between *Init* and *Top* will be found in a breadth-first way with low efficiency. Therefore, providing an appropriate value for k is key to the solution. For large models, we recommend a relatively small k for the bounded searching firstly. If Algorithm 1 can not terminate within a reasonable amount of time, gradually increase k until an adequate number of searching branches have been cut down so that the algorithm gets terminated.

4. Fuel Supply System Example

In this section, we exemplify our approach with a fuel supply system for small aircraft. Figure 8 is the schematic diagram of this system. The engine is supplied with fuel pumped at high pressure from a collector tank—a small tank located close to the engine. This demonstration is not concerned with the high-pressure fuel system. The main fuel storage in the aircraft is in the left and right main tanks. Each tank contains a low-pressure pump (P and Q in the diagram) which transfers fuel to the collector tank via valves A and B as required. In

Input: *Reduced*(DG), *BasicFaults*, *Ksets*
Output: *MCSList* is a list of minimal cut sets.
(1) Push *Reduced*(DG).*Init* in stack *S* and set it *visited*;
(2) *MCSList* ≔ *Ksets*;
(3) cs ≔ *Null*;
(4) **while** *S is not empty* **do**
(5) $v \coloneqq S.top()$; // Get the top element of stack *S*
(6) **if** *There exist a vertex u satisfying* $((v, b, u) \in Reduced(\mathrm{DG}) \wedge u$ *is unvisited)* **then**
(7) **if** $b \in BasicFaults$ **then**
(8) Add basic fault *b* into the set cs;
(9) **if** cs $\notin$ *MCSList* **then**
(10) Push *u* in stack *S*;
(11) **else**
(12) Remove *a* from cs;
(13) Set *u visited*;
(14) **else**
(15) Pop *v* from stack *S* and set *v* as well as its successors *unvisited*;
(16) *Update*(cs);
(17) **if** *the current top element of the stack is Reduced*(DG).*Top* **then**
(18) Add a copy of cs to the end of *MCSList*;
(19) Pop out *Reduced*(DG).*Top* and set it *unvisited*;
(20) *Update*(cs);
(21) *Filter*(*MCSList*);
(22) *Return*(*MCSList*);

Algorithm 1: Generation of minimal cut sets.

flight, valves *A* and *B* are normally left open. The aircraft also has a smaller reserve tank, also fitted with its own low-pressure pump *R*. All pumps are protected by nonreturn valves *W*, *X*, *Y*, and *Z*. Valves *C* and *D* (normally closed and opened when required) allow fuel to be transferred from the reserve to either wing tank as necessary. The pumps have built-in overpressure protection; in the event of attempting to pump into a closed or blocked pipe, the overpressure relief system will simply return fuel to the tank.

We model this system at interface level by three components interacting with each other, as shown in Figure 9. The automaton at the top left, denoted by P_{Left}, describes the interface behavior of the left tank, pump *P*, and valves *W* and *A*. The top right model P_{Right} consists of the right tank, pump *Q*, and valves *X* and *B*. The reserve tank, pump *R*, and valves *C*, *D*, *Y*, and *Z* are modeled as P_{Bottom} at the bottom. The solid part of the figure depicts the nominal interactions among these components.

In order to analyze the system behavior in presence of faults, we would like to extend this nominal system model with the given failure modes. In Table 1, we list all faults under consideration, defined as input or output actions, and their intuitive meaning. Those dash lines as well as the new added actions in Figure 9 demonstrate our model extension. The parallel composition $\mathrm{FSS} = P_{\mathrm{Left}} \times P_{\mathrm{Bottom}} \times P_{\mathrm{Right}}$ describes the behavior of this fuel supply system in the presence of faults. There are 140 states and 560 transitions in the state space $\mathrm{DG}_{\mathrm{FSS}}$.

For this example, assume that the safety requirement is as follows:

SR 2: simultaneous loss of fuel supply from the left and right main tank will not occur.

That is to say, it must never happen that P_{Left} is at the state p_2 and at the same time P_{Right} at q_2. Thus, the top-level event is $\mathrm{TLE} = p_2 * q_2$, where $*$ is used as a wildcard to substitute for any state of automaton P_{Bottom}. The set of all basic faults could be obtained from Table 1, that is,

$$\mathscr{E}^{\mathrm{bf}} = \{A\_F, B\_F, C\_F, D\_F, X\_F, Y\_F, Z\_F, W\_F, Empty\_P, Empty\_Q, Empty\_R\}. \quad (5)$$

According to Definition 5, $\mathrm{DG}_{\mathrm{FSS}}$ could be divided into three parts: $\mathrm{SafetyArea}^{\mathrm{FSS}}$, $\mathrm{TriggeringArea}^{\mathrm{FSS}}$, and $\mathrm{HazardCore}^{\mathrm{FSS}}$, while $\mathrm{TriggeringArea}^{\mathrm{FSS}}$ is the focus of our attention. Using the reconstruction approach given in Definition 6, we get a reduced state space $Reduced(\mathrm{DG}_{\mathrm{FSS}})$. In contrast, the new state space only contains 88 states and 442 transitions.

Table 1: Parameters of the fuel supply system interface models.

Name	Action	Type	Meaning
A_F, *B_F*	Input	Basic fault	Unintended shutdown of valve *A* or *B*
C_F, *D_F*	Input	Basic fault	Failure to open valve *C* or *D*
W_F, *X_F*, *Y_F*, *Z_F*	Input	Basic fault	Clogging of valve *W*, *X*, *Y*, or *Z*
P_F, *Q_F*, *R_F*	Input	Basic fault	Pump failure in *P*, *Q*, or *R*
OutputP, *OutputQ*	Output	Propagating fault	Fuel supplied successfully by pump *P* or *Q*
No_outputP, *No_outputQ*	Output	Propagating fault	No Fuel supplied by pump *P* or *Q*
Empty_P, *Empty_Q*, *Empty_R*	Input	Basic fault	Left, right, or reserve tank is empty
InputPR, *InputQR*	Input & output	Propagating fault	Fuel supplied successfully from reserve tank to the left or right one
No_inputPR, *No_inputQR*	Input & output	Propagating fault	No Fuel supplied from reserve tank to the left or right one

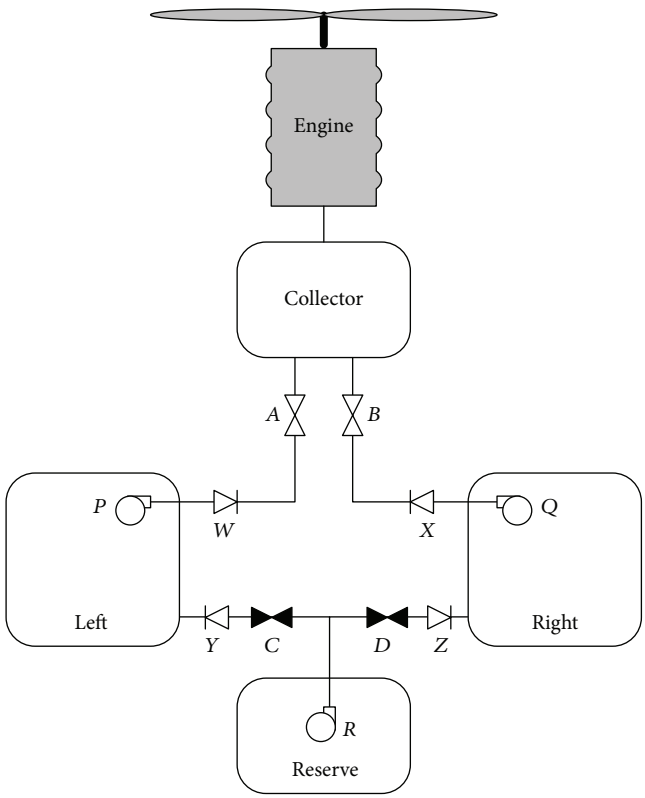

Figure 8: The fuel supply system for a small aircraft.

In our case, we choose $k = 4$ for the bounded breadth-first search which returns a few cut sets *K*sets as a key parameter for the further computation, where

$$K\text{sets} = \{\{P\_F, Q\_F\}, \{P\_F, X\_F\}, \{P\_F, B\_F\}, \{W\_F, Q\_F\}, \{W\_F, X\_F\}, \{W\_F, B\_F\}, \{A\_F, Q\_F\}, \{A\_F, X\_F\}, \{A\_F, B\_F\}\}. \quad (6)$$

Then, Algorithm 1 is performed with *K*sets and its successful termination returns the following *MCSList*, including 39 minimal cut sets:

{*P_F*, *Q_F*} {*P_F*, *X_F*} {*P_F*, *B_F*} {*W_F*, *Q_F*} {*W_F*, *X_F*}

{*W_F*, *B_F*} {*A_F*, *Q_F*} {*A_F*, *X_F*} {*A_F*, *B_F*} {*P_F*, *R_F*, *EmptyQ*}

{*P_F*, *EmptyR*, *EmptyQ*} {*P_F*, *D_F*, *EmptyQ*} {*P_F*, *Z_F*, *EmptyQ*}

{*W_F*, *R_F*, *EmptyQ*} {*W_F*, *EmptyR*, *EmptyQ*} {*W_F*, *D_F*, *EmptyQ*}

{*W_F*, *Z_F*, *EmptyQ*} {*A_F*, *R_F*, *EmptyQ*} {*A_F*, *EmptyR*, *EmptyQ*}

{*A_F*, *D_F*, *EmptyQ*} {*A_F*, *Z_F*, *EmptyQ*} {*EmptyP*, *R_F*, *Q_F*}

{*EmptyP*, *R_F*, *X_F*} {*EmptyP*, *R_F*, *B_F*} {*EmptyP*, *R_F*, *EmptyQ*}

{*EmptyP*, *EmptyR*, *Q_F*} {*EmptyP*, *EmptyR*, *X_F*} {*EmptyP*, *EmptyR*, *B_F*}

{*EmptyP*, *Y_F*, *B_F*} {*EmptyP*, *C_F*, *Q_F*} {*EmptyP*, *C_F*, *X_F*}

{*EmptyP*, *C_F*, *B_F*} {*EmptyP*, *Y_F*, *Q_F*} {*EmptyP*, *Y_F*, *X_F*}

{*EmptyP*, *EmptyR*, *EmptyQ*} {*EmptyP*, *C_F*, *D_F*, *EmptyQ*}

{*EmptyP*, *C_F*, *Z_F*, *EmptyQ*} {*EmptyP*, *D_F*, *EmptyQ*, *Y_F*}

{*EmptyP*, *Y_F*, *Z_F*, *EmptyQ*}

Additionally, this kind of automatic analysis on interface models provides a convenient way to explore the feasibility of different architectures and design choices. For instance, consider the following safety requirement:

SR 3: any loss of fuel supply from the left or right main tank is not allowed.

An interface automaton implicitly represents both assumptions about the environment and guarantees about the specified component. One interesting note about this formalism is that while the environment changed, it would exhibit different system behavior. The environment could also be modeled explicitly by another interface automaton. For safety requirement SR 3, any occurrence of output actions *No_outputP* or *No_outputQ* will lead to danger. The automaton in Figure 10 provides such an environment by accepting these actions as legal inputs. Using the composition

Table 2: The comparison of experimental results.

	RC + SR 1	FSS + SR 2	FSS2 + SR 3
States in DG	30	140	132
States in *Reduced*(DG)	16	88	26
Transitions in DG	63	560	536
Transitions in *Reduced*(DG)	31	442	176
Paths generated by naive searching	19	59721	603
Paths generated by Algorithm 1	8	34875	316
Minimal cut sets	2	39	14

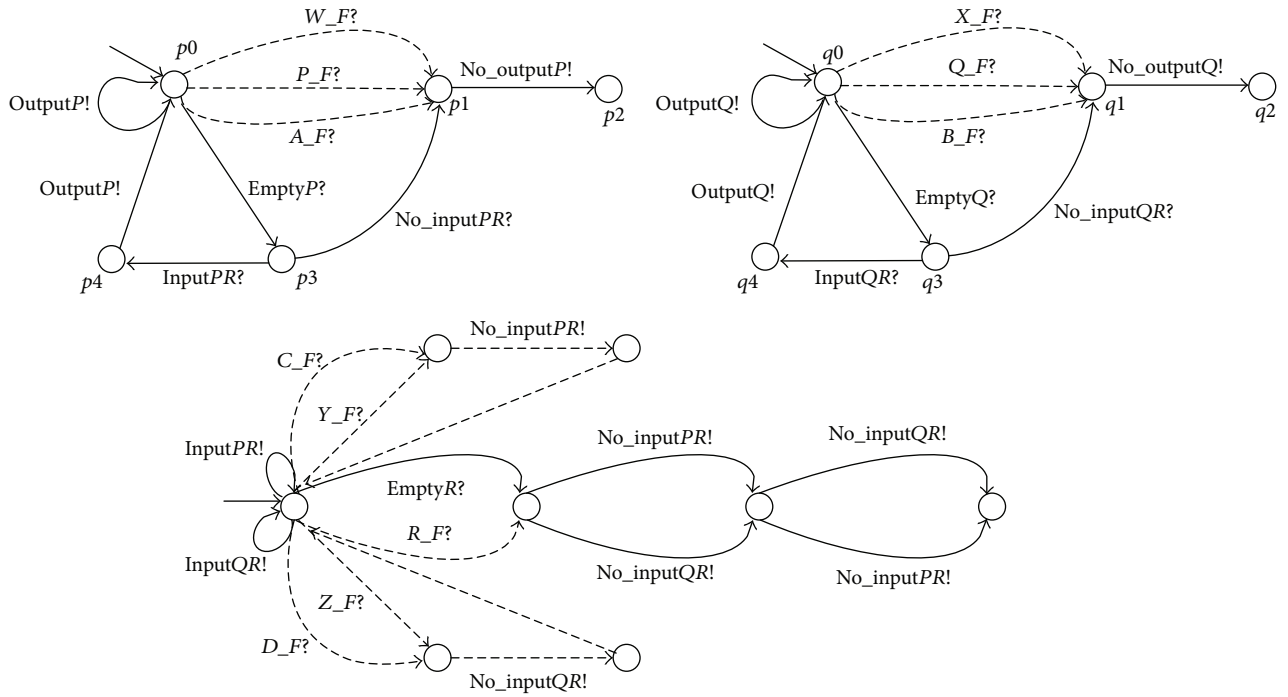

Figure 9: The interface models of fuel supply system.

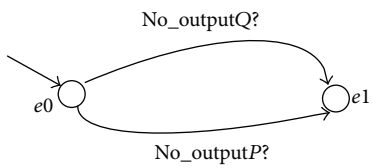

Figure 10: An environment model of fuel supply system.

of FSS and Env, we can quickly locate all dangerous states by TLE = $***\ e_1$ in the new interface model FSS2 = FSS×Env, which consist of 132 states and 536 transitions. In a similar way, the state space can be reduced to *Reduced*(DG_{FSS2}), containing only 26 states and 176 transitions, and then the corresponding minimal cut sets are generated as follows (with the choice of parameter $k = 2$):

$\{P\_F\}$ $\{W\_F\}$ $\{A\_F\}$ $\{Q\_F\}$ $\{X\_F\}$ $\{B\_F\}$
$\{EmptyP, R\_F\}$

$\{EmptyP, EmptyR\}$ $\{EmptyP, C\_F\}$ $\{EmptyP, Y\_F\}$
$\{R\_F, EmptyQ\}$

$\{EmptyR, EmptyQ\}$ $\{D\_F, EmptyQ\}$
$\{Z\_F, EmptyQ\}$

The above demonstration and experimental results shown in Table 2 indicate that not only is the state space reduction effect satisfactory, but also the improved searching algorithm has more quick convergence speed than naive exhaustive searching. Both of these models can benefit from state space reconstruction, but the impact is more pronounced on FSS2 where nearly eighty percent of the states and seventy percent of the transitions are eliminated. The number of simple paths generated by the searching process is considered as an index of efficiency. The naive searching strategy will deliver all corresponding simple paths in the state space, while Algorithm 1 discards some unnecessary branches for further exploration. Essentially, these two technical measures contribute to the efficiency improvement by narrowing down the search region from different perspectives.

5. Conclusions and Future Directions

Safety analysis is indispensable for ensuring the system safety but is very time-consuming and error-prone. The approach presented in this paper has shown that applying interface automata and restricted reachability analysis techniques to faults modeling and minimal cut sets generation yields a promising means to improve automation and reduce the effort of the analysis. We believe that it is in these areas that formal methods could be most effectively used to aid in safety analysis.

Although several search-based failure analysis approaches have been proposed, this is the first reported application of using the characteristics of faults propagation and cut sets to speed up the search process in a reduced state space (i.e., via our state space reconstruction and guided searching strategy). Besides taking full advantage of domain knowledge, a further very important merit is the flexibility of this approach. With different setting of environment parameters, interface automata could exhibit different behavior which provides an efficient way for engineers to explore different design choices, as we have shown in the case study.

However, we note that directly adding complex fault behaviors to nominal system model tends to severely clutter the model with failure information. This added complexity typically obscures the actual nonfailure system functionality which will make model evolution and maintenance difficult. Without favorable tool supporting, manual incorporation of the fault behaviors may also lead to error-prone extension of the nominal model. Therefore, it is crucial to separately specify fault behavior with a formal notation (e.g., FPTN) and provide a merge mechanism for automatic model extension.

In this paper, we concentrated our attention on fault propagation analysis, but the other important features such as failure ordering analysis and fault tree generation and optimization were not discussed. We will work on those issues and larger case studies aimed at analyzing the scalability of this approach will be the emphasis of our further work. Furthermore, we find some useful characteristics of our state space partition strategy, such as the identification of HazardCore and TriggeringArea, can provide valuable information for runtime monitoring, failure forecast, and fault diagnosis. That might be an interesting attempt to explore the role of model-based safety analysis in system verification and validation.

Competing Interests

The authors declare that they have no competing interests.

Acknowledgments

This work was partially supported by the National Basic Research Program of China (no. 2014CB340703), the Foundation of State Key Laboratory of Rail Traffic Control and Safety (no. RCS2015ZT002), and the Fundamental Research Funds for the Central Universities (no. 2015JBM113).

References

[1] M. Bozzano, A. Villafiorita, O. Åkerlund et al., "ESACS: an integrated methodology for design and safety analysis of complex systems," in *Proceedings of the European Safety and Reliability Conference*, pp. 237–245, 2003.

[2] O. Akerlund, P. Bieber, E. Boede et al., "ISAAC, a framework for integrated safety analysis of functional, geometrical and human aspects," in *Proceedings of 3rd European Congress on Embedded Real Time Systems (ERTS '06)*, pp. 109–120, Toulouse, France, January 2006.

[3] A. Arnold, G. Point, A. Griffault, and A. Rauzy, "The AltaRica formalism for describing concurrent systems," *Fundamenta Informaticae*, vol. 40, no. 2-3, pp. 109–124, 1999.

[4] M. Boiteau, Y. Dutuit, A. Rauzy, and J.-P. Signoret, "The AltaRica data-flow language in use: modeling of production availability of a multi-state system," *Reliability Engineering and System Safety*, vol. 91, no. 7, pp. 747–755, 2006.

[5] P. Bieber, C. Castel, and C. Seguin, "Combination of fault tree analysis and model checking for safety assessment of complex system," in *Proceedings of the European Dependable Computing Conference*, pp. 19–31, Toulouse, France, 2002.

[6] P. Fenelon and J. A. McDermid, "New directions in software safety: causal modelling as an aid to integration," Tech. Rep., High Integrity Systems Engineering Group, Department of Computer Science, University of York, 1992.

[7] P. Fenelon and J. A. McDermid, "An integrated tool set for software safety analysis," *The Journal of Systems and Software*, vol. 21, no. 3, pp. 279–290, 1993.

[8] Y. Papadopoulos and M. Maruhn, "Model-based synthesis of fault trees from Matlab-Simulink models," in *Proceedings of the International Conference on Dependable Systems and Networks (DSN '01)*, pp. 77–82, Goteborg, Sweden, July 2001.

[9] P. Feiler and A. Rugina, "Dependability modeling with the architecture analysis & design language (AADL)," Tech. Rep., Software Engineering Institute, Carnegie Mellon University (SEI/CMU), 2007.

[10] J. Bowen and V. Stavridou, "Safety-critical systems, formal methods and standards," *Software Engineering Journal*, vol. 8, no. 4, p. 189, 1993.

[11] A. Rauzy, "Mode automata and their compilation into fault trees," *Journal of Logic and Algebraic Programming*, vol. 78, no. 1, pp. 1–12, 2002.

[12] M. Bozzano and A. Villafiorita, "Improving system reliability via model checking: the FSAP/NuSMV-SA safety analysis platform," in *Computer Safety, Reliability, and Security*, S. Anderson, M. Felici, and B. Littlewood, Eds., vol. 2788 of *Lecture Notes in Computer Science*, pp. 49–62, 2003.

[13] L. D. Alfaro and T. A. Henzinger, "Interface automata," in *Proceedings of ACM SIGSOFT International Symposium on Foundations of Software Engineering*, pp. 109–120, September 2001.

Hindawi Publishing Corporation
Mathematical Problems in Engineering
Volume 2016, Article ID 9798406, 8 pages
http://dx.doi.org/10.1155/2016/9798406

Research Article

Geometric Process-Based Maintenance and Optimization Strategy for the Energy Storage Batteries

Yan Li, Peng Han, Jinkuan Wang, and Xin Song

School of Computer Science and Engineering, Northeastern University, Shenyang 110819, China

Correspondence should be addressed to Peng Han; hp@mail.neuq.edu.cn

Received 1 February 2016; Accepted 2 March 2016

Academic Editor: Jurgita Antucheviciene

Renewable energy is critical for improving energy structure and reducing environment pollution. But its strong fluctuation and randomness have a serious effect on the stability of the microgrid without the coordination of the energy storage batteries. The main factors that influence the development of the energy storage system are the lack of valid operation and maintenance management as well as the cost control. By analyzing the typical characteristics of the energy storage batteries in their life cycle, the geometric process-based model including the deteriorating system and the improving system is firstly built for describing the operation process, the preventive maintenance process, and the corrective maintenance process. In addition, this paper proposes an optimized management strategy, which aims to minimize the long-run average cost of the energy storage batteries by defining the time interval of the detection and preventive maintenance process as well as the optimal corrective maintenance times, subjected to the state of health and the reliability conditions. The simulation is taken under the built model by applying the proposed energy storage batteries' optimized management strategy, which verifies the effectiveness and applicability of the management strategy, denoting its obvious practicality on the current application.

1. Introduction

Along with the quality of environment being more and more emphasized, the microgrid, which regards the renewable resources as the major energy source, is growing rapidly in recent years. Energy storage technology in the microgrid system indicates tremendous development potential since it could solve the fluctuation and randomness problems of the renewable energy generation to a great extent [1, 2]. It achieves a smooth output of the power by effectively regulating the voltage, frequency, or phase changes so that the large-scale wind power and photovoltaic power generation will be incorporated into the microgrid reliably [3].

Main energy storage devices in the microgrid include the energy storage batteries, energy storage inductors, and energy storage capacitors, where the energy storage batteries are mostly used. Aimed at achieving integrated scheduling for regulating both the generation side and distribution side, all of the energy storage batteries are installed centrally in the charging room, considering the energy storage batteries' deteriorating characteristics with aging as well as the degradation of performance during times of charging and discharging. Strict maintenance and management aimed at the energy storage batteries are necessary for improving the electric energy efficiency, prolonging the service life, and reducing the life cycle costs [4, 5].

Munoz-Condes et al. [6] take into account the battery operating conditions and establish the mathematical relation between the impedance of simultaneous cells and the temperature for any model of lead-acid battery. Ure et al. [7] present a development and hardware implementation of an autonomous battery maintenance mechatronic system for the unmanned aerial vehicles. Li et al. [8] develop a multistep-ahead prediction model to predict the state of health and remaining life of the battery based on the mean entropy and relevance vector machine. Ablay [9] proposes a robust nonlinear estimator-based online condition monitoring method to determine the state of health of the battery systems online in the industry. Zhao et al. [10] develop an optimization model considering the lifetime characteristics of lead-acid batteries to realize the economic operation of a standalone microgrid via the nondominated sorting

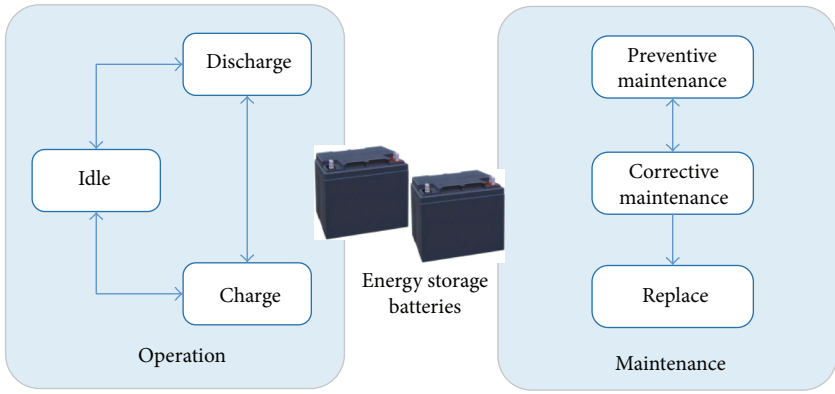

Figure 1: The states of operation and maintenance.

genetic algorithm. Liao and Köttig [11] focus on the hybrid prognostics approaches and leverage the advantages of the combining prognostics models for the battery's remaining useful life prediction. Han et al. [12] propose a novel health prediction model of the battery based on sample entropy and establish the prediction model by calculating the sample entropy. Wang and Liu [13] estimate the battery state of charge and implement the fault diagnosis according to the battery status to achieve the full and efficient use of battery power.

However, the previous estimation and monitoring studies related to the battery management mainly focus on the battery's prediction and monitoring but seldom distinguish and analyze the impact on the different states in the battery's life cycle including the operation, preventive maintenance, and corrective maintenance. And the geometric process-based (GP-based) method, with its practical advantages in characterizing the whole life cycle of component or system [14], gains large attention in recent years, and many researches have been taken based on GP in different application domains. Lam [15] introduces a geometric process δ-shock maintenance model and adopts a replacement policy for minimizing the long-run average cost per unit time. Zhang [16] proposes a GP-based preventive repairment policy to solve the efficiency for a deteriorating and valuable system to minimize the average cost rate. Wang and Zhang [17] apply a bivariate preventive repair policy to solve the efficiency for a deteriorating and valuable system to minimize the average cost rate. Huang et al. [18] propose a delayed geometric process for the degenerative repairable systems by supposing the system to be returned to the "as good as former" state and the "worse" state with two different certain probabilities. Considering the application of the GP-based method on the energy storage batteries, the aging with the repeating charging and discharging, and the effect on the operation, preventive maintenance or corrective maintenance should be taken into account. Aimed at solving the energy storage batteries' optimized management, a GP-based model with the deteriorating system and the improving system of the energy storage batteries is firstly built, and then the long-run average cost of the energy storage batteries is optimized under the constraint of the detection or preventive maintenance time interval as well as the reliability demand through the proposed optimized management strategy.

2. Typical State of the Energy Storage Battery

Aimed at the daily behaviors of the energy storage batteries, the states of operation and maintenance are divided to distinguish the operation and maintaining processes, as is described in Figure 1.

In the operation process, the energy storage batteries are scheduled to charge if the excess renewable generated energy exists and discharge if the energy is deficient; otherwise, the energy storage batteries are on idle state. In the maintenance process, preventive maintenance is performed in certain time intervals depending on the defined function to enhance the energy storage batteries' performance and reduce the frequency of breakdown. The corrective maintenance is performed when the energy storage batteries break down or an obvious fault has occurred. After a period of time, the energy storage batteries would be replaced for some secondary applications when a certain index is unsatisfied.

Considering the aging of the energy storage batteries during the life cycle, the performance comparison analysis under the preventive maintenance state and corrective maintenance state are shown in Figure 2. The preventive maintenance process is helpful to improve the performance of the energy storage batteries to a certain extent, but the descending overall trend is indubitable for their chemical properties. The corrective maintenance process makes the disabled ones to work again, which avoids the premature discard of the energy storage batteries. Each of the maintenance processes is absolutely helpful and necessary at the exact time so that the appropriate maintenance strategy should be established based on the service condition.

3. Mathematical Model of the Energy Storage Batteries

The studied life cycle of the energy storage batteries starts from the first use and ends with the replacement, or the time interval between two contiguous replacements. Under the fact that the chemical property of the energy storage batteries is irreversible and degraded, the GP-based mathematical model of the studied life cycle is firstly proposed aimed at the typical processes, which includes the operation process, the detecting process, the preventive maintenance process, the

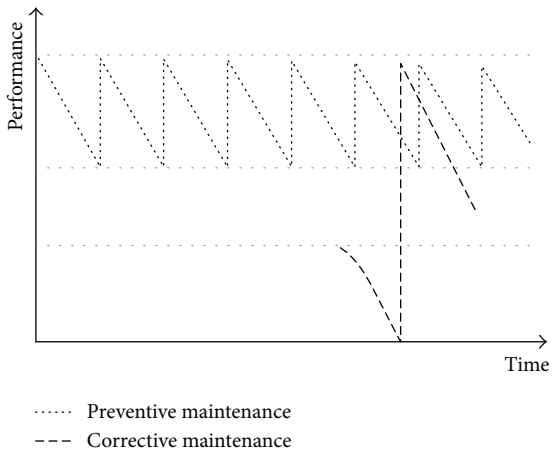

Figure 2: The comparison analysis under the two maintenance states.

corrective maintenance process, and so on [19]. The whole life cycle will be described in Figure 3.

For $n = 1, 2, \ldots, N$, the time interval between the $(n-1)$th and the nth corrective maintenance in the life cycle can be defined as the nth period. Let $\{X_n^i,\ n = 1, 2, \ldots,\ i = 1, 2, \ldots\}$ be the ith operation time of the energy storage batteries after $i-1$th preventive maintenance in the nth period. Let $\{Y_n^i,\ n = 1, 2, \ldots,\ i = 1, 2, \ldots\}$ be the ith preventive maintenance in the nth period. Given that each preventive maintenance is accompanied by a detecting process, the detections have the same number of the preventive maintenances $\{M_n,\ n = 1, 2, \ldots, N\}$ in the nth period. Besides, the corrective maintenance time in the nth period is $\{Z_n,\ n = 1, 2, \ldots\}$, and the replacement time is H.

Now, the definitions and assumptions are made as follows to establish the related mathematical model of the energy storage batteries.

Definition 1. The successive operation time $\{X_n^i,\ i = 1, 2, \ldots\}$ in the nth period forms a GP with ratio a and $E(X_1^1) = \lambda$, and the preventive maintenance time $\{Y_n^i,\ i = 1, 2, \ldots\}$ in the nth period forms a GP with ratio b and $E(Y_1^1) = \mu$, while the consecutive corrective maintenance time $\{Z_n,\ n = 1, 2, \ldots\}$ constitutes a GP with radio c and $E(Z_1) = \nu$. Besides, the replacement time H is a random variable with $E(H) = \tau$.

Definition 2. The distribution function and probability density function of X_n^i are $F(a^{n-1}x)$ and $a^{n-1}f(a^{n-1}x)$, respectively.

Definition 3. The preventive and corrective maintenance cost rates are, respectively, c_p and c_c, the benefit rate of the operation is c_b, the detection cost rate is c_d, the replacement cost rate is c_r corresponding to the replacement time H, the unit price of a new energy storage battery is c_N, and the secondary applications benefit of the depleted one is c_s.

Assumption 4. $\{X_n^i,\ i = 1, 2, \ldots\}$, $\{Y_n^i,\ i = 1, 2, \ldots\}$, and $\{Z_n,\ n = 1, 2, \ldots\}$ are independent. In addition, the processes $X_n^i,\ i = 1, 2, \ldots, M_n + 1,\ n = 1, 2, \ldots, N$ and $Y_n^i,\ i = 1, 2, \ldots, M_n,\ n = 1, 2, \ldots, N$ are independent and identically distributed (i.i.d.) random variables.

Assumption 5. The operation time decreases with age; thus it is a stochastically decreasing GP-based model with $a > 1$. And the preventive maintenance and corrective maintenance processes are stochastically increasing GP-based model with $0 < b < 1$ and $0 < c < 1$.

4. GP-Based Optimized Management Strategy

Economy and reliability are the focus of most concern for the construction of microgrid and even the energy storage system. The evaluation aimed at the economy of the energy storage system will be expressed as the average cost of the energy storage batteries. Generally, the average cost is given by the ratio of the total cost and the life cycle, as is shown in function (1):

$$C(T) = \lim_{t\to\infty} \frac{C(t)}{t}. \tag{1}$$

Depending on the definitions of the energy storage batteries above, the successive periods form a renewal process; therefore, the successive periods together with the cost rates incurred in each period constitute a renewal process. Supposing an optimized management strategy (T, N) is applied, the long-run average cost $C(T, N)$ that is expressed by the defined GP-based processes is given by

$$C(T, N) = \frac{C(N)}{T_{\text{Total}}}, \tag{2}$$

where

$$\begin{aligned} C(N) &= E\left(c_d \sum_{n=1}^{N} M_n + c_p \sum_{n=1}^{N}\sum_{i=1}^{M_n} Y_n^i + c_c \sum_{n=1}^{N-1} Z_n + c_r H \right.\\ &\quad \left. + c_N - c_s - c_b \sum_{n=1}^{N} X_n\right), \\ T_{\text{Total}} &= E\left(\sum_{n=1}^{N} X_n + \sum_{n=1}^{N}\sum_{i=1}^{M_n} Y_n^i + \sum_{n=1}^{N-1} Z_n + H\right). \end{aligned} \tag{3}$$

Then, from function (2)-(3) the long-run average cost of the energy storage batteries is shown as function (4):

$$\begin{aligned} C(T, N) &= E\left(c_d \sum_{n=1}^{N} M_n + c_p \sum_{n=1}^{N}\sum_{i=1}^{M_n} Y_n^i + c_c \sum_{n=1}^{N-1} Z_n \right.\\ &\quad \left. + c_r H + c_N - c_s - c_b \sum_{n=1}^{N} X_n\right) \\ &\quad \cdot \left(E\left(\sum_{n=1}^{N} X_n + \sum_{n=1}^{N}\sum_{i=1}^{M_n} Y_n^i + \sum_{n=1}^{N-1} Z_n + H\right)\right)^{-1} \end{aligned}$$

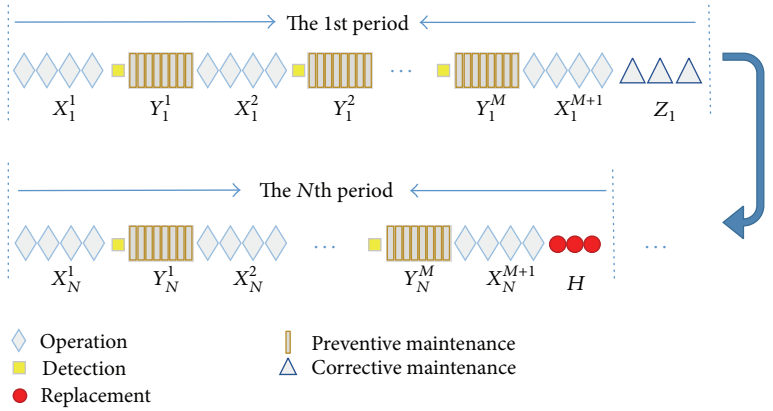

Figure 3: The whole life cycle of the energy storage batteries.

$$= \left(c_d \sum_{n=1}^{N} E(M_n) + c_p \sum_{n=1}^{N} \frac{\mu}{b^{n-1}} E(M_n) + c_c \sum_{n=1}^{N-1} \frac{\nu}{c^{n-1}} + c_r \tau + c_N - c_s - c_b \sum_{n=1}^{N} E(X_n) \right) \left(\sum_{n=1}^{N} E(X_n) + \sum_{n=1}^{N} \frac{\mu}{b^{n-1}} E(M_n) + \sum_{n=1}^{N-1} \frac{\nu}{c^{n-1}} + \tau \right)^{-1}. \tag{4}$$

To further obtain the explicit result of $C(T,N)$, the number of preventive maintenances M_n is supposed to have a geometric distribution, that is $M_n \sim G(p_n)$, and then

$$P\left(X_n^1 \le T\right) = F\left(a^{n-1}T\right) = q_n^i p_n, \quad i = 0, 1, 2, 3, \ldots, \qquad q_n = P\left(X_n^1 > T\right) = 1 - p_n. \tag{5}$$

Consequently,

$$E(M_n) = \frac{q_n}{p_n} = \frac{1 - p_n}{p_n}. \tag{6}$$

Then, the detection time and preventive maintenance time in the life cycle are transformed into

$$E\left(\sum_{n=1}^{N} M_n\right) = \sum_{n=1}^{N} \frac{1 - p_n}{p_n}, \tag{7}$$

$$E\left(\sum_{n=1}^{N} \sum_{i=1}^{M_n} Y_n^i\right) = \sum_{n=1}^{N} \frac{\mu}{b^{n-1}} \frac{1 - p_n}{p_n}. \tag{8}$$

Let $E(X_n) = \psi(T,n)$ be the expected operation time in the nth period:

$$E(X_n) = \psi(T,n) = E\left(\frac{1}{F\left(a^{n-1}T\right)} \int_0^T \left(a^{n-1}t\right) dF\left(a^{n-1}t\right) \right) = \frac{1}{F\left(a^{n-1}T\right)} \int_0^T \left(1 - F\left(a^{n-1}t\right)\right) dt. \tag{9}$$

Given that the operation time has a Weibull distribution with density function,

$$f(t) = \begin{cases} \frac{k}{\lambda} \left(\frac{t}{\lambda}\right)^{k-1} \exp\left(-\left(\frac{t}{\lambda}\right)^k\right), & t > 0 \\ 0, & \text{else.} \end{cases} \tag{10}$$

Then,

$$p_n = F\left(a^{n-1}T\right) = 1 - \exp\left(-\left(\frac{1}{\lambda} a^{n-1}T\right)^k\right), \qquad q_n = 1 - p_n = \exp\left(-\left(\frac{1}{\lambda} a^{n-1}T\right)^k\right), \qquad \psi(T,n) = \frac{1}{1 - \exp\left(-\left((1/\lambda)\, a^{n-1}T\right)^k\right)} \cdot \int_0^t \exp\left(-\left(\frac{1}{\lambda} a^{n-1}t\right)^k\right) dt = \frac{\lambda}{a^{n-1}}. \tag{11}$$

From function (4), (6), and (10)-(11), $C(N,T)$ will be further expressed as

$$C(T,N) = \left(c_d \sum_{n=1}^{N} \frac{\exp\left(-\left((1/\lambda)\, a^{n-1}T\right)^k\right)}{1 - \exp\left(-\left((1/\lambda)\, a^{n-1}T\right)^k\right)} + c_p \sum_{n=1}^{N} \frac{\mu}{b^{n-1}} \frac{\exp\left(-\left((1/\lambda)\, a^{n-1}T\right)^k\right)}{1 - \exp\left(-\left((1/\lambda)\, a^{n-1}T\right)^k\right)} + c_c \sum_{n=1}^{N-1} \frac{\nu}{c^{n-1}} + c_r \tau + c_N - c_s - c_b \sum_{n=1}^{N} \frac{\lambda}{a^{n-1}} \right)$$

$$\cdot\left(\sum_{n=1}^{N}\frac{\lambda}{a^{n-1}}+\sum_{n=1}^{N}\frac{\mu}{b^{n-1}}\frac{\exp\left(-\left((1/\lambda)\,a^{n-1}T\right)^{k}\right)}{1-\exp\left(-\left((1/\lambda)\,a^{n-1}T\right)^{k}\right)}+\sum_{n=1}^{N-1}\frac{\nu}{c^{n-1}}+\tau\right)^{-1}. \tag{12}$$

Assuming that the preventive maintenance process would be taken before the state of health (SOH) is down to R, one has

$$F\left(a^{n-1}T\right)\le 1-R. \tag{13}$$

From function (10), the constraint of T has the following derivation:

$$\begin{aligned}1-\exp\left(-\left(\frac{1}{\lambda}a^{n-1}T\right)^{k}\right)&\le 1-R,\\ \left(\frac{1}{\lambda}a^{n-1}T\right)^{k}&\le \ln\left(\frac{1}{R}\right),\\ \frac{1}{\lambda}a^{n-1}T&\le\left(\ln\left(\frac{1}{R}\right)\right)^{1/k},\\ T&\le\frac{\lambda}{a^{n-1}}\left(\ln\left(\frac{1}{R}\right)\right)^{1/k}.\end{aligned} \tag{14}$$

The reliability of the energy storage batteries is a representation of the full operation capability. Generally, it is defined as $A(T)=\lim_{t\to\infty}(A(t)/t)$. Under the proposed optimized management strategy aimed at the life cycle of the energy storage batteries, the reliability $A(N,T)$ will be expressed as the ratio of the operation time and the whole life cycle; that is,

$$A(T,N)=\frac{E\left(\sum_{n=1}^{N}X_n\right)}{E\left(\sum_{n=1}^{N}X_n+\sum_{n=1}^{N}\sum_{i=1}^{M_n}Y_n^i+\sum_{n=1}^{N-1}Z_n+H\right)}. \tag{15}$$

Furtherly, from function (6), (8), (10)-(11), and (15),

$$A(T,N)=\sum_{n=1}^{N}\frac{\lambda}{a^{n-1}}\left(\sum_{n=1}^{N}\frac{\lambda}{a^{n-1}}+\sum_{n=1}^{N}\frac{\mu}{b^{n-1}}\frac{\exp\left(-a^{n-1}T/\lambda\right)}{1-\exp\left(-a^{n-1}T/\lambda\right)}+\sum_{n=1}^{N-1}\frac{\nu}{c^{n-1}}+\tau\right)^{-1}. \tag{16}$$

Based on the above analysis, the objective function of the proposed optimized management strategy is to find the minimum value of $C(T^*,N^*)$ against T^* and N^* under the constraint of the reliability threshold, which would be expressed as

$$\begin{aligned}C\left(T^*,N^*\right):\ \min\quad & C(T,N)\\ \text{s.t.}\quad & A\left(T^*,N^*\right)\ge A_0,\\ & T\le\frac{\lambda}{a^{n-1}}\left(\ln\left(\frac{1}{R}\right)\right)^{1/k},\end{aligned} \tag{17}$$

where A_0 is the threshold of the availability.

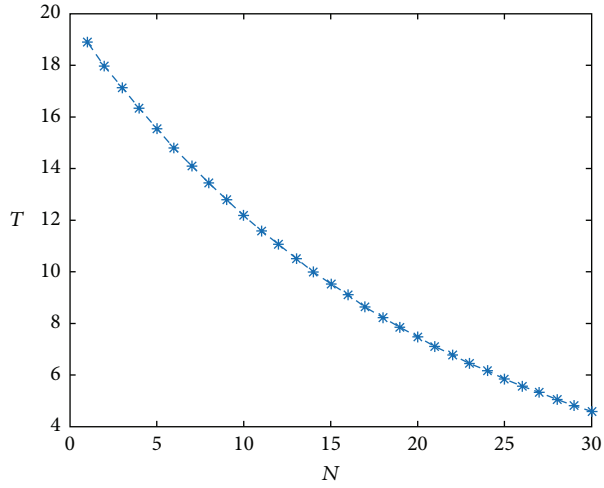

Figure 4: The constraint of T against N.

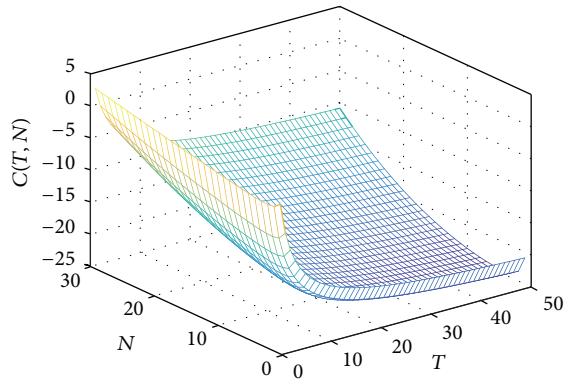

Figure 5: $C(T,N)$ against T and N.

5. Simulation Analysis

To verify the proposed optimized management strategy of the energy storage batteries, numerical examples are analyzed as follows. Originally from the lead-acid storage battery, the main parameters are listed in Table 1. Under the constraint of function (14), the time interval T that determines the detection and preventive maintenance processes have a certain relation to the maximum number of corrective maintenances N, which satisfies the area under the curve, as is shown in Figure 4.

Considering the long-run average cost of the energy storage batteries $C(T,N)$ under the proposed optimized management strategy (T,N), the simulation is firstly carried out to gain the minimum $C(T^*,N^*)$, and the result is illustrated in Figure 5. It indicates that the long-run average costs increase as the number of corrective maintenances goes up and decrease as the time interval of detection and preventive maintenance goes down. So the dense and multiple times of detection, preventive maintenance, and corrective maintenance would certainly raise the cost of the energy storage batteries.

Table 1: Main parameters of the simulation.

Parameter	a	b	c	λ	μ	ν	τ	c_b	c_d	c_p	c_c	c_r	c_N	c_s	R	k
Value	1.05	0.95	0.9	100	0.3	0.7	10	50	60	100	300	200	2000	200	0.8	0.9

Table 2: The main explicit values of $C(T, N)$.

N	T								
	7	9	10	11	12	14	16	17	18
1	−14.94	−16.17	−16.64	−17.04	−17.39	−17.96	−18.41	−18.61	**−18.78**
2	−16.88	−18.23	−18.74	−19.18	−19.57	−20.19	−20.69	**−20.90**	*−21.09*
3	−17.33	−18.72	−19.26	−19.71	−20.11	−20.76	−21.28	**−21.50***	*−21.70*
4	−17.41	−18.83	−19.37	−19.84	−20.24	−20.91	**−21.44**	*−21.67*	*−21.87*
6	−17.16	−18.62	−19.18	−19.66	−20.08	**−20.77**	*−21.31*	*−21.55*	*−21.76*
9	−16.42	−17.91	−18.48	−18.97	**−19.40**	*−20.11*	*−20.67*	*−20.91*	*−21.13*
11	−15.80	−17.29	−17.87	**−18.36**	*−18.79*	*−19.51*	*−20.08*	*−20.32*	*−20.54*
13	−15.10	−16.59	**−17.16**	*−17.66*	*−18.09*	*−18.81*	*−19.38*	*−19.62*	*−19.85*
15	−14.33	**−15.80**	*−16.37*	*−16.87*	*−17.30*	*−18.01*	*−18.58*	*−18.82*	*−19.04*
19	**−12.57**	*−13.98*	*−14.53*	*−15.00*	*−15.41*	*−16.10*	*−16.65*	*−16.88*	*−17.09*

*The minimum long-run average cost of the energy storage batteries.

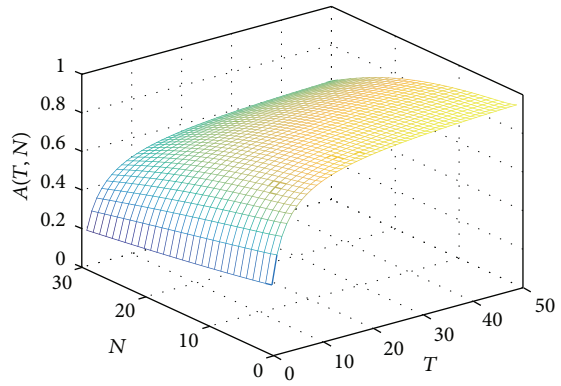

Figure 6: $A(T, N)$ against T and N.

The main explicit values of the long-run average cost $C(T, N)$ are lists in Table 2.

The values that are formatted in the bold text are the constraint of T, the ones with the italic font are the invalid values. Comparing to the values which are accordant with the certain condition, the minimum long-run average cost of the energy storage batteries is $C(17, 3) = -21.50$; that is, the lowest long-run average cost is gained when the time interval of detection and preventive maintenance is set to 17 and the maximum number of corrective maintenances is 3.

The next simulation is taken to verify another constraint $A(T, N)$ of the proposed optimized management strategy. The threshold A_0 is set to 0.8. Under the same conditions of the previous simulations, the reliability curve in the different values of T and N is shown in Figure 6, and the explicit values of $A(T, N)$ corresponding to Table 2 are listed in Table 3. Considering the optimized management strategy $(17, 3)$, the corresponding reliability is 0.84 that meets the 0.8 threshold, which indicates a strong applicability of the proposed optimized management strategy.

6. Conclusions

Oriented to the centralized schedule and management of the energy storage batteries in the microgrid for dealing with the strong fluctuation and randomness of the renewable energy, this paper firstly analyzes the different main states in the life cycle of the energy storage batteries, which includes the operation state, the preventive maintenance state, and the corrective maintenance state. Considering the energy storage batteries' deteriorating characteristics during the repeating charging and discharging as well as the negative impact of aging, the deteriorating system and the improving system are distinguished in the built GP-based model for describing the operation process, preventive maintenance process, and corrective maintenance process. Moreover, this paper proposes the optimized management strategy to minimize the long-run average cost on the specified condition of the SOH and reliability, which adaptively schedules the time interval of the detection and preventive maintenance as well as the maximum number of corrective maintenances. Finally, the simulation with the specified SOH and reliability thresholds is taken to verify its effectiveness. The results denote that the built GP-based model is suitable to study the management of the energy storage batteries, and the proposed optimized management strategy will reduce the long-run average cost of the energy storage batteries on the promise of the normal operation, which is of much suitability for the energy storage batteries' optimized management.

Competing Interests

The authors declare that they have no competing interests.

Table 3: The explicit values of $A(T, N)$.

N	T								
	7	9	10	11	12	14	16	17	18
1	0.74	0.78	0.80	0.81	0.82	0.84	0.85	0.86	0.87
2	0.73	0.77	0.79	0.80	0.81	0.83	0.84	0.85	*0.85*
3	0.73	0.76	0.78	0.79	0.80	0.82	0.84	**0.84**[*]	*0.85*
4	0.72	0.76	0.77	0.79	0.80	0.81	0.83	*0.84*	*0.84*
6	0.70	0.74	0.76	0.77	0.78	0.80	*0.82*	*0.82*	*0.83*
9	0.68	0.72	0.74	0.75	0.76	*0.78*	*0.80*	*0.80*	*0.81*
11	0.66	0.70	0.72	0.73	*0.75*	*0.77*	*0.78*	*0.79*	*0.79*
13	0.65	0.69	0.70	*0.72*	*0.73*	*0.75*	*0.76*	*0.77*	*0.78*
15	0.63	0.67	*0.69*	*0.70*	*0.71*	*0.73*	*0.75*	*0.75*	*0.76*
19	0.59	*0.63*	*0.65*	*0.66*	*0.67*	*0.69*	*0.71*	*0.71*	*0.72*

[*] The reliability corresponding to (17, 3).

Acknowledgments

This work is supported by the National Natural Science Foundation of China (61374097 and 61473066), the Program for New Century Excellent Talents in University (NCET-12-0103), the Basic Science & Research Fund of Northeastern University (N152303010) and of Northeastern University at Qinhuangdao (XNB201601), and the Science and Technology Research Project of Higher Education of Hebei Province (QN2016315).

References

[1] P. Han, J. Wang, Y. Han, and Y. Li, "Resident Plug-In Electric Vehicle charging modeling and scheduling mechanism in the smart grid," *Mathematical Problems in Engineering*, vol. 2014, Article ID 540624, 8 pages, 2014.

[2] D. Tran and A. M. Khambadkone, "Energy management for lifetime extension of energy storage system in micro-grid applications," *IEEE Transactions on Smart Grid*, vol. 4, no. 3, pp. 1289–1296, 2013.

[3] B. Liu, F. Zhuo, Y. Zhu, and H. Yi, "System operation and energy management of a renewable energy-based DC micro-grid for high penetration depth application," *IEEE Transactions on Smart Grid*, vol. 6, no. 3, pp. 1147–1155, 2015.

[4] Y. Han, J. Wang, Q. Zhao, and P. Han, "An optimal operating strategy for battery life cycle costs in electric vehicles," *Journal of Applied Mathematics*, vol. 2014, Article ID 305905, 6 pages, 2014.

[5] H. Peng, W. Jinkuan, S. Xin, and L. Yan, "Geometric-process-based battery management modeling and optimization in the electric vehicle battery switching station," in *Proceedings of the 11th International Conference on Natural Computation*, pp. 897–901, IEEE, Zhangjiajie, China, August 2015.

[6] P. Munoz-Condes, M. Gomez-Parra, C. Sancho et al., "On condition maintenance based on the impedance measurement for traction batteries: development and industrial implementation," *IEEE Transactions on Industrial Electronics*, vol. 60, no. 7, pp. 2750–2759, 2013.

[7] N. K. Ure, G. Chowdhary, T. Toksoz, J. P. How, M. A. Vavrina, and J. Vian, "An automated battery management system to enable persistent missions with multiple aerial vehicles," *IEEE/ASME Transactions on Mechatronics*, vol. 20, no. 1, pp. 275–286, 2015.

[8] H. Li, D. Pan, and C. L. P. Chen, "Intelligent prognostics for battery health monitoring using the mean entropy and relevance vector machine," *IEEE Transactions on Systems, Man, and Cybernetics: Systems*, vol. 44, no. 7, pp. 851–862, 2014.

[9] G. Ablay, "Online condition monitoring of battery systems with a nonlinear estimator," *IEEE Transactions on Energy Conversion*, vol. 29, no. 1, pp. 232–239, 2014.

[10] B. Zhao, X. Zhang, J. Chen, C. Wang, and L. Guo, "Operation optimization of standalone microgrids considering lifetime characteristics of battery energy storage system," *IEEE Transactions on Sustainable Energy*, vol. 4, no. 4, pp. 934–943, 2013.

[11] L. Liao and F. Köttig, "Review of hybrid prognostics approaches for remaining useful life prediction of engineered systems, and an application to battery life prediction," *IEEE Transactions on Reliability*, vol. 63, no. 1, pp. 191–207, 2014.

[12] H. Han, H. Xu, Z. Yuan, and Y. Shen, "A new SOH prediction model for lithium-ion battery for electric vehicles," in *Proceedings of the 17th International Conference on Electrical Machines and Systems (ICEMS '14)*, pp. 997–1002, Hangzhou, China, October 2014.

[13] Y. Wang and Y. Liu, "Electronic control system design and test of pure electric vehicle battery management system," in *Proceedings of the 2nd International Conference on Mechanic Automation and Control Engineering (MACE '11)*, pp. 1289–1292, Hohhot, China, July 2011.

[14] Y. Lam and Y. L. Zhang, "A geometric-process maintenance model for a deteriorating system under a random environment," *IEEE Transactions on Reliability*, vol. 52, no. 1, pp. 83–89, 2003.

[15] Y. Lam, "A geometric process δ-shock maintenance model," *IEEE Transactions on Reliability*, vol. 58, no. 2, pp. 389–396, 2009.

[16] Y. L. Zhang, "A geometric-process repair-model with good-as-new preventive repair," *IEEE Transactions on Reliability*, vol. 51, no. 2, pp. 223–228, 2002.

[17] G. J. Wang and Y. L. Zhang, "Optimal periodic preventive repair and replacement policy assuming geometric process repair," *IEEE Transactions on Reliability*, vol. 55, no. 1, pp. 118–122, 2006.

[18] A. L. Huang, Q. M. Li, M. Z. Ruan, and D. J. Mao, "Optimal replacement policies for degenerative repairable systems based

on delayed geometric process," *Journal of Systems Engineering and Electronics*, vol. 33, no. 11, pp. 2449–2452, 2011.

[19] Y. Li, J.-K. Wang, P. Han, and Y.-H. Han, "Geometric-process-based battery management optimizing policy for the electric bus," *Mathematical Problems in Engineering*, vol. 2015, Article ID 624130, 7 pages, 2015.

Hindawi Publishing Corporation
Mathematical Problems in Engineering
Volume 2016, Article ID 1659549, 7 pages
http://dx.doi.org/10.1155/2016/1659549

Research Article

Reliability of Foundation Pile Based on Settlement and a Parameter Sensitivity Analysis

Shujun Zhang,[1,2] Luo Zhong,[1] and Zhijun Xu[3]

[1] *Wuhan University of Technology, School of Civil Engineering and Architecture, Wuhan 430070, China*
[2] *Nanyang Institute of Technology, School of Civil Engineering, Nanyang 473004, China*
[3] *Henan University of Technology, School of Civil Engineering and Architecture, Zhengzhou 450001, China*

Correspondence should be addressed to Shujun Zhang; s-j-z668@163.com

Received 19 November 2015; Accepted 14 February 2016

Academic Editor: Egidijus R. Vaidogas

Based on the uncertainty analysis to calculation model of settlement, the formula of reliability index of foundation pile is derived. Based on this formula, the influence of coefficient of variation of the calculated settlement at pile head, coefficient of variation of the permissible limit of the settlement, coefficient of variation of the measured settlement, safety coefficient, and the mean value of calculation model coefficient on reliability is analyzed. The results indicate that (1) high reliability index can be obtained by increasing safety coefficient; (2) reliability index will be reduced with increasing of the mean value of calculation model coefficient and coefficient of variation of the permissible limit of settlement; (3) reliability index will not always monotonically increase or decrease with increasing of coefficient of variation of the calculated settlement and coefficient of variation of calculation model coefficient. To get a high reliability index, coefficient of variation of calculation model coefficient or value range of coefficient of variation of calculation model coefficient should be determined through the derived formula when values of other independent variables are determined.

1. Introduction

Analysis on reliability of foundation pile is one of the important research topics in the field of geotechnical engineering. In order to make in-depth research to this topic, experts and scholars have done a lot of work. But most of these researches are conducted based on bearing capacity of foundation pile [1, 2]. Some theoretical methods which are used to analyze settlement of single foundation pile and foundation pile group have emerged so far such as load transfer method, integral equation method, finite element method, approximate analysis method, and hybrid analysis approach [3]. However, in these researches, parameter of soil property is basically considered as a fixed value. It is obviously limited because the soil mass is variable in space, there are many uncertainties in sample test, and the test data obtained from the testing site has very high variability. Thus, it has become a trend in analysis and research on settlement of foundation pile to take into account some variability parameters as variables and adopt uncertainty analysis method.

Bian [3], after analyzing the influence of spatial variability of soil mass on settlement of single foundation pile using random finite element method, pointed out that settlement of pile tip is influenced by uncertainty and randomness of parameter and then performed analysis to reliability of settlement of foundation pile by taking these uncertainties into account. Quek et al. [4] performed analysis to reliability of settlement of foundation pile using design drawing method based on uncertain parameters, and they also considered relationship between parameters as uncertainties. Zhang and Ng [5] investigated probability distribution of permissible limit of settlement under serviceability limit state of foundation pile using a large quantity of data they collected, laying a certain foundation for design of foundation pile under serviceability limit state from design based on certainty to reliability design. Zhang and Phoon [6] took into account all the uncertain factors when they research reliability design of foundation pile. They considered the measured settlement, estimated settlement, and permissible limit of settlement as random variables, thus giving the method for reliability

design under serviceability limit state. Bian et al. [7] got formula of reliability of single pile under several common design methods of foundation pile and analyzed the influence of deviation factor of these several foundation pile design methods on the bearing capacity reliability of foundation pile. Bian et al. [8] got formula for reliability of foundation pile under ultimate limit state and serviceability limit state and studied the influence of randomness of allowable settlement of pile head on reliability analysis result under serviceability limit state. By combining failure probability of intact pile and pile which has sediment at the base; Li and Yan [9] obtained failure probability of single pile and got formula of deviation factor and coefficient of variation of foundation pile which has sediment at the base.

It can be seen from the above that research on reliability of settlement of foundation pile has become a focus in the field of engineering. However, the actual settlement of foundation pile is small and the difficulty for measurement is a little high. Meanwhile, the measurement result has large deviation and discreteness. All these above mentioned would influence the reliability index and make the investigation on the reliability index of foundation pile highly rich. Although a lot of formulas have been derived in the literature, and the effectiveness of these formulas has been proved through some testing data, it is still necessary and beneficial to recognize sensitive parameters in many affecting variables. In this paper, formula of reliability index of settlement of foundation pile (single pile) is derived through the establishment of limit state equation based on uncertainty analysis on settlement model of foundation pile. The influence of coefficient of variation of the calculated settlement, coefficient of variation of the permissible limit of settlement, and coefficient of variation of the measured settlement on reliability is studied as well. The result of analysis can be used as reference and guide for design, construction, and quality inspection of foundation pile engineering.

2. Model Coefficient and Limit State Equation

Load transfer method is a commonly used method to calculate settlement of a foundation pile. It divides the foundation pile into several elastic units. It is assumed that each unit is connected with the soil mass (including pile tip) through nonlinear spring to simulate load transfer mechanism between foundation pile and soil. Nonlinearity of interaction between foundation pile and soil as well as stratification characteristic of soil can be correctly described through this method, which is suitable for calculation of settlement of single pile. However, continuity of soil property is not fully considered in this method [10].

As one of the difficult problems in foundation pile engineering, settlement estimation of foundation pile is influenced by many uncertainties, such as physical dimension of pile body, pile formation technology, property of soil around the pile, and measurement error [11]. Thus, the calculation result of settlement of foundation pile is of high uncertainty. Under vertical load, the measured settlement of pile head is assumed to be S_m and the estimated settlement of pile head according to settlement formula of foundation pile is S_p. The calculated settlement of pile head S_p is considered as a random variable to reflect uncertainty of calculation model of settlement.

In order to make quantitative evaluation to uncertainty of calculation model of settlement, the ratio of the measured settlement S_m to the calculated one S_p is used to define model coefficient:

$$\lambda_s = \frac{S_m}{S_p}. \tag{1}$$

Then, the uncertainty of calculation model of foundation pile can be described through the mean value and the coefficient of variation of λ_s.

Xu [12] collected static load test data of 60 foundation piles with H-type steel frame and studied its settlement property by nonlinear load transfer method. After statistical analysis, the mean value of calculation model λ_s and coefficient of variation were arrived: that is, $\mu_{\lambda_s} = 1.25$ and $\mathrm{COV}_{\lambda_s} = 0.23$.

In addition, under the influence of site environment, construction condition, measurement equipment, and test technology, the permissible limit of settlement S_{tol} and the measured settlement S_m are of highly uncertain. Therefore, the permissible limit of settlement S_{tol} and the measured settlement S_m are considered as random variables in reliability analysis of settlement of foundation pile.

Vertical settlement of pile head cannot exceeds the permissible limit of settlement S_{tol} under normal working condition. A function can be established according to the permissible limit of settlement S_{tol} and the measured settlement S_m:

$$g\left(S_{\mathrm{tol}}, S_m\right) = S_{\mathrm{tol}} - S_m. \tag{2}$$

A two-dimensional state space is established through formula (2), which takes the permissible limit of settlement S_{tol} and the measured settlement S_m as the variables, wherein

(1) $g(S_{\mathrm{tol}}, S_m) = S_{\mathrm{tol}} - S_m = 0$ means that foundation pile reaches the limit state under the working vertical load, which is the critical state. It can be used as the limit state curve, dividing the entire state space into security domain and failure domain;

(2) $g(S_{\mathrm{tol}}, S_m) = S_{\mathrm{tol}} - S_m > 0$ indicates that foundation pile is in a safe state and the representative domain is a security domain;

(3) $g(S_{\mathrm{tol}}, S_m) = S_{\mathrm{tol}} - S_m < 0$ means that foundation pile is in a failure state and the representative domain is a failure domain.

In order to effectively make reliability analysis of the settlement with probability method, distribution pattern of the permissible limit of settlement S_{tol} and the measured settlement S_m should be determined. The scholars have made a lot of investigations on this topic. Zhang and Xu [13] researched the vertical settlement of pile head of 149 foundation piles into which H-steel is inserted under static

load test condition and analyzed relevant results using load-settlement model of foundation pile. Zhang and Phoon [6] took logarithmic normal distribution as the distribution pattern of the measured settlement S_m of pile head in their researches. Zhang and Ng [5] collected a huge mass of data about settlement of foundation pile of bridge. By using statistical analysis method, they found that a logarithmic normal distribution can be used for the permissible limit of settlement S_{tol}.

3. Calculation of Reliability Index

According to (2), if the measured settlement S_m is greater than the permissible limit of settlement S_{tol}, the foundation pile is invalid and cannot meet the design requirement of foundation pile engineering.

Let p_f and β represent the failure probability of foundation pile due to settlement and the corresponding reliability index, respectively. According to knowledge of mathematical statistics and reliability theory [14, 15], relation between failure probability and reliability index reads

$$p_f = \text{Prob}\left(S_{\text{tol}} < S_m\right) = \Phi\left(-\beta\right) \tag{3}$$

wherein $\Phi(\cdot)$ is the cumulative probability distribution function of the standard normal distribution.

According to the existing research data, the permissible limit of settlement S_{tol}, the measured settlement S_m, and model coefficient λ_s are assumed to obey the logarithmic normal distribution. Then the failure probability of a foundation pile can be written in

$$\begin{aligned} p_f &= \text{Prob}\left(S_{\text{tol}} < S_m\right) = \text{Prob}\left(\frac{S_{\text{tol}}}{S_m} < 1\right) \\ &= \text{Prob}\left[\ln\left(\frac{S_{\text{tol}}}{S_m}\right) < 0\right] \\ &= \text{Prob}\left\{\ln\left[\left(\frac{S_{\text{tol}}}{S_p}\right) \times \left(\frac{S_p}{S_m}\right)\right] < 0\right\} \\ &= \text{Prob}\left\{\ln\left[\frac{\left(S_{\text{tol}}/S_p\right)}{\lambda_s}\right] < 0\right\} \\ &= \text{Prob}\left[\ln\left(S_{\text{tol}}\right) - \ln\left(S_p\right) - \ln\left(\lambda_s\right) < 0\right] \\ &= \Phi\left(-\frac{\mu_{S_{\text{tol}}^N} - \mu_{S_p^N} - \mu_{\lambda_s^N}}{\sqrt{\sigma_{S_{\text{tol}}^N}^2 + \sigma_{S_p^N}^2 + \sigma_{\lambda_s^N}^2}}\right) \end{aligned} \tag{4}$$

wherein $\mu_{S_{\text{tol}}^N}$, $\mu_{S_p^N}$, and $\mu_{\lambda_s^N}$ are the mean value of $\ln(S_{\text{tol}})$, $\ln(S_p)$ and $\ln(\lambda_s)$, respectively. While $\sigma_{S_{\text{tol}}^N}$, $\sigma_{S_p^N}$, and $\sigma_{\lambda_s^N}$ are standard deviation of $\ln(S_{\text{tol}})$, $\ln(S_p)$, and $\ln(\lambda_s)$, respectively.

According to (3) and (4), the reliability index β of foundation pile based on settlement analysis is

$$\begin{aligned} \beta &= \frac{\mu_{S_{\text{tol}}^N} - \mu_{S_p^N} - \mu_{\lambda_s^N}}{\sqrt{\sigma_{S_{\text{tol}}^N}^2 + \sigma_{S_p^N}^2 + \sigma_{\lambda_s^N}^2}} = \frac{\ln\left[\mu_{S_{\text{tol}}}/\sqrt{1+\text{COV}_{S_{\text{tol}}}^2}\right] - \ln\left[\mu_{S_p}/\sqrt{1+\text{COV}_{S_p}^2}\right] - \ln\left[\mu_{\lambda_s}/\sqrt{1+\text{COV}_{\lambda_s}^2}\right]}{\sqrt{\ln\left[\left(1+\text{COV}_{S_{\text{tol}}}^2\right)\left(1+\text{COV}_{S_p}^2\right)\left(1+\text{COV}_{\lambda_s}^2\right)\right]}} \\ &= \frac{\ln\left[\left(\text{FS}/\mu_{\lambda_s}\right)\sqrt{\left(1+\text{COV}_{S_p}^2\right)\left(1+\text{COV}_{\lambda_s}^2\right)/\left(1+\text{COV}_{S_{\text{tol}}}^2\right)}\right]}{\sqrt{\ln\left[\left(1+\text{COV}_{S_{\text{tol}}}^2\right)\left(1+\text{COV}_{S_p}^2\right)\left(1+\text{COV}_{\lambda_s}^2\right)\right]}} \end{aligned} \tag{5}$$

wherein $\mu_{S_{\text{tol}}}$, μ_{S_p}, and μ_{λ_s} are the mean value of variables S_{tol}, S_p, and λ_s, respectively; $\text{COV}_{S_{\text{tol}}}$, COV_{S_p}, and COV_{λ_s} are the variable coefficient of variables S_{tol}, S_p, and λ_s, respectively; FS is safety coefficient defined by

$$\text{FS} = \frac{\mu_{S_{\text{tol}}}}{\mu_{S_p}}. \tag{6}$$

In the investigation of settlement, Skempton and MacDonald [16] suggested that the basic safety coefficient should not be lower than 1.25 for differential settlement and maximum settlement and that the safety coefficient should not be lower than 1.50 for buildings under torsion. Thus, reliability analysis of foundation pile based on characteristic of settlement should use higher safety coefficient.

According to (1),

$$S_m = \lambda_s S_p. \tag{7}$$

Based on (7), we assume that λ_s and S_p are uncorrelated. The statistical characteristic of the measured settlement S_m of pile head can be estimated by

$$\begin{aligned} \mu_{S_m} &= \mu_{\lambda_s}\mu_{S_p}, \\ \text{COV}_{S_m} &= \sqrt{\text{COV}_{S_p}^2 + \text{COV}_{\lambda_s}^2}. \end{aligned} \tag{8}$$

4. Parameter Sensitivity Analysis

According to (5), the settlement reliability of foundation pile is influenced by safety coefficient FS, the mean value μ_{λ_s} of calculation model coefficient, coefficient of variation $\text{COV}_{S_{\text{tol}}}$ of the permissible limit of settlement of foundation pile, coefficient of variation COV_{S_p} of the calculated settlement of foundation pile, and coefficient of variation COV_{λ_s} of calculation model coefficient. Thus, it is difficult to

determine settlement reliability of foundation pile. However, the influence of each parameter on reliability index can be recognized through parameter sensitivity analysis, and then high reliability domain and low reliability domain can be obtained, which can be used as reference in engineering.

4.1. Influence of Coefficient of Variation of the Permissible Limit of Settlement. According to (5),

$$\frac{\partial\beta}{\partial \mathrm{COV}_{S_{\mathrm{tol}}}} = -\frac{\mathrm{COV}_{S_{\mathrm{tol}}}}{\left(1+\mathrm{COV}_{S_{\mathrm{tol}}}^2\right)\sqrt{\ln\left[\left(1+\mathrm{COV}_{S_{\mathrm{tol}}}^2\right)\left(1+\mathrm{COV}_{S_p}^2\right)\left(1+\mathrm{COV}_{\lambda_s}^2\right)\right]}} - \frac{\mathrm{COV}_{S_{\mathrm{tol}}}\ln\left(\left(\mathrm{FS}/\mu_{\lambda_s}\right)\sqrt{\left(1+\mathrm{COV}_{S_p}^2\right)\left(1+\mathrm{COV}_{\lambda_s}^2\right)/\left(1+\mathrm{COV}_{S_{\mathrm{tol}}}^2\right)}\right)}{\left(1+\mathrm{COV}_{S_{\mathrm{tol}}}^2\right)\left(\ln\left[\left(1+\mathrm{COV}_{S_{\mathrm{tol}}}^2\right)\left(1+\mathrm{COV}_{S_p}^2\right)\left(1+\mathrm{COV}_{\lambda_s}^2\right)\right]\right)^{3/2}}. \tag{9}$$

According to the scope of independent variable and formula (5), $\partial\beta/\partial\mathrm{COV}_{S_{\mathrm{tol}}}$ is constantly smaller than 0. Thus, the reliability index will always decrease with the increase of the coefficient of variation of the permissible limit of settlement of foundation pile.

Figure 1, based on formula (5), shows the influence of the permissible limit of settlement of foundation pile on reliability index in the circumstance of a set of special parameters, wherein FS = 3.0, $\mu_{\lambda_s} = 1.25$, and $\mathrm{COV}_{\lambda_s} = 0.23$.

It can be seen that, with the increase of the coefficient of variation of the permissible limit of settlement, reliability index gradually decreases, which is consistent with the law given by (9). In the particular condition given in Figure 1, a greater reliability index can be obtained when coefficient of variation $\mathrm{COV}_{\mathrm{tol}}$ of the permissible limit of settlement is between 0.0 and 0.4, and coefficient of variation COV_{S_p} of the measured settlement is near zero. In this domain, however, reliability index will be significantly changed when $\mathrm{COV}_{\mathrm{tol}}$ changes within 0.0–0.4.

4.2. Influence of Coefficient of Variation of Calculation Model Coefficient. In a similar way, from (5)

$$\frac{\partial\beta}{\partial \mathrm{COV}_{\lambda_s}} = \frac{\mathrm{COV}_{\lambda_s}}{\left(1+\mathrm{COV}_{\lambda_s}^2\right)\sqrt{\ln\left[\left(1+\mathrm{COV}_{S_{\mathrm{tol}}}^2\right)\left(1+\mathrm{COV}_{S_p}^2\right)\left(1+\mathrm{COV}_{\lambda_s}^2\right)\right]}} - \frac{\mathrm{COV}_{\lambda_s}\ln\left(\left(\mathrm{FS}/\mu_{\lambda_s}\right)\sqrt{\left(1+\mathrm{COV}_{S_p}^2\right)\left(1+\mathrm{COV}_{\lambda_s}^2\right)/\left(1+\mathrm{COV}_{S_{\mathrm{tol}}}^2\right)}\right)}{\left(1+\mathrm{COV}_{S_p}^2\right)\left(\ln\left[\left(1+\mathrm{COV}_{S_{\mathrm{tol}}}^2\right)\left(1+\mathrm{COV}_{S_p}^2\right)\left(1+\mathrm{COV}_{\lambda_s}^2\right)\right]\right)^{3/2}}. \tag{10}$$

It can be seen from formula (10) that the sign of $\partial\beta/\partial\mathrm{COV}_{\lambda_s}$ is related to the value of the independent variables: that is, the reliability index can increase and decrease with the increase of the coefficient of variation of calculation model coefficient. The reliability index reaches its maximum value when the value of COV_{λ_s} meets $\partial^2\beta/\partial^2\mathrm{COV}_{\lambda_s} = 0$. In the real engineering, (10) can be used as a guidance for obtaining high reliability index. For example, the sign of $\partial\beta/\partial\mathrm{COV}_{\lambda_s}$ can be determined using formula (10) when the safety coefficient FS, the mean value μ_{λ_s} of calculation model coefficient and coefficient of variation $\mathrm{COV}_{\mathrm{tol}}$ of the permissible limit of settlement are known. Subsequently, this result can be used to determine the range of independent variable (coefficient of variation COV_{λ_s} of calculation model coefficient and coefficient of variation COV_{S_p} of the measured settlement) which can make the reliability reaches the desired level.

According to (5), the influence of coefficient of variation of calculation model coefficient on reliability index under this set of special circumstance can be obtained taking COV_{λ_s} as 0.0, 0.2, 0.4, 0.6, 0.8, and 1.0 in sequence, FS = 3.0, $\mu_{\lambda_s} = 1.25$, and $\mathrm{COV}_{\mathrm{tol}} = 0.583$, and taking coefficient of variation of the measured settlement as independent variable. The calculation result is as shown in Figure 2.

It can be seen from Figure 2 that reliability index does not continuously decrease with increasing of coefficient of variation of calculation model coefficient. Reliability index increases with increasing of coefficient of variation of calculation model coefficient when coefficient of variation COV_{S_p} of the measured settlement is greater than 0.9. This is consistent with the law given by (10). At the same time, when COV_{λ_s} changes within [0, 1], reliability index is only in the variation

region [1.06, 1.32]. This indicates that the change of coefficient of variation of calculation model coefficient does not significantly influence reliability index under the particular circumstance of this set of parameter representative.

4.3. Influence of Coefficient of Variation of the Measured Settlement. From (5),

$$\frac{\partial\beta}{\partial \mathrm{COV}_{S_p}} = \frac{\mathrm{COV}_{S_p}}{\left(1+\mathrm{COV}_{S_p}^2\right)\sqrt{\ln\left[\left(1+\mathrm{COV}_{S_{\mathrm{tol}}}^2\right)\left(1+\mathrm{COV}_{S_p}^2\right)\left(1+\mathrm{COV}_{\lambda_s}^2\right)\right]}} - \frac{\mathrm{COV}_{S_p}\ln\left(\left(\mathrm{FS}/\mu_{\lambda_s}\right)\sqrt{\left(1+\mathrm{COV}_{S_p}^2\right)\left(1+\mathrm{COV}_{\lambda_s}^2\right)/\left(1+\mathrm{COV}_{S_{\mathrm{tol}}}^2\right)}\right)}{\left(1+\mathrm{COV}_{S_p}^2\right)\left(\ln\left[\left(1+\mathrm{COV}_{S_{\mathrm{tol}}}^2\right)\left(1+\mathrm{COV}_{S_p}^2\right)\left(1+\mathrm{COV}_{\lambda_s}^2\right)\right]\right)^{3/2}}. \tag{11}$$

It can be seen from (11) that the sign of $\partial\beta/\partial\mathrm{COV}_{S_p}$ is related to the value of the independent variables: that is, reliability index can increase and decrease with the increase of coefficient of variation of the measured settlement. This result is similar to the value of $\partial\beta/\partial\mathrm{COV}_{\lambda_s}$. In real engineering, the sign of $\partial\beta/\partial\mathrm{COV}_{S_p}$ can be determined using (11) when the safety coefficient FS, the mean value μ_{λ_s} of calculation model coefficient, and coefficient of variation $\mathrm{COV}_{\mathrm{tol}}$ of the permissible limit of settlement are known. This result can also be used to determine the range of independent variable (coefficient of variation COV_{λ_s} of calculation model coefficient and coefficient of variation COV_{S_p} of the measured settlement) which can make the reliability reaches the desired level.

It can also be seen from the particular case shown in Figures 1 and 2 that coefficient of variation COV_{S_p} of the measured settlement has influence on the reliability index and that the reliability index can increase and decrease with the increase of COV_{S_p}, which is consistent with the law given by (11).

4.4. Influence of Safety Coefficient. According to (5),

$$\frac{\partial\beta}{\partial \mathrm{FS}} = \frac{1}{\mathrm{FS}\sqrt{\ln\left[\left(1+\mathrm{COV}_{S_{\mathrm{tol}}}^2\right)\left(1+\mathrm{COV}_{S_p}^2\right)\left(1+\mathrm{COV}_{\lambda_s}^2\right)\right]}}. \tag{12}$$

Since the independent variables in formula (12) are greater than 0, we can easily know that $\partial\beta/\partial\mathrm{FS} > 0$, which means reliability index will always increase with the increase of the safety coefficient.

Figure 3, based on (5), shows the influence of the safety coefficient on the reliability index in the circumstance of a set of special parameter: that is, $\mathrm{COV}_{\lambda_s} = 0.23$, $\mu_{\lambda_s} = 1.25$, and $\mathrm{COV}_{\mathrm{tol}} = 0.583$. It can be seen that the law given by Figure 3 is consistent with that by (12) and that the reliability index always increases with safety coefficient.

4.5. Influence of the Mean Value of Calculation Model Coefficient. According to (5),

$$\frac{\partial\beta}{\partial\mu_{\lambda_s}} = -\frac{1}{\mu_{\lambda_s}\sqrt{\ln\left[\left(1+\mathrm{COV}_{S_{\mathrm{tol}}}^2\right)\left(1+\mathrm{COV}_{S_p}^2\right)\left(1+\mathrm{COV}_{\lambda_s}^2\right)\right]}}. \tag{13}$$

In a similarly way, independent variables in formula (13) are greater than 0, and thus $\partial\beta/\partial\mu_{\lambda_s} < 0$, which means that the increase of the mean value of calculation model coefficient reduces the reliability index.

According to (5), the influence of the mean value of calculation model coefficient on reliability index under this particular condition can be obtained taking $\mathrm{COV}_{\lambda_s} = 0.23$, $\mathrm{COV}_{\mathrm{tol}} = 0.583$, FS = 3.0, and $\mathrm{COV}_{S_p} = 0.5$, as shown in Figure 4. It can be seen that reliability index continuously reduces with the increase of the mean value of calculation model coefficient, which is consistent with the conclusion obtained through (13).

5. Analysis of Discussion Result

It can be seen from (9) and Figure 1 that the lower the coefficient of variation of the permissible limit of settlement is, the greater the reliability index is, and ideal reliability index can be obtained when coefficient of variation of the permissible limit of settlement takes value from 0 to 0.2. It indicates that it is easier to obtain high reliability index when discreteness of the permissible limit of settlement is small. In real engineering, it is very important engineering value to try to obtain accurate permissible limit of settlement.

The result shown in (12) and Figure 3 indicates that reliability index can be improved when safety coefficient is increased, which means that it has a clear positive significance to improve reliability index of engineering using greater safety coefficient in engineering practice.

Formula (13) and Figure 4 show that high reliability index can be obtained with a low mean value of calculation model coefficient. This indicates that it is easier to obtain high reliability index when the ratio of the measured settlement

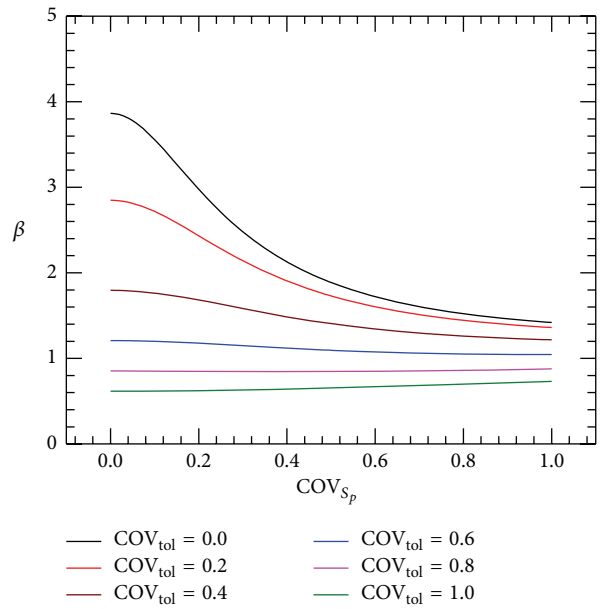

Figure 1: Relation between reliability index β and coefficient of variable $\mathrm{COV}_{\mathrm{tol}}$.

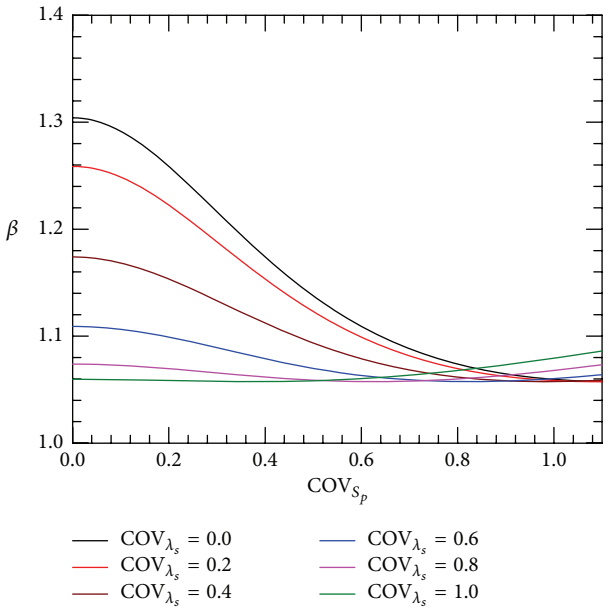

Figure 2: Relation between reliability index β and coefficient of variable COV_{λ_s}.

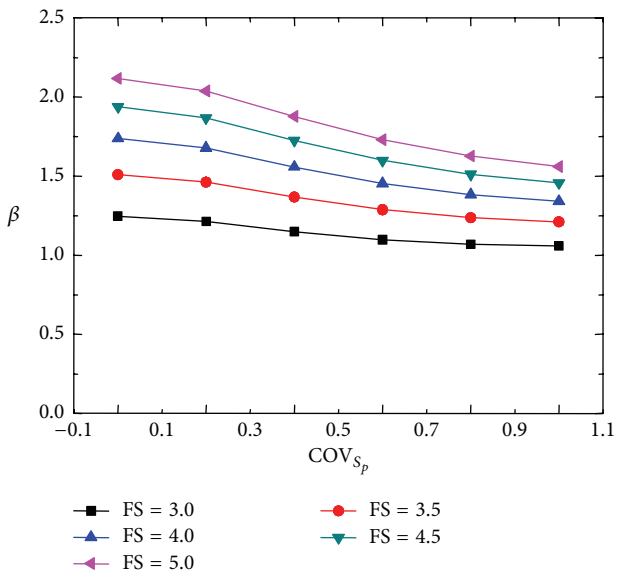

Figure 3: Relation between reliability index β and coefficient of variable COV_{S_p}.

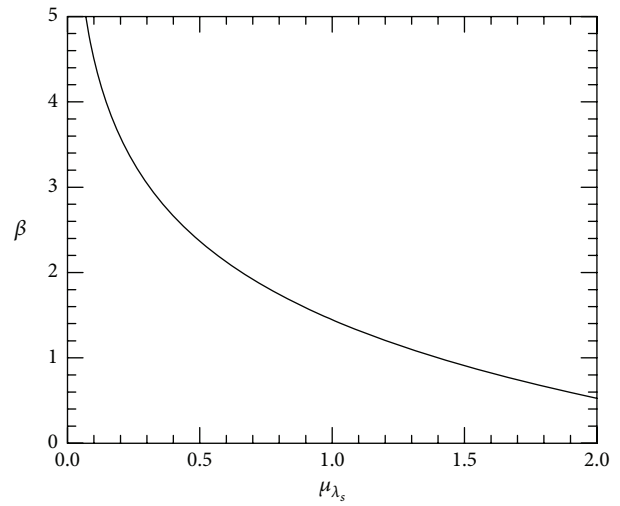

Figure 4: Relation between reliability index β and the mean value of calculation model coefficient.

value to the calculated settlement value is small, which obviously agrees with the logic and the practical engineering. It means that we should try our best to obtain detailed settlement observation data to reduce the ratio of the measured settlement value to the calculated settlement value and finally improve the reliability index.

Formulas (10) and (11) indicate that partial derivative of the reliability index to the coefficient of variation of the calculated settlement and the coefficient of variation of calculation model coefficient can be great than 0 or less than 0, which means that reliability index will not always monotonically increase or decrease with increasing of coefficient of variation of the calculated settlement and coefficient of variation of calculation model coefficient. Instead, it increases sometimes and then decreases in the other cases. This can be seen from the particular circumstance shown in Figures 1 and 2. Therefore, to get a high reliability index, coefficient of variation of calculation model coefficient or value range of coefficient of variation of calculation model coefficient should be determined through the derived formula when values of other independent variables are determined.

6. Conclusion

In this paper, based on analysis to settlement of foundation pile, limit state equations are established. Formula for reliability index of foundation pile settlement is derived, and a parameter sensitivity analysis is conducted. The following conclusion can be arrived:

(1) With the increase of the coefficient of variation of the permissible limit of settlement, the reliability index gradually reduces.

(2) Gradual increase of the reliability index can be obtained by the increase of the safety coefficient.

(3) The reliability index always decreases with the increase of the mean value of calculation model coefficient.

(4) Reliability index will not always monotonically increase or decrease with the increase of the coefficient of variation of the calculated settlement and the coefficient of variation of calculation model coefficient.

Conflict of Interests

The authors declare that there is no conflict of interests regarding the publication of this paper.

Acknowledgments

Thanks are due to the National Natural Science Foundation of China (51178165), High-Level Talent Fund Program of Henan University of Technology (2013BS010), and Henan Basic and Cutting-Edge Technology Research Plan Program (132300410024) for supporting the present work.

References

[1] E. Momeni, R. Nazir, D. Jahed Armaghani, and H. Maizir, "Prediction of pile bearing capacity using a hybrid genetic algorithm-based ANN," *Measurement*, vol. 57, pp. 122–131, 2014.

[2] F. Milad, T. Kamal, H. Nader, and O. E. Erman, "New method for predicting the ultimate bearing capacity of driven piles by using Flap number," *KSCE Journal of Civil Engineering*, vol. 19, no. 3, pp. 611–620, 2015.

[3] X. Y. Bian, *Reliability Analysis and Design of Pile Foundations for Serviceability Limit State*, Huazhong University of Science and Technology, Wuhan, China, 2014 (Chinese).

[4] S. T. Quek, Y. K. Chow, and K. K. Phoon, "Further contributions to reliability-based pile settlement analysis," *Journal of Geotechnical Engineering*, vol. 118, no. 5, pp. 726–742, 1992.

[5] L. M. Zhang and A. M. Y. Ng, "Probabilistic limiting tolerable displacements for serviceability limit state design of foundations," *Geotechnique*, vol. 55, no. 2, pp. 151–161, 2005.

[6] L. Zhang and K. Phoon, "Serviceability considerations in reliability-based foundation design," *Foundation Analysis and Design: Innovative Methods*, GSP 153, pp. 127–136, 2006.

[7] X.-Y. Bian, J.-J. Zheng, and Z.-J. Xu, "Reliability analysis of bearing capacity of foundation piles considering pile foundation design approach," *Chinese Journal of Geotechnical Engineering*, vol. 35, no. 2, pp. 1099–1102, 2013 (Chinese).

[8] X.-Y. Bian, J.-J. Zheng, and Z.-J. Xu, "Reliability analysis of serviceability limit state of foundation piles considering uncertainties of parameter and model," *Rock and Soil Mechanics*, vol. 35, no. 11, pp. 3317–3322, 2014 (Chinese).

[9] D.-Q. Li and L.-L. Yan, "Reliability evaluation of bored pile considering possibility of toe debris presence," *Rock and Soil Mechanics*, vol. 29, no. 1, pp. 155–160, 2008.

[10] M.-H. Zhao, D. Zou, and X.-J. Zou, "Settlement calculation of pile groups by load transfer method," *Engineering Mechanics*, vol. 23, no. 7, pp. 119–123, 2006.

[11] M.-H. Zhao, D. Zou, and X.-J. Zou, "Settlement calculation of pile foundations with elevated caps by load transfer method," *Chinese Journal of Rock Mechanics and Engineering*, vol. 24, no. 13, pp. 2310–2314, 2005.

[12] Y. Xu, *Calibration of Settlement Analysis Models for Single Piles and Pile Groups*, Hong Kong University of Science and Technology, Hong Kong, 2006.

[13] L. Zhang and Y. Xu, "Settlement of building foundations based on field pile load tests," in *Proceedings of the 16th International Conference on Soil Mechanics and Geotechnical Engineering (ICSMGE '05)*, pp. 2871–2874, Osaka, Japan, September 2005.

[14] A. H.-S. Ang and W. H. Tang, *Probability Concepts in Engineering: Emphasis on Applications to Civil and Environmental Engineering*, John Wiley & Sons, New York, NY, USA, 2nd edition, 2007.

[15] G. B. Baecher and J. T. Christian, *Reliability and Statistics in Geotechnical Engineering*, John Wiley & Sons, Chichester, UK, 2003.

[16] A. W. Skempton and D. H. MacDonald, "The allowable settlement of buildings," *Proceedings of the Institution of Civil Engineers*, vol. 3, no. 5, pp. 727–768, 1956.

Hindawi Publishing Corporation
Mathematical Problems in Engineering
Volume 2016, Article ID 9564801, 10 pages
http://dx.doi.org/10.1155/2016/9564801

Research Article

The Method of Oilfield Development Risk Forecasting and Early Warning Using Revised Bayesian Network

Yihua Zhong, Yuxin Liu, Xuxu Lin, and Shiming Luo

School of Science, Southwest Petroleum University, Chengdu, Sichuan 610500, China

Correspondence should be addressed to Yihua Zhong; zhongyh_65@126.com

Received 26 November 2015; Revised 14 January 2016; Accepted 27 January 2016

Academic Editor: Egidijus R. Vaidogas

Oilfield development aiming at crude oil production is an extremely complex process, which involves many uncertain risk factors affecting oil output. Thus, risk prediction and early warning about oilfield development may insure operating and managing oilfields efficiently to meet the oil production plan of the country and sustainable development of oilfields. However, scholars and practitioners in the all world are seldom concerned with the risk problem of oilfield block development. The early warning index system of blocks development which includes the monitoring index and planning index was refined and formulated on the basis of researching and analyzing the theory of risk forecasting and early warning as well as the oilfield development. Based on the indexes of warning situation predicted by neural network, the method dividing the interval of warning degrees was presented by "3σ" rule; and a new method about forecasting and early warning of risk was proposed by introducing neural network to Bayesian networks. Case study shows that the results obtained in this paper are right and helpful to the management of oilfield development risk.

1. Introduction

Because the oilfield development has the basic characteristics of high risk and high investment as well as complicated process, it is very important to study oilfield development risk forecasting and early warning in order to keep the oil production safe and reduce decision-making mistakes to be caused by risk. Up to now, many scholars have studied the problems on safety related risk and risk-based decision-making [1–17]. For example, Khan et al. summarized and reviewed methods and models on process safety and risk management in recent years; moreover, they figured out their present research trends and future research direction which includes dynamic risk assessment and management as well as advanced consequence modeling [1]. Khan et al. pointed out challenges on development of natural resources in harsh environments [2]. Because Bayesian network (BN) is currently being used for applications related to safety and risk assessment, we first highlight those works that were solved by using Bayesian network (BN) and its improved methods in different industries as follows. Musharraf et al. presented a data collection methodology using a virtual environment for a simplified BN model of offshore emergency evacuation and the probability of failure in the offshore emergency evacuation calculated by BN model aiming at human reliability analysis [3]. Khakzad et al. demonstrated the application of bow-tie and BN methods in conducting quantitative risk analysis of drilling operations and verified BN method which may provide a better vision of well control safety issues and greater value than the bow-tie model [4]. Abimbola et al. presented a risk assessment methodology based on BN for analyzing the safety critical components and consequences of possible pressure regimes in constant bottom-hole pressure techniques of managed pressure drilling [5]. Vinnem et al. developed a dynamic risk analysis methodology that focuses on translating the blowout flowchart directly into BN and showed that BN is an effective technique, which can be used in risk analysis and failure prediction for the offshore industry [6]. Bhandari et al. proposed applying BN to conduct a dynamic safety analysis of deepwater managed pressure drilling operations (MPD) and underbalanced drilling (UBD) operations [7]. Khakzad et al. illustrated how BN helps to overcome the limitations of bow-tie (BT) method; and pointed out that BN can be used in dynamic safety analysis of a wide range of accident scenarios [8]. Yu et al. proposed a two-stage fault diagnosis

technique for process operations [9], in which the modified independent component analysis is used in the first stage for fault detection and to identify the faulty monitored variable, and BN is in the second stage with considering the process variables and their dependence obtained from the process flow diagram. Yuan et al. proposed a methodology for risk analysis of dust explosion scenarios based on BN and a bow-tie diagram [10]. Khakzad presented a methodology based on dynamic BN to model both the spatial and the temporal evolutions of domino effects and also to quantify the most probable sequence of accidents in a potential domino effect with having significance of foreseeing the temporal evolution of domino effects and predicting the most probable sequence of accidents on a domino effect in the allocation of preventive and protective safety measure [11]. Khakzad et al. developed a methodology based on event tree and hierarchical Bayesian analysis to establish informative distributions for offshore blowouts using data of near accidents and implemented the methodology in a Markov Chain Monte Carlo framework and applied it to risk assessment of offshore blowouts in the Gulf of Mexico [12]. Baksh et al. improved the shortcomings of the existing accident model to propose predictive accident modeling methodologies through mitigating restrictive sequential progression assumption and using BN approach [13]. Yang et al. performed a similar analysis as Kalantarnia et al. (2009) [14] to reduce the uncertainty of fault tree calculation using Bayes' theorem [15]. Besides above methods, some scholars also developed other research methods. For example, Alaneme and Igboanugo provided a veritable tool that systematically transforms the qualitative risk variables from its linguistic expressions to quantitative functions using fuzzy logic in combination with conventional risk analysis techniques with marginal oilfield risks [16]. Lavasani et al. proposed a fuzzy logic based risk assessment methodology to perform quantitative risk assessment for offshore oil and gas wells [17].

The above works mainly used BN combined with fault tree and event tree and other methods to solve the analysis and assessment as well as diagnostics on risk. These revised Bayesian networks may provide a convincing basis for BN structure learning and parameter learning from another aspect. The concept of integrating neural network with BN has been present for a long time [18]. Works on this concept include two fields: one is to deal with the problems related to NN from Bayesian perspective [18–22]; the other is to deal with the problems related to BN from NN perspective. However, the latter is seldom studied. As an example, Maschio and Schiozer proposed replacing the flow simulator by proxy models generated by artificial neural network (ANN) to formulate the posterior distribution of Bayesian inference in the history matching [23]. Based on the ability for NN to be known as 100% fitting any function, we propose introducing NN to BN to calculate the posterior probability distribution of BN node under the evidence.

In a word, the literature investigation showed that there are a few studies focusing on safety related risk or risk-based decision-making of petroleum industry, and they mainly concentrated on risk analysis, risk assessment, and prediction in microscopic aspects such as drilling and blowout, while the researches in the macro-aspect are almost focused on the monitoring, predicting, and early warning of operation risk about oilfield enterprise [24–26]. However, they are seldom concerned with risk problem of oilfield block development from the point of microcosmic perspective and control.

This paper aims to forecast and early warn of oilfield block development risk to study risk management in the oilfield development and its related issues, including theory of risk forecast and early warning, model and method of forecast, and early warning oilfield development risk which may provide the technique support for controlling risk by using the theory of oilfield development, forecasting warning, Bayesian networks, neural network and so forth, as well as case study to test the correctness of model and method presented in this paper. Particularly, we extract five blocks' development index based on the law of single well producing oil and transform them successfully into risk nodes using "3σ" rule. Then, we predict oil production by neural network; subsequently, those values were used for decision-making whether they are in the normal interval of yield or not. If one of them is not in the normal interval of yield, then we diagnose what makes prediction result of yield is abnormal by using BN and trace the source of risk.

2. Theoretical Studies of Risk Predicting and Early Warning

The risk is the root or state that makes events be in danger or cause loss; its theories of prediction and early warning include concepts and methods of risk identification, risk assessment, prediction, and early warning [27].

The base of forecasting and early warning is to identify risk and risk source. The risk sources are generally divided into two categories, the first category is innate existence and is not controlled by human; the second category is arising under the influence of people or things [28, 29].

In the study of forecasting and early warning of oilfield development risk, we classified all the indicators in three categories that are the index of warning situation, the index of warning sign, and the index of warning source. Indexes of warning situation are the events that are most taken care of in oilfield development, such as oil production and liquid production; indexes of warning sign are the indexes in contact with the indexes of warning situation and they are easily monitored. Indexes of warning source are causes of the risk. The key of risk prediction and early warning is measuring risk, but now there is no appropriate method to measure risk of oilfield development. At present, the main methods of risk prediction and early warning are neural network method [30], Monte Carlo method [31–33], fuzzy comprehensive evaluation method [34, 35], and Bayesian network method [36, 37]. In order to study the problem of oilfield development risk forecasting and early warning, we will present an improved Bayesian network method by introducing neural network to the structure learning of BN in this paper.

3. Research of Prediction and Early Warning on Oilfield Development Risk

3.1. Early Warning Index System of Oilfield Development Risk. Since the process of oilfield development is very complex, it is quite difficult to identify, evaluate, predict, and early warn of the risks implied in this process. After studying reservoir physical and geological exploration, we adopt the thinking mode proposed in the book named *Early Warning Dynamic System in the Oilfield Development* [38] to construct the early warning index system of oilfield development risk, that is, first analyzing the association relationship among the testing indexes of single well to select testing index with larger association degree, then explaining these test indexes of single well to layer index, and finally refining the index system of oilfield block development risk. This index system contains oil production (OPRO), liquid production (LPRO), oil producing capacity (OPC), liquid producing capacity (LPC), water absorbing capacity (WAC), percolating capacity (PEC), and pressure maintaining level (PML). Among them, oil production and liquid production are the indexes of warning situation; other indexes are the indexes of warning sign [39].

3.2. Method to Forecast Oilfield Development Risk

3.2.1. Neural Network Prediction of Warning Situation Indexes. Neural network is abstracting and modeling of the human brain or biological neural network, which is connected by a large number of neurons. The artificial neuron is a simple mapping model; artificial neuron model can be expressed as

$$S = \sum_{i=1}^{n} \omega_i x_i - \theta, \qquad y = \sigma(s), \tag{1}$$

where x_i $(i = 1, 2, \ldots, n)$ is the input signal added to the input; ω_i is the weight coefficient of corresponding connection which is a coefficient to simulate the strength of synaptic transmission; $\sum$ shows the summation of the postsynaptic potential pulse signal; θ is the critical value of neurons; $\sigma(s)$ is the excitation function of artificial neurons, which is commonly expressed as one of two S (Sigmoid) functions as follows [40, 41]:

$$\sigma(s) = \frac{1}{1 + e^{-1}}, \qquad \sigma(s) = \tanh(\beta s). \tag{2}$$

A lot of the same-form artificial neurons are arranged in layers to form neural network. The neurons receiving signal are called the input layer, the neurons of output signal are called the output layer, and the neurons not directly involved in the input or output are called the intermediate layer or hidden layer.

Input of neural network used in the prediction of oilfield development risk is warning sign indexes (five-block indexes); its output is warning situation indexes (two production indexes). Parameter ω_i of the network was trained by historical data to be determined. This paper trained 1367 networks to select the best model as its predictive model. Its fitting precision is up to 0.002, and the prediction accuracy reaches 0.08.

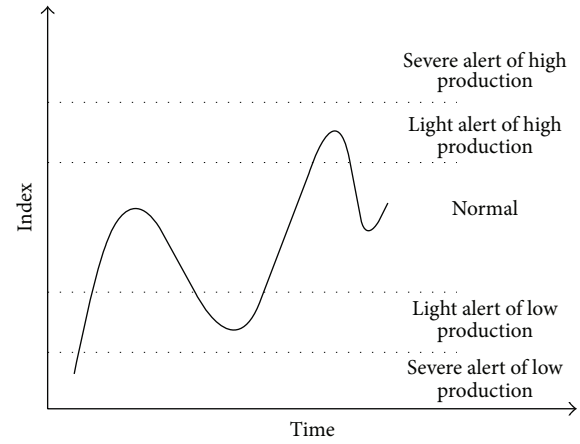

Figure 1: Interval of warning degree.

3.2.2. Method to Determinate the Degree of Oilfield Development Risk. After predicting indexes of warning situation by neural network trained model, the interval of warning degree is determined by "3σ" rule, where σ is the standard deviation which means the discrete degree of data in statistics. According to the statistical principle, if the value of sample deviating from its mathematical expectation μ is more than 1 time the standard deviation, then probability is only 31.74%; if its value is more than 2 times the standard deviation, then probability is only 5%; if its value is more than 3 times the standard deviation, then probability is less than 1%, which is usually said to be the small probability event. Therefore, we may determine the degree that indexes of warning situation happen to risk according to the interval that sample value belongs to. The steps of this method are as follows.

Step 1. Calculate the expected value μ and standard deviation σ of indexes of warning situation by their historic data.

Step 2. Divide the interval of warning degree into the normal interval $[\mu-\sigma, \mu+\sigma]$, the light abnormal intervals $[\mu-2\sigma, \mu-\sigma]$ and $[\mu+\sigma, \mu+2\sigma]$, and the severe abnormal intervals $(-\infty, \mu-2\sigma]$ and $[\mu+2\sigma, +\infty)$ by "3σ" rule [42]; see Figure 1.

Step 3. Predict indexes of warning situation by neural network trained model.

Step 4. Determine the warning degree on the indexes of warning situation. If the prediction value of index of warning situation falls in the normal interval, then it has no risk; if the prediction value of index of warning situation falls in the light abnormal interval, then it has lesser risk; if the prediction value of index of warning situation falls in the severe abnormal interval, then it has bigger risk.

3.3. The Early Warning Method of Oilfield Development Risk by Revised Bayesian Network

3.3.1. Bayesian Network Model of Early Warning

(1) Structure Learning. Bayesian network is a structure to connect the nodes of causal relationship, which is usually determined by two kinds of methods. One is the manual learning method where people use experience to determine whether there is the directed edge connecting nodes or not; the other is machine learning method based on data driven learning, which uses K2 algorithm to search gradually to meet the conditions and score the highest network. The steps of machine learning are as follows.

Step 1. Define a random variable S^h.

Step 2. Determine its prior probability distribution $p(S^h)$.

Step 3. Calculate the posterior probability distribution $p(S^h \mid D)$; that is,

$$p\left(S^h \mid D\right) = \frac{p\left(S^h, D\right)}{p\left(D\right)} = \frac{p\left(S^h\right) p\left(D \mid S^h\right)}{p\left(D\right)}, \tag{3}$$

where $p(D)$ is a constant which is not related with the structure; $p(D \mid S^h)$ is the likelihood function of boundary; it is calculated by [43]

$$p\left(D \mid S^h\right) = \prod_{i=1}^{n} \prod_{j=1}^{q_i} \frac{\Gamma\left(\partial_{ij}\right)}{\Gamma\left(\partial_{ij} + N_{ij}\right)} \prod_{k=1}^{r_i} \frac{\Gamma\left(\partial_{ijk} + N_{ijk}\right)}{\Gamma\left(\partial_{ijk}\right)}. \tag{4}$$

(2) Parameter Learning. The goal of parameter learning is to update the prior distribution of network variables. Let the joint probability distribution of variables $X = \{x_1, x_2, \ldots, x_n\}$ be stored in network S (see [44]):

$$p\left(x \mid \theta_s, S^h\right) = \prod_{i=1}^{n} p\left(x_i \mid pa_i, \theta_i, S^h\right), \tag{5}$$

where S^h means that the joint distribution can be decomposed according to S; $D = \{X_1, X_2, \ldots, X_n\}$ is the random sample of the joint probability distribution of X; θ_s is parameters variable of network, whose vector θ_i represents its uncertainty; $p(\theta_S, S^h)$ is a given prior probability density function. Thus, the learning problem of Bayesian network parameters can be expressed as calculating posterior distribution $p(\theta_S \mid D, S^h)$ after giving a random sample D [45].

(3) Bayesian Network Inference. The essence of Bayesian network inference is to calculate the conditional probability distribution. Let the set of evidence variable be E and let the set of query variable be Q; then, the Bayesian network inference is to calculate the posterior probability distribution of the query variable Q in $E = e$, which is formulated as follows:

$$\begin{aligned} P\left(Q \mid E = e\right) &= \sum_{X-E} P\left(x_1, x_2, \ldots, x_n\right) \\ &= \sum_{X-E} \prod_{i=1}^{n} P\left(x_i \mid Pa_i\right). \end{aligned} \tag{6}$$

3.3.2. The Method of Forecasting and Early Warning Based on Neural Network and Bayesian Network.

Because warning sign index is called fault source in the Bayesian network diagnostic theory, it is also risk source. Generally, the key problem in early warning is to predict whether risk source fault occurs or not, thus warning sign indexes may be dealt with with Boolean variables. Combining the method of risk prediction using neural network in Section 3.2 with diagnostic and inference function of Bayesian network, we presented a new method of forecasting and early warning for oilfield development risk as follows.

Step 1. Construct early warning index system of oilfield development risk using the method in Section 3.1.

Step 2. Generate an appropriate neural network model of forecasting warning situation indexes, whose input is the historical sample data of five warning signs indicators; its output is the historical sample data of warning situation indexes.

Step 3. Predict the value of warning situation indexes by neural network trained model in Step 2.

Step 4. Determine the warning degree of predictive value about warning situation indexes by using the method in Section 3.2.2.

Step 5. Use the history data and the experience of experts to learn Bayesian network structure and parameter.

Step 6. Input the neural network prediction results into Bayesian networks and calculate posterior probability distribution under this evidence.

Step 7. Compare the posterior probability of fault and identify the source of the risk caused by warning situation indexes.

4. Case Studies

In this section, we will analyze and validate that the predictive models established and the new methods of early warning proposed above are correct and feasible by the historical data of oilfield block development in Table 1.

4.1. The Predicting of Warning Situation Index (Production) on Oilfield Development Risk.

According to the methods in Sections 3.1 and 3.2.1, we build a neural network model which takes the warning signs indexes (OPC, LPC, PEC, WAC, and PML) as input and the warning situation indexes (OPRP, LPRO) as output to predict the warning situation index

Table 1: The historical data of an oilfield from 2007.07 to 2009.12.

Date	OPRP	LPRO	LPC	OPC	PEC	WAC	PML
2007.07	5637	92297	0.3018	0.0075	1549.26	1.5842	5.1452
2007.08	5248	92695	0.3016	0.0072	1629.54	1.6147	3.4864
2007.09	4855	91884	0.3017	0.0074	1302.18	1.6174	6.0758
⋮	⋮	⋮	⋮	⋮	⋮	⋮	⋮
2009.10	4254	112409	0.3017	0.007	234.916	1.504	1.5744
2009.11	3439	98884	0.3018	0.0069	231.74	1.5106	1.6142
2009.12	3260	97499	0.3018	0.0069	226.067	1.5154	1.5144

Table 2: Comparison table of neural network predictive value and the actual value.

	Predictive value		Actual value	
	Oil production (t)	Liquid production (t)	Oil production (t)	Liquid production (t)
2010.01	2330	99000	2552	98026
2010.02	3060	105800	3398	97475
2010.03	3690	109240	3705	117607

(production) of the oilfield development risk from 2010.01 to 2010.03 based on the data in Table 1. Their predictive values and actual values are shown in Table 2.

4.2. The Determining of Warning Degree on the Oilfield Development Risk. Firstly, we draw the trend figure of actual production change as Figure 2. This figure shows that the liquid production appears as upward trend during the whole period, but oil production appears as downward trend after 2007.07, which means that this oilfield development has entered the high water-cut period, which needs to be injected by a large amount of water to increase oil production after 2007.07. Then, we use the method in Section 3.2.2 to determine the interval of warning degree as in Table 3 and the warning degree of the predicted values on warning situation index as in Table 4.

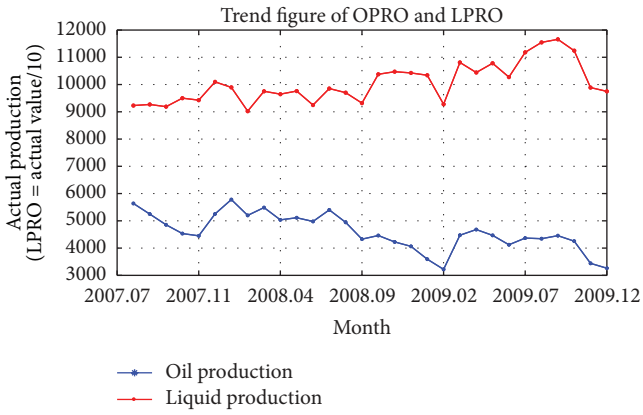

Figure 2: Trend of actual production change.

4.3. Early Warning for Oilfield Development Risk

4.3.1. The Establishing of the Bayesian Network Model. We use genie software to construct the Bayesian network model for the index system of oilfield block development risk which contains OPRO, LPRO, OPC, LPC, PEC, WAC, and PML as in Figure 3 and learn the parameter of Bayesian network based on the history data and the experience of experts as in Figure 4. It shows that the probability of oil output occurring at low production risk is bigger according to its historical data. It is the reason that we do not use Bayesian network to forecast oilfield block development risk. If the value of five warning sign indexes is higher than the average value plus standard deviation or lower than the sum of average value and standard deviation, then we defined its state as fault. Otherwise, its state is normal.

4.3.2. The Inference of Bayesian Network. We shall take the prediction results of neural network in Section 4.1 as observational evidence and use the inference of Bayesian network to get warning signs indexes which is the most risky under this evidence. That is to input the forecast results into the Bayesian networks and calculate posterior probability distribution of the warning signs indexes to find the origin of the risks. Three group evidences and their inference results are as in Figures 5–7.

Figure 5 shows that the most likely risk point which causes such evidence is LPC, for the posterior probability of LPC fault is much larger than others, which is 76%. Reasoning results are matching with the actual situation.

Figure 6 shows that the most likely risk point which causes such evidence is PEC, for the posterior probabilities

Table 3: The interval of warning degree based on 3σ rule.

Warning level	Warning degree	Oil production		Liquid production	
Low production heavy warning (Lhw)	1	0	3249	0	85825
Low production light warning (Llw)	2	3249	3919	85825	93142
Normal (Nor)	3	3919	5259	93142	107776
High production light warning (Hlw)	4	5259	5929	107776	115093
High production heavy warning (Hhw)	5	5929	$+\infty$	115093	$+\infty$

Table 4: The predicted values of productions and the warning degree of them.

	Oil production (t)	Warning degree	Liquid production (t)	Warning degree
2010.01	2330	1	99000	3
2010.02	3260	2	105800	3
2010.03	3690	2	109240	4

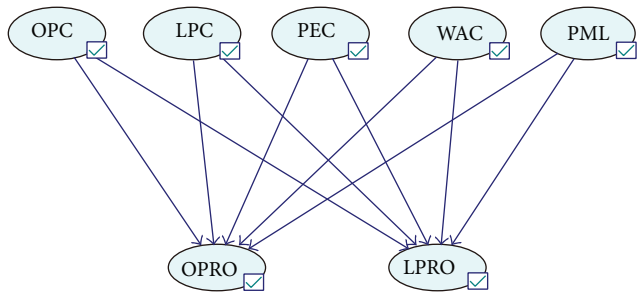

Figure 3: The Bayesian network construction model of oilfield block development risk.

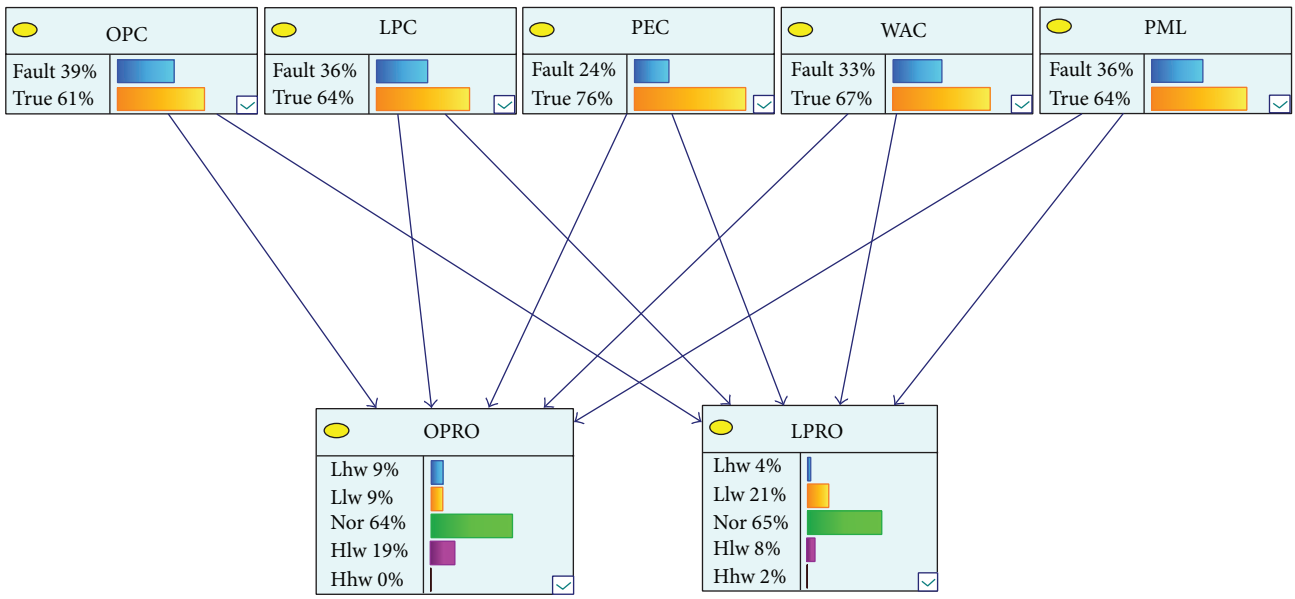

Figure 4: The parameter learning of Bayesian network.

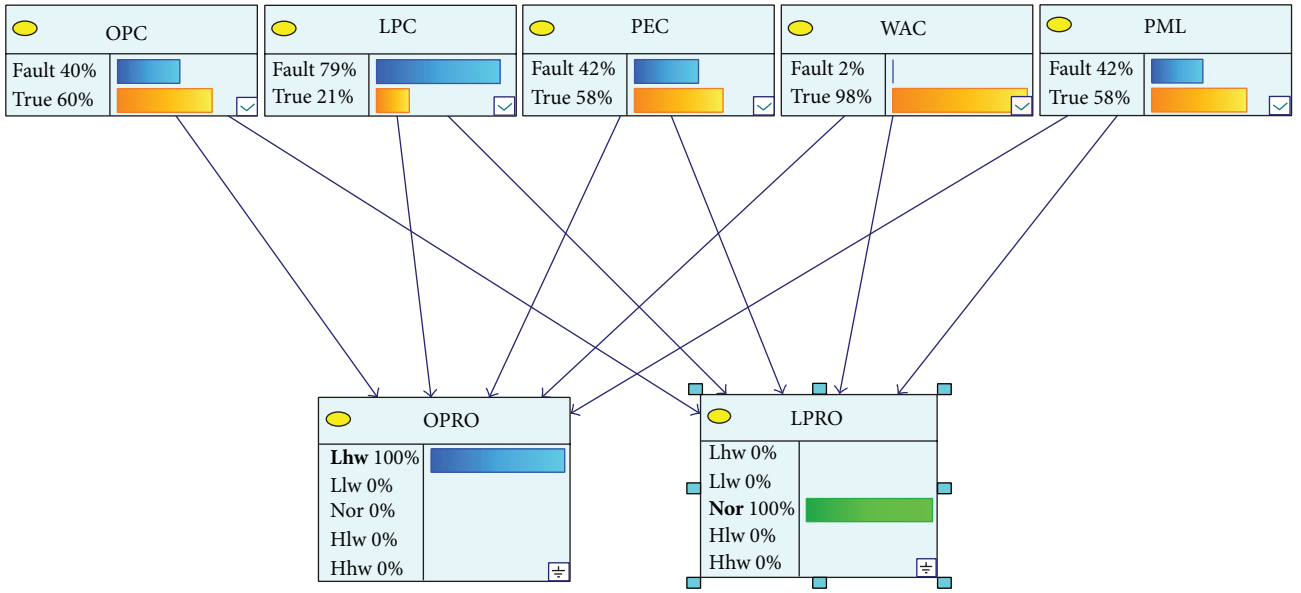

Figure 5: The posterior probability distribution under the evidence of OPRO heavy warning and LPRO Normal.

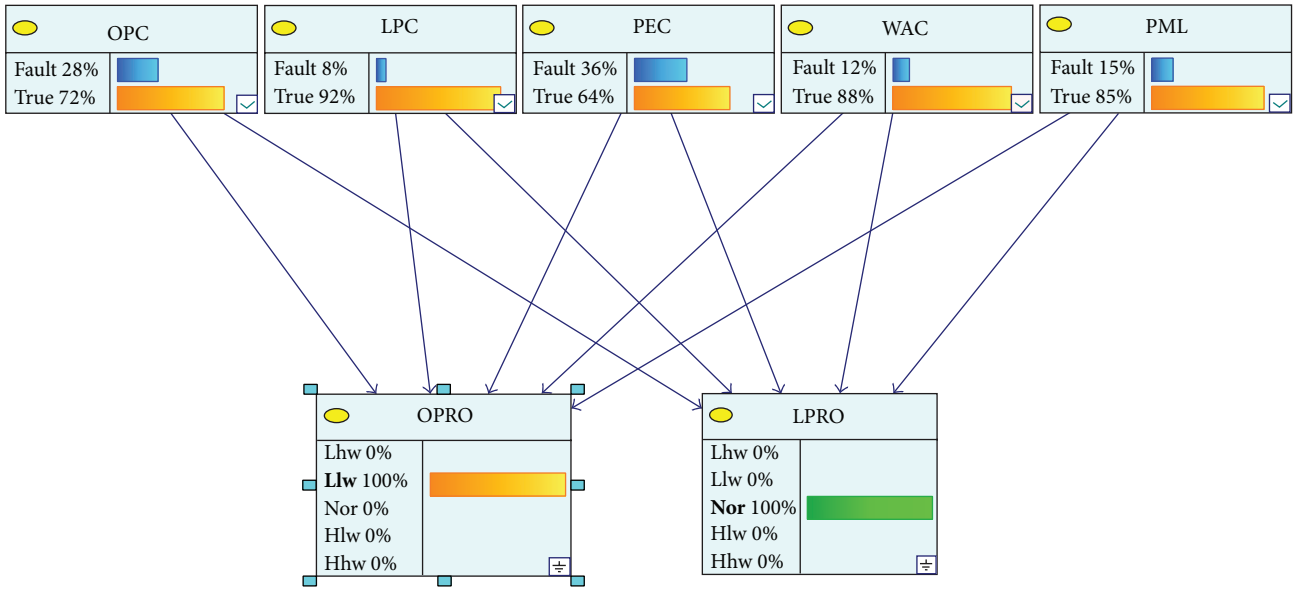

Figure 6: The posterior probability distribution under the evidence of OPRO light warning and LPRO Normal.

of PEC fault are 36%. Reasoning results are consistent with the reality.

Figure 7 shows that the most likely risk point which causes such evidence is WAC, for the posterior probabilities of WAC fault are 69%. Reasoning results correspond to the actual situation.

4.3.3. The Analysis of the Results. It can be drawn from the three-group reasoning results above that the most influential indexes are WAC and LPC in the high water-cut period of oilfield development. They contact closely with the amount of water injected, which are positively correlated. In other words, we can increase the water injection to raise the oil production in the later stages of oilfield development. The inference result is very consistent with the engineering practice.

5. Conclusion

Based on the studies for oilfield development risk forecasting and early warning of Bayesian network, we integrated the neural networks and Bayesian networks successfully to

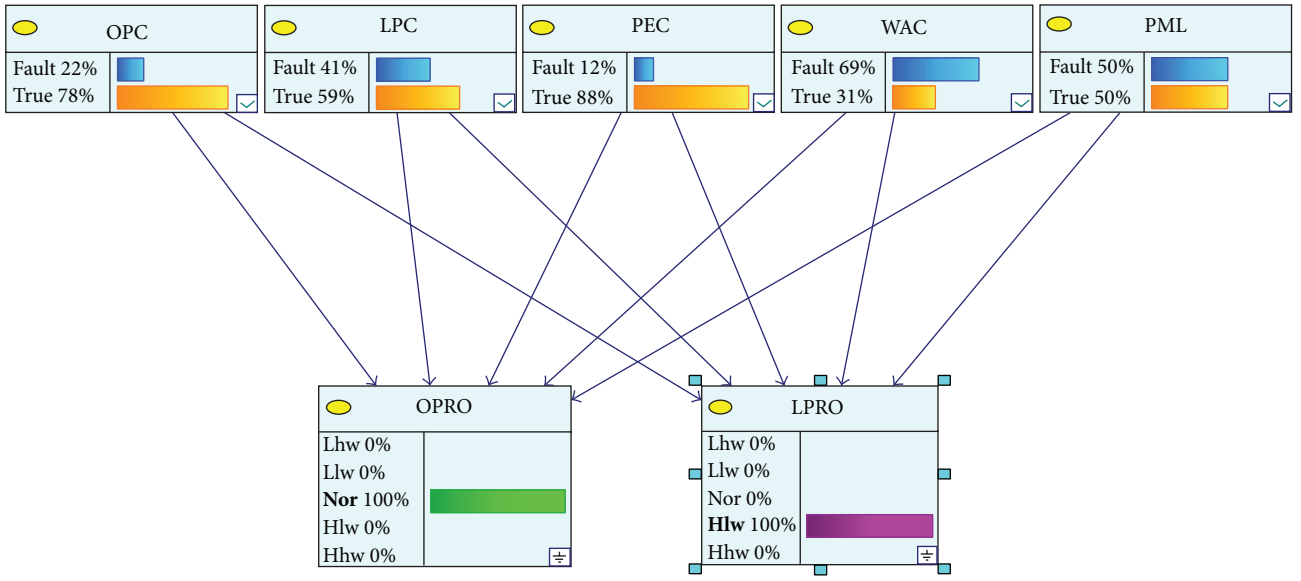

Figure 7: The posterior probability distribution under the evidence of OPRO Normal and LPRO light warning.

present a new method of forecasting and early warning of oilfield development risk. This method uses neural network to predict the warning situation indexes of oilfield development risk, uses "3σ" rule to determine the interval of risk warning degree, and uses Bayesian network to diagnose the reasons causing the risk. The case study shows that the new method proposed can provide help and guidance for discovering and controlling oilfield development risk. The revised BN method proposed by us is different from the existing BN method revised by fault trees or event trees or other methods. In the existing revised BN methods, the structure model and parameter of the Bayesian network are determined largely by fault trees or event trees or other methods, and the main purpose of the BN is to calculate posterior probability distribution of node (risk) after joining the evidence, while in our revised BN method, neural network is first used to predict warning situation indexes. Subsequently, ascertain the degree of the predicted value, and the degree value will be as input evidence of BN whose structure model is built by historical experience and parameter model based on the sample data to calculate the posterior probability distribution of node under the evidence. The future works may be to expand our research by introducing dynamic BN or to develop the software on oilfield development risk forecasting and early warning.

Conflict of Interests

The authors declare that there is no conflict of interests regarding the publication of this paper.

Acknowledgment

The authors are grateful for financial support from scientific research innovation team fund of Southwest Petroleum University (2013XJZT004): "The Optimization Theory and Control."

References

[1] F. Khan, S. Rathnayaka, and S. Ahmed, "Methods and models in process safety and risk management: past, present and future," *Process Safety and Environmental Protection*, vol. 98, pp. 116–147, 2015.

[2] F. Khan, S. Ahmed, M. Yang et al., "Safety challenges in harsh environments: lessons learned," *Process Safety Progress*, vol. 34, no. 2, pp. 191–195, 2015.

[3] M. Musharraf, D. Bradbury-Squires, F. Khan, B. Veitch, S. Mackinnon, and S. Imtiaz, "A virtual experimental technique for data collection for a Bayesian network approach to human reliability analysis," *Reliability Engineering and System Safety*, vol. 132, pp. 1–8, 2014.

[4] N. Khakzad, F. Khan, and P. Amyotte, "Quantitative risk analysis of offshore drilling operations: a Bayesian approach," *Safety Science*, vol. 57, pp. 108–117, 2013.

[5] M. Abimbola, F. Khan, N. Khakzad et al., "Safety and risk analysis of managed pressure drilling operation using Bayesian network," *Safety Science*, vol. 76, pp. 133–144, 2015.

[6] J. E. Vinnem, R. Bye, B. A. Gran et al., "Risk modelling of maintenance work on major process equipment on offshore petroleum installations," *Journal of Loss Prevention in the Process Industries*, vol. 25, no. 2, pp. 274–292, 2012.

[7] J. Bhandari, R. Abbassi, V. Garaniya, and F. Khan, "Risk analysis of deepwater drilling operations using Bayesian network," *Journal of Loss Prevention in the Process Industries*, vol. 38, pp. 11–23, 2015.

[8] N. Khakzad, F. Khan, and P. Amyotte, "Dynamic safety analysis of process systems by mapping bow-tie into Bayesian network," *Process Safety and Environmental Protection*, vol. 91, no. 1-2, pp. 46–53, 2013.

[9] H. Yu, F. Khan, and V. Garaniya, "Modified independent component analysis and bayesian network-based two-stage fault diagnosis of process operations," *Industrial & Engineering Chemistry Research*, vol. 54, no. 10, pp. 2724–2742, 2015.

[10] Z. Yuan, N. Khakzad, F. Khan, and P. Amyotte, "Risk analysis of dust explosion scenarios using Bayesian networks," *Risk Analysis*, vol. 35, no. 2, pp. 278–291, 2015.

[11] N. Khakzad, "Application of dynamic Bayesian network to risk analysis of domino effects in chemical infrastructures," *Reliability Engineering & System Safety*, vol. 138, pp. 263–272, 2015.

[12] N. Khakzad, S. Khakzad, and F. Khan, "Probabilistic risk assessment of major accidents: application to offshore blowouts in the Gulf of Mexico," *Natural Hazards*, vol. 74, no. 3, pp. 1759–1771, 2014.

[13] A.-A. Baksh, F. Khan, V. Gadag, and R. Ferdous, "Network based approach for predictive accident modelling," *Safety Science*, vol. 80, pp. 274–287, 2015.

[14] M. Kalantarnia, F. Khan, and K. Hawboldt, "Dynamic risk assessment using failure assessment and Bayesian theory," *Journal of Loss Prevention in the Process Industries*, vol. 22, no. 5, pp. 600–606, 2009.

[15] X. Yang, W. J. Rogers, and M. S. Mannan, "Uncertainty reduction for improved mishap probability prediction: application to level control of distillation unit," *Journal of Loss Prevention in the Process Industries*, vol. 23, no. 1, pp. 149–156, 2010.

[16] C. E. Alaneme and A. C. Igboanugo, "A fuzzy-logic theoretic approach to modelling marginal oilfield risks," *Research Journal of Applied Sciences, Engineering and Technology*, vol. 6, no. 4, pp. 557–567, 2013.

[17] S. M. M. Lavasani, Z. Yang, J. Finlay, and J. Wang, "Fuzzy risk assessment of oil and gas offshore wells," *Process Safety and Environmental Protection*, vol. 89, no. 5, pp. 277–294, 2011.

[18] D. J. C. Mackay, "Probable networks and plausible predictions—a review of practical bayesian methods for supervised neural networks," *Network: Computation in Neural Systems*, vol. 6, no. 3, pp. 469–505, 1995.

[19] R. M. Neal, *Bayesian Learning for Neural Networks*, Springer, New York, NY, USA, 1996.

[20] J. F. G. Freitas, *Bayesian methods for neural networks [Ph.D. thesis]*, Trinity College University of Cambridge and Cambridge University Engineering Department, Cambridge, UK, 2000.

[21] N. Chitsazan, A. A. Nadiri, and F. T.-C. Tsai, "Prediction and structural uncertainty analyses of artificial neuralnetworks using hierarchical Bayesian model averaging," *Journal of Hydrology*, vol. 528, pp. 52–62, 2015.

[22] J. L. Ticknor, "A Bayesian regularized artificial neural network for stock market forecasting," *Expert Systems with Applications*, vol. 40, no. 14, pp. 5501–5506, 2013.

[23] C. Maschio and D. J. Schiozer, "Bayesian history matching using artificial neural network and Markov Chain Monte Carlo," *Journal of Petroleum Science and Engineering*, vol. 123, pp. 62–71, 2014.

[24] W. Mingda, C. Guoming, F. Jianmin, and L. Weijun, "Safety analysis approach of MFM-HAZOP and its application in the dehydration system of oilfield united station," *Procedia Engineering*, vol. 43, pp. 437–442, 2012.

[25] R. Sadiq, T. Husain, B. Veitch, and N. Bose, "Risk-based decision-making for drilling waste discharges using a fuzzy synthetic evaluation technique," *Ocean Engineering*, vol. 31, no. 16, pp. 1929–1953, 2004.

[26] J. Kang, W. Liang, L. Zhang et al., "A new risk evaluation method for oil storage tank zones based on the theory of two types of hazards," *Journal of Loss Prevention in the Process Industries*, vol. 29, no. 1, pp. 267–276, 2014.

[27] J. E. Horner, J. W. Castle, and J. H. Rodgers Jr., "A risk assessment approach to identifying constituents in oilfield produced water for treatment prior to beneficial use," *Ecotoxicology and Environmental Safety*, vol. 74, no. 4, pp. 989–999, 2011.

[28] D. Baca and K. Petersen, "Countermeasure graphs for software security risk assessment: an action research," *Journal of Systems and Software*, vol. 86, no. 9, pp. 2411–2428, 2013.

[29] T. Wang, P. Wang, J. Meng et al., "A review of sources, multimedia distribution and health risks of perfluoroalkyl acids (PFAAs) in China," *Chemosphere*, vol. 129, pp. 87–99, 2015.

[30] D. Kim, S. Kim, and T. Yoo, "Osteoarthritis and cartilage," in *Proceedings of the World Congress of the Osteoarthritis Research Society International (OARSI '14)*, p. S379, Elsevier Science, Paris, France, April 2014.

[31] R. S. Targino, G. W. Peters, and P. V. Shevchenko, "Sequential Monte Carlo samplers for capital allocation under copula-dependent risk models," *Insurance: Mathematics and Economics*, vol. 61, pp. 206–226, 2015.

[32] M. Hofmann, R. Lux, and H. R. Schultz, "Constructing a framework for risk analyses of climate change effects on the water budget of differently sloped vineyards with a numeric simulation using the Monte Carlo method coupled to a water balance model," *Frontiers in Plant Science*, vol. 5, article 645, 2014.

[33] E. J. D. S. Pereira, J. T. Pinho, M. A. B. Galhardo, and W. N. Macêdo, "Methodology of risk analysis by Monte Carlo Method applied to power generation with renewable energy," *Renewable Energy*, vol. 69, pp. 347–355, 2014.

[34] L. Han, Y. Song, L. Duan, and P. Yuan, "Risk assessment methodology for Shenyang Chemical Industrial Park based on fuzzy comprehensive evaluation," *Environmental Earth Sciences*, vol. 73, no. 9, pp. 5185–5192, 2015.

[35] Y. Wang, J. Zhang, E. Guo, and Z. Sun, "Fuzzy comprehensive evaluation-based disaster risk assessment of desertification in Horqin Sand Land, China," *International Journal of Environmental Research and Public Health*, vol. 12, no. 2, pp. 1703–1725, 2015.

[36] A. C. Constantinou, N. E. Fenton, and M. Neil, "Profiting from an inefficient association football gambling market: prediction, risk and uncertainty using Bayesian networks," *Knowledge-Based Systems*, vol. 50, pp. 60–86, 2013.

[37] E. Sharifahmadian and S. Latifi, "Water environment risk prediction using Bayesian network," in *Proceedings of the IEEE SoutheastCon*, pp. 1–5, Jacksonville, Fla, USA, April 2013.

[38] Z. Zhao, Z. Liu, J. Xu, and H. Jiang, "Analysis and prediction of Block detection indexes," in *Early Warning Dynamic System in the Oilfield Development*, Z. Zhiyong, Ed., Petroleum Industry Press, Beijing, China, 2010.

[39] Y. Zhong, *Research on the Dynamic Prediction Methods for Extra High Water Cut Oilfield Development Planning*, Southwest Petroleum University, 2008.

[40] J. Botzheim and P. Földesi, "Novel calculation of fuzzy exponent in the sigmoid functions for fuzzy neural networks," *Neurocomputing*, vol. 129, pp. 458–466, 2014.

[41] D. Xia, L. Kong, Y. Hu, and P. Ni, "Silicon microgyroscope temperature prediction and control system based on BP neural network and fuzzy-PID control method," *Measurement Science & Technology*, vol. 26, no. 2, Article ID 025101, 2015.

[42] R. Lehmann, "3 Sigma-rule for outlier detection from the viewpoint of geodetic adjustment," *Journal of Surveying Engineering*, vol. 139, no. 4, pp. 157–165, 2013.

[43] D. Fu, "Research on the learning algorithm of Bayesian Network," *Journal of Daqing Normal University*, vol. 31, no. 3, pp. 36–38, 2011.

[44] M. R. Martins, A. M. Schleder, and E. L. Droguett, "A methodology for risk analysis based on hybrid bayesian networks: application to the regasification system of liquefied natural gas onboard a floating storage and regasification unit," *Risk Analysis*, vol. 34, no. 12, pp. 2098–2120, 2014.

[45] X. Li, "Research on learning Bayesian network parameters," *Journal of Shenyang Agricultural University*, vol. 38, no. 1, pp. 125–128, 2007.

Hindawi Publishing Corporation
Mathematical Problems in Engineering
Volume 2016, Article ID 1718257, 10 pages
http://dx.doi.org/10.1155/2016/1718257

Research Article

Risk Analysis Based on AHP and Fuzzy Comprehensive Evaluation for Maglev Train Bogie

Chengxin Fan, Fengshan Dou, Baiming Tong, and Zhiqiang Long

Engineering Research Center of Maglev Technology, College of Mechatronics Engineering and Automation, National University of Defense Technology, Changsha 410073, China

Correspondence should be addressed to Zhiqiang Long; lzq@maglev.cn

Received 15 September 2015; Revised 17 December 2015; Accepted 22 December 2015

Academic Editor: Jurgita Antucheviciene

The maglev bogie is the key subsystem for maglev train security. To ensure life and property security, it is essential to evaluate its risk level before its operation. In this paper, a combinational method of analytic hierarchy process and fuzzy comprehensive evaluation is proposed to assess hazards in a complex maglev bogie system associated with multiple subsystems' failures. The very comprehensive identification of risk sources has been done by analyzing the structure of maglev bogie. Furthermore, based on the fuzzy theory, linguistic evaluation set is classified according to risk tolerance. The score of each risk factor is obtained by weighted sum of the result of fuzzy comprehensive evaluation. Our results show that the degree of maglev bogie's risk is within the range of acceptability. The merits of this work facilitate finding the weak links and determining the maintenance of maglev bogie system.

1. Introduction

Rail safety and reliability are highly related to national development, and the lives and property of people. As a new kind of railway vehicle, the maglev train faced the difficulties which form the performance analysis of safety due to lack of experiences on the long-term operations. Hence, the safety analysis should be carried out through the risk analysis, which is very different from that for the traditional train. Maglev train system includes a number of subsystems, where the bogie that has a significant impact on maglev train safety is an important part. In this paper, we focus on the risk analysis of low-medium speed maglev train bogie.

In recent years, several researchers have carried out investigations to gain a deep insight into the reliability evaluation of a bogie frame. Han et al. evaluated experimentally static strength for bogie frame of an urban maglev train including performing fatigue analysis, cumulative damage, and fatigue test based on a developed fatigue load and as a final outcome, aimed at proposing a fatigue strength evaluation method for the bogie frame of urban maglev [1]. Cui et al. corroborated the carrying capacity of a maglev train on the horizontal curve through the analysis of a single magnetic bogie to ensure reliability and safety [2]. However, the research about the risk analysis of low-medium speed maglev train bogie has been rarely done from a holistic point of view.

Since we realize that describing the reason of a bogie failure is a difficult issue because of comprehensive risk sources, for example, it is more complex to describe failures by a chain of events in a modeling process [1]. Furthermore, the probabilities of various basic events are difficult to collect and estimate. As a result, some common methods are unsuitable for the risk analysis of bogie system. In this case, it is necessary to propose a risk analysis method which is able to handle multiple factors and fuzziness combined with quantitative analysis. Hence, fuzzy set theory [3] is a useful tool to deal with imprecise and uncertain data. Meanwhile, analytic hierarchy process (AHP), proposed by Saaty [4], is a practical decision-making method [5, 6]. The AHP could handle uncertain, imprecise, and subjective data and it also has robustness when solving practical ranking problems [7]. Fuzzy comprehensive evaluation (FCE) is a common method to analyze the risk of the environmental resources and construction of bridges, mines, and dams [8, 9]. It is also used in the safety areas of public facilities and transportation [10, 11]. Song et al. corroborated that the triangular extent fuzzy AHP approach was more effective to evaluate self-ignition risks of coal piles than the trapezoidal fuzzy AHP method.

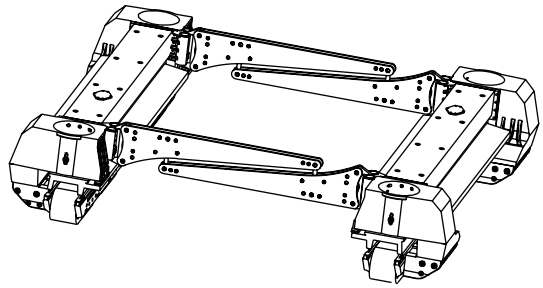

Figure 1: Bogie structure of low-medium speed maglev train.

They evaluated self-ignition risks of coal piles from a holistic point of view [12]. Yang et al. constructed a combination of AHP and FCE method to evaluate road transport system vulnerability against meteorological disasters from the view of risk analysis theory [13]. In our study, to overcome the complexity of structure and the uncertainty of various basic events' probabilities, a combinational method of AHP and FCE is proposed.

In Section 2, the maglev bogie structure and the relevant risk sources are analyzed. In Section 3, the three-layer hierarchical model is established to compute the weights distribution by using AHP. In Section 4, the risk degree of maglev bogie is assessed by using FCE. Finally, the discussion and concluding remarks are given in Sections 5 and 6.

2. Risk Source Analysis of Maglev Bogie

2.1. The Structure of a Maglev Bogie. Low-medium speed maglev train has five bogies. Air springs are installed on the four corners of each bogie. The bogies are connected with cars by 20 air springs, and the air suspension system consists of vertical and horizontal rod and steering mechanism. The bogies are not only the chassis of a train, but also the mounting platform of linear motors, solenoids, air springs, and other important power subassemblies. The bogies play an important role in delivering suspension force and steering force. Meanwhile, they also exert effect on geometric decoupling.

Figure 1 shows bogie structure of low-medium speed maglev train. A bogie consists of two left and two right modules which are connected together by two anti-roll beams. Each module consists of a linear motor beam, corbel, corbel connection, integrated bracket, transverse rod seat bracket, supporting slider, and hydraulic supporting wheel. The linear motor beam, corbel, and corbel connection are connected by bolts. The corbel connection and electromagnet are connected by keys and secured by bolts. The integrated bracket, corbel, and linear motor beam are connected together. The antiroll beam is installed outside the integrated bracket. The hydraulic supporting wheel is installed inside it. Antiroll beams are connected by suspenders. The linear motor is hanged by eight bolts in the lower part of linear motor beam [2].

2.2. Risk Source Analysis. According to the analysis of bogie structure, the main failures of bogie system and the reasons and consequences of these failures are as follows [14].

2.2.1. Corbel. The main reasons of corbel damage are foundry lacuna, fracture, losing suspension point, and split of wire rope seat. The corbel's damage and fracture may lead to air spring and electromagnet falling on track. Severe cases may cause train's damage and even casualties.

2.2.2. Corbel Connection. The faults of corbel connection are mainly due to the internal foundry lacuna and the damage of fatigue. The faults may lead to electromagnet's shedding. Severe cases may cause train's damage and even casualties.

2.2.3. Integrated Bracket. The main reasons of integrated bracket fracture are foundry lacuna and fatigue. This failure may lead to antiroll beam failing to connect with the left and right modules and disbanding of bogie structure. Severe cases may cause train's damage and even casualties.

2.2.4. Antiroll Beam. The causes of antiroll beam's fracture may be quality's defect and damage of knocking. If these faults happen, they will influence train's operation. They may cause train's damage and even casualties, especially when antiroll beam stuck between sleeper and train [15].

2.2.5. Linear Motor. The foundry lacuna and fatigue of linear motor beam can lead to the faults of linear motor. Snow and other obstructions on the track may lead to linear motor's burning out. The failures of linear motor may lead to losing power. Severe cases may cause train's damage and even casualties.

2.2.6. Electromagnet. The link package of electromagnet may have overcurrent faults. The outer plates of electromagnet and inner plates of electromagnet may be collided with obstacles. The failures of electromagnet may lead to critical consequences, such as abnormal suspension, train's smoking, and outbreak of a fire.

2.2.7. Air Spring. The main reasons of air spring's burst may be external force and aging. The failures of air spring may lead to train's abnormal operation, and the train may slow down or be rescued back to a maintenance location.

2.2.8. Mechanical Brake. The main reason of mechanical brake failure is screws' loosening of the outer plate of electromagnet. When the train carries out air brake, mechanical brake failure may lead to insufficient braking force. If the air brake and electric brake are both ineffective in extreme cases, the train will only execute brake by falling on the track. Therefore, normal train's operations will be interrupted [16].

The most of risk sources described above are foundry lacuna and abrasion of mechanical parts. These risk sources all can lead to the failures of maglev bogie. As a result, there are multiple initiating events. It is more complex to describe failures by a chain of events in a modeling process [1]. Furthermore, the probabilities of various basic events are difficult to collect and estimate. Hence, some common risk analysis techniques, for example, event tree analysis (ETA) and fault tree analysis (FTA), are not suitable for the risk analysis of bogie system. However, AHP and its extensions

were developed to solve alternative selection criteria and justification issues that are capable of capturing a human's appraisal of ambiguity when complex multicriteria decision-making problems are considered [9, 17]. FCE is an effective method which can use the experiences of engineers and analysts to express the uncertain relations of risk analysis [18]. It can give the level of risk for this system qualitatively. Therefore, this paper employs AHP and FCE to analyze the risk for maglev bogie system.

3. Establishment of Analytic Hierarchy Process for Maglev Bogie

3.1. Establishment of the Level Hierarchical Model. According to the analysis of the structure of maglev bogie, the eight sources of maglev bogie risk have been found, because there are a few subsystems' devices installed on the maglev bogie. These devices' faults can reduce different size risks. In order to analyze the contribution degree for total risk from each subsystem, it is essential to classify risk sources in accordance with the subsystems. The subsystems include the supporting unit, drive unit, architecture, brake unit, and suspension unit. The fifth risk source includes linear motor and linear motor beam. The linear motor and linear motor beam are part of drive unit. Meanwhile, the linear motor beam is also part of the architecture of maglev bogie. The sixth risk source includes line package, outer plates of electromagnet, and inner plates of electromagnet. These three factors are part of suspension unit. Because mechanical braking device is installed on the outer plate of electromagnet, the outer plate of electromagnet can affect brake unit at the same time. Therefore, there are 11 factors included in the five subsystems. The relationship between the 11 factors and the five subsystems are as follows:

(i) The support unit is a component or structure on the bogie which provides support for the quadratic suspension system. The structure of support unit includes air spring and corbel, and the air spring is installed in the corbel.

(ii) The drive unit is a component or structure which is used to drive maglev train. Linear motor and linear motor beam are part of drive unit. The linear motor is installed on the linear motor beam.

(iii) The architecture is the main mechanical structure of maglev bogie. It includes linear motors beam, corbel, integrated bracket, antiroll beam, and corbel connection. The integrated bracket is installed on the corbel. The antiroll beam is connected with the integrated bracket. The corbel connection is installed on the corbel.

(iv) The brake unit is the component which is installed on the bogie for braking. Mechanical braking device, outer plate of electromagnet, and corbel connection are part of brake unit. Mechanical braking device is installed on the outer plate of electromagnet. The outer plate of electromagnet is connected with the main structure of bogie by corbel connection.

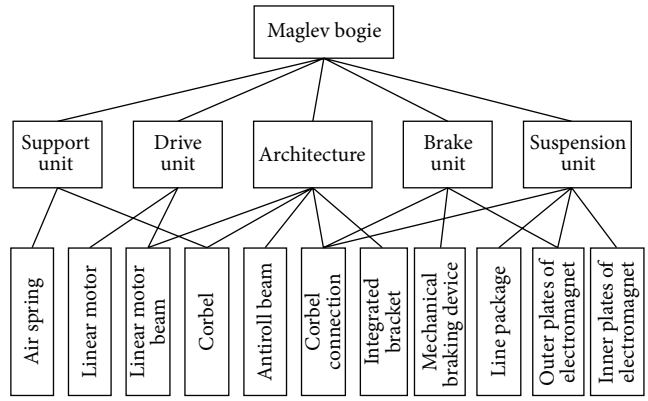

Figure 2: Level hierarchical model of bogie.

(v) The suspension unit provides vertical suspension force for maglev train. Link package, outer plates of electromagnet, inner plates of electromagnet, and corbel connection are part of the suspension unit. The suspension electromagnet line package and core are installed between the inner plates of electromagnet and outer plates of electromagnet. The inner plates of electromagnet and outer plates of electromagnet are connected with the main structure of bogie by corbel connections.

Accordingly, a three-layer hierarchical model is established to describe maglev bogie reasonably [19, 20]. The target layer is the risk of maglev bogie. The first layer (criterion layer) is the subsystems of maglev bogie, which includes the supporting unit, drive unit, architecture, brake unit, and suspension unit. The second layer (scheme layer) includes air spring, linear motor, linear motor beam, corbel, antiroll beam, corbel connection, integrated bracket, mechanical braking device, line package, outer plates of electromagnet, and inner plates of electromagnet.

The level hierarchical model of bogie is shown in Figure 2.

To describe the hierarchical model more clearly, we give the corresponding notations in Table 1.

The set of factors can be represented as

$$\mathbf{U} = \left\{u_{i1}^{(l)}, u_{i2}^{(l)}, \ldots, u_{in_i}^{(l)}\right\}, \tag{1}$$

where $u_{in_i}^{(l)}$ is the n factor of the l layer dominated by the i factor of the $l-1$ layer.

The weight vector of factors is represented as

$$\begin{aligned} \mathbf{W} &= \left\{w_1^{(l)}, w_2^{(l)}, \ldots, w_n^{(l)}\right\}, \\ \mathbf{A} &= \left\{a_1^{(l)}, a_2^{(l)}, \ldots, a_n^{(l)}\right\}, \end{aligned} \tag{2}$$

where $\mathbf{W}$ is the weight which is determined by normalizing the eigenvector and $\mathbf{A}$ is the weight vector of factors.

3.2. Calculation of Factors' Weights under a Single Criterion

3.2.1. Determination of the Weights of the Second Layer Factor Set with respect to the First Layer Criterion Set. It is assumed that the factor $u_i^{(l-1)}$ of the $l-1$ layer is a criterion. The next

Table 1: Factor set partitions and symbolic representations of bogie's level hierarchical mode.

Target layer	Layer 1 (criterion layer)		Layer 2 (scheme layer)	
	Factor	Weight	Factor	Weight
The risk of maglev bogie	Support unit $u_1^{(1)}$	$w_1^{(1)}a_1^{(1)}$	Air spring, $u_{11}^{(2)}$ or $u_1^{(2)}$	$w_{11}^{(2)}$ or $w_1^{(2)}$, $a_1^{(2)}$
			Corbel, $u_{12}^{(2)}$ or $u_4^{(2)}$	$w_{12}^{(2)}$ or $w_4^{(2)}$, $a_4^{(2)}$
	Drive unit $u_2^{(1)}$	$w_2^{(1)}a_2^{(1)}$	Linear motor, $u_{21}^{(2)}$ or $u_2^{(2)}$	$w_{21}^{(2)}$ or $w_2^{(2)}$, $a_2^{(2)}$
			Linear motor beam, $u_{22}^{(2)}$ or $u_3^{(2)}$	$w_{22}^{(2)}$ or $w_3^{(2)}$, $a_3^{(2)}$
	Architecture $u_3^{(1)}$	$w_3^{(1)}a_3^{(1)}$	Linear motor, $u_{31}^{(2)}$ or $u_2^{(2)}$	$w_{31}^{(2)}$ or $w_2^{(2)}$, $a_2^{(2)}$
			Corbel, $u_{32}^{(2)}$ or $u_4^{(2)}$	$w_{23}^{(2)}$ or $w_4^{(2)}$, $a_4^{(2)}$
			Antiroll beam, $u_{33}^{(2)}$ or $u_5^{(2)}$	$w_{33}^{(2)}$ or $w_5^{(2)}$, $a_5^{(2)}$
			Corbel connection, $u_{34}^{(2)}$ or $u_6^{(2)}$	$w_{34}^{(2)}$ or $w_6^{(2)}$, $a_6^{(2)}$
			Integrated bracket, $u_{35}^{(2)}$ or $u_7^{(2)}$	$w_{35}^{(2)}$ or $w_7^{(2)}$, $a_7^{(2)}$
	Brake unit $u_4^{(1)}$	$w_4^{(1)}a_4^{(1)}$	Corbel connection, $u_{41}^{(2)}$ or $u_6^{(2)}$	$w_{41}^{(2)}$ or $w_6^{(2)}$, $a_6^{(2)}$
			Outer plates of electromagnet, $u_{42}^{(2)}$ or $u_{10}^{(2)}$	$w_{42}^{(2)}$ or $w_{10}^{(2)}$, $a_{10}^{(2)}$
			Mechanical braking device, $u_{43}^{(2)}$ or $u_8^{(2)}$	$w_{43}^{(2)}$ or $w_8^{(2)}$, $a_8^{(2)}$
	Suspension unit $u_5^{(1)}$	$w_5^{(1)}a_5^{(1)}$	Corbel connection, $u_{51}^{(2)}$ or $u_6^{(2)}$	$w_{51}^{(2)}$ or $w_6^{(2)}$, $a_6^{(2)}$
			Line package, $u_{52}^{(2)}$ or $u_9^{(2)}$	$w_{52}^{(2)}$ or $w_9^{(2)}$, $a_9^{(2)}$
			Outer plates of electromagnet, $u_{53}^{(2)}$ or $u_{10}^{(2)}$	$w_{53}^{(2)}$ or $w_{10}^{(2)}$, $a_{10}^{(2)}$
			Inner plates of electromagnet, $u_{54}^{(2)}$ or $u_{11}^{(2)}$	$w_{54}^{(2)}$ or $w_{11}^{(2)}$, $a_{11}^{(2)}$

layer factors $u_{i1}^{(l)}, u_{i2}^{(l)}, \ldots, u_{in_i}^{(l)}$ are dominated by the criterion. The judgment matrix is determined by comparing relative importance between two arbitrary factors from $u_{i1}^{(l)}, u_{i2}^{(l)}, \ldots, u_{in_i}^{(l)}$ [4].

In this study, the judgment matrix is determined by expert decision along with field investigation and other related research results [16], given as follows:

$$\mathbf{C}_1^{(1)} = \begin{bmatrix} 1 & 5 \\ \frac{1}{5} & 1 \end{bmatrix}, \tag{3}$$

where $\mathbf{C}_1^{(1)}$ is the judgment matrix of the first layer's first factor.

The maximum eigenvalue, $\lambda_{1,\max}^{(1)} = 2$, is determined by $\mathbf{C}_1^{(1)}$.

The eigenvector can be calculated by

$$\mathbf{C}_i^{(l-1)} w_i'^{(l-1)} = \lambda_{i,\max}^{(l-1)} w_i'^{(l-1)}, \tag{4}$$

where $\mathbf{C}_i^{(l-1)}$ the judgment matrix, $\lambda_{i,\max}^{(l-1)}$ is the maximum eigenvalue, and $w_i'^{(l-1)}$ is the eigenvector [4].

$w_1^{(1)}$ is the weight which is determined by normalizing the eigenvector:

$$w_1^{(1)} = \left[w_{11}^{(2)}, w_{12}^{(2)}\right]^T = [0.8333, 0.1667]^T. \tag{5}$$

It is essential to check the consistency of the judgment matrix to ensure that the calculated weights are acceptable. The consistency ratio can be determined by

$$\begin{aligned} \mathbf{C.I.}_1^{(1)} &= \frac{\lambda_{1,\max}^{(1)} - n_1^{(l)}}{n_1^{(l)} - 1} = 0, \\ \mathbf{C.R.}_1^{(1)} &= \frac{\mathbf{C.I.}_1^{(1)}}{\mathbf{R.I.}_1^{(1)}} = 0 < 0.1, \end{aligned} \tag{6}$$

where $\mathbf{C.I.}_1^{(1)}$ is the consistency index, $\mathbf{R.I.}_1^{(1)}$ is the random index, and $\mathbf{C.R.}_1^{(1)}$ is the consistency ratio (C.R.). Saaty has proposed a consistency index (CI) and calculated the random indices shown in Table 2 [4].

Table 2: The random consistency index (R.I.).

Size	1	2	3	4	5	6	7	8	9
R.I.	0	0	0.52	0.89	1.12	1.26	1.36	1.41	1.46

The consistency of the judgment matrix is acceptable only if $\mathbf{C.R.} < 0.1$. Hence, $\mathbf{C}_1^{(1)}$ satisfies consistency requirement.

Similarly, based on the AHP which is introduced by Saaty [4], the other four judgment matrixes and their consistency are given as

$$\begin{aligned} \mathbf{C}_2^{(1)} &= \begin{bmatrix} 1 & 5 \\ \frac{1}{5} & 1 \end{bmatrix}, \\ \lambda_{2,\max}^{(1)} &= 2, \\ w_2^{(1)} &= \left[w_{21}^{(2)}, w_{22}^{(2)}\right]^T = [0.8333, 0.1667]^T, \\ \mathbf{C.I.}_2^{(1)} &= \frac{\lambda_{2,\max}^{(1)} - n_2^{(1)}}{n_2^{(1)} - 1} = 0, \\ \mathbf{C.R.}_2^{(1)} &= \frac{\mathbf{C.I.}_2^{(1)}}{\mathbf{R.I.}_2^{(1)}} = 0 < 0.1. \end{aligned} \tag{7}$$

Hence, $\mathbf{C}_2^{(1)}$ satisfies consistency requirement. Consider

$$\mathbf{C}_3^{(1)} = \begin{bmatrix} 1 & 2 & \frac{1}{5} & \frac{1}{2} & \frac{1}{5} \\ \frac{1}{2} & 1 & \frac{1}{3} & \frac{1}{5} & \frac{1}{5} \\ 5 & 3 & 1 & 1 & 1 \\ 2 & 5 & 1 & 1 & 1 \\ 5 & 5 & 1 & 1 & 1 \end{bmatrix},$$

$$\begin{aligned}
\lambda_{3,\max}^{(1)} &= 5.1703,\\
w_3^{(1)} &= \left[w_{31}^{(2)}, w_{32}^{(2)}, w_{33}^{(2)}, w_{34}^{(2)}, w_{35}^{(2)}\right]^T\\
&= [0.0884, 0.0605, 0.2852, 0.2573, 0.3086]^T,\\
\mathbf{C.I.}_3^{(1)} &= \frac{\lambda_{3,\max}^{(1)} - n_3^{(1)}}{n_3^{(1)} - 1} = 0.0426,\\
\mathbf{C.R.}_3^{(1)} &= \frac{\mathbf{C.I.}_3^{(1)}}{\mathbf{R.I.}_3^{(1)}} = \frac{5.1703}{1.12} = 0.0380 < 0.1.
\end{aligned} \tag{8}$$

Hence, $\mathbf{C}_3^{(1)}$ satisfies consistency requirement. Consider

$$\mathbf{C}_4^{(1)} = \begin{bmatrix} 1 & 3 & 7\\ \frac{1}{3} & 1 & 5\\ \frac{1}{7} & \frac{1}{5} & 1 \end{bmatrix},$$

$$\begin{aligned}
\lambda_{4,\max}^{(1)} &= 3.0649,\\
w_4^{(1)} &= \left[w_{41}^{(2)}, w_{42}^{(2)}, w_{43}^{(2)}\right]^T\\
&= [0.6491, 0.2790, 0.0719]^T,\\
\mathbf{C.I.}_4^{(1)} &= \frac{\lambda_{4,\max}^{(1)} - n_4^{(1)}}{n_4^{(1)} - 1} = 0.0324,\\
\mathbf{C.R.}_4^{(1)} &= \frac{\mathbf{C.I.}_4^{(1)}}{\mathbf{R.I.}_4^{(1)}} = \frac{0.0324}{0.52} = 0.0624 < 0.1.
\end{aligned} \tag{9}$$

Hence, $\mathbf{C}_4^{(1)}$ satisfies consistency requirement. Consider

$$\mathbf{C}_5^{(1)} = \begin{bmatrix} 1 & 1 & 5 & 7\\ 1 & 1 & 3 & 5\\ \frac{1}{5} & \frac{1}{3} & 1 & 3\\ \frac{1}{7} & \frac{1}{5} & \frac{1}{3} & 1 \end{bmatrix},$$

$$\begin{aligned}
\lambda_{4,\max}^{(1)} &= 4.0820,\\
w_5^{(1)} &= \left[w_{51}^{(2)}, w_{52}^{(2)}, w_{53}^{(2)}, w_{54}^{(2)}\right]^T\\
&= [0.4532, 0.3633, 0.1253, 0.0581]^T,\\
\mathbf{C.I.}_5^{(1)} &= \frac{\lambda_{5,\max}^{(1)} - n_5^{(1)}}{n_5^{(1)} - 1} = 0.0273,\\
\mathbf{C.R.}_5^{(1)} &= \frac{\mathbf{C.I.}_5^{(1)}}{\mathbf{R.I.}_5^{(1)}} = \frac{0.0273}{0.89} = 0.0307 < 0.1.
\end{aligned} \tag{10}$$

Hence, $\mathbf{C}_5^{(1)}$ satisfies consistency requirement.

3.2.2. Determination of the Weights of the First Layer Criterion Set with respect to the Target Set. The judgment matrix is given as follows:

$$\mathbf{C}^{(0)} = \begin{bmatrix} 1 & \frac{1}{3} & \frac{1}{5} & 3 & \frac{1}{6}\\ 3 & 1 & \frac{1}{5} & 1 & \frac{1}{5}\\ 5 & 5 & 1 & 6 & 1\\ \frac{1}{3} & 1 & \frac{1}{6} & 1 & \frac{1}{5}\\ 6 & 5 & 1 & 5 & 1 \end{bmatrix}. \tag{11}$$

The results of the maximum eigenvalue and weight vector are given as

$$\begin{aligned}
\lambda_{\max}^{(0)} &= 5.4135,\\
w^{(0)} &= \left[w_1^{(1)}, w_2^{(1)}, w_3^{(1)}, w_4^{(1)}, w_5^{(1)}\right]^T\\
&= [0.0805, 0.1027, 0.3762, 0.0608, 0.3798]^T.
\end{aligned} \tag{12}$$

The consistency ratio can be determined by

$$\begin{aligned}
\mathbf{C.I.}^{(0)} &= \frac{\lambda_{\max}^{(0)} - n^{(0)}}{n^{(0)} - 1} = 0.1034,\\
\mathbf{C.R.}^{(0)} &= \frac{\mathbf{C.I.}^{(0)}}{\mathbf{R.I.}^{(0)}} = \frac{0.1034}{1.12} = 0.0923 < 0.1.
\end{aligned} \tag{13}$$

Hence, $\mathbf{C}^{(0)}$ satisfies consistency requirement.

3.3. Calculation of Combining Weights of Each Layer Factor. The weight of the first layer factors with respect to the total target is $\mathbf{A}^{(1)} = w^{(0)}$. The single criterion layer weights of the second layer factors are as follows:

$$\begin{aligned}
\overline{w}_1^{(1)} &= \left[w_1^{(2)}, w_2^{(2)}, \ldots, w_{n_l}^{(2)}\right]^T\\
&= \left[0.8333 \;\; 0 \;\; 0 \;\; 0.1667 \;\; 0 \;\; 0 \;\; 0 \;\; 0 \;\; 0 \;\; 0 \;\; 0\right]^T,
\end{aligned} \tag{14}$$

where $\overline{w}_1^{(1)}$ is the weight vector of the first layer's first factor in a single order and n_l is the number of factors in l ($l = 2$) layer. The factors dominated by an upper layer are nonzero:

$$\begin{aligned}
&\overline{w}_2^{(1)} = \left[0 \;\; 0.8333 \;\; 0.1667 \;\; 0 \;\; 0 \;\; 0 \;\; 0 \;\; 0 \;\; 0 \;\; 0 \;\; 0\right]^T,\\
&\overline{w}_3^{(1)}\\
&= \left[0 \;\; 0 \;\; 0.0884 \;\; 0.0605 \;\; 0.2852 \;\; 0.2573 \;\; 0.3086 \;\; 0 \;\; 0 \;\; 0 \;\; 0\right]^T,\\
&\overline{w}_4^{(1)} = \left[0 \;\; 0 \;\; 0 \;\; 0 \;\; 0 \;\; 0.6491 \;\; 0.2790 \;\; 0.0719 \;\; 0 \;\; 0 \;\; 0\right]^T,\\
&\overline{w}_5^{(1)} = \left[0 \;\; 0 \;\; 0 \;\; 0 \;\; 0 \;\; 0.4532 \;\; 0 \;\; 0 \;\; 0.3633 \;\; 0.1253 \;\; 0.0581\right]^T,\\
&\mathbf{W}^{(2)} = \left[\overline{w}_1^{(1)} \;\; \overline{w}_2^{(1)} \;\; \cdots \;\; \overline{w}_{n_{l-1}}^{(1)}\right],
\end{aligned} \tag{15}$$

where $\mathbf{W}^{(2)}$ is a $n_l \times n_{l-1}$ matrix and n_{l-1} is the number of factors in $l-1$ ($l = 2$) layer.

The weight vector of the second layer factors with respect to the total target in a combinational order can be calculated

Table 3: Risk matrix.

	Hazardous event severity level				
	Negligible	Slight	Moderate	Serious	Disastrous
Possibility of hazardous event					
Frequently	Higher	Higher	Very high	Highest	Highest
Very likely	Middle	High	Higher	Very high	Highest
Occasionally	Lower	Middle	High	Very high	Very high
Small possible	Very low	Lower	Middle	Higher	Very high
Impossible	Very low	Very low	Low	High	Higher

by $\mathbf{A}^{(2)} = \mathbf{W}^{(2)}\mathbf{A}^{(1)}$. The results of vector $\mathbf{A}^{(2)}$ are $a_1^{(2)} = 0.0671$, $a_2^{(2)} = 0.0856$, $a_3^{(2)} = 0.0504$, $a_4^{(2)} = 0.0362$, $a_5^{(2)} = 0.1073$, $a_6^{(2)} = 0.3084$, $a_7^{(2)} = 0.1331$, $a_8^{(2)} = 0.0044$, $a_9^{(2)} = 0.1380$, $a_{10}^{(2)} = 0.0476$, and $a_{11}^{(2)} = 0.0221$.

The overall consistency of the weights of each layer factor with respect to the total target should be checked. For the first layer, because of $\mathbf{C.R.}^{(1)} = \mathbf{C.R.}^{(0)}$ it has a satisfactory overall consistency.

For the second layer,

$$\begin{aligned}
\mathbf{C.I.}^{(2)} &= \left[\mathbf{C.I.}_1^{(1)} \ \mathbf{C.I.}_2^{(1)} \ \mathbf{C.I.}_3^{(1)} \ \mathbf{C.I.}_4^{(1)} \ \mathbf{C.I.}_5^{(1)}\right] \\
&\quad \cdot \mathbf{A}^{(1)} = 0.0284, \\
\mathbf{R.I.}^{(2)} &= \left[\mathbf{R.I.}_1^{(1)} \ \mathbf{R.I.}_2^{(1)} \ \mathbf{R.I.}_3^{(1)} \ \mathbf{R.I.}_4^{(1)} \ \mathbf{R.I.}_5^{(1)}\right] \\
&\quad \cdot \mathbf{A}^{(1)} = 0.7910, \\
\mathbf{C.R.}^{(2)} &= \frac{\mathbf{C.I.}^{(2)}}{\mathbf{R.I.}^{(2)}} = \frac{0.0284}{0.7910} = 0.0359 < 0.1.
\end{aligned} \tag{16}$$

The overall consistency of the second layer satisfies the requirement.

According to calculations of this section, the weights of factors with respect to the total target are obtained.

4. Risk Analysis Based on Fuzzy Comprehensive Evaluation for Maglev Bogie

4.1. Division of Risk Level and Tolerance. Risk can be defined as follows [21]:

$$\text{Risk} = \text{probability} \times \text{severity}. \tag{17}$$

The mishap probability factor is the probability of the hazard components occurring and transforming into the mishap. The mishap severity factor is the overall consequence of the mishap.

The probability of fault maglev bogie occurring and the level of hazardous event severity are difficult to determine quantitatively. Therefore, linguistic terms [10] are applied to describe the probability and severity qualitatively. The probabilities of hazardous event are frequently, very likely, occasionally, small possible, and impossible. The hazardous event severity levels are disastrous, serious, moderate, slight, and negligible, respectively. The risks of maglev bogie are divided into eight levels, very low, lower, low, middle, high, higher, very high, and highest, respectively.

The risk matrix used to evaluate the level of risk for maglev bogie is shown in Table 3. It is determined by referencing IEC 62278: 2002 combined with engineering practice [16, 22].

Linguistic terms have been found intuitively easy to use in expressing the subjectiveness and imprecision of risk assessments [3, 23]. In fact, the risk levels given by experts are fuzzy. Such an uncertain and imprecise issue can be expressed by the use of the fuzzy set theory [3].

In this paper the triangular fuzzy number is used for fuzzy numbers, because it is simpler than trapezoidal fuzzy number [24] and in accordance with the actual case. The definition of triangular fuzzy number is as follows, based on the operations on fuzzy numbers of Dubois and Prade [25]:

$$\mu_M(x) = \begin{cases} \dfrac{1}{m-x}x - \dfrac{l}{m-l} & x \in [l, m], \\ \dfrac{1}{m-u}x - \dfrac{u}{m-u} & x \in [m, u], \\ 0 & \text{otherwise}, \end{cases} \tag{18}$$

where M is the fuzzy number, μ_M is the membership function of M, m is called the most possible value of triangular fuzzy number M, and l and u are called lower and upper limits of M, respectively.

The eight linguistic terms of risk level are characterized by triangular fuzzy numbers for representing their approximate value range between 1 and 8 [26]. Figure 3 shows the memberships of these linguistic terms. The eight top points' membership functions are 1, which represents the most possible eight linguistic terms of risk level, respectively. When each linguistic term's membership grade decreases, the other one will increase accordingly.

The risk levels which include very low, lower, and low are divided into acceptable risk. The middle, high, and higher risk levels are considered to be undesirable risk. The very high and highest risk levels are regarded as unacceptable. These rules are given according to the practical engineering experience. Through the analysis, three broken blue line triangles are drawn in Figure 4.

The x-coordinates of the crossover point of the two broken blue line triangles are 3.33 and 6.5, respectively. The ranges of risk tolerance are obtained by comparing the size of memberships. They are given as follows:

(i) Acceptable risk: [1, 3.33).

(ii) Undesirable risk: [3.33, 6.5].

(iii) Unacceptable risk: (6.5, 8].

Figure 4 shows the division of risk tolerance.

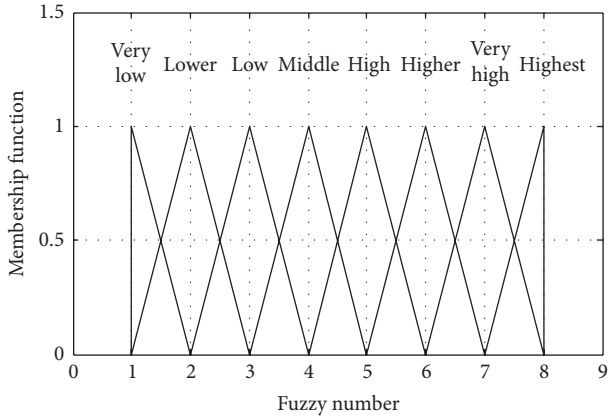

Figure 3: Membership functions of linguistic terms.

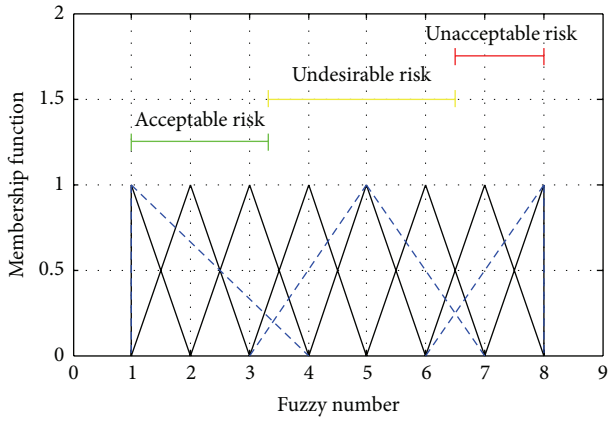

Figure 4: Division of risk tolerance.

4.2. Fuzzy Comprehensive Risk Assessment. The weights of each layer factor with respect to the total target are obtained by using AHP. The weights used in FCE are obtained by normalizing them.

For the first level FCE, the weight vectors of the second layer's factors with respect to the total target are as follows:

$$\begin{aligned}
\mathbf{A}_1^{(2)} &= \left[a_1^{(2)} \quad a_4^{(2)}\right] = \left[0.0671 \quad 0.0362\right], \\
\mathbf{A}_2^{(2)} &= \left[a_2^{(2)} \quad a_3^{(2)}\right] = \left[0.0856 \quad 0.0504\right], \\
\mathbf{A}_3^{(2)} &= \left[a_3^{(2)} \quad a_4^{(2)} \quad a_5^{(2)} \quad a_6^{(2)} \quad a_7^{(2)}\right] \\
&= \left[0.0504 \quad 0.0362 \quad 0.1073 \quad 0.3084 \quad 0.1331\right], \\
\mathbf{A}_4^{(2)} &= \left[a_6^{(2)} \quad a_8^{(2)} \quad a_{10}^{(2)}\right] = \left[0.3084 \quad 0.0044 \quad 0.0476\right], \\
\mathbf{A}_5^{(2)} &= \left[a_6^{(2)} \quad a_9^{(2)} \quad a_{10}^{(2)} \quad a_{11}^{(2)}\right] \\
&= \left[0.3084 \quad 0.1380 \quad 0.0476 \quad 0.0221\right].
\end{aligned} \tag{19}$$

Before starting the first level FCE, the above-mentioned five weights should be normalized, given as

$$\begin{aligned}
\underset{\sim}{\mathbf{A}}_1^{(2)} &= \left[0.6496 \quad 0.3504\right], \\
\underset{\sim}{\mathbf{A}}_2^{(2)} &= \left[0.6294 \quad 0.3706\right], \\
\underset{\sim}{\mathbf{A}}_3^{(2)} &= \left[0.0793 \quad 0.0570 \quad 0.1689 \quad 0.4854 \quad 0.2095\right], \\
\underset{\sim}{\mathbf{A}}_4^{(2)} &= \left[0.8557 \quad 0.0122 \quad 0.1321\right], \\
\underset{\sim}{\mathbf{A}}_5^{(2)} &= \left[0.5976 \quad 0.2674 \quad 0.0922 \quad 0.0428\right].
\end{aligned} \tag{20}$$

For the second level FCE, the weight of the first layer factor set is $\underset{\sim}{\mathbf{A}}^{(1)}$, that is, $\mathbf{A}^{(1)}$.

According to Table 3, the evaluation set of FCE can be written as $\mathbf{V} = \{$very low, lower, low, middle, high, higher, very high, highest$\}$. In order to make the index quantitative, the grade is provided for the corresponding evaluation set: $N = (1, 2, 3, 4, 5, 6, 7, 8)$ [5].

When the first level FCE starts, risk analysts give the single-factor evaluation matrix $\mathbf{R}_i^{(2)}$ of the second layer. This can be calculated by using model $M(\cdot, +)$ to begin fuzzy compositional operation "$\circ$". $\mathbf{R}_i^{(2)}$ is determined by [27]

$$\mathbf{R}_i^{(2)} = \begin{bmatrix}
r_{i11}^{(2)} & r_{i12}^{(2)} & \cdots & r_{i1m}^{(2)} \\
r_{i21}^{(2)} & r_{i22}^{(2)} & \cdots & r_{i2m}^{(2)} \\
\vdots & \vdots & & \vdots \\
r_{in_i^{(2)}1}^{(2)} & r_{in_i^{(2)}2}^{(2)} & \cdots & r_{in_i^{(2)}m}^{(2)}
\end{bmatrix} \quad i = 1, 2, \ldots, n^{(1)}, \tag{21}$$

where $n^{(1)}$ ($n^{(1)} = 5$) represents the number of factors included in the first layer, $n_i^{(2)}$ denotes the number of factors included in the second layer with respect to the factor i of the first layer, and m ($m = 8$) stands for the number of the evaluative sets.

Hence, the matrix $\mathbf{R}_1^{(2)}$ can be derived as follows:

$$\mathbf{R}_1^{(2)} = \begin{bmatrix}
0.1 & 0.2 & 0.3 & 0.3 & 0.06 & 0.04 & 0 & 0 \\
0.2 & 0.3 & 0.3 & 0.1 & 0.1 & 0 & 0 & 0
\end{bmatrix}. \tag{22}$$

Similarly, the matrices $\mathbf{R}_2^{(2)}$, $\mathbf{R}_3^{(2)}$, $\mathbf{R}_4^{(2)}$, and $\mathbf{R}_5^{(2)}$ are obtained. They are shown as follows:

$$\mathbf{R}_2^{(2)} = \begin{bmatrix}
0.06 & 0.2 & 0.2 & 0.3 & 0.2 & 0.04 & 0 & 0 \\
0.05 & 0.3 & 0.3 & 0.3 & 0.05 & 0 & 0 & 0
\end{bmatrix},$$

$$\mathbf{R}_3^{(2)} = \begin{bmatrix}
0.05 & 0.3 & 0.3 & 0.3 & 0.05 & 0 & 0 & 0 \\
0.2 & 0.3 & 0.3 & 0.1 & 0.1 & 0 & 0 & 0 \\
0.04 & 0.25 & 0.25 & 0.25 & 0.2 & 0.01 & 0 & 0 \\
0.1 & 0.3 & 0.3 & 0.2 & 0.1 & 0 & 0 & 0 \\
0.1 & 0.2 & 0.3 & 0.3 & 0.1 & 0 & 0 & 0
\end{bmatrix},$$

$$\mathbf{R}_4^{(2)} = \begin{bmatrix} 0.1 & 0.3 & 0.3 & 0.2 & 0.1 & 0 & 0 & 0 \\ 0.05 & 0.1 & 0.2 & 0.2 & 0.3 & 0.1 & 0.05 & 0 \\ 0.1 & 0.1 & 0.2 & 0.3 & 0.2 & 0.1 & 0 & 0 \end{bmatrix},$$

$$\mathbf{R}_5^{(2)} = \begin{bmatrix} 0.1 & 0.3 & 0.3 & 0.2 & 0.1 & 0 & 0 & 0 \\ 0.05 & 0.18 & 0.36 & 0.3 & 0.1 & 0.01 & 0 & 0 \\ 0.1 & 0.1 & 0.2 & 0.3 & 0.2 & 0.1 & 0 & 0 \\ 0.1 & 0.2 & 0.3 & 0.25 & 0.15 & 0 & 0 & 0 \end{bmatrix}. \tag{23}$$

The results of evaluation can be obtained through multiplying the vector of the factor weight and the matrix $\mathbf{R}$ of single-factor evaluation [5]:

$$\begin{aligned} \underset{\sim}{\mathbf{B}}_1^{(2)} &= \underset{\sim}{\mathbf{A}}_1^{(2)} \circ \mathbf{R}_1^{(2)} \\ &= [0.1350 \;\; 0.2350 \;\; 0.3000 \;\; 0.2299 \;\; 0.0740 \;\; 0.0260 \;\; 0 \;\; 0], \end{aligned} \tag{24}$$

where $\underset{\sim}{\mathbf{B}}_1^{(2)}$ is the evaluation result of the first layer's first factor. The elements in $\underset{\sim}{\mathbf{B}}_1^{(2)}$ are membership of the evaluation object with regard to the elements in the evaluation set. The conclusion of the comprehensive evaluation can be obtained by the maximum membership principle [5].

Similarly, the results of the first level FCE are given, respectively, by

$$\begin{aligned} \underset{\sim}{\mathbf{B}}_2^{(2)} &= \underset{\sim}{\mathbf{A}}_2^{(2)} \circ \mathbf{R}_2^{(2)} \\ &= [0.0563 \;\; 0.2371 \;\; 0.2371 \;\; 0.3000 \;\; 0.1444 \;\; 0.0252 \;\; 0 \;\; 0], \\ \underset{\sim}{\mathbf{B}}_3^{(2)} &= \underset{\sim}{\mathbf{A}}_3^{(2)} \circ \mathbf{R}_3^{(2)} \\ &= [0.0916 \;\; 0.2706 \;\; 0.2916 \;\; 0.2316 \;\; 0.1129 \;\; 0.0017 \;\; 0 \;\; 0], \\ \underset{\sim}{\mathbf{B}}_4^{(2)} &= \underset{\sim}{\mathbf{A}}_4^{(2)} \circ \mathbf{R}_4^{(2)} \\ &= [0.0994 \;\; 0.2711 \;\; 0.2856 \;\; 0.2132 \;\; 0.1157 \;\; 0.0144 \;\; 0.0006 \;\; 0], \\ \underset{\sim}{\mathbf{B}}_5^{(2)} &= \underset{\sim}{\mathbf{A}}_5^{(2)} \circ \mathbf{R}_5^{(2)} \\ &= [0.0866 \;\; 0.2452 \;\; 0.3068 \;\; 0.2381 \;\; 0.1114 \;\; 0.0119 \;\; 0 \;\; 0]. \end{aligned} \tag{25}$$

The results of the second level FCE are given by

$$\begin{aligned} \underset{\sim}{\mathbf{B}}^{(1)} &= \mathbf{A}^{(1)} \circ \mathbf{R}^{(1)} = \mathbf{A}^{(1)} \circ \begin{bmatrix} \underset{\sim}{\mathbf{A}}_1^{(2)} \circ \mathbf{R}_1^{(2)} \\ \underset{\sim}{\mathbf{A}}_2^{(2)} \circ \mathbf{R}_2^{(2)} \\ \vdots \\ \underset{\sim}{\mathbf{A}}_5^{(2)} \circ \mathbf{R}_5^{(2)} \end{bmatrix} \\ &= [0.0900 \;\; 0.2547 \;\; 0.2921 \;\; 0.2399 \;\; 0.1126 \;\; 0.0107 \;\; 0 \;\; 0], \end{aligned} \tag{26}$$

where $\underset{\sim}{\mathbf{B}}^{(1)}$ is the fuzzy comprehensive evaluation result of risk level for maglev bogie.

The maximum membership of $\underset{\sim}{\mathbf{B}}^{(1)}$ is the three-factor 0.2921 which indicates the total risk level of maglev bogie is low. The maximum membership of $\underset{\sim}{\mathbf{B}}_1^{(2)}$, $\underset{\sim}{\mathbf{B}}_2^{(2)}$, $\underset{\sim}{\mathbf{B}}_3^{(2)}$, $\underset{\sim}{\mathbf{B}}_4^{(2)}$, and $\underset{\sim}{\mathbf{B}}_5^{(2)}$ are 0.3, 0.3, 0.2916, 0.2856, and 0.3068, respectively. Similarly, the risk level of supporting unit, architecture, brake unit, and suspension unit is low. The risk level of drive unit is middle. Hence, maintainers should pay more attention to the drive unit.

4.3. Results of Risk Assessment. In order to get the risk tolerance of each factor, weighted sum of the result of risk level is proposed.

The index is determined by

$$\text{Index} = \underset{\sim}{\mathbf{B}} \cdot \mathbf{N}, \tag{27}$$

where Index is the score of risk evaluation and $\mathbf{N}$ ($\mathbf{N} = [1 \;\; 2 \;\; 3 \;\; 4 \;\; 5 \;\; 6 \;\; 7 \;\; 8]^T$) is the grade of evaluation set.

The single-factor evaluation matrix of scheme layer is corresponding to the row vector of $\mathbf{R}_i^{(2)}$, and $\mathbf{A}^{(3)} = 1$.

Table 4 shows the risk assessment of bogie system determined by results of FCE.

According to Figure 3, the risk index of bogie system is acceptable in Table 4. The risks of five subsystems are also acceptable. However, there are four parts' risk indexes undesirable. They are linear motor, antiroll beam, mechanical braking device, and outer plates of electromagnet, respectively. Clearly, they are the weak links which affect the safety of bogie system. Accordingly, making decisions for the maintenance of maglev train is convenient. Meanwhile, the cost is dropped remarkably when putting the limited resources into the most needed place.

5. Discussion

The main difficulties in risk analysis for mechatronics systems are the complexity of mechanism and the uncertainty of various basic events' probabilities. The research about risk analysis for maglev bogie is very rare.

As a response to this dilemma, various methods have been proposed for solving risk analysis problems for mechatronics systems. For example, the frequently used methods are ETA and FTA. However, ETA is unable to handle the process of identifying safety risk because of multiple no related events. FTA can identify hazards that present mishap risk with an assessment of the risk [21]. But as the probabilities of various basic events are difficult to collect and estimate, FTA is unable to give quantitative risk assessment.

In this paper, the combinational method of analytic hierarchy process and fuzzy comprehensive evaluation has been proposed to solve the complex and uncertain problems in the area of risk analysis for maglev bogie. First, the complex structure of maglev bogie should be taken into consideration. There are a few subsystems' devices installed on the maglev bogie. These devices' faults can reduce different size risks. To deal with this challenge, based on the analysis of maglev bogie's structure, 11 risk sources have been divided into five groups in accordance with the subsystems to determine the contribution degree for total risk. Risk sources and risk sources' reasons and effects have influence on finding the relationship between failures and grading risks. In this study, the identification of risk sources has been very comprehensive. But the analysis of risk sources' reasons and effects is limited, and it is also the importance of future research.

Second, the application of AHP in this study is mainly based on Saaty's research [4]. The hierarchy relationships of risk factors have been built clearly by AHP. Certainly, AHP still suffers from some theoretical disputes. The assumption of

Table 4: Results of risk assessment.

Level	Item	Index	Risk	Ratio
System	Bogie	3.0627	Acceptable	
Subsystem	Support unit	2.9506	Acceptable	0.1919
	Drive unit	3.3150	Acceptable	0.2156
	Architecture	3.0090	Acceptable	0.1957
	Brake unit	3.0203	Acceptable	0.1965
	Suspension unit	3.0782	Acceptable	0.2002
Component	Air spring	3.1400	Acceptable	0.0877
	Corbel	2.6000	Acceptable	0.0726
	Linear motor	3.5000	Undesirable	0.0978
	Linear motor beam	3.0000	Acceptable	0.0838
	Antiroll beam	3.3500	Undesirable	0.0936
	Corbel connection	2.9000	Acceptable	0.0810
	Integrated rated bracket	3.1000	Acceptable	0.0866
	Mechanical braking device	4.1000	Undesirable	0.1146
	Line package	3.2500	Acceptable	0.0908
	Outer plates of electromagnet	3.7000	Undesirable	0.1034
	Inner plates of electromagnet	3.1500	Acceptable	0.0880

criteria independence may be sometimes a limitation of AHP [6]. The selection of judgment matrix is completed by experts' engineering practice experience. In fact, exact numbers are inappropriate for linguistic judgments. Hence, fuzzy AHP [28] may be considered in the next research.

Third, the conclusion of maglev bogie's risk level obtained by the maximum membership principle [5] is low. However, each factor's risk performance should be considered into risk analysis to find the weak links of maglev bogie. Based on the fuzzy theory [3], linguistic evaluation set has been classified according to risk tolerance. The fuzzy comprehensive evaluation method is utilized to assess the score and ratio of each factor. Accordingly, it is convenient for people to make decisions for the maintenance of maglev bogie system.

6. Conclusion

In this paper, we have proposed an effective risk analysis method, a combinational method of analytic hierarchy process and fuzzy comprehensive evaluation, which provides a quantitative risk assessment for low-medium speed maglev train.

The very comprehensive identification of risk sources has been done by analyzing the structure of maglev bogie. The weight of each layer is calculated by analytic hierarchy process. The results of risk level for maglev bogie are obtained by fuzzy comprehensive evaluation, and based on the maximum membership principle, the total risk level of maglev bogie is low. As the risk level of drive unit is middle, maintainers should pay more attention to the drive unit.

The triangular fuzzy number has been used to determine the ranges of risk tolerance. The score of each risk factor is obtained by weighted sum of the result of fuzzy comprehensive evaluation. The results of risk assessment show that the risk degree of maglev bogie is acceptable. However, the risk degrees of linear motor, antiroll beam, mechanical braking device, and outer plates of electromagnet are undesirable. Clearly, they are the weak links which affect the safety of bogie system.

The evaluated results can provide a reasonable guide to analyze the risk of maglev bogie system. The merits of the approach facilitate finding the weak links and making decisions for the maintenance of maglev bogie system. The costs will also decrease significantly when putting the limited resources into the most needed place.

Conflict of Interests

The authors declare that there is no conflict of interests regarding the publication of this paper.

Acknowledgment

This work is supported by the National Key Technology R&D Program of the 12th Five-Year Plan, Systematic Study on Engineering Integration of High Speed Maglev Transportation, 2013BAG19B01.

References

[1] J.-W. Han, J.-D. Kim, and S.-Y. Song, "Fatigue strength evaluation of a bogie frame for urban maglev train with fatigue test on full-scale test rig," *Engineering Failure Analysis*, vol. 31, pp. 412–420, 2013.

[2] P. Cui, J. Li, and D. S. Liu, "Carrying capacity for the electromagnetic suspension low-speed maglev train on the horizontal curve," *Science China Technological Sciences*, vol. 53, no. 4, pp. 1082–1087, 2010.

[3] L. A. Zadeh, "Fuzzy sets," *Information and Computation*, vol. 8, pp. 338–353, 1965.

[4] T. L. Saaty, "A scaling method for priorities in hierarchical structures," *Journal of Mathematical Psychology*, vol. 15, no. 3, pp. 234–281, 1977.

[5] J.-F. Chen, H.-N. Hsieh, and Q. H. Do, "Evaluating teaching performance based on fuzzy AHP and comprehensive evaluation approach," *Applied Soft Computing Journal*, vol. 28, pp. 100–108, 2015.

[6] A. Ishizaka and A. Labib, "Review of the main developments in the analytic hierarchy process," *Expert Systems with Applications*, vol. 38, no. 11, pp. 14336–14345, 2011.

[7] B. Srdjevic and Y. D. P. Medeiros, "Fuzzy AHP assessment of water management plans," *Water Resources Management*, vol. 22, no. 7, pp. 877–894, 2008.

[8] Q. Nian, S. Shi, and R. Li, "Research and application of safety assessment method of gas explosion accident in coal mine based on GRA-ANP-FCE," *Procedia Engineering*, vol. 45, pp. 106–111, 2012.

[9] S. Su, X. Chen, S. D. DeGloria, and J. Wu, "Integrative fuzzy set pair model for land ecological security assessment: a case study of Xiaolangdi Reservoir Region, China," *Stochastic Environmental Research and Risk Assessment*, vol. 24, no. 5, pp. 639–647, 2010.

[10] C.-H. Yeh, H. Deng, and Y.-H. Chang, "Fuzzy multicriteria analysis for performance evaluation of bus companies," *European Journal of Operational Research*, vol. 126, no. 3, pp. 459–473, 2000.

[11] A. Roozbahani, B. Zahraie, and M. Tabesh, "Integrated risk assessment of urban water supply systems from source to tap," *Stochastic Environmental Research and Risk Assessment*, vol. 27, no. 4, pp. 923–944, 2013.

[12] Z. Song, H. Zhu, G. Jia, and C. He, "Comprehensive evaluation on self-ignition risks of coal stockpiles using fuzzy AHP approaches," *Journal of Loss Prevention in the Process Industries*, vol. 32, no. 1, pp. 78–94, 2014.

[13] J. Yang, H. Sun, L. Wang, L. Li, and B. Wu, "Vulnerability evaluation of the highway transportation system against meteorological disasters," *Procedia—Social and Behavioral Sciences*, vol. 96, pp. 280–293, 2013.

[14] Z. Ren, *Fatigue Analysis and Simulation of Maglev Bogie in Low-Medium Speed Maglev Train*, National University of Defense Technology, Changsha, China, 2005.

[15] C. Huang, W. Xu, S. Yao, and B. Zheng, "Low-medium speed maglev train bogie anti-roll beam structure optimization," *Rolling Stock*, vol. 51, 2013.

[16] B. Tong, *Risk Analysis of the Critical Systems in Medium-Low Speed Maglev Train and its Application Research*, National University of Defense Technology, Changsha, China, 2014.

[17] J. K. Levy, "Multiple criteria decision making and decision support systems for flood risk management," *Stochastic Environmental Research and Risk Assessment*, vol. 19, no. 6, pp. 438–447, 2005.

[18] Y. Han, W. Zhou, and X. Zhang, "Fuzzy comprehensive evaluation of the adaptability of an expressway system," *Journal of Highway and Transportation Research and Development*, vol. 8, no. 4, pp. 97–103, 2014.

[19] H. Yuan and W. Cai, "The model combined the BT project and land development risk assessment research," *Systems Engineering Procedia*, vol. 1, pp. 250–256, 2011.

[20] E. Cagno, F. Caron, and A. Perego, "Multi-criteria assessment of the probability of winning in the competitive bidding process," *International Journal of Project Management*, vol. 19, no. 6, pp. 313–324, 2001.

[21] C. A. Ericson, *Hazard Analysis Techniques for System Safety*, John Wiley & Sons, Hoboken, NJ, USA, 2005.

[22] International Electrotechnical Commission, *IEC 62278: Railway Applications—Specification and Demonstration of Reliability, Availability, Maintainability and Safety (RAMS)*, IEC Central Office, Geneva, Switzerland, 2002.

[23] G.-S. Liang, "Fuzzy MCDM based on ideal and anti-ideal concepts," *European Journal of Operational Research*, vol. 112, no. 3, pp. 682–691, 1999.

[24] E. Triantaphyllou and L. Chi-Tun, "Development and evaluation of five fuzzy multiattribute decision-making methods," *International Journal of Approximate Reasoning*, vol. 14, no. 4, pp. 281–310, 1996.

[25] D. Dubois and H. Prade, "Operations on fuzzy numbers," *International Journal of Systems Science*, vol. 9, no. 6, pp. 613–626, 1978.

[26] E. K. Zavadskas and J. Antucheviciene, "Multiple criteria evaluation of rural building's regeneration alternatives," *Building and Environment*, vol. 42, no. 1, pp. 436–451, 2007.

[27] X. Yihong and S. Mengju, "Fuzzy comprehensive evaluation of beverage enterprise risks from system engineering perspective," *Systems Engineering Procedia*, vol. 3, pp. 240–248, 2012.

[28] O. S. Vaidya and S. Kumar, "Analytic hierarchy process: an overview of applications," *European Journal of Operational Research*, vol. 169, no. 1, pp. 1–29, 2006.

Hindawi Publishing Corporation
Mathematical Problems in Engineering
Volume 2015, Article ID 129787, 12 pages
http://dx.doi.org/10.1155/2015/129787

Research Article

A Novel Approach to Evaluate the Time-Variant System Reliability of Deteriorating Concrete Bridges

Hao Tian,[1,2,3] Yuanli Chen,[3] and Fangyuan Li[4]

[1]*Zhejiang Scientific Research Institute of Transport, Hangzhou 310006, China*
[2]*State Key Laboratory Breeding Base of Mountain Bridge and Tunnel Engineering, Chongqing Jiaotong University, Chongqing 400074, China*
[3]*Zhejiang Institute of Communications, Hangzhou 311112, China*
[4]*Department of Bridge Engineering, College of Civil Engineering, Tongji University, Shanghai 200092, China*

Correspondence should be addressed to Fangyuan Li; fyli@tongji.edu.cn

Received 8 October 2015; Revised 6 December 2015; Accepted 9 December 2015

Academic Editor: Egidijus R. Vaidogas

Bridge time-variant system reliability is a useful measure to evaluate the lifetime performance of deteriorating bridge structures under uncertainty and is an influential performance indicator in bridge maintenance management programs. This paper proposes a computational methodology based on the Monte Carlo simulations for evaluating the time-variant system reliability of concrete bridges under environmental attacks. Methods related to the reduction of concrete sections and the variation of the load effects acting on the components are investigated using a finite element-based computational program, CBDAS (Concrete Bridge Durability Analysis System), to perform the assessment of lifetime structural performance. With regard to system reliability, a practical technique for searching the structural failure mode is also presented and a program, SRMCS (System Reliability by Monte Carlo Simulations), based on the Monte Carlo simulations is written to calculate and evaluate the structural system reliability of deteriorating concrete bridges. Finally, three numerical examples are presented to display the CBDAS and SRMCS functions.

1. Introduction

A large percentage of the bridges all over the world are constructed with concrete and reinforcing steel, because of their relatively low cost [1]. In recent years, however, significant distress and deterioration have been observed in many concrete bridges, mainly due to the environmental stressors such as concrete carbonation, chloride penetration, and freeze-thaw cycles. Thus, maintenance intervention to keep the structure healthy during its service life is necessary. The primary task in selecting and performing an appropriate maintenance strategy for a deteriorating concrete bridge is to evaluate and predict its lifetime structural performance [2]. To achieve this, the computational prediction should be probabilistic based, due to the inherent randomness reflected in the structural configuration, materials properties, live loads, and different environments. A comprehensive consideration of time-variant performance and uncertainty is a useful measure to assess the lifetime performance of a deteriorating bridge structure and is one of the key performance indicators in bridge maintenance management programs [3, 4]. However, though widely accepted and used, current techniques and methods may still not be accurate enough in measuring the time-variant reliability of bridges for the following reasons: (1) the effects of the aggressive environments on the structural performance have not been precisely simulated, (2) the structural failure mode (i.e., the relationship between the overall structural failure and the individual component failure) is hard to measure; and (3) the correlation coefficients among the individual components or failure modes are difficult to determine [5–7].

Because of the shortcomings of previous techniques and methods, a finite element- and Monte Carlo simulations-based computational methodology is proposed for evaluating the time-variant system reliability of deteriorating concrete bridges [8–10]. For time-variant performance, methods related to the reduction of concrete sections and the variation of structural load effect are discussed. For system reliability,

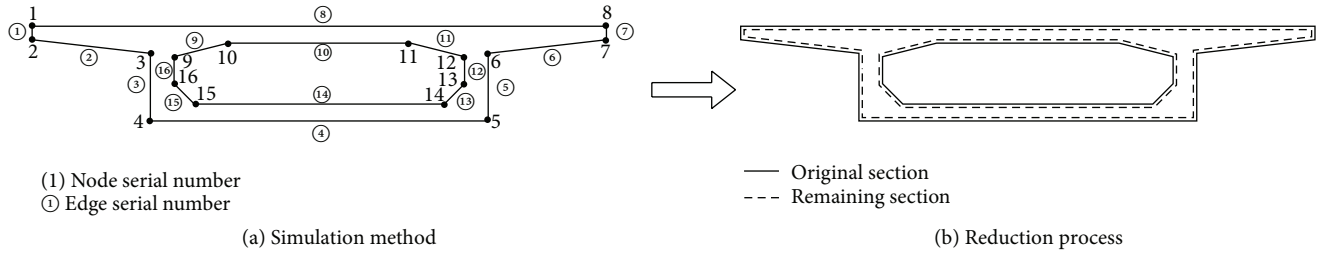

(a) Simulation method (b) Reduction process

Figure 1: Reduction of concrete section.

a technique for searching the structural failure mode is presented, and a Monte Carlo simulations-based program, SRMCS, is presented. Finally, three numerical examples are illustrated to display the functions of CBDAS and SRMCS and of the combination of the two programs: (1) in the first example, the time-variant performance of a reinforced concrete continuous bridge under chloride-induced corrosion is evaluated by means of CBDAS; (2) in the second example, the procedure for computing the system reliability of a two-story truss is displayed in terms of SRMCS; and (3) in the third example, the time-variant system reliability of the same model as the first example is investigated by combining CBDAS with SRMCS.

2. Time-Variant Performance

It is well known that the variation of structural performance with respect to the deteriorating concrete bridges may be significant during their entire service lifetime due to the environmental attacks [9, 10]. Also, because the resistances of the individual components are time variant, it is necessary to evaluate the time-variant structural performance in an effective way by selecting an appropriate maintenance schedule.

2.1. Finite Element-Based Approach. The essential problems encountered in the assessment of lifetime performance are as follows: (1) the deterioration of the materials properties, (2) the reduction of sectional areas, and (3) the variation of the overall structural performance induced by the first two problems. Furthermore, the last two problems can be divided into the reductions of reinforcing steel and concrete sections, the deterioration of resistances of the individual components, and the variation of load effects acting on these components. The two main problems to be investigated in this paper are the reduction of concrete sections due to environmental attacks and the variation of the load effects acting on the individual components.

2.1.1. Reduction of Concrete Sections. When considering the reduction of a concrete section, it is necessary to simulate the accurate shape of the section, as it is one of the critical factors related to measuring the actual reduction process. One way to accurately do this is to simulate the section by using the concrete edge as the basic unit because the reduced depths of the concrete edges in the same section are likely to be not identical due to the different values of the environmental parameters and other design variables among the concrete edges. It can be seen from Figure 1(a) that the number of the edges is equal to that of the nodes. Thus, the edge information can be obtained from the coordinates of the control nodes. The cross-sectional geometrical properties can be thus calculated associated with the node coordinates and the Triangle Partitioning Method [11, 12] and by using the edge as basic unit, the reduction process of concrete section can be described as the movement of the concrete edges. The specific steps are as follows: (1) the corrosion rate of the reinforcing steel related to each concrete edge is calculated by means of the corrosion numerical model, (2) the reduced depths of the two adjacent concrete edges are obtained in association with the corrosion rates of the reinforcing steels on the two edges, (3) each edge moves a distance equal to the respective reduced depth along its normal direction and a group of new control nodes are obtained as the intersections of the moved concrete edges, and (4) the remaining concrete section can be generated with the same method as the original one. The reduction process is shown in Figure 1(b), where the figure surrounded by solid lines is the original concrete section and the one encircled by dashed lines is the remaining section.

2.1.2. Variation of Load Effect. The key problems derived from the variation of the load effects acting on the individual components are the loss of dead weight and internal force redistribution due to the reduced concrete and steel bar sections. In the case of a concrete section, the computation of the lost dead weight is similar to assessment by conventional analyses. Only two problems are required to be modified: (1) the area of the original concrete section should be replaced by the reduced concrete section when forming the load vector caused by the lost dead weight and (2) the load induced by the lost dead weight should be applied on the deteriorating structure in the opposite direction of the original dead weight. In the reinforcing steel and prestressing steel sections, corrosion cannot lead to the loss of dead weight because they are wrapped in the concrete section and the dead weight of the rust is consistently acting on the structure over its life cycle. The internal forces acting on the reduced concrete section, reinforcing the steel section and its prestressing section, need to be redistributed on the deteriorating structure. The internal force redistribution of reduced concrete section is shown in Figure 2, where $I_{c,c}$, I_c, and $I_{c,h}$ are the geometric centers of the reduced, original, and remaining concrete sections, respectively. $N_{c,c}$ and $N_{c,h}$ are the internal forces acting on the reduced and remaining

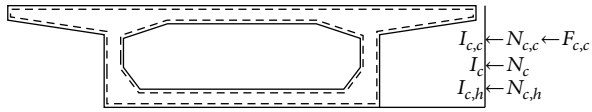

Figure 2: Redistribution of the internal forces.

concrete sections, respectively, which are decomposed from N_c, the internal force acting on the original concrete section, based on the cross-sectional geometric properties of the reduced, original, and remaining concrete sections. Thus, load $F_{c,c}$ caused by the reduction of the concrete section is identical to the internal force $N_{c,c}$. In a similar way, loads $F_{s,c}$ and $F_{p,c}$ induced by the reduction of reinforcing steel and prestressing steel sections are obtained. Finally, load F_c due to the internal force redistribution of the reduced sections is composed of $F_{c,c}$, $F_{s,c}$, and $F_{p,c}$.

2.2. Computational Program: CBDAS. The analysis procedure of the structural time-variant performance is displayed in Figure 3. A finite element-based approach to evaluate the time-variant performance of deteriorating concrete bridges is set up based on the solutions of the abovementioned essential problems. Accordingly, a program named CBDAS (i.e., Concrete Bridge Durability Analysis System) [13] has been developed to perform this approach by using FORTRAN. The program has two major functions. The first is to simulate the physical events from the initiation of construction to its completion, which can be characterized as the construction process analysis, and the second is to evaluate the time-variant structural performance from structural completion to the occurrence of the limit state or the end of service life, which can be defined as the degradation process analysis. Figure 3 displays the flow chart of CBDAS.

3. System Reliability

Structural system reliability defines safety as the condition in which a system failure will not occur from a probabilistic standpoint. To accurately evaluate system reliability, it is necessary to follow an approach called "Structure-Component-Structure." This approach can be divided into two steps: (1) deduction from the overall structure to individual components and (2) induction from the individual components to overall structure [14]. In the first step, the resistances of individual components and the load effects acting on these components are calculated based on the structural configuration, loads, and construction method. The limit state functions of these individual components or failure modes are formulated by equations relating the load effects to the relative resistances and the components reliabilities are evaluated accordingly. In the second step, the structural failure mode is required to be searched according to the relationship between the overall structure failure and the individual component failure. Finally, the system reliability can be assessed in association with the components' reliabilities and the structural failure mode. The schematic for calculating the system reliability is shown in Figure 4.

In the following part of this section, the conventional methods for calculating the structural system reliability are briefly reviewed. Afterwards, an approach for evaluation of the system reliability associated with Monte Carlo simulations and a practical structural failure mode searching technique is proposed.

3.1. The Conventional Methods. The commonly used methods for calculating the structural system reliability are (1) the incremental method and (2) the series-parallel modeling method.

3.1.1. The Incremental Method. The incremental method [15] is used to search the structural failure mode and thus formulate the limit state function of the overall structure. The objective of this method is to find out an expression for the system resistance in terms of the component resistances. The method identifies a system failure mode by following a load path from initial component failure to final system collapse and leads to a linear system failure expression such as [2, 16]

$$g_j = \sum C_{jk} R_k - S_j, \tag{1}$$

where the failure function $g_j < 0$ means that the jth failure has occurred. C_{jk} is the coefficient representing the participation of the kth component in the jth failure mode; R_k is the resistance of the kth component; and S_j is the load term in the jth failure mode. The system reliability R_s is expressed as [2, 16, 17]

$$R_s = \text{Probability}\left[\text{All } g_j > 0\right]. \tag{2}$$

It is clear that (1) is a system limit state function, based on which the system reliability can be calculated directly by using the integration method or Monte Carlo simulations. In this method, the deduction from structure to components and the induction from components to structure are both implied in the process of searching the load path from initial component failure to final system collapse. This method is applicable to straightforwardly estimating the probability of system failure related to some simple structures. The drawback of the method, however, is the difficulty in finding all the system failure modes with respect to the complex structures. Therefore, it is hard to be applied in evaluating system reliabilities of complex structures.

3.1.2. The Series-Parallel Modelling Method. Another conventional method is the series-parallel modeling method [17]. The goal of this method is to simplify the overall structure to a series-parallel model. The system reliability is a function of the series-parallel model, the individual reliabilities of all possible failure modes for each of the components in the model, and the correlations among the failure modes [10, 16, 18]. A series system is sometimes referred to as the weakest link system, since the failure of the system corresponds to the failure of the weakest component in the system [17]. The probability of system failure of a series system can be expressed as

$$P_s = \text{Probability}\left[\text{Any } g_i < 0\right], \tag{3}$$

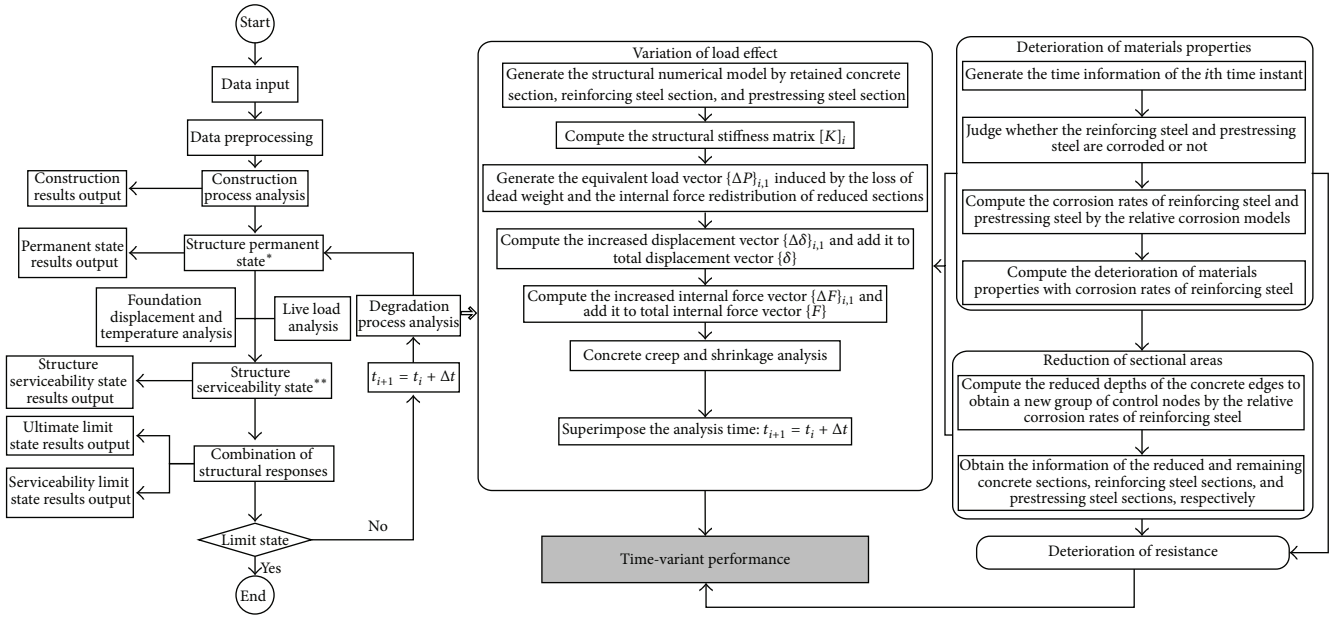

FIGURE 3: The flow chart of CBDAS for the analysis procedure of the time-variant performance. ∗: structure permanent state is the structural response with dead loads, such as structural weight, construction process, deck pavement, lost dead weight, and internal force redistribution. ∗∗: structure serviceability state is the structural response with variable loads, such as vehicle, people, and temperature.

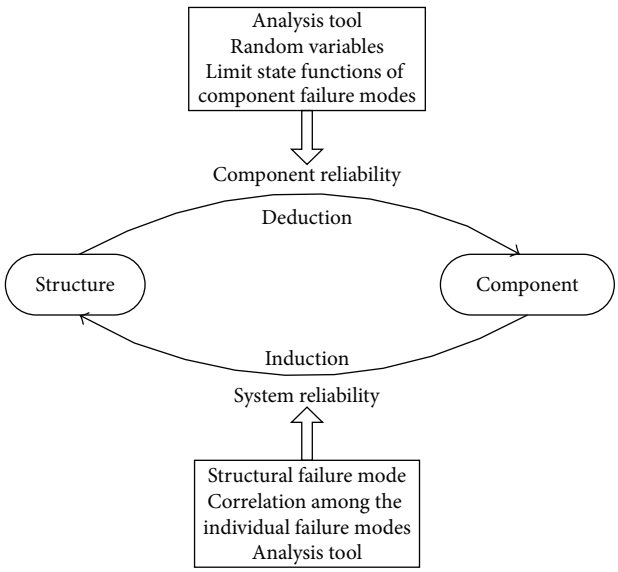

FIGURE 4: Schematic for calculating the system reliability.

where P_s is the probability of system failure and g_i is the limit state function of the ith component failure mode. A parallel system is in a state of failure when all of its elements fail [17] and its probability of system failure should be

$$P_s = \text{Probability}\left[\text{All } g_i < 0\right]. \quad (4)$$

Actually, most of the structures should be considered as the combination of series and parallel systems. Such systems are referred to as hybrid or combined systems. This method provides a rather comprehensive insight into the relationship between the overall structure and the individual components and, as a consequence, induction from the components to the structure is effectively solved. Furthermore, deduction from structure to components can be performed by using finite element analysis with respect to the complex structures or calibrated limit state functions with respect to the simple structures. The obstacle of this method, however, is in the determination of the correlations among the individual components failure modes. For this reason, the assumed values of the correlation coefficients are commonly used in previous studies and thus the accuracy of the results cannot be guaranteed.

3.2. Monte Carlo Simulations-Based Method. To overcome the deficiencies involved in the conventional methods, a Monte Carlo simulations-based approach is presented herein, which can be divided into two sections: (1) a component reliability calculating method and (2) a structural failure mode searching technique. The first section presents the analysis related to deduction from the structure to components associated with the geometry and layout of the structure, its external loads, along with a construction method. The objective of the second section is to determine the relationship between individual component failure and overall structural failure.

3.2.1. Component Reliability. The two essential ingredients for calculating component reliability are the limit state function and the analysis method. A limit state function is related to the difference between the resistance and load effect [18–20]. Based on finite element analysis, the state function of component failure mode i can be formulated by means of

the physical quantity of interest (e.g., flexural moment and shear force) as

$$g_i(\mathbf{q}_i) = R_i - S_i, \tag{5}$$

where $\mathbf{q}_i$ represents a group of variables with respect to the physical quantity of component failure mode I and R_i and S_i are the resistance and load effect in component failure mode i. Hence, the effect of the structural configuration, construction method, and external loads on R_i and S_i can be comprehensively taken into account by using the proposed approach. The finite element-based method proposed in the previous section is utilized to evaluate R_i and S_i, and several analytical methods can be used to calculate the component reliability, such as the first-order (FORM) or second-order (SORM) moment methods. First-order [21] or, more accurately, second-order [22] method is applicable to accounting for the correlations among the resistances and load effects reflected in the component limit state functions and can estimate the component reliabilities efficiently. Alternatively, Monte Carlo simulations can be performed to directly evaluate the probability of individual failure more accurately. Monte Carlo simulations are selected herein to evaluate the component reliability, in order to better combine with the searching technique of the structural failure mode introduced in the latter section.

3.2.2. Structural Failure Mode. To determine the structural failure mode, the most formidable task is to determine the relationship between overall structure failure and individual component failure to determine when the failure of an individual component has occurred and whether the overall structure is still safe or not [23, 24]. In this study, a practical technique for searching the structural failure mode proposed is mainly based on the degree of static indeterminacy of the overall structure [25]. The proposed technique can be described as the following steps:

(1) Search out the subsets of component failure modes according to the geometry and layout of the overall structure. Each subset, composed of several component failure modes, represents one of the local behaviors or the overall performance of the structure. The reasons for defining these subsets as such are as follows: (1) local failure can induce the overall structure collapse and (2) the number of component failure modes in a subset triggering the local failure may be less than the one in the subset leading to the system failure. At least one subset should be taken into account, in which all the component failure modes of the structure are included and, furthermore, the same component failure mode can appear in the different subsets simultaneously.

(2) Decide the minimum degree of static indeterminacy of the structure based on the structural original degree of static indeterminacy and the expert advice. The minimum degree should be between 0 and the original degree of static indeterminacy.

(3) Determine the minimum number of the occurring component failures that can trigger the local failure or the system failure in each subset. The minimum number related to the subset, where all the component failure modes are included, should be equal to

$$N_s = D_o - D_a + 1, \tag{6}$$

where N_s is the minimum number of the occurring component failures triggering the system failure, D_o is the original degree of static indeterminacy of the structure, and D_a is the designated minimum degree of static indeterminacy of the structure. In the case of other subsets, the smallest numbers can be determined in terms of the local configuration and the expert advice, and meanwhile, they should be less than N_s.

Finally, it is clear that the structural failure mode should be composed of the subsets related to the component failure modes, the designated minimum degree of static indeterminacy of the structure, and the minimum number of occurring component failures triggering the local failure or the system failure in each of the subsets. In the ith deterministic analysis, if the number of the occurring component failures in any of the subsets is equal to or even more than the designated minimum number, the overall structure is failure.

Two examples are illustrated to display the proposed structural failure mode searching technique. The first example is a one-story truss shown in Figure 5(a). The truss is composed of five bars (components) and the original degree of static indeterminacy of the structure is 1. The tensile or compressive failure of each bar is considered and thus the total component failure modes are 5. Based on the proposed technique, two different structural failure modes can be searched out, in which only one subset is included, respectively. The subset is composed of all the component failure modes in the structure. The difference of the two structural failure modes is the designated minimum degree of static indeterminacy of the structure. If the minimum degree is defined as 0, the minimum number of the occurring component failures in the subset should be 2. If the structure is required to be conservatively constructed according to the expert advice, however, the minimum degree is assumed to be 1. Therefore, the minimum number of the occurring component failures is 1. In this case, the overall structure is similar to a series system, since the occurrence of any component failure can trigger the system failure.

The second example shown in Figure 5(b) is a two-story truss with 10 bars (components). Based on the structural mechanics analysis, the original degree of static indeterminacy is investigated to be 2, and the proposed technique is used to search the structural failure modes. The overall structure can be divided into two one-story trusses including bars 1–5 and bars 6–10, respectively. Thus, three subsets should be considered and the component failure modes included in these subsets are tensile (compressive) failures of bars 1–5, bars 6–10, and bars 1–10, respectively. In this example, three structural failure modes can be sought out, and in the first failure mode, the minimum degree of static

Table 1: Critical parameters involved in the structural failure modes.

Parameters Examples	Structural failure mode	Minimum degree of static indeterminacy	Subset	Minimum number of the occurring CFMs*	Including CFMs
One-story truss	1	0	1	2	1–5
	2	1	1	1	1–5
Two-story truss	1	0	1	2	1–5
			2	2	6–10
			3	3	1–10
	2	1	1	2	1–10
	3	2	1	1	1–10

*CFMs: component failure modes.

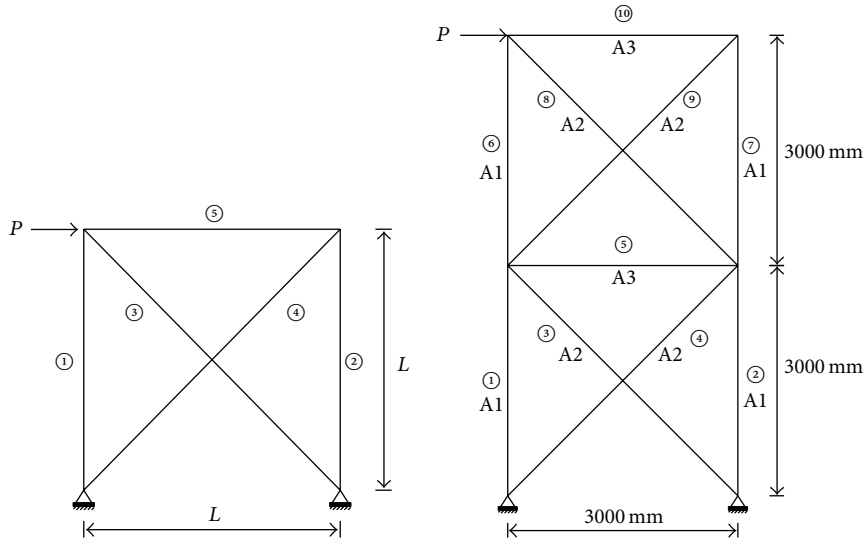

(a) The geometry of a one-story truss (b) The geometry of a two-story truss

Figure 5: The geometry of example truss.

indeterminacy is defined as 0 (i.e., the static determinacy is allowable). Consequently, minimum numbers of the occurring component failures in the subsets are 2, 2, and 3, respectively. In the case of the second failure mode, the minimum degree of static indeterminacy is assumed as 1 with conservative consideration derived from the expert advice, and the minimum numbers of the occurring component failures in the three subsets are all identical to 2. In this case, since the third subset includes all the component failure modes, the other two subsets are included in this subset and the number of the subsets is reduced to 1. As for the third failure mode, if more conservative consideration is required, the minimum degree of static indeterminacy is assumed to be 2. Similar to the second structural failure mode, only the subset containing all the component failure modes is necessary to be investigated and its minimum number of the occurring component failures should be 1. The values of critical parameters encountered in the structural failure modes relating to the abovementioned two examples are summarized in Table 1.

A Monte Carlo simulations-based method for evaluating the system reliability is set up based on the proposed structural failure mode searching technique. Accordingly, a program named SRMCS (System Reliability by Monte Carlo Simulations) [13] and written in MATLAB has been developed to perform this approach. Figure 6 shows the schematic of the proposed method for calculating the system reliability.

4. Numerical Examples

Three numerical examples are illustrated to display the functions of CBDAS, SRMCS, and the combination of the two programs. In the first example, the time-variant performance of a reinforced concrete continuous bridge under chloride-induced corrosion is evaluated by means of CBDAS; in the second example, the procedure to calculate the system reliability of a two-story truss is displayed by using SRMCS; and in the last example, the time-variant system reliability related to the same model as the first example is calculated by combination of CBDAS and SRMCS.

4.1. Example 1. In the first example, the lifetime performance of a reinforced concrete continuous bridge shown in Figure 7

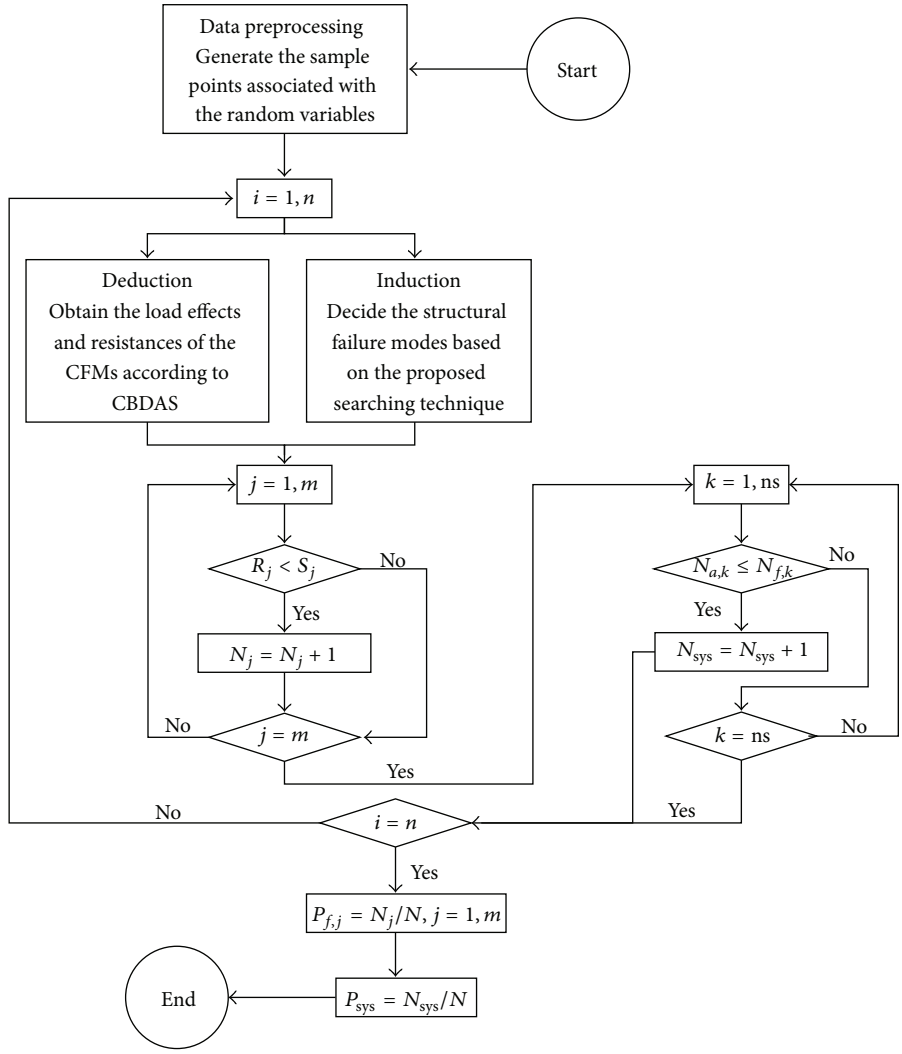

Figure 6: Schematic of the proposed method for calculating the system reliability.

is discussed. This bridge, located in Shanghai, China, is a 3 × 22 m three-span reinforced concrete continuous girder bridge with a single-box section. In this study, since the model bridge is near East China Sea and the concentration of chloride ion in the atmosphere may be relatively high, chloride-induced corrosion is taken into account. The values of the major parameters are listed in Table 2. It should be noted that the chloride ion concentrations at the different surfaces of the concrete section may be not identical. For this reason, the values of the chloride ion concentrations at different concrete edges are determined as shown in Table 3. The prescribed service life is defined as 100 years.

Figure 8 shows three critical times in the degradation process related to all the edges involved in the concrete section at the midspan center in the model bridge. The differences of the same critical time among the concrete edges are evident since the values of the design parameters among the concrete edges are not identical. The shortest critical times appear on edge 7, with the values of 19, 22, and 24 years, because the minimum concrete cover depth, the highest concentration of chloride ion, and the largest diameter of reinforcing steel happen to appear in this edge. On the contrary, the critical times of edge 18 are the longest among all the edges in the concrete section. The corrosion initiation

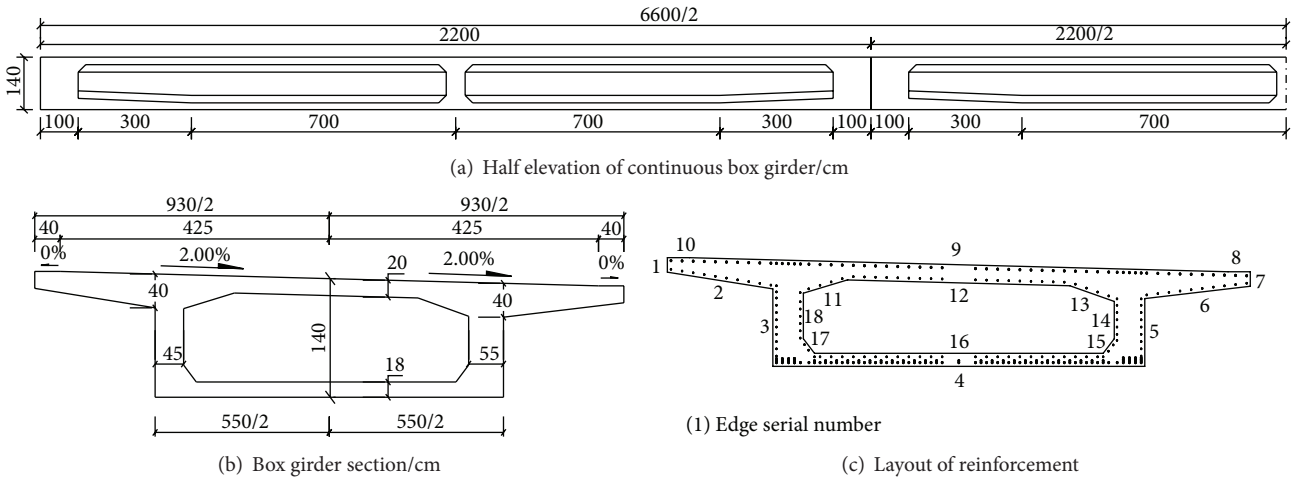

Figure 7: Profile of reinforced concrete continuous bridge.

Table 2: Values of the major parameters.

Variable	Value	Variable description
E_c	34,500 MPa	Concrete elastic modulus
f_c	32.4 MPa	Concrete compressive strength
E_s	200,000 MPa	Reinforcing steel elastic modulus
f_s	335 MPa	Reinforcing steel tensile strength
C	C_{nom} [a]	Concrete cover thickness
d_s	$d_{s,\text{nom}}$ [b]	Reinforcing steel diameter
γ_c	25 kN/m^3	In situ concrete unit weight
γ_s	78.5 kN/m^3	Reinforcing steel unit weight
γ_a	23 kN/m^3	Deck paving unit weight
Q	10.5 kN	Uniform live load
P	250 kN	Concentrated live load
M_s	6.9 kg/m^3	Surface chloride concentration
M_{cr}	1.5 kg/m^3	Critical chloride concentration
D_c	22.5 mm^2/year	Diffusion coefficient

[a] C_{nom} is the cover thickness of some concrete edge in the section.
[b] $d_{s,\text{nom}}$ is the reinforcing steel diameter of some concrete edge in the section.

Table 3: Values of chloride ion concentrations at different concrete edges.

Concrete edge	Environmental condition	Value
5, 6, 7	Face to the sea	100% of the value in Table 2
1, 2, 3	Back to the sea	70% of the value in Table 2
4, 8, 9, 10	Between the first two conditions	85% of the value in Table 2
11–18	Interior edges	Half of the value of relative exterior edges

times of 10 concrete edges from the total eighteen concrete edges are less than 100 years (i.e., the prescribed service life), and as a consequence, the corrosion of reinforcing steel and concrete cracking have only occurred in the 10 edges. Compared with the concrete edges in exterior surface, the

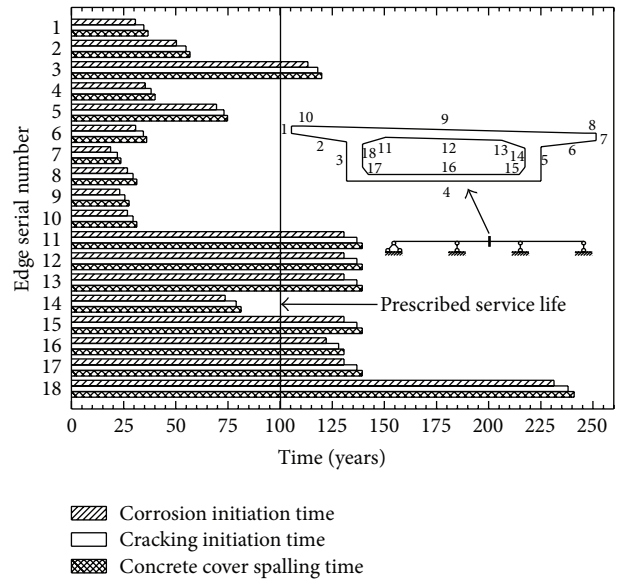

Figure 8: Critical times in the degradation process.

edges of the interior surface have relatively long critical times due to the low concentrations of chloride ion. The corrosion initiation times of all the interior concrete edges are longer than 100 years except edge 14, where the cover thickness is comparatively thin. Since the critical times related to the concrete edges may be significantly different as a result of the various values of the environmental and other design parameters, the conclusion can be drawn that it is necessary to form the concrete section by using its edges as the basic unit based on the above results, when the lifetime structural performance is investigated.

Figure 9 displays the time-variant area loss rates of reinforcing steel and concrete sections at the midspan center in the model bridge. It is clear that the area loss of reinforcing steel section initiates at about 19 years, which corresponds to the results shown in Figure 8 where the earliest corrosion initiation time is also 19 years. The corrosion rate gradually

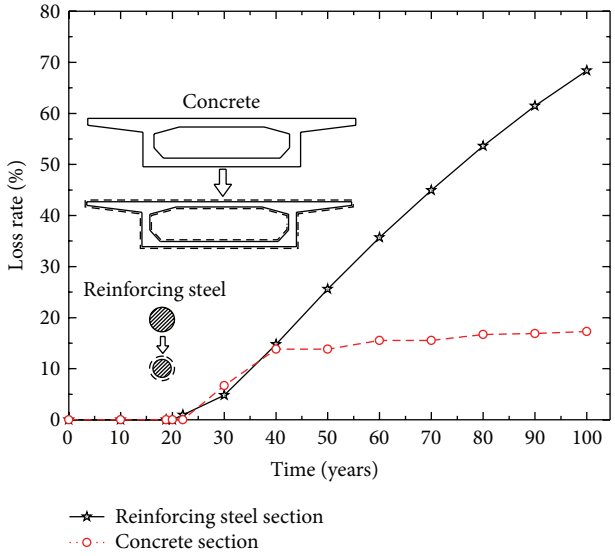

Figure 9: Time-variant area loss rates of reinforcing steel and concrete sections.

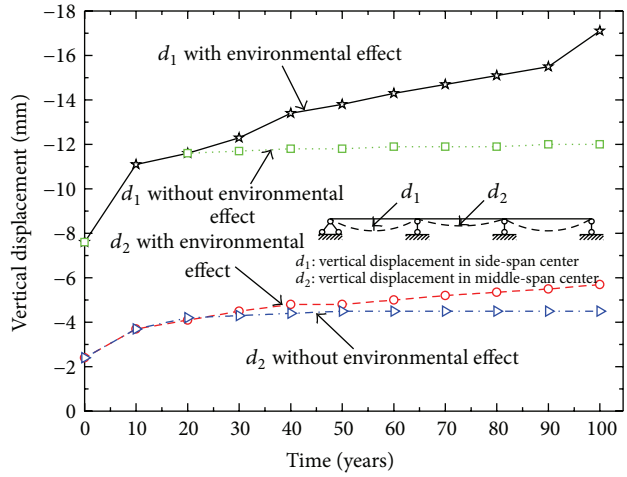

Figure 10: Variations of vertical displacements at critical locations.

increases from 20 years to 40 years, since the concrete at seven edges begins to crack during this period accelerating the corrosion of reinforcing steels wrapped in these concrete edges. At the end of service life, the area loss rate of reinforcing steels wrapped in the entire concrete section reaches about 70%. In the case of concrete, it is clear from Figure 9 that its section begins to reduce at about 22 years. Note that the increase in area loss rate of the concrete section is not significant after 40 years. This is because (1) the entire concrete covers at seven edges are all spalling during the first 40 years and the concrete is assumed not to continue cracking in these edges and (2) the concrete at only three edges cracks and leads to the reduction of concretion section after 40 years. Finally, the area loss rate of the concrete section is about 17.3% at 100 years.

To determine the effect of environmental attack on the lifetime structural performance, two time-variant performance cases with and without the environmental effect are now considered the structural vertical displacement. Figure 10 displays the variations of the vertical displacements at two critical locations (i.e., the side-span and middle-span centers). Note that the displacement along the direction of y-axis in the global coordinate system is assumed as positive. In the first 10 years after structural completion, the variations of the vertical displacements are significant due to the concrete creep and shrinkage. When the environmental effect is considered, the time-variant vertical displacements after the first 10 years can be described as follows: (1) from 10 years to 20 years, the variations of vertical displacements are not evident, since the effect of concrete creep and shrinkage is gradually weak and the corrosion initiation times related to most of the reinforcing steels are longer than 20 years; (2) from 20 years to 100 years, the variations of vertical displacements are gradually significant again due to the reductions of reinforcing steel and concrete sections as a result of the reinforcing steel corrosion and concrete cracking. The degree of variation caused by the environmental effect is similar to the one induced by concrete creep and shrinkage. When the environmental effect is not considered, the vertical displacements at the two critical locations are nearly invariant after 10 years.

The flexural moment and the ultimate limit stage are now discussed where the variations of the flexural moments at two critical locations (i.e., the side-span center and the middle-pier top) are shown in Figure 11. The flexural moment leading to tensile stress at the bottom of the concrete section is assumed to be positive and the time-variant flexural moment throughout the service life can be described as follows. In the first 10 years after structural completion, the evident variations of the flexural moments are the result of concrete creep and shrinkage. If the environmental effect is considered, the variations of the flexural moments during the subsequent 10 years and from 20 years to 100 years are apparent and significant, due to the same reasons as that of the vertical displacement. When the environmental effect is not considered, the variations of the flexural moments at the two critical locations are insignificant after 10 years. It should be noticed, from this figure, that the variations of the flexural moments at the two critical locations with the environmental effect are not monotonic during service life. This is because of (1) the time-variant location of the neutral axis of concrete section due to the reduction of the section; (2) the loss of dead weight induced by the reduction of concrete section; and (3) the redistribution of the internal force caused by the reductions of reinforcing steel and concrete sections. For these results, the flexural moment may increase or decrease over the life cycle of a structure.

4.2. Example 2. In the third example, the same model as the first example shown in Figure 7 is used to illustrate the computation of time-variant system reliability associated with the proposed methods for calculating the time-variant performance and system reliability. The distribution types and associated statistical descriptors of the random variables involved in the structural configuration, materials properties, live loads, and environment are summarized in Table 4,

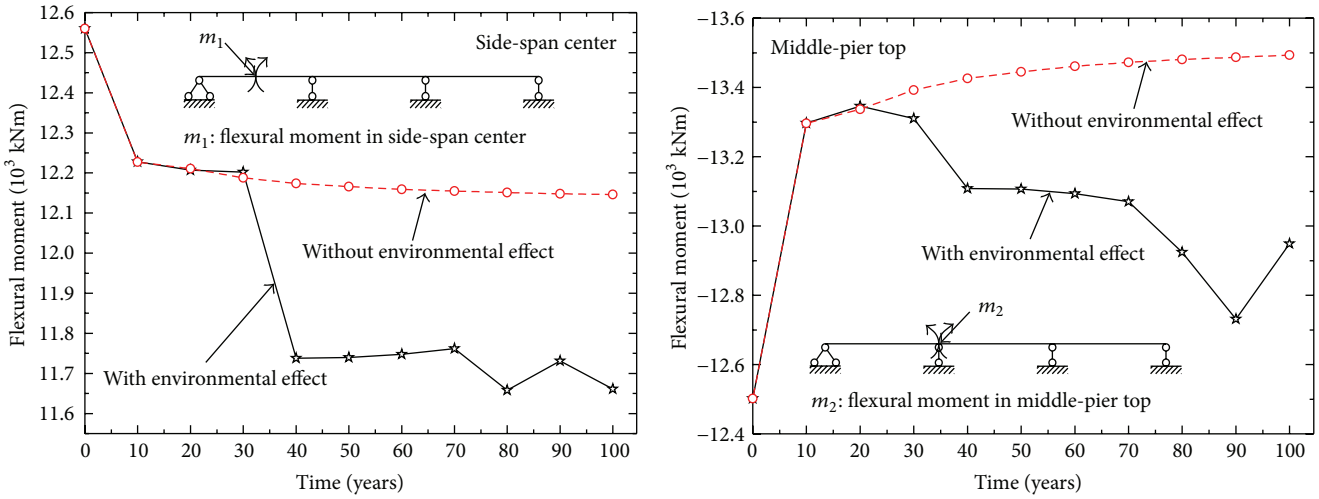

(a) Side-span center (b) Middle-pier top

Figure 11: Variations of flexural moments at critical locations.

Table 4: Statistical parameters of random variables.

Variable	Nominal	Mean	COV[a]	Distribution type
E_c	34,500 MPa	34,500 MPa	0.10	Normal[b]
f_c	32.4 MPa	40.5 MPa	0.12	Normal[b]
E_s	200,000 MPa	200,000 MPa	0.06	Normal[b]
f_s	335 MPa	375 MPa	0.065	Normal[b]
C	C_{nom}	$1.02C_{\text{nom}}$	0.05	Normal[b]
d_s	$d_{s,\text{nom}}$	$1.0d_{s,\text{nom}}$	0.02	Normal[b]
γ_c	25 kN/m^3	26 kN/m^3	0.06	Normal[b]
γ_s	78.5 kN/m^3	80.1 kN/m^3	0.05	Normal[b]
γ_a	23 kN/m^3	23 kN/m^3	0.04	Normal[b]
Q	10.5 kN	9.03 kN	0.08	Extreme value type I
P	250 kN	215 kN	0.08	Extreme value type I
M_s	6.9 kg/m^3	6.9 kg/m^3	0.1	Normal[b]
M_{cr}	1.5 kg/m^3	1.5 kg/m^3	0.15	Normal[b]
D_c	22.5 mm^2/year	22.5 mm^2/year	0.45	Lognormal

[a]COV is the coefficient of variation.
[b]Truncated distributions with nonnegative outcomes are adopted in the simulation process.

according to the structural drawing and relative literatures [26]. The prescribed service life and the unit calculating time are assumed as 100 years and 10 years, respectively. The same as the second example, the number of samples in Monte Carlo simulations is defined as 200,000.

Based on the structural decomposition technique presented in [13], the three-span reinforced concrete bridge is divided into 21 components, with seven components in each span. Ultimate limit state is only discussed here, since the structural resistance is more likely to deteriorate significantly due to the area loss of reinforcing steel section over the life cycle of a structure. When two component failure modes, flexure failure and shear failure, are taken into account, the number of the component failure modes is 42 for overall structure and 14 for each span as shown in Figure 12, and the key parameters of the structural failure mode are summarized in Table 5. Three structural failure modes can be sought out

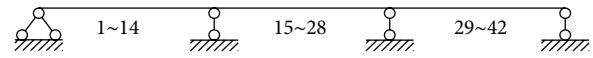

(1) Serial number of component failure mode

Figure 12: The component failure modes.

from the model bridge, in which the designated minimum degrees of static indeterminacy are 0, 1, and 2, respectively.

The variation of the system reliabilities for different structural failure modes throughout the service life is displayed in Figure 13, showing that the time-variant system reliabilities with respect to the structural failure modes 2 and 3 are identical. This is because (1) the minimum individual reliability of component failure mode appears on the side span and (2) the structure is symmetrical. Thus, when a component failure mode in a side span occurs, its

Table 5: Key parameters of the structural failure mode.

Structural failure mode	Minimum degree of static indeterminacy	Subset serial number	Minimum number of the occurring CFMs*	Including CFMs
1	0	1	2	1–14
		2	2	29–42
		3	3	1–42
2	1	1	2	1–42
3	2	1	1	1–42

*CFMs: component failure modes.

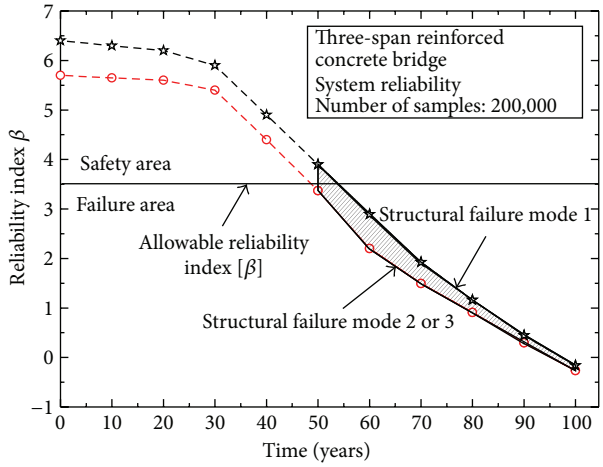

Figure 13: Variation of the system reliability.

counterpart in another side span has also appeared. The system reliabilities of different structural failure modes from 0 to 50 years are shown as the dash lines, since they cannot be calculated by using the prescribed number of samples (i.e., 200,000). However, we are concerned with the variation of system reliability below the allowable reliability index $[\beta]$ (i.e., in the failure area), which can be evaluated and is shown as solid lines in the figure. The actual system reliability of the overall structure should be between the star-solid line and the circle-solid line, the shadow region of Figure 13, showing that the difference of the system reliabilities among the structural failure modes gradually decreases from 50 to 100 years. In addition, the system reliabilities with respect to all the structural failure modes reduce to negative values at the end of service life. Thus, maintenance interventions are required to improve the structural performance during that life. According to the obtained system reliability profile, the appropriate maintenance application time should be at 50 years when the system reliability is about to decrease to the failure area.

5. Conclusions

A finite element- and Monte Carlo simulations-based computational methodology is proposed in this paper to evaluate the time-variant system reliability of deteriorating concrete bridges under environmental attacks. Methods for solving the reduction of concrete section and the variation of structural load effect are investigated for time-variant performance. For system reliability, a novel structural failure mode searching technique is proposed. Accordingly, two programs, CBDAS and SRMCS, are written to perform these analyses from which the time-variant system reliability of deteriorating concrete bridge can be calculated. Finally, two examples are presented to demonstrate the functions of CBDAS, SRMCS, and the combination of the two programs. The following conclusions can be drawn:

(1) The first example shows that the differences of the critical time variants between the edges in a concrete section may be significant due to the various values of the design parameters among the concrete edges. These differences have great influence on deterioration in the reinforcing steel and concrete sections of bridges. Thus, to simulate the actual reduction process of concrete sections, it is necessary to delineate the concrete section by using its edge as the basic unit.

(2) Again from the first example, it is clear that the variations of the performance indicators reflecting the structural serviceability and strength, such as the structural vertical displacement and flexural moment, are significant due to the effect of concrete creep and shrinkage and reduction of sectional areas at the beginning and end of service life and the degree of variation related to the serviceability-performance indicator is more significant than that of strength-performance indicator. This is because the reduction of reinforcing steel and concrete sections has a great effect on vertical displacement but little effect on flexural moment. Moreover, since essential variables such as the construction process, concrete creep, and shrinkage and the reduction of sectional areas and variations in overall structural performance can be measured collectively by using the finite element-based approach, the lifetime performance of concrete bridges exposed to aggressive environments can be accurately evaluated.

(3) The time-variant system reliability of concrete bridges with environment attacks can be evaluated accurately using the Monte Carlo simulations-based and the finite element-based approach because (a) determination of the correlation coefficients of the individual component failure modes is not needed in the proposed method; (b) by using the proposed

finite element-based assessment method, the limit state functions of the individual component failure modes are sufficient to obtain good results; and (c) based on the structural failure mode searching technique, the relationship between the individual component failures and the overall structural failure can be effectively simulated during the lifetime of bridges negatively affected by adverse environmental conditions.

Conflict of Interests

The authors declare that there is no conflict of interests regarding the publication of this paper.

Acknowledgment

This research was supported by Zhejiang Provincial Natural Science Foundation of China (no. LQ14E080001).

References

[1] M. G. Richardson, *Fundamentals of Durable Reinforced Concrete*, CRC Press, London, UK, 2002.

[2] R. Rackwitz, "Reliability analysis—a review and some perspective," *Structural Safety*, vol. 23, no. 4, pp. 365–395, 2001.

[3] L. Burgazzi, "About time-variant reliability analysis with reference to passive systems assessment," *Reliability Engineering and System Safety*, vol. 93, no. 11, pp. 1682–1688, 2008.

[4] Z. Wang and P. Wang, "A new approach for reliability analysis with time-variant performance characteristics," *Reliability Engineering & System Safety*, vol. 115, pp. 70–81, 2013.

[5] W. Zhang and H. Yuan, "Corrosion fatigue effects on life estimation of deteriorated bridges under vehicle impacts," *Engineering Structures*, vol. 71, pp. 128–136, 2014.

[6] J. S. Kong and D. M. Frangopol, "Prediction of reliability and cost profiles of deteriorating bridges under time- and performance-controlled maintenance," *Journal of Structural Engineering*, vol. 130, no. 12, pp. 1865–1874, 2004.

[7] A. A. Czarnecki and A. S. Nowak, "Time-variant reliability profiles for steel girder bridges," *Structural Safety*, vol. 30, no. 1, pp. 49–64, 2008.

[8] S. Kim and D. M. Frangopol, "Inspection and monitoring planning for RC structures based on minimization of expected damage detection delay," *Probabilistic Engineering Mechanics*, vol. 26, no. 2, pp. 308–320, 2011.

[9] F. Biondini and D. M. Frangopol, "Lifetime reliability-based optimization of reinforced concrete cross-sections under corrosion," *Structural Safety*, vol. 31, no. 6, pp. 483–489, 2009.

[10] A. Titi, F. Biondini, and D. M. Frangopol, *Lifetime Resilience of Aging Concrete Bridges under Corrosion*, CRC Press, London, UK, 2014.

[11] G. P. Li, *Bridge Structure Analysis Composite System*, Tongji University Press, Shanghai, China, 1998.

[12] P. Lu, F. Li, and C. Shao, "Analysis of a T-frame bridge," *Mathematical Problems in Engineering*, vol. 2012, Article ID 640854, 14 pages, 2012.

[13] H. Tian, *Research on Structure Performance Evolution of Concrete Bridges in Given Service Life*, Department of Bridge Engineering, Tongji University, Shanghai, China, 2009.

[14] Q. Gu, "Performance and risk assessment of soil-structure interaction systems based on finite element reliability methods," *Mathematical Problems in Engineering*, vol. 2014, Article ID 704804, 16 pages, 2014.

[15] S.-I. Yang, D. M. Frangopol, Y. Kawakami, and L. C. Neves, "The use of lifetime functions in the optimization of interventions on existing bridges considering maintenance and failure costs," *Reliability Engineering & System Safety*, vol. 91, no. 6, pp. 698–705, 2006.

[16] N. M. Okasha and D. M. Frangopol, "Lifetime-oriented multi-objective optimization of structural maintenance considering system reliability, redundancy and life-cycle cost using GA," *Structural Safety*, vol. 31, no. 6, pp. 460–474, 2009.

[17] A. S. Nowak and K. R. Collins, *Reliability of Structures*, McGraw-Hill, New York, NY, USA, 2000.

[18] E. Bastidas-Arteaga, P. Bressolette, A. Chateauneuf, and M. Sánchez-Silva, "Probabilistic lifetime assessment of RC structures under coupled corrosion-fatigue deterioration processes," *Structural Safety*, vol. 31, no. 1, pp. 84–96, 2009.

[19] S. Y. Kim and D. M. Frangopol, "Optimal planning of structural performance monitoring based on reliability importance assessment," *Probabilistic Engineering Mechanics*, vol. 25, no. 1, pp. 86–98, 2010.

[20] H. Tian, X.-P. Jin, and A.-R. Chen, "Probabilistic-based effect analysis of different maintenance actions on reinforced concrete bridges," *Journal of Zhejiang University Engineering Science*, vol. 46, no. 6, pp. 1097–1121, 2012.

[21] C. A. Cornell, "Bounds on the reliability of structural systems.93(ST1)," *Journal of Structural Division*, vol. 93, no. 1, pp. 171–200, 1967.

[22] A. Der Kiureghian, H.-Z. Lin, and S.-J. Hwang, "Second-order reliability approximations," *Journal of Engineering Mechanics*, vol. 113, no. 8, pp. 1208–1225, 1987.

[23] H.-C. Liu, L. Liu, and N. Liu, "Risk evaluation approaches in failure mode and effects analysis: a literature review," *Expert Systems with Applications*, vol. 40, no. 2, pp. 828–838, 2013.

[24] R. Kanapady and R. Adib, "Application of modeling and simulation for high risk failure modes," in *Proceedings of the Annual Reliability and Maintainability Symposium*, pp. 1–6, IEEE, Reno, Nev, USA, January 2012.

[25] P. Wei, Z. Lu, and B. Ren, "Reliability analysis of structural system with multiple failure modes and mixed uncertain input variables," *Proceedings of the Institution of Mechanical Engineers Part C: Journal of Mechanical Engineering Science*, vol. 227, no. 7, pp. 1441–1453, 2013.

[26] *Code for Design Reinforced Concrete and Prestressed Concrete Bridges and Culverts*, China Communications Press, Beijing, China, 2004.

Hindawi Publishing Corporation
Mathematical Problems in Engineering
Volume 2015, Article ID 296394, 11 pages
http://dx.doi.org/10.1155/2015/296394

Research Article

Real-Time Track Reallocation for Emergency Incidents at Large Railway Stations

Wei Liu, Xiaoning Zhu, and Liujiang Kang

School of Traffic and Transportation, Beijing Jiaotong University, Beijing 100044, China

Correspondence should be addressed to Liujiang Kang; 243525771@qq.com

Received 16 September 2015; Revised 13 November 2015; Accepted 16 November 2015

Academic Editor: Egidijus R. Vaidogas

After track capacity breakdowns at a railway station, train dispatchers need to generate appropriate track reallocation plans to recover the impacted train schedule and minimize the expected total train delay time under stochastic scenarios. This paper focuses on the real-time track reallocation problem when tracks break down at large railway stations. To represent these cases, virtual trains are introduced and activated to occupy the accident tracks. A mathematical programming model is developed, which aims at minimizing the total occupation time of station bottleneck sections to avoid train delays. In addition, a hybrid algorithm between the genetic algorithm and the simulated annealing algorithm is designed. The case study from the Baoji railway station in China verifies the efficiency of the proposed model and the algorithm. Numerical results indicate that, during a daily and shift transport plan from 8:00 to 8:30, if five tracks break down simultaneously, this will disturb train schedules (result in train arrival and departure delays).

1. Introduction

To solve the track allocation problem in a railway station, a conflict-free route must be found for each arrival/departure train. This optimization problem, known as the train routing problem or the train platform problem, is one of the basic scheduling problems for railway companies. In terms of complexity, this problem is NP-hard [1]. Nevertheless, it can be modeled and solved using operation research techniques. Due to the signal problem, frequent use, or other reasons, available tracks at a railway station may break down (may be unavailable). In addition, track incidents are generally uncertain and often disturb train schedules such that trains will be delayed if station tracks are not effectively reallocated. In this paper, we consider the problem of real-time reallocation of trains to available tracks (except accidental tracks) at a large railway station, given one daily and shift transport timetable and the structural and operational constraints.

There are many existing studies that solve the track allocation problem. Zwaneveld et al. [2] proposed a node packing formulation, and infrastructure capacity requirements were developed to evaluate future demand for rail transportation. To improve the solution method, Zwaneveld et al. [3] conducted an extension of [2]. Zwaneveld et al. assumed that trains prefer certain paths to others and this problem was formulated as a weighted node packing problem. A branch-and-cut solution approach was adopted to solve this NP-hard problem.

Cardillo and Mione [4], Billionnet [5], and Carey and Carville [6] studied a version of the problem termed *train platform problem* (TPP). Cardillo and Mione [4] proposed a heuristic algorithm with a backtracking method. The work of [5] demonstrated how the TPP models could be strengthened through the addition of clique inequalities. Carey and Carville [6] studied the problem at busy complex stations and developed scheduling heuristics analogous to train operators using the manual method.

TPP is affected by the structure of stations and yards, the bottleneck section structure, station operations, train timetables, train punctuality, and many other factors among which the train working diagram (TWD) plays an important role because it determines the start and end times of tracks utilized at railway stations [7]. Barber et al. [8] presented a set of heuristics for a constraint-based TWD tool and formulated

TWD as a constraint optimization problem. According to TWD and train routing in stations, Kang et al. [7] combined TPP with the station bottleneck carrying capacity. A case study that focused on bottleneck section optimization in passenger stations illustrated that TPP affects not only bottleneck capacity but also station capacity. D'Ariano et al. [9] introduced a new concept aimed at less planning on the timetable and solving more intertrain conflicts to improve punctuality without decreasing line capacity. A detailed model for conflict resolution was illustrated, and different algorithms based on the alternative graph formulation were analyzed in their work. Heydar et al. [10] investigated the capacity of a single track, bidirectional rail line that adheres to a cyclic timetable.

When probabilities for unexpected events are estimated, efficiency is a major concern and can be addressed through multilevel splitting or staged simulation [11]. After major service disruption in the railway operational system, dispatchers need to generate a series of train meet-pass plans at different decision times of the rescheduling stage to recover the impacted train schedule from current and future disturbances and minimize the expected additional delay under different forecasted operational conditions. Thus, railway controllers play a pivotal role in the service recovery of normal rail system operations when accidents occur. Cheng and Tsai [12] adopted Taiwan's railway system to diagnose railway-controller-perceived competence when facing diverse tasks during incidents and accidents that were derived from a proposed conceptual model. Belmonte et al. [13] presented an application of functional resonance accident models (FRAM) for the safety analysis of complex sociotechnological systems, that is, systems with not only technological components but also human and organizational components. The examples illustrated the principal advantages of FRAM in comparison to classical safety analysis models, which allowed true multidisciplinary cooperation between specialists from the different domains involved.

Operationally robust solutions are usually synonymous with compact, nonoverlapping routes with little or no intraroute crossover [14]. Railway companies are also interested in schedule reliability (assessed by means of cancelling the number of operating trains) and robustness (the ability to resist schedule perturbations). Intuitively, a more robust track allocation schedule is less likely to propagate delays to the following trains. Clearly, an efficient use of the railway infrastructure and the prospects of recovery cause TPP to become a more complex optimization problem in engineering theory and practice.

The aforementioned studies mainly focus on the track allocation optimization problem. After the track capacity breakdown(s) at a railway station, train dispatchers need to generate appropriate track reallocation plans to recover the impacted train schedule and minimize the expected total train delay time under stochastic scenarios. As a result, reallocating tracks in railway stations for emergency incidents to ensure service remains a significant issue. A model that can be exactly solvable by a global optimization method is also desired.

On the basis of station track incidents, a model considering the minimum average use time of bottleneck sections is proposed to reduce technical process time and improve the antijamming capacity. The bottleneck and station carrying capacity can be improved simultaneously by tapping the potential and more effective occupation of normal tracks and bottleneck equipment. The contributions of this paper are listed as follows:

(1) A mathematical programming model is proposed to describe TPP after track incidents, which fully considers the tight capacity of station bottlenecks when some tracks break down.

(2) Virtual trains are introduced to represent track incidents. The novelty of this formulation is the use of virtual trains to occupy these unavailable tracks. In the Baoji passenger station, an incident in which five tracks break down simultaneously will lead to the delay of trains' arrival/departure.

(3) Genetic simulated annealing (GSA) focused on TPP is adopted. In addition, a genuine case in China is studied, and the station track allocation plan is given. The carrying capacity of the left side bottleneck is approximately 1.29 times more than the right side bottleneck.

This paper will be organized as follows. First, the model formulation section draws the TPP model out. In addition, the GSA of TPP is developed in the solution algorithm section. Furthermore, a real case from China is illustrated in Case Study. Finally, the Conclusions summarize this paper and discuss the future study.

2. Track Reallocation Model

2.1. Notations. Notations in this paper are as follows

Sets

I: set of groups of turnouts (GTs), $i \in I$, $I = \{i/i = 1, 2, \ldots, n\}$, where n is the total number of GTs. Herein, turnout is also called switch in stations.

I_L: set of GTs in the left station bottleneck, which consists of the number of GTs.

I_R: set of GTs in the right station bottleneck.

J: set of trains, $j \in J$, $J = \{j/j = 1, 2, \ldots, m\}$, where m is the total number of trains scheduled within TWD.

R: set of reception-departure tracks, $r \in R$, $R = \{r/r = 1, 2, \ldots, l\}$, where l is the total number of reception-departure tracks at a passenger station.

Parameters

T_S: security interval time between two neighboring trains that occupy the same track.

t_{rj}^S: starting time of train j occupying track r.

t_{rj}^E: ending time of train j occupying track r.

t_{ij}: traversing time of train j occupying GT i.

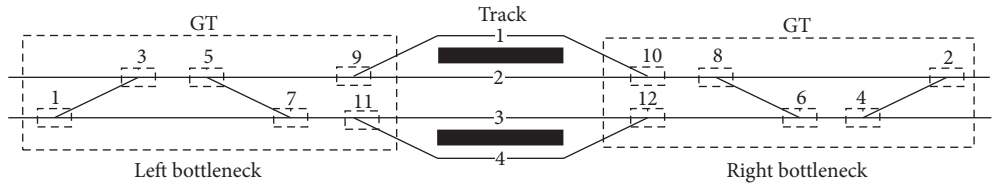

Figure 1: A sample station structure.

Variables

$x_{ij} = \begin{cases} 1, & \text{if train } j \text{ occupies GT } i; \\ 0, & \text{otherwise.} \end{cases}$

$x_{rj} = \begin{cases} 1, & \text{if train } j \text{ stays at track } r; \\ 0, & \text{otherwise.} \end{cases}$

T_j: the total time cost of GTs by train j.

T_L: the total time cost of GTs in the left bottleneck (detailed illustration of the left bottleneck can be found in Figure 1), $T_L = \sum_i \sum_j t_{ij}$.

T_R: the total time cost of GTs in the right bottleneck (detailed illustration of the right bottleneck can be found in Figure 1), $T_R = \sum_i \sum_j t_{ij}$.

2.2. Basic Assumptions. To solve and optimize TPP, several assumptions are used throughout this paper to simplify practical cases:

(1) Train arrival/departure times at/from the station are collected according to the existing timetable and cannot be changed. That is, there is no train shifting from the original timetable. In this case, the track reallocation plan is ordered by train arrival-departure times.

(2) Different trains traverse the same GT with equal time. This assumption eliminates the complexity of considering train types (e.g., train formation, train ranks). Thus, the total occupation time of a certain route composed of GTs can be accumulated.

(3) The security interval time (T_S) is assumed as a constant. Generally, there are different ranks of trains passing through stations, for example, passenger trains and freight trains. Obviously, T_S varies between different ranks of trains for their unique braking performance. This assumption can help substantially reduce the complexity of the model.

2.3. Model Formulations. To better explain the model formulations, a sample station is illustrated in Figure 1. There are four tracks and twelve GTs numbered from 1 to 4 and from 1 to 12, respectively, in the sample station. In Figure 1, the left bottleneck section contains six GTs, which are marked with odd numbers. On the contrary, the right bottleneck section consists of six even numbered GTs.

2.3.1. Constraints of TPP and Track Accidents. Operational constraints in a passenger station set limits on the track allocations of trains. To fulfill the service requirements and enable safety, the following constraints should be satisfied.

One Time, One GT, and One Train. For each GT $i \in I$ and $j \in J$, constraints (1) set the uniqueness occupation of each GT in a certain period of time punctually, where x_{ij} is a binary variable representing whether train j occupies GT i. A fixed GT cannot be traversed by other trains until it is released by the preceding train. Thus, during the periods of $[t_{rj}^S - T_s, t_{rj}^S]$ and $[t_{rj}^E, t_{rj}^E + T_s]$, where t_{rj}^S and t_{rj}^E represent the starting and ending times of train j occupying track r, constraints (1) should be satisfied:

$$\begin{aligned} \left[t_{rj}^S - T_s, t_{rj}^S\right] &: \sum_{j=1}^{m} x_{ij} \le 1, \\ \left[t_{rj}^E, t_{rj}^E + T_s\right] &: \sum_{j=1}^{m} x_{ij} \le 1. \end{aligned} \tag{1}$$

Obviously, if a train pulls in from the left bottleneck and stays on track 1 in Figure 1, it will traverse GTs [2, 3, 5, 8–10]. At the same time, if another train also pulls in from the left bottleneck, it cannot stay on track 2 because GTs [2, 3, 5, 8–10] have been occupied. However, this train can sit on track 3 or track 4 because GTs [1, 4, 6, 7, 11, 12] are free at that moment.

One Time, One Track, and One Train. x_r is a binary variable. $x_r = 1$ means track r breaks down, and $x_r = 0$ means track r can receive trains. Constraint (2) indicates that, during the period of $[t_{rj}^S, t_{rj}^E]$, track r is reserved for train j. Apart from this period, track r is released. Thus, constraint (2) examines the track state and limits the unique utilization of station tracks as well:

$$\left[t_{rj}^S, t_{rj}^E\right] : \sum_{j=1}^{m} x_{rj} \le (1 - x_r). \tag{2}$$

When x_r is equal to one, we have $\sum_{j=1}^{m} x_{rj} \le (1 - x_r) = 0$. This track breaks down and is occupied by one virtual train. On the contrary, when x_r is equal to zero, the right hand side $\sum_{j=1}^{m} x_{rj} \le (1 - x_r) = 1$ and track r is ready for allocation. With the binary variable x_r so defined, track incidents are described accurately.

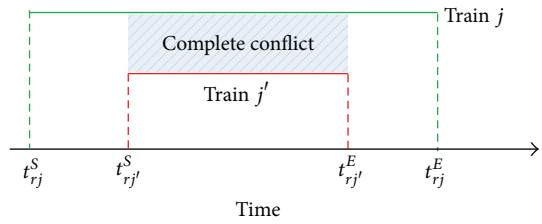

FIGURE 2: Complete conflict. Train j occupies track r from time t^S_{rj} to time t^E_{rj}, and train j' occupies track r from time $t^S_{rj'}$ to time $t^E_{rj'}$, where $t^S_{rj} \le t^S_{rj'} \le t^E_{rj'} \le t^E_{rj}$.

One Time, One Train, and One Track. Clearly, each coming train should be allocated with only one track. In the period of $[t^S_{rj}, t^E_{rj}]$, train j will stay on track r. Hence,

$$\left[t^S_{rj}, t^E_{rj}\right] : \sum_{r=1}^{l} x_{rj} = 1. \tag{3}$$

One Track, Two Trains, and Two Conflicts. A two-train conflict or greater can be decomposed by two trains. There are two types of conflicts on a track that must be avoided: complete conflict and partial conflict as referred to in Figures 2 and 3, respectively. To fulfill the requirements, there is a minimum security interval time, denoted by T_S, for two trains pulling on the same track. Figure 4 shows how two trains can stay on one identical track successively.

According to Figure 4, a conflict avoidance constraint can be built as (4); that is, one train cannot pull on to track r until the preceding train has departed from track r for at least T_S min. Hence, $\forall j \in J$, $j' \in J$, and $r \in R$,

$$x_{rj'} \cdot T^S_{rj'} - x_{rj} \cdot T^E_{rj} \ge T_S. \tag{4}$$

2.3.2. Objective Function of TPP. Many other urgent problems may be induced under sudden incidents on station reception-departure tracks, such as a delay in the train's arrival and departure and decreasing the carrying capacity of station bottleneck sections. These problems are brought about directly from one phenomenon: decreasing the number of available station tracks. In this case, station operators must repair tracks as quickly as possible and reallocate tracks effectively with a limited number of available tracks.

Figure 5 illustrates the flow of track reallocation after station track incidents. First, if the tracks have incidents, then the station capacity will definitely decrease. In this situation, the station bottleneck capacity also decreases because some tracks and GTs are frozen. Then, the predetermined routes (consisting of GTs) are changed and a new track reallocation plan is formulated.

The occupation time of each route to each track can be accumulated by GTs. For any train j, the traversing time of GTs is calculated in (5). In addition, different routes consist of different GTs. The average occupation time of each GT is used to express the cost of the route. Clearly, the less average occupation time a GT has, the better the route we choose.

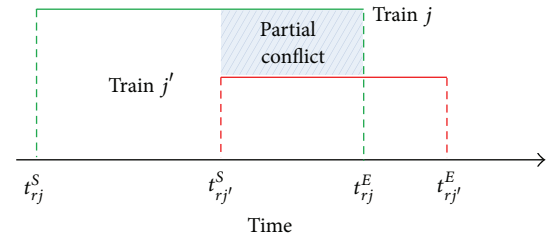

FIGURE 3: Partial conflict. Train j occupies track r from t^S_{rj} to t^E_{rj}, and train j' occupies track r from $t^S_{rj'}$ to $t^E_{rj'}$, where $t^S_{rj} \le t^S_{rj'} \le t^E_{rj} \le t^E_{rj'}$.

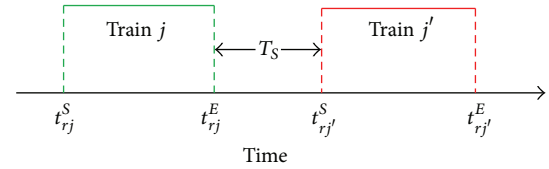

FIGURE 4: Conflict avoidance. Train j occupies track r from t^S_{rj} to t^E_{rj}, and train j' occupies track r from $t^S_{rj'}$ to $t^E_{rj'}$, where $t^S_{rj} \le t^E_{rj} \le t^S_{rj'} - T_s \le t^E_{rj'} - T_s$.

Therefore, (6) evaluates the average occupation time of GTs in a route. Therefore,

$$T_j = \sum_{i=1}^{n}\sum_{j=1}^{m} x_{ij} \cdot t_{ij}, \tag{5}$$

$$f = \frac{\sum_{i=1}^{n}\sum_{j=1}^{m} x_{ij} \cdot t_{ij}}{\sum_{i=1}^{n}\sum_{j=1}^{m} x_{ij}}. \tag{6}$$

As we know, if some tracks are in incidents, the carrying capacity of the tracks will decrease immediately. In addition, the capacity of the bottleneck sections is also reduced. Therefore, the objective function of our model should pursue the minimum average use time of GTs in bottleneck sections that constitute different routes and lead to normal and abnormal station tracks. For all $i \in I$, $j \in J$, $j' \in J$, and $r \in R$,

$$\begin{aligned} f = \min \quad & \frac{\sum_{i=1}^{n}\sum_{j=1}^{m} x_{ij} \cdot t_{ij}}{\sum_{i=1}^{n}\sum_{j=1}^{m} x_{ij}} \\ \text{s.t.} \quad & \left[t^S_{rj} - T_s, t^S_{rj}\right] : \sum_{j=1}^{m} x_{ij} \le 1 \\ & \left[t^E_{rj}, t^E_{rj} + T_s\right] : \sum_{j=1}^{m} x_{ij} \le 1 \\ & \left[t^S_{rj}, t^E_{rj}\right] : \sum_{j=1}^{m} x_{rj} \le (1 - x_r) \\ & \left[t^S_{rj}, t^E_{rj}\right] : \sum_{r=1}^{l} x_{rj} = 1 \\ & x_{rj'} \cdot T^S_{rj'} - x_{rj} \cdot T^E_{rj} \ge T_S. \end{aligned} \tag{7}$$

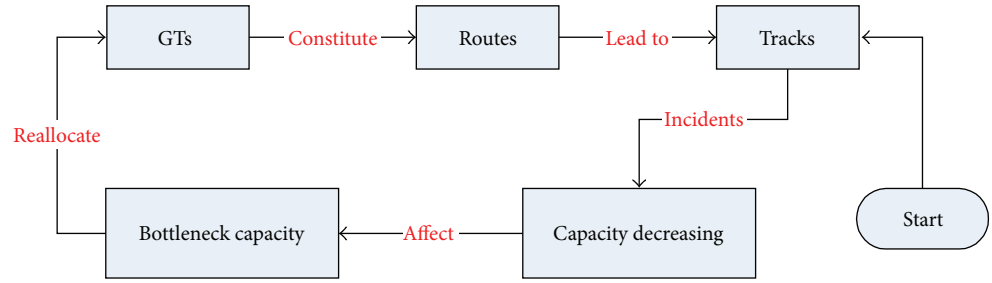

Figure 5: Track reallocation flow.

3. Solution Algorithm and Sample Test

Artificial intelligence algorithms have been widely adopted to solve NP-hard problems. Gandibleux et al. [15] proposed Ant Colony Optimization heuristics to solve the track allocation problem. As evolution of [15], the algorithm described in [16] improved the local search heuristic and stopping criterion. The node packing formulation used in [17] found robust routing for the train routing problem. In addition, [17] adopted the fixed-point iteration heuristic to exploit the clique structure. The improved research by [18] used the same fixed-point heuristic to consider both deterministic and probabilistic robust problem. Similarly, [7, 19] studied the track allocation problem at railway stations using the simulated annealing (SA) algorithm.

Studies [20, 21] designed a stochastic search scheme based on SA and the genetic algorithm (GA). For a nonconvex optimization system, GA may suffer from premature convergence on a local optimum. Escaping from local optima is accomplished with an SA search scheme, which is a stochastic process. Intervention in the SA is accomplished with a GA search scheme that provides promising search locations or directions when an SA search slows down or "freezes." Considering the nice compatibility of both GA and SA algorithms, a genetic simulated annealing (GSA) algorithm approach is created. Herein, the GSA algorithm will be briefly reviewed.

3.1. Genetic Simulated Annealing. SA starts from an initial solution at a high temperature and makes a series of changes according to an annealing schedule. For each change, an objective value f_{new} (f_{new} becomes f_{old} after an iteration) is obtained. The difference between the objective values ($\Delta f = f_{\text{new}} - f_{\text{old}}$) is calculated after each iteration. If $\Delta f \le 0$, the new solution is accepted with probability $\rho = 1$. On the contrary, it is accepted with a small probability ρ, which can be tracked as $\rho = \exp(-\Delta f/T)$, where T is the current temperature parameter. Thus, SA avoids being trapped in a local optimum [22]. Moreover, at each temperature, the above process will repeat L times, where L represents the Markov length. The temperature T is gradually decreased by cooling coefficient ω, where T is defined as $T = T \times \omega$ ($0 < \omega < 1$). SA terminates either when the optimum solution is obtained or when the initial temperature decreases to the given value [7].

A matrix $[\underline{x_{11}, x_{21}, \ldots, x_{r1}, \ldots, x_{l1}}; \underline{x_{12}, x_{22}, \ldots, x_{r2}, \ldots, x_{l2}}; \ldots; \underline{x_{1j}, x_{2j}, \ldots, x_{rj}, \ldots, x_{lj}}; \ldots; \underline{x_{1m}, x_{2m}, \ldots, x_{rm}, \ldots, x_{lm}}]$ forms the genes of a chromosome in the algorithm. Here, from $j = 1:m$, $r = 1:l$, each gene $x_{rj} = 1$ represents the notion that train j stays on track r. The matrix above is a unit matrix and ensures that each coming train has a track. A common operator used in GA is crossover, which generates chromosomes [23]. A replacing method is adopted in the crossover operation. Taking the sample station as an example (four tracks), the track for a certain train is replaced by the track for the same train in another chromosome (see Figure 6), where the x-axis represents trains and the y-axis represents the timeline. The mutation operation changes the track for one train randomly. If the generated chromosome is unavailable, then it will be deleted.

The following GSA searches solutions for the track reallocation problem in railway stations. The detailed algorithmic steps are described as follows.

Step 1 (initialization). (1.1) Set initial parameters: population size p ($p = 1000$), iteration mark $k := 0$, initial temperature $t_k := 100$, lowest temperature $\tau = 0.01$, and cooling coefficient $\omega = 0.95$.

(1.2) Read the timetables for the arrival-departure trains.

Step 2 (creating and selecting new chromosome). (2.1) Update $k = k + 1$.

(2.2) If $t_k := \tau$, stop; otherwise, turn to 2.2.

(2.3) Obtain a new chromosome j from each old chromosome $i \in \text{POP}(k)$ from the crossover operation to chromosome i.

(2.4) Calculate $\sigma(j) - \sigma(i)$, where $\sigma(j)$ and $\sigma(i)$ are objective values of chromosomes j and i, respectively.

(2.5) If $\sigma(j) - \sigma(i) \le 0$, chromosome j replaces chromosome i; otherwise, chromosome j replaces chromosome i by probability $\rho = \exp((f(i) - f(j))/t_k)$.

(2.6) Repeat steps 2.2 through 2.5 until a new population POP1(k) is generated.

(2.7) Use the mutation operation to population POP1(k). Check the generated solutions with constraints in (7) and accept them if they are available. Otherwise, delete them.

(2.8) Find the best solution in POP1(k) by comparing objective values.

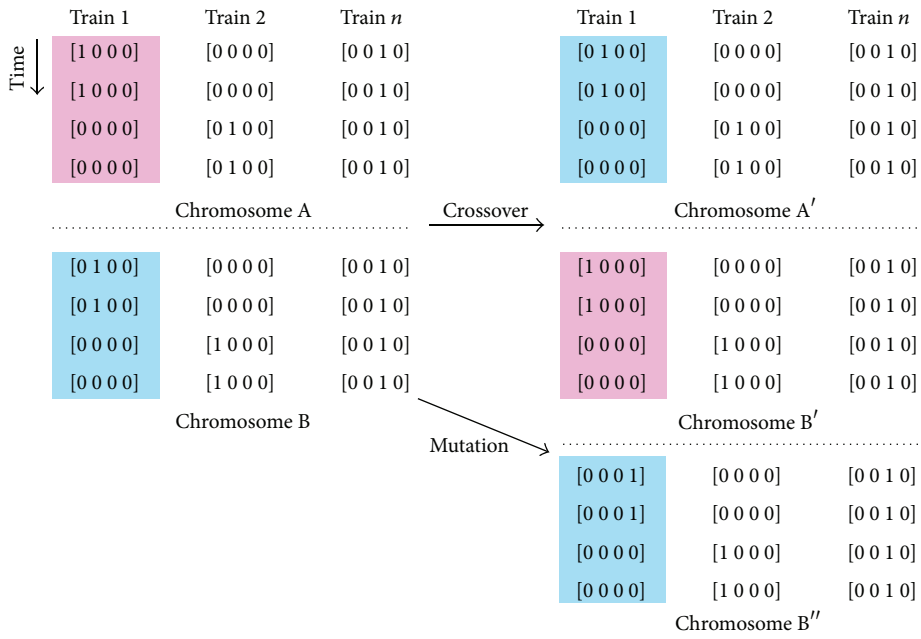

Figure 6: Samples of crossover and mutation operations.

Step 3 (stop or do not stop). 3.1 If temperature $t_k \leq \tau$, stop; otherwise, $t_k = t_k \cdot \omega$. Return to Step 2.

3.2. Sample Test. A sample station in Figure 1 is used to verify the feasibility of the proposed model. Table 1 shows the different components for the routes and the corresponding occupation time of the GTs. For example, GTs (3, 5, 9/10, 8, 2) consist of the path to reception-departure track 1. The corresponding occupation times of the above GTs are (2, 2, 2/2, 2, 2) seconds.

Table 2 gives the arrival and departure times of trains that should be dispatched in this station. There are six trains from 8:00 to 8:25 among which three trains pull in from the right bottleneck section and three pull in from the left bottleneck section. Figure 7 depicts the timetable intuitively. As observed, T2, T4, T5, and T6 arrive/depart at/from the station simultaneously. In other words, these four trains will occupy the station bottlenecks at 8:15, which means this station stays in the thick of the bottleneck capacity at this time.

Experiments are tested on a personal computer with an Intel Pentium 4 2.80 GHz CPU and 2 GB RAM. The track allocation optimizing results are given in Table 3, when $\sum_{i\in I} t_{ij} / \sum_{i\in I} x_{ir}$ of tracks 1 and 2 are smaller than those of tracks 3 and 4. Thus, tracks 1 and 2 have been occupied twice, while tracks 3 and 4 are only used once.

We also simulate the track accidental experiment (track 1 is randomly selected by the programming). Computing results are shown in Table 4. When we simulate two track incidents simultaneously, a feasible reallocation plan could not be returned because the bottleneck capacity is not large enough to receive all trains. The computer simulation indicates that if there are two or more tracks that are not ready for service, trains cannot stay on the tracks according to the existing timetable. The track capacity decreases and some trains are delayed for arrival.

Table 1: Component GTs of each track in Figure 1.

Track	Groups of turnouts	$\sum_{i\in I} x_{ir}$	t_{ij} (sec)	$\sum_{i\in I} t_{ij} / \sum_{i\in I} x_{ir}$ (sec)
1	3, 5, 9/10, 8, 2	3/3	2, 2, 2/2, 2, 2	2
2	3, 5, 9/10, 8, 2	3/3	2, 2, 2/2, 2, 2	2
3	1, 7, 11/12, 6, 4	3/3	3, 3, 3/3, 3, 3	3
4	1, 7, 11/12, 6, 4	3/3	3, 3, 3/3, 3, 3	3

4. Case Study

This section illustrates the quality of the proposed model for a real case in China. Figure 8 shows the structure of the Baoji railway station in China. There are two bottleneck sections in this station: the left bottleneck section and the right bottleneck section. The left bottleneck is made up of 13 GTs that are marked with odd Arabic numbers, and the right bottleneck is made of 14 even GTs. Eleven reception-departure tracks, numbered from 1 to 11, are in the middle of the station. Here, the data sources for the computation come from the Xi'an Railway Administration, and the detailed TWD is given in Table 5.

As seen from Table 5, there are 30 trains that are scheduled in this daily and shift transport plan (from approximately 8:00 to 10:00). For example, train T22 arrives at 8:09 and departs at 8:22. The *Direction* column indicates that train T22

Table 2: TWD of trains.

Train	Direction	Reception	Departure	Train	Direction	Reception	Departure
T1	Right	8:00:00	8:10:00	T2	Left	8:00:00	8:15:00
T3	Right	8:00:00	8:05:00	T4	Left	8:10:00	8:15:00
T5	Right	8:10:00	8:15:00	T6	Left	8:15:00	8:25:00

Table 3: Track allocation results of sample station.

Train	Track	Reception	Departure	Train	Track	Reception	Departure
T1	3	8:00:00	8:10:00	T2	1	8:00:00	8:15:00
T3	2	8:00:00	8:05:00	T4	2	8:10:00	8:15:00
T5	4	8:10:00	8:15:00	T6	1	8:15:00	8:25:00

Table 4: Track reallocation results.

Train	Track	Arrival	Departure	Train	Track	Arrival	Departure
T1	4	8:00:00	8:10:00	T2	3	8:00:00	8:15:00
T3	2	8:00:00	8:05:00	T4	2	8:10:00	8:15:00
T5	4	8:10:00	8:15:00	T6	2	8:15:00	8:25:00

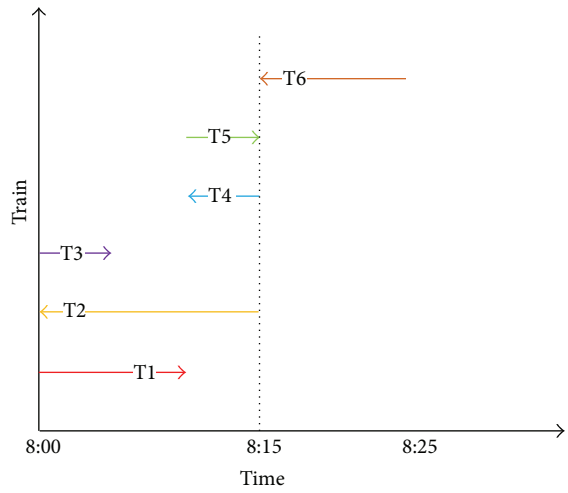

Figure 7: Train arrival-departure time axes.

pulls in from the right bottleneck section and pulls out from the opposite bottleneck.

In Table 6, each row gives the component GTs of a station route from track 1 to track 11. The occupation time of each route is calculated according to Table 7, which shows the occupation time of each GT. Here, safety interval times have been taken into consideration [24].

4.1. Unavailable Tracks Simulation. Some virtual trains are introduced to solve the simulation work. It is undoubted that if a certain track is unavailable because of incidents, this track cannot be occupied until it recovers. According to different accident degrees, different repairing times are required. Therefore, the track repairing time is represented by the track occupation time of a virtual train. Actually, each track has a hidden virtual train, which will be activated as long as the track remains unavailable. Figure 9 illustrates how virtual trains simulate the unavailable tracks. TWD is transformed into a track occupation timeline. The dotted lines represent virtual trains, and the solid lines are real trains with train running directions. Train numbers are marked above the lines with the tracks in brackets. One virtual train will occupy a track when this track breaks down. The virtual train will evacuate when the track recovers.

4.2. Optimization Results. Four accidental tracks are randomly selected by the computer, that is, tracks 2, 3, 8, and 10. Track 3 and track 8 are unavailable from 8:00 to 9:00, while track 1 and track 10 are unavailable from 9:00 to 10:00. In this case, the optimization results are shown in Table 8. Clearly, no train should stay on tracks 3 and 8 between 8:00 and 9:00. Additionally, tracks 1 and 10 are not occupied between 9:00 and 10:00. Figure 10 shows the track occupation frequency and route occupation time (cost) in a line chart, where "cost" means the necessary occupation time (min) of GTs with respect to a certain track. Compared with the original allocation results, the total cost of the optimal results is reduced from 64.3 to 62.2 in 30 min (Table 9).

It is easy to find that the higher the route costs, the smaller the occupation frequency of the corresponding track is. For example, tracks 10, 5, 9, and 7 have been occupied four times, while tracks 8 and 11 are occupied only once because track 8 is unavailable from 8:00 to 9:00 and because its time cost reaches up to 2.3. For instance, track 10 has been occupied four times in one hour. This is mainly because its time cost is only 1.833, which is the least among all station tracks.

4.3. Limited Carrying Capacity. According to the train arrival times in Table 8, different track allocation plans are given by discrete algorithm parameters. Table 10 lists the specific values of the left and right bottlenecks after analyzing two bottleneck capacities under each given plan. As seen, the program has been run by separate iterations (from 60 to

Table 5: TWD of trains.

Train	Direction	Arrival	Departure	Train	Direction	Arrival	Departure
T22	Right	8:09:00	8:22:00	K375	Left	8:24:00	8:31:00
T75	Left	9:12:00	9:22:00	D5082	Right	8:41:00	9:11:00
T117	Left	9:42:00	9:52:00	T23	Left	8:09:00	8:22:00
T193	Left	8:29:00	8:33:00	T116	Right	9:42:00	9:52:00
T223	Left	8:12:00	8:22:00	T192	Right	8:29:00	8:33:00
K621	Left	9:04:00	9:12:00	T222	Right	8:12:00	8:22:00
10176	Right	9:24:00	9:29:00	K624	Right	9:04:00	9:12:00
10452	Right	9:14:00	9:22:00	10175	Left	9:24:00	9:29:00
10454	Right	9:16:00	9:46:00	10420	Right	8:08:00	8:19:00
10448	Right	8:08:00	8:38:00	10450	Right	8:30:00	9:00:00
1486	Right	9:27:00	9:40:00	10456	Right	9:32:00	10:02:00
T7	Left	9:35:00	9:45:00	D5081	Left	8:51:00	9:21:00
1150	Right	9:35:00	10:00:00	1147	Left	9:35:00	10:00:00
2669	Left	9:20:00	9:50:00	K245	Left	8:39:00	8:49:00
K248	Right	8:39:00	8:49:00	K378	Right	8:24:00	8:31:00

Table 6: Component GTs of each train track.

Track	Groups of turnouts	$\sum_{i\in I} x_{ir}$	$\sum_{i\in I} t_{ij}$	$\sum_{i\in I} t_{ij} / \sum_{i\in I} x_{ir}$
1	11, 13, 21/16, 18, 26, 28	3/4	8/8	2.286
2	11, 13, 21/16, 18, 26, 28	3/4	8/8	2.286
3	11, 13, 21/6, 8, 10, 20, 24, 28	3/6	8/13	2.333
4	11, 13, 23/16, 18, 20, 24	3/4	7/8	2.143
5	11, 13, 15, 23, 25/6, 8, 10, 12, 22	5/5	9/10	1.900
6	1, 7, 9, 17/6, 8, 10, 12, 14	4/5	9/10	2.111
7	1, 3, 9/6, 8, 10, 12, 14	3/5	6/10	2.000
8	3, 5, 7, 9/6, 8, 10, 12, 14, 4	4/6	10/13	2.300
9	1, 3, 5/6, 8, 10, 12, 14, 4	3/6	5/13	2.000
10	1, 3, 5/2, 4	3/2	5/6	1.833
11	3, 5, 7, 9/6, 8, 10, 12, 14, 4	4/6	10/13	2.300

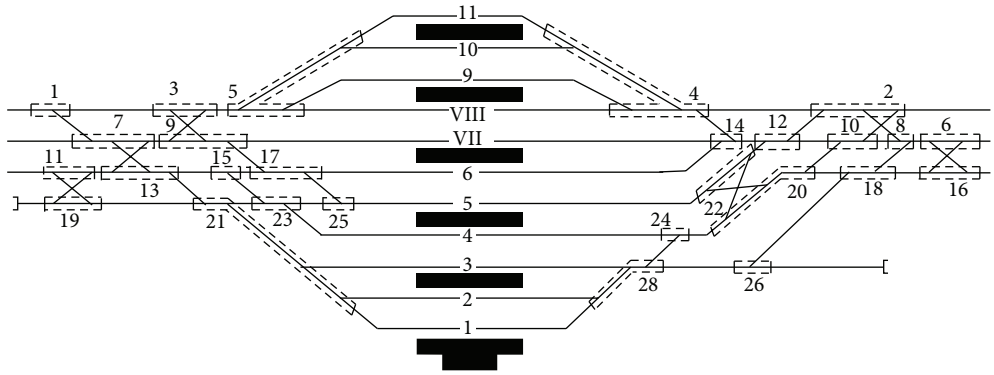

Figure 8: Map of station bottleneck structure (Baoji, China).

2800). T_L and T_R are calculated each time. It is found that the carrying capacity of the left bottleneck is approximately 1.29 times more than the right bottleneck. Thus, the limited carrying capacity is the right bottleneck section in this railway station.

4.4. Track Unavailable Analysis. From 8:00 to 8:30, the capacity of the station tracks is excessive if there is no track accident. What if the station tracks have a larger area of failures? If the number of unavailable tracks exceeds a certain figure, this will lead to a delay in a train's arrival/departure.

Table 7: Occupation time of each GT (min).

GT	1	3	5	7	9	11	13	15	17	19	21	23	25	
t_{ij}	1	2	2	3	3	2	3	1	2	2	3	2	1	
GT	2	4	6	8	10	12	14	16	18	20	22	24	26	28
t_{ij}	3	3	2	2	2	2	2	2	2	3	2	1	1	3

Table 8: Track allocation results.

Train	Track	Arrival	Departure	Train	Track	Arrival	Departure
10420	9	8:08:00	8:19:00	K624	9	9:04:00	9:12:00
10448	6	8:08:00	8:38:00	K621	7	9:04:00	9:12:00
T23	7	8:09:00	8:22:00	T75	5	9:12:00	9:22:00
T22	5	8:09:00	8:22:00	10452	3	9:14:00	9:22:00
T222	1	8:12:00	8:22:00	10454	9	9:16:00	9:46:00
T223	10	8:12:00	8:22:00	2669	2	9:20:00	9:50:00
K378	10	8:24:00	8:31:00	10175	5	9:24:00	9:29:00
K375	9	8:24:00	8:31:00	10176	4	9:24:00	9:29:00
T192	1	8:29:00	8:33:00	1486	8	9:27:00	9:40:00
T193	7	8:29:00	8:33:00	1147	11	9:35:00	10:00:00
10450	2	8:30:00	9:00:00	1150	5	9:35:00	10:00:00
K248	10	8:39:00	8:49:00	10456	4	9:32:00	10:02:00
K245	1	8:39:00	8:49:00	T7	6	9:35:00	9:45:00
D5082	6	8:41:00	9:11:00	T117	7	9:42:00	9:52:00
D5081	10	8:51:00	9:21:00	T116	3	9:42:00	9:52:00

Thus, the maximum antijamming capacity in this station is tested. We performed a track unavailable experiment. The results indicate that the maximum number of unavailable tracks at the Baoji station is five from 8:00 to 8:30. Table 11 shows the experimental results.

Table 10 shows that the Baoji station tolerates five unavailable tracks at most. Therefore, we observe the relationships for the number of unavailable tracks, lasting time, and station capacity in Figure 11. There are two parameters related to the size of dispatching trains that have been tested here. It is clear that, with a smaller number of unavailable tracks and shorter lasting time, a larger number of trains tend to be received. As shown in Figure 11, the number of unavailable tracks changes from 6 to 11, the lasting time changes from 5 to 30 min, and the different number of trains that can stay in the station is obtained.

4.5. Convergence Test. To further illustrate the efficiency of the GSA algorithm, a convergence test is given in this case study as shown in Figure 12. The program stops after approximately 30 min with 1000 generations. The result indicates that the algorithm can converge to a steady state. For the real-time usage, operators can set a smaller value of generation or a limited running time. In addition, as the convergence curve indicates, solutions are acceptable when iterations reach one-fourth of the total iterations.

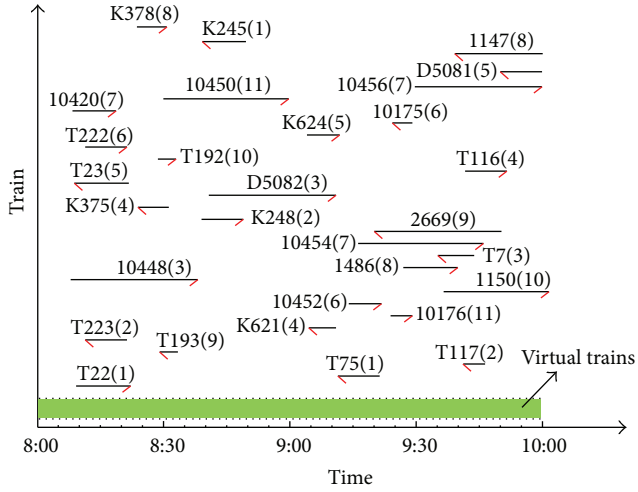

Figure 9: Track occupations timeline.

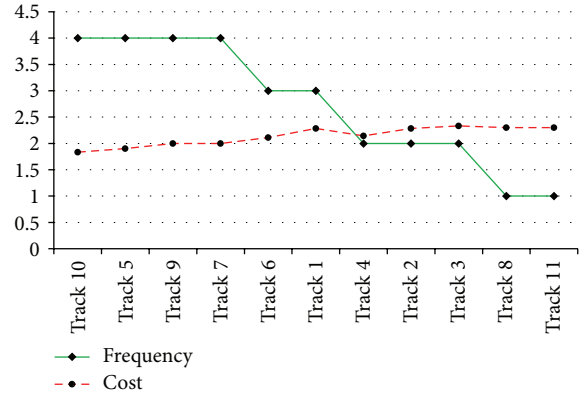

Figure 10: Track occupation frequency and track cost.

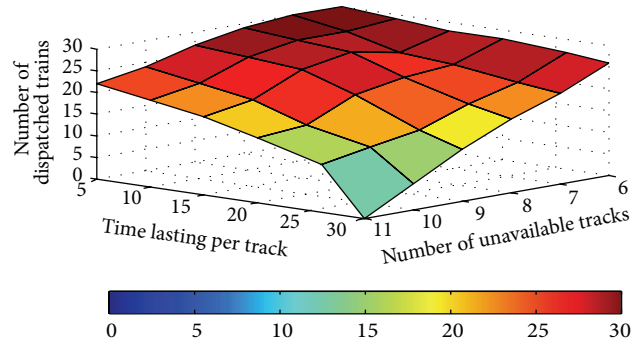

Figure 11: Relationships for the number of unavailable tracks, lasting time, and station capacity.

5. Conclusions

This paper is motivated by the need to formulate and solve a track reallocation problem in large railway stations. We first explain the key features of using virtual trains to formulate track incidents. A mathematical programming model is developed, which aims at minimizing the total occupation

Table 9: Comparison of optimization results.

Track	Cost of GTs (min)	Optimal results		Original results	
		Frequency	Cost (min)	Frequency	Cost (min)
1	2.286	3	6.858	3	6.858
2	2.286	2	4.572	3	6.858
3	2.333	2	4.666	3	6.999
4	2.143	2	4.286	3	6.429
5	1.9	4	7.6	3	5.7
6	2.111	3	6.333	3	6.333
7	2	4	8	3	6
8	2.3	1	2.3	3	6.9
9	2	4	8	2	4
10	1.833	4	7.332	2	3.666
11	2.3	1	2.3	2	4.6

Table 10: Bottleneck capacity analysis.

Algorithm parameters					Track allocations	T_L	T_R	T_R/T_L	$T_L + T_R$
T_0	τ	ω	L	Run					
50	0.1	0.8	100	2800	7, 5, 8, 10, 4, 1, 7, 4, 2, 10, 1, 10, 2, 4, 9, 7, 10, 2, 10, 7, 1, 11, 4, 10, 11, 4, 3, 9, 6, 10	208	268	1.29	476
30	0.1	0.8	100	2600	9, 6, 10, 1, 5, 4, 10, 2, 5, 11, 7, 10, 2, 1, 10, 2, 4, 4, 2, 11, 9, 10, 4, 5, 1, 2, 3, 4, 10, 6	219	270	1.23	489
10	0.1	0.8	100	2100	10, 8, 7, 1, 9, 2, 10, 1, 9, 11, 2, 4, 10, 9, 1, 4, 5, 10, 4, 2, 7, 10, 4, 8, 11, 1, 10, 4, 9, 6	211	280	1.33	491
50	0.5	0.8	100	2100	10, 7, 5, 2, 8, 4, 4, 10, 8, 2, 6, 11, 7, 1, 4, 9, 10, 6, 11, 1, 7, 10, 4, 5, 2, 4, 8, 6, 10, 9	223	281	1.26	504
50	1	0.8	100	1800	6, 4, 10, 11, 1, 5, 10, 5, 9, 11, 1, 10, 9, 2, 7, 5, 10, 6, 8, 5, 3, 10, 7, 11, 2, 1, 4, 7, 10, 6	223	283	1.27	506
50	0.1	0.5	100	900	10, 11, 4, 5, 7, 1, 8, 5, 7, 10, 6, 10, 7, 8, 7, 5, 4, 10, 8, 1, 4, 10, 6, 2, 6, 11, 10, 9, 2, 8	226	283	1.25	509
50	0.1	0.2	100	400	9, 7, 10, 5, 11, 1, 3, 1, 9, 10, 5, 11, 7, 3, 1, 8, 10, 4, 10, 7, 8, 5, 6, 10, 2, 5, 1, 6, 10, 3	223	290	1.30	513
50	0.1	0.8	50	1400	5, 4, 10, 3, 7, 2, 10, 11, 5, 1, 6, 10, 3, 7, 10, 9, 11, 4, 5, 11, 8, 10, 5, 2, 7, 10, 3, 1, 4, 2	223	284	1.27	507
50	0.1	0.8	30	840	9, 6, 7, 5, 1, 10, 10, 9, 1, 7, 2, 10, 1, 6, 10, 9, 7, 5, 3, 9, 2, 5, 4, 8, 11, 5, 4, 6, 7, 3	217	294	1.35	511
10	1	0.2	30	60	7, 1, 8, 9, 11, 5, 3, 7, 5, 2, 9, 4, 6, 1, 7, 5, 2, 9, 1, 6, 4, 10, 8, 9, 5, 10, 1, 11, 8, 3	230	306	1.33	536
Average				1500	—	220	284	1.29	504

Table 11: Test of the number of unavailable tracks.

Track unavailable	Track allocation	Occupation time of GTs
1	10, 5, 9, 7, 6, 4, 10, 5, 9, 7, 6	21.831
1, 2	10, 5, 9, 7, 6, 4, 10, 5, 9, 7, 6	21.831
1, 2, 3	10, 5, 9, 7, 6, 4, 10, 5, 9, 7, 6	21.831
1, 2, 3, 4	10, 5, 9, 7, 6, 8, 10, 5, 9, 7, 6	21.988
1, 2, 3, 4, 5	10, 9, 7, 6, 8, 11, 10, 9, 7, 6, 8	22.788
1, 2, 3, 4, 5, 6	Reallocation failure	Train delay

time of station bottleneck sections to avoid train delays. In addition, a hybrid algorithm between the genetic algorithm and the simulated annealing algorithm is designed. The case study for the Baoji railway station in China verifies the efficiency of the proposed model and the algorithm.

Our future study will focus on (1) developing different optimization or reformulation methods that can reduce the CPU time, improving the solution efficiency, and (2) modeling different scenarios for station incidents, for example, signal problems and switching problems, to address problems in railway station operations.

Conflict of Interests

The authors declare that there is no conflict of interests regarding the publication of this paper.

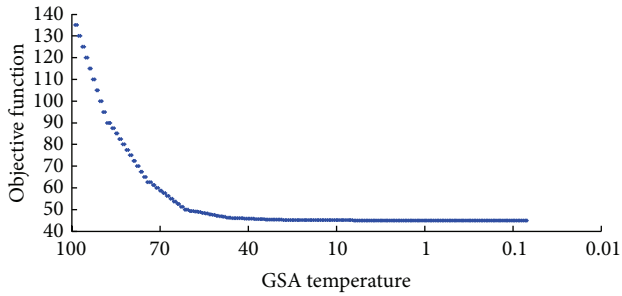

Figure 12: Convergence test.

Acknowledgments

This paper is supported by the NSFC (71473259, 71390332), the Fundamental Research Funds for the Central Universities (2015YJS101), and the Specialized Research Fund for the Doctoral Program of Higher Education (20130009110001).

References

[1] A. Caprara, M. Fischetti, and P. Toth, "Modeling and solving the train timetabling problem," *Operations Research*, vol. 50, no. 5, pp. 851–861, 2002.

[2] P. J. Zwaneveld, L. G. Kroon, and S. P. M. Van Hoesel, "Routing trains through a railway station based on a node packing model," *European Journal of Operational Research*, vol. 128, no. 1, pp. 14–33, 2001.

[3] P. J. Zwaneveld, L. G. Kroon, H. E. Romeijn et al., "Routing trains through railway stations: model formulation and algorithms," *Transportation Science*, vol. 30, no. 3, pp. 181–194, 1996.

[4] D. D. L. Cardillo and N. Mione, "kL-list λ colouring of graphs," *European Journal of Operational Research*, vol. 106, no. 1, pp. 160–164, 1998.

[5] A. Billionnet, "Using integer programming to solve the train-platforming problem," *Transportation Science*, vol. 37, no. 2, pp. 213–222, 2003.

[6] M. Carey and S. Carville, "Scheduling and platforming trains at busy complex stations," *Transportation Research Part A: Policy and Practice*, vol. 37, no. 3, pp. 195–224, 2003.

[7] L. J. Kang, J. J. Wu, and H. J. Sun, "Using simulated annealing in a bottleneck optimization model at railway stations," *Journal of Transportation Engineering*, vol. 138, no. 11, pp. 1396–1402, 2012.

[8] F. Barber, M. A. Salido, L. P. Ingolotti, M. Abril, A. L. Lova, and M. P. Tormos, "An interactive train scheduling tool for solving and plotting running maps," in *Current Topics in Artificial Intelligence*, vol. 3040 of *Lecture Notes in Computer Science*, pp. 646–655, Springer, Berlin, Germany, 2004.

[9] A. D'Ariano, D. Pacciarelli, and M. Pranzo, "Assessment of flexible timetables in real-time traffic management of a railway bottleneck," *Transportation Research Part C: Emerging Technologies*, vol. 16, no. 2, pp. 232–245, 2008.

[10] M. Heydar, M. E. H. Petering, and D. R. Bergmann, "Mixed integer programming for minimizing the period of a cyclic railway timetable for a single track with two train types," *Computers & Industrial Engineering*, vol. 66, no. 1, pp. 171–185, 2013.

[11] S. Narayanaswami and N. Rangaraj, "Modelling disruptions and resolving conflicts optimally in a railway schedule," *Computers & Industrial Engineering*, vol. 64, no. 1, pp. 469–481, 2013.

[12] Y.-H. Cheng and Y.-C. Tsai, "Railway-controller-perceived competence in incidents and accidents," *Ergonomics*, vol. 54, no. 12, pp. 1130–1146, 2011.

[13] F. Belmonte, W. Schön, L. Heurley, and R. Capel, "Interdisciplinary safety analysis of complex socio-technological systems based on the functional resonance accident model: an application to railway traffic supervision," *Reliability Engineering and System Safety*, vol. 96, no. 2, pp. 237–249, 2011.

[14] B. L. Hollis and P. J. Green, "Real-life vehicle routing with time windows for visual attractiveness and operational robustness," *Asia-Pacific Journal of Operational Research*, vol. 29, no. 4, Article ID 1250017, 2012.

[15] X. Gandibleux, X. Delorme, and V. T'Kindt, "An ant colony optimisation algorithm for the set packing problem," in *Ant Colony Optimization and Swarm Intelligence*, vol. 3172 of *Lecture Notes in Computer Science*, pp. 49–60, Springer, Berlin, Germany, 2004.

[16] X. Gandibleux, J. Jorge, S. Angibaud, X. Delorme, and J. Rodriguze, "An ant colony optimization inspired algorithm for the set packing problem with application to railway infrastructure," in *Proceedings of the 6th Metaheuristics International Conference*, pp. 309–396, Vienna, Austria, 2005.

[17] G. Caimi, D. Burkolter, and T. Herrmann, "Finding delay-tolerant train routings through stations," in *Operations Research Proceedings 2004*, vol. 2004 of *Operations Research Proceedings*, pp. 136–143, Springer, Berlin, Germany, 2005.

[18] T. M. Herrmann, *Stability of timetables and train routing the station regions [Ph.D. thesis]*, Swiss Federal Institute of Technology, Zürich, Switzerland, 2006.

[19] J. J. Wu, L. J. Kang, H. J. Sun, and X. L. Jia, "Track allocation optimization in railway station: mean-variance model and case study," *Journal of Transportation Engineering*, vol. 139, no. 5, pp. 540–547, 2013.

[20] F. Zhao and X. G. Zeng, "Simulated annealing–genetic algorithm for transit network optimization," *Journal of Computing in Civil Engineering*, vol. 20, no. 1, pp. 57–68, 2006.

[21] L. J. Kang, X. N. Zhu, J. J. Wu, H. J. Sun, S. Siriya, and K. Kanokvate, "Departure time optimization of last trains in subway networks: mean-variance model and GSA algorithm," *Journal of Computing in Civil Engineering*, Article ID 04014081, pp. 1–12, 2014.

[22] C. Koulamas, S. R. Antony, and R. Jaen, "A survey of simulated annealing applications to operations research problems," *Omega*, vol. 22, no. 1, pp. 41–56, 1994.

[23] C. R. Reeves, "Genetic algorithms for the operations researcher," *INFORMS Journal on Computing*, vol. 9, no. 3, pp. 231–250, 1997.

[24] P. Sels, P. Vansteenwegen, T. Dewilde, D. Cattrysse, B. Waquet, and A. Joubert, "The train platforming problem: the infrastructure management company perspective," *Transportation Research Part B: Methodological*, vol. 61, pp. 55–72, 2014.